RECORD COPY
C.1

SANDIA REPORT

SAND93—1342 • UC—132
Unlimited Release
Printed July 1993

MICROFICHE

Rationale for Finding and Exploiting Fractured Reservoirs, Based on the MWX/SHCT-Piceance Basin Experience

John C. Lorenz, Norman R. Warpinski, Lawrence W. Teufel

8592116

SANDIA NATIONAL
LABORATORIES
TECHNICAL LIBRARY

Prepared by
Sandia National Laboratories
Albuquerque, New Mexico 87185 and Livermore, California 94550
for the United States Department of Energy
under Contract DE-AC04-76DP00789

SF2900Q(8-81)

150p.

Issued by Sandia National Laboratories, operated for the United States Department of Energy by Sandia Corporation.

NOTICE: This report was prepared as an account of work sponsored by an agency of the United States Government. Neither the United States Government nor any agency thereof, nor any of their employees, nor any of their contractors, subcontractors, or their employees, makes any warranty, express or implied, or assumes any legal liability or responsibility for the accuracy, completeness, or usefulness of any information, apparatus, product, or process disclosed, or represents that its use would not infringe privately owned rights. Reference herein to any specific commercial product, process, or service by trade name, trademark, manufacturer, or otherwise, does not necessarily constitute or imply its endorsement, recommendation, or favoring by the United States Government, any agency thereof or any of their contractors or subcontractors. The views and opinions expressed herein do not necessarily state or reflect those of the United States Government, any agency thereof or any of their contractors.

Printed in the United States of America. This report has been reproduced directly from the best available copy.

Available to DOE and DOE contractors from
Office of Scientific and Technical Information
PO Box 62
Oak Ridge, TN 37831

Prices available from (615) 576-8401, FTS 626-8401

Available to the public from
National Technical Information Service
US Department of Commerce
5285 Port Royal Rd
Springfield, VA 22161

NTIS price codes
Printed copy: A07
Microfiche copy: A01

SAND93–1342
Unlimited Release
Printed August 1993

Distribution
Category UC–132

Rationale for Finding and Exploiting Fractured Reservoirs, Based on the MWX/SHCT-Piceance Basin Experience

John C. Lorenz
Geomechanics Department

Norman R. Warpinski
Geotechnology Research Department

Lawrence W. Teufel
Geomechanics Department

Sandia National Laboratories
Albuquerque, NM 87185

Abstract

The deliverability of a reservoir depends primarily on its permeability, which, in many reservoirs, is controlled by a combination of natural fractures and the in situ stresses. Therefore it is important to be able to predict which parts of a basin are most likely to contain naturally fractured strata, what the characteristics of those fractures might be, and what the most likely in situ stresses are at a given location. This paper presents a set of geologic criteria that can be superimposed onto factors, such as levels of maturation and porosity development, in order to predict whether fractures are present once the likelihood of petroleum presence and reservoir development have been determined. Stress causes fracturing, but stresses are not permanent. A natural-fracture permeability pathway opened by one system of stresses may be held open by those stresses, or narrowed or even closed by changes of the stress to an oblique or normal orientation. The origin of stresses and stress anisotropies in a basin, the potential for stress to create natural fractures, and the causes of stress reorientation are examined in this paper. The appendices to this paper present specific techniques for exploiting and characterizing natural fractures, for measuring the present-day in situ stresses, and for reconstructing a computerized stress history for a basin.

Acknowledgments

Reviews by James T. Neal and David A. Northrop have improved this manuscript. This work was supported by the U.S. Department of Energy under contract DE-AC04-76DP00789.

Contents

Introduction 9
1. Importance of Natural Fractures in Western Basins 10
2. Effects of Stresses on Natural Fractures 11
3. Fracture Mechanisms 14
4. Sources of Anisotropic Stress in a Basin 14
   4.1 Horizontal Compression as a Source of Stress 16
      4.1.1 Thrusting 16
      4.1.2 Basin Subsidence 17
      4.1.3 Basin Uplift 18
   4.2 Calculating Stress Trajectories Due to Thrusts 19
   4.3 Calculating the Horizontal Stress Due to Basin-Wide Strain 21

5. Local Modifications of Regional Stresses in a Basin 21
   5.1 Variations in Pore Pressure 21
   5.2 Stress Decollements 22
   5.3 Stress Refraction 25
   5.4 Local Stress Due to Flexure 26
   5.5 Effects of Severe Topography 27
   5.6 Relaxation of Stresses 29

6. Analysis: Reconstructing the Stress/Fracture History of a Basin 31
   6.1 Paleostress Indicators 31
      6.1.1 Microscopic Indicators 31
      6.1.2 Mesoscopic Indicators 33
      6.1.3 Macroscopic Indicators 34
   6.2 Present-Day, In Situ Stress Indicators 35
   6.3 Pore Pressure 36
   6.4 Summary 38

7. Prediction of Fracture and Stress Orientations in a Basin and at a Well Site 39
   7.1 Tectonic Stress History 41
   7.2 Calculated Stress History 41
   7.3 Fracture-Susceptibility History 43
   7.4 Integration 44
Conclusion 45
References 47

APPENDIX A—Wellbore Geometries for Optimum Fracture Characterization and Drainage 51
APPENDIX B—Measurement and Analysis of Fractures in Core 61
APPENDIX C—Viscoelastic Stress History Equations for Basin Stress Modeling 87
APPENDIX D—Techniques for In Situ Stress Measurement: Anelastic Strain Recovery (ASR), and Circumferential Velocity Anisotropy (CVA) 89
APPENDIX E—Computer Codes for Calculating the Effects of Topography on Stress 95
APPENDIX F—Computer Code for Stress-History Calculations 107

Figures

1 Laboratory measurements of the permeabilities through mineralized fractures in sandstones of the MWX reservoirs compared to the matrix permeabilities of adjacent, unfractured samples 11
2 Laboratory measurements of the stress sensitivity of MWX mineralized fractures. Higher conductivity fractures from the Cozzette sandstone have less sensitivity than the lower conductivity fracture from the fluvial interval 13
3 Measured permeability anisotropy in the Ekofisk reservoir, relative to the observed fracture orientations and the maximum stress orientation 13
4 Characteristics of rock failure as a function of confining stress. Rocks show brittle behavior with only small amounts of strain prior to failure if the confining stress is low; they are ductile and accommodate significant strain if confining stresses are high 15
5 Natural fracture pattern that radiates out from the White River Uplift, created by stress trajectories radiating away from the thrust front during thrusting 17
6 Strain due to lengthening of a depositional surface to a hypotenuse during asymmetric subsidence in a narrow, deep basin such as the Late Cretaceous foredeep in southwestern Wyoming 18
7 Stresses in strata created by uniform uplift and radial release of confining stresses 19
8 Schematic of the geometry for a constant distributed load applied to a semi-infinite region 20
9 Stress trajectories calculated from simple distributed loads as representations of the White Rover thrusts. Line orientations indicate the orientations of the maximum stress; length of the line indicates the relative stress magnitudes. (Compare to Figure 5.) 20
10 Measured variation in the minimum horizontal stress, as represented by the fracture gradient, as a function of the pore pressure for the Vicksburg Formation 23
11 Measured variation in the minimum horizontal stress, as represented by the fracture gradient, as a function of the pore pressure for the MWX site 23
12 Stress in the Jura Region. (a): Stress variations across a ductile boundary layer in front of the Alpine thrust belt (from Muller et al., 1987); (b): Inferred planview stress trajectories of upper stress array and lower stress array in the same area as (a) (from Becker, 1989) 24
13 Example of horizontally layered stress domains caused by buttress-induced thrusting (from Kulick and Schmidt, 1988). Measurements of paleostresses within strata with a similar configuration have suggested that the stresses in the upper, unbuttressed layers had been largely relieved (Genovese and Schmidt, 1989) 25
14 Stress trajectories deflected by inhomogeneities in strata (from Bell and Lloyd, 1989) 26
15 The changes in stress orientation and magnitude with depth, due to topographic loading near the MWX site (from Clark, 1983) 28
16 Schematic of the geometry for a linearly increasing distributed load applied to a semi-infinite region. 28
17 Calculated stress reorientation due to a mesa and escarpment as a function of the angle of the escarpment relative to the far-field maximum stress orientation. A high mesa can significantly reorient the stress field. 29
18 Map of the Piceance basin showing the trends and occurrences of paleostress indicators 32
19 Rapid subsidence in a narrow basin that led to asymmetric stresses and fracturing parallel to the basin axis despite thrust-fault compression normal to the basin axis: Cretaceous foredeep of the Green River basin, southwestern Wyoming 34

Figures (continued)

20 Orientation of the stress field at MWX based on Anelastic Strain Recovery (ASR) data in three wells, Differential Strain Curve Analysis (DSCA) on selected samples, an open-hole hydraulic fracture (impression packer), and four hydraulic fracture experiments where borehole seismic instrumentation was used to map the fracture azimuth....37
21 Time/Burial-depth/Surface-elevation diagram for the strata at the MWX site in the Piceance basin....38
22 Reconstructed stress history for the strata at the MWX site....40
23 Stresses (from previous figure) plotted within an empirical failure envelope, indicating the most likely times of fracturing. Outer envelope is failure plane from laboratory data. Inner envelope indicates failure plane corrected for geologic criteria....40
24 Calculation of the shear stress, through time, that would have developed at three sites in the southern Piceance basin. Increased shear stress indicates increased potential for fracturing....44
25 Flow diagram summarizing fracture-assessment techniques and their integration into the procedures described in this paper....46

Table

1 Information for Predicting Subsurfaces Stress and Fracture Patterns at a Well Site....39

Rationale for Finding and Exploiting Fractured Reservoirs, Based on the MWX/SHCT-Piceance Basin Experience

Introduction

Insights into naturally fractured reservoirs and in situ stresses were gained through extensive studies and experiments performed at the U.S. Department of Energy's Multiwell Experiment site. This report uses those insights to develop a rationale for the identification and efficient exploitation of naturally fractured, low-permeability, natural gas reservoirs. The lessons of the Multiwell Experiment have a wide range of applications because most reservoirs are fractured, and because in situ stresses commonly control the conductivity of natural fractures. Therefore the efficiency of stimulation and production of such reservoirs often depends on an understanding of the fractures and the stresses present in the strata. Moreover, such an understanding allows for the prediction of areas within a basin where optimum conditions of stress and fracturing may have occurred and thus leads to an exploration methodology.

The Multiwell Experiment (MWX) was a field laboratory designed (1) to characterize low-permeability (tight) natural-gas reservoirs, (2) to assess the existing technologies for the exploitation (stimulation) of this large but generally inaccessible resource, and (3) to develop new stimulation technologies (Northrop and Frohne, 1990). The project consisted of three closely spaced wells located in the Colorado River valley in the east-central Piceance basin of northwestern Colorado near the town of Rifle. The reservoirs of interest were sandstones of the Mesaverde Formation, which occur between the depths of 4000 and 8350 ft at this site. Different depositional zones within the formation contain reservoirs of different character, varying from blanket-shaped marine sandstones to narrow, lenticular sandstones (Lorenz, 1989), but all have low matrix permeabilities (usually less than a microdarcy), all are enclosed in shale or mudstone, and all are extensively fractured despite the absence of major structural deformation of the local strata.

The three MWX wells are arranged in a triangle with interwell spacing varying from about 150–250 ft, depending on depth. A total of 4200 ft of 4-inch core were taken from the three wells for extensive rock property testing and reservoir characterization. During the eight-year program, six individual reservoir zones were isolated one at a time, and each tested and characterized with extensive reservoir draw-down, build-up, interference tests, in situ stress measurements, and stimulation experiments. Complimentary geologic studies of the core and of nearby outcrops helped to characterize reservoir shapes, sizes, and internal heterogeneity.

Subsequent to the MWX program, a new project was undertaken at the same site, the Slant Hole Completion Test (SHCT), the design of which was based on the MWX findings (Myal and Frohne, 1991). The SHCT project consisted of a deviated well, locally cored, through the Mesaverde reservoirs. The hole azimuth was normal to the subsurface fracture trend. This well and core confirmed (1) that vertical natural fractures are pervasive throughout the formation, (2) that they constitute the primary permeability system in the reservoirs, and (3) that the gas in the formation can be accessed with deviated wellbores.

In addition to the SHCT, DOE has also funded a cooperative program to extrapolate the MWX/SHCT technology to other parts of the Piceance basin. This program has relied on

industry wells for which DOE has funded coring, logging, or testing activities. These wells have provided fracture and stress orientation data in other parts of the basin that can then be correlated with the established data base.

Several important understandings came out of these programs: (1) natural fractures are more common in reservoirs than is usually recognized, (2) natural fractures may dominate a reservoir permeability system, especially where the matrix permeability is low, (3) natural fractures may be stress sensitive, in that a) they can be closed when the in situ stresses change during reservoir production, and that b) they may be closed when the maximum horizontal stress is not parallel to fracture trend due to a complex tectonic history of the strata, and (4) natural-fracture permeability systems may be damaged by stress or fluid perturbations of the reservoir during drilling, stimulation, and/or production.

This report will show how these understandings, along with ancillary studies conducted by Sandia, may be used to explore for naturally fractured reservoirs and to enhance production from them. The sections of this report outline the significance of fractures to the system permeability of reservoirs (section 1), and give the principles and examples of the interactions between stress and natural fractures in a basin, both in terms of the origin of the fractures (section 3), and in terms of the significance of stress and fractures in a reservoir (section 2). The report also outlines a methodology by which these interactions can be documented, studied, and ultimately, predicted for an unknown basin, by discussing the sources of stress (section 4), as well as potential local modifications to regional stresses (section 5). The report then discusses the compilation of these data into a stress history of a basin and how fracturing might be predicted from that history (sections 6,7).

The appendices to the report list specific techniques for fracture studies. These include techniques for optimizing the chances for fracture intersection with a wellbore (A) and for characterizing fractures in core (B). Appendix C presents equations for a stress history model (the computer code for this model is presented in appendix F), while appendix D discusses two of the more reliable techniques for measurement of the present-day in situ stress from core. Finally, a computer code that allows the caluclation of the effects of severe topography on in situ stresses is given in appendix E.

This report is intended to provide a fracture analysis toolbox, with instructions and insights for the investigator wishing to find and exploit naturally fractured reservoirs.

1. Importance of Natural Fractures in Western Basins

Fractures create quasi-planar breaks in the continuity of a reservoir that may or may not provide an enhancement of the permeability system. Enhancement depends on the ratio of the fracture permeability to the matrix-rock permeability. The permeability of an individual fracture is a function of the width of the fracture, the roughness of the fracture walls, the stress acting on it, and the completeness of cementation (if any).

Fracture *system* permeability includes the additional factors of fracture interconnectedness, distribution, and trend(s) within a reservoir. Narrow fractures in a high-permeability reservoir will be of little consequence, but fracture importance increases as reservoir matrix permeability decreases. Even fractures that appear to be completely filled with calcite may offer significant permeability, especially to gas, under high-pressure, in situ reservoir conditions in otherwise "tight" (less than 10 microdarcy) reservoirs. Laboratory measurements of the fractures in the MWX sandstone reservoirs (Figure 1) show that permeability even through tight fractures may be several orders of magnitude higher than the sub-microdarcy matrix permeability. Open fractures that are confined to thin beds within laminated reservoirs or that do not connect to adjacent fractures may also be of limited significance to production; each fracture intersected by the wellbore, although individually highly permeable, may not drain enough of the reservoir to be of consequence. This is because

the essentially two-dimensional volume of most fracture systems is insignificant compared to the three-dimensional volume of matrix rock, even if it is rock of relatively low-porosity.

Fracture strike is also an important characteristic. If a single set of fractures is present at depth, reservoir system permeability may be highly anisotropic, producing a drainage area that is significantly elongate along the fracture trend. Documented horizontal permeability anisotropy due to unidirectional fracturing at the MWX site ranges from 8:1 to 100:1 (Branagan et al., 1984), and limits lateral communication between closely spaced wells in the direction orthogonal to the fracture trend. Similar fracture-controlled permeability anisotropies have been measured in other formations (e.g., Kempthorne and Irish, 1981; Elkins and Skov, 1960).

Tightly cemented fractures within a relatively permeable matrix rock may also produce elongate drainage areas by creating permeability barriers rather than permeability conduits. In this case, reservoir flow would still be directed along the trend of fractures, but would occur between rather than within the fractures.

Accordingly, it is important to characterize the nature of a reservoir fracture system in order to be able to predict and understand the effects of natural fractures on production and drainage patterns.

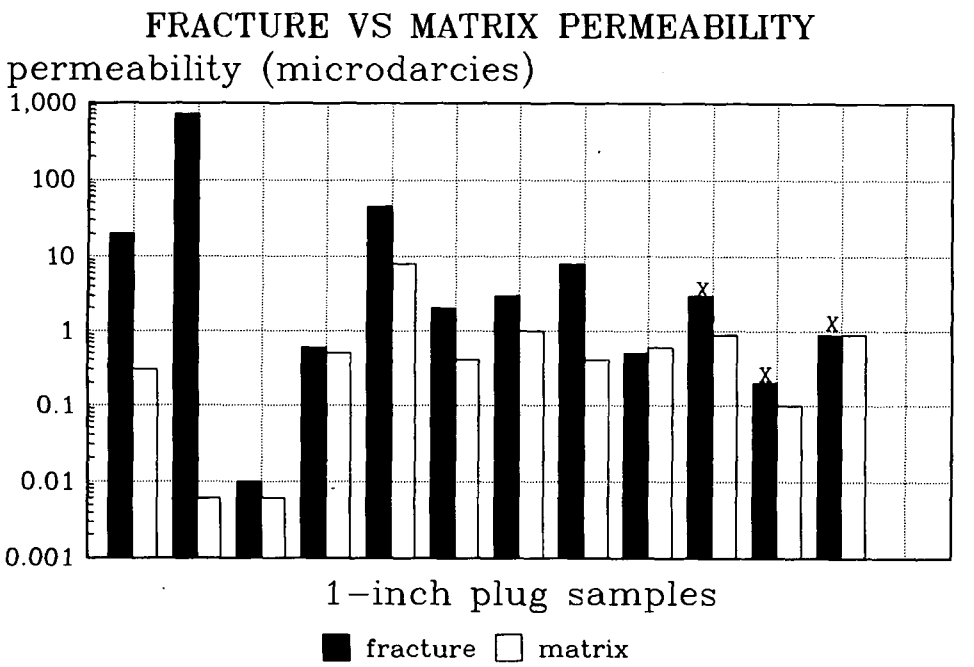

(dry klinkenberg corrected permeability)
X = fracture oblique to plug, k may be higher

Figure 1. Laboratory measurements of the permeabilities through mineralized fractures in sandstones of the MWX reservoirs compared to the matrix permeabilities of adjacent, unfractured samples.

2. Effect of Stresses on Natural Fractures

Fracturing of strata results from the anisotropic stresses that build up in formations during tectonic movements of the earth. Fractures generally form parallel to a plane defined by the maximum and intermediate principal stresses, and open in the direction of the least principal stress. Thus, where the tectonic history of the strata is not complicated, fractures commonly have a strike that is parallel to the maximum horizontal principal stress, and there may be few or no cross fractures to provide the interconnections. In such cases, the in situ

stresses act to keep fractures open and permeable. However, hydraulic stimulation fractures, which also parallel the maximum horizontal stress, will not efficiently access such a reservoir permeability system because the stimulation fracture will parallel the natural fractures. This was apparent in the results of most of the MWX stimulation experiments (Branagan et al., 1985) where the hydraulic fractures did not produce the expected production enhancement (although formation damage was also an important factor).

Where tectonic activity has continued to evolve after fracturing of the strata, the subsurface stresses may have changed orientation and may no longer be aligned with the fractures that were formed at an earlier stage of basin evolution. In some wells near the MWX site, severe topography has resulted in locally reoriented stresses such that stimulation fractures may be directed across the natural fracture trend, enhancing stimulation potential.

Existing fractures may also act as planes of weakness that were reactivated during later tectonic stages. However, if the existing fractures were either well-cemented or highly oblique to the reoriented stresses, entirely new fractures may form if stresses are sufficient. The Ekofisk field in the North Sea is an example of radial fractures caused by doming of the strata being superimposed on regional northeast trending fractures (Teufel and Farrell, 1990).

Whether or not new fractures form, reoriented stresses will act to press fractures of the initial set closed, limiting permeability. Moreover, the conductivity of many fractures is sensitive to changes in the in situ stress magnitudes, regardless of whether the stress orientation has changed. For example, the permeability of the natural fractures in the Cozzette sandstone at the MWX site was degraded when the well was allowed unrestricted flow (formation pressure was reduced, higher effective stresses were created, and the fractures were forced to close), whereas enhanced fracture permeability was created when formation pressures were increased during injection tests (Warpinski, 1991).

Fluid flow along mineralized natural fractures has been documented in the laboratory, although flow through completely mineralized fractures is limited (e.g., Morrow, 1990). Tests were performed at Sandia on two fractures from the SHCT Cozzette core that, although mineralized, are considerably more conductive than previous samples, having visible remnant apertures within the mineralization. The results (Figure 2) show that even the highly conductive samples have some stress sensitivity, although the planar fractures typical of MWX samples were much more stress sensitive. The two Cozzette fractures were both about 60–80% filled with cement, but the available porosity was vuggy in nature. The highest conductivity sample has a fracture permeability of several darcys.

Thus it is important to reconstruct the geologic/tectonic history that strata have been subjected to, and to characterize in detail both the stresses and the fractures within the strata in order to predict (1) the behavior of a reservoir permeability system, and (2) the locations for the optimum development of fractures and stresses. For example, a set of numerous fractures, if it is oriented at a high angle to the maximum or intermediate principal stresses, may not be as important to the permeability of a reservoir as a set of less numerous or narrower fractures that are oriented normal to the least principal stress. As noted, the Ekofisk reservoir provides an example of this behavior (Figure 3). The maximum permeability orientation was found to be aligned with the maximum stress orientation rather than with the maximum fracture orientation (Teufel and Farrell, 1992).

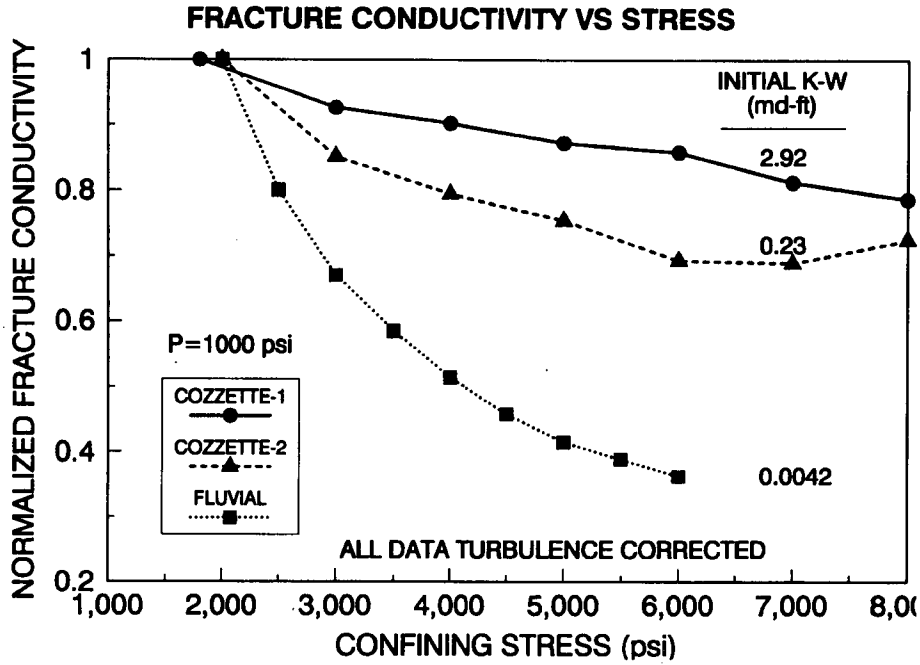

Figure 2. Laboratory measurements of the stress sensitivity of MWX mineralized fractures. Higher conductivity fractures from the Cozzette sandstone have less sensitivity than the lower conductivity fracture from the fluvial interval.

Effect of In Situ Stress on Permeability Anisotropy

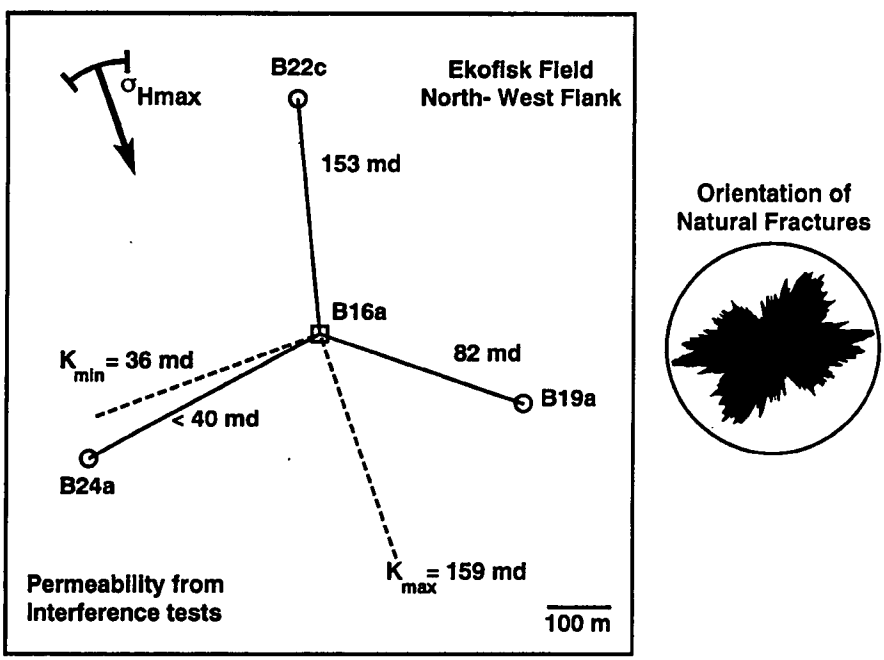

Figure 3. Measured permeability anisotropy in the Ekofisk reservoir, relative to the observed fracture orientations and the maximum stress orientation.

3. Fracture Mechanisms

Regional fracture systems are the primary concern in reservoirs of the western tight-gas basins. Therefore, regional fractures are the focus of this section, but it should be recognized that structurally induced fractures can provide additional fracture sets that significantly enhance the "system" permeability.

Regional natural fractures are often attributed to natural hydraulic fracturing, but this is a mistaken belief that was formulated without a thorough understanding of the mechanics, poro- mechanics, and failure properties of sedimentary rocks. Most regional natural fractures are likely due to load-parallel extensional failure of the rocks. Such a failure mechanism is well-known in the rock mechanics literature (Figure 4), and the characteristics of the type of fracturing match the characteristics of the observed regional natural fractures.

The basic mechanism of regional fracturing has two criteria that must be met in order to achieve load-parallel extensional failure (Lorenz, et al., 1991). First, there must be a horizontal stress anisotropy, as due to tectonics or basinal subsidence behavior. Second, the net confining stress on the rocks must be low, as would occur in overpressured regions. The first requirement is the mechanism that causes extensional failure of the rock and preferentially aligns the natural fractures. The second requirement allows the fractures to be created under relatively small amounts of horizontal stress anisotropy. If the net confining stress is not low, then large stress anisotropies are needed, and the characteristics of the fracturing (if it occurs) become shear in nature, oblique to the stress. Such fracturing is more typical of more intensely deformed, folded, and faulted areas.

Regional fractures created under such conditions have characteristics that make them particularly suitable as flow conduits. Since they are induced by compression in the direction of the fracture strike, there is a dilatancy associated with the process that opens the fractures and holds them open as long as the stress anisotropy exists. This persistent dilatancy allows for the fractures to be mineralized and, commonly, propped open.

The drawback of regional natural fractures is that they tend to be unidirectional, as there is no mechanism to create cross fracture sets. As a result, the interconnectivity of these systems is poor, and any hydrocarbon drainage will be highly elliptical.

Structurally induced fractures, on the other hand, may have conjugate or other multiple sets, and these are superposed on the regional fractures if the structure post-dates the regional-fracturing episode. Therefore, structure is important in these tight-gas reservoirs for its contribution to the fracture system rather than for its usefulness as a trapping mechanism (although trapping is obviously important for conventional oil and gas reservoirs).

4. Sources of Anisotropic Horizontal Stress in a Basin

Because stresses both cause and control fracture permeability, they are an important part of a fractured reservoir permeability system and must be understood before fracture location and behavior can be predicted.

Under ideal conditions, both horizontal stresses in a formation are equal and are the result of lateral expansion of the strata due to the weight of the overburden. The magnitudes of the horizontal stresses are primarily a function of the weight of the overburden as modified by the Poisson's ratio of the strata (Jaeger and Cook, 1976). Pore pressure and elevated temperatures, attained by strata as they are buried, also contribute an isotropic stress component to the total stress system (Warpinski, 1989). However, the ideal situation of isotropic horizontal stress is rarely obtained under actual geologic conditions, and horizontal stresses are most commonly unequal due to tectonic movements. Worldwide measurements have shown that horizontal stress anisotropy exists even in quiescent basins, far from active orogenic regions (e.g., Zoback and Zoback, 1980).

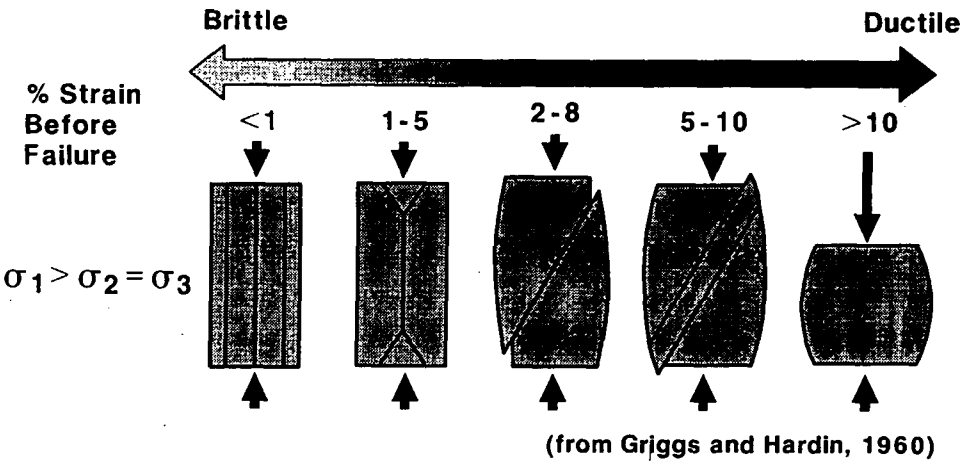

Figure 4. Characteristics of rock failure as a function of confining stress. Rocks show brittle behavior with only small amounts of strain prior to failure if the confining stress is low; they are ductile and accommodate significant strain if confining stresses are high.

The equation for the effect of the overburden stress on the horizontal stresses is simply derived. First, however, the calculations must be performed in effective-stress space because the effective stresses are the only component of the total stress that contribute to deformation. Defining the total stresses as S_v, the overburden stress, S_h, the minimum horizontal stress, and S_H, the maximum horizontal stress, the effective stresses are then given as

$$\sigma_v = S_v - \alpha P,$$
$$\sigma_h = S_h - \alpha P, \text{ and}$$
$$\sigma_H = S_H - \alpha P,$$

where α is the poroelastic parameter (often called Biot's modulus) and P is the pore pressure. Linear elasticity requires that

$$E\epsilon_h = \sigma_h - \nu(\sigma_H + \sigma_v),$$
$$E\epsilon_H = \sigma_H - \nu(\sigma_h + \sigma_v), \text{ and}$$
$$E\epsilon_v = \sigma_v - \nu(\sigma_H + \sigma_h),$$

where ν is Poisson's ratio, E is Young's modulus, and the various ϵ are the strains in the three principal directions. If it is stipulated that there is no strain in any horizontal direction (uniaxial strain), then $\epsilon_h = \epsilon_H = 0$ and $\sigma_h = \sigma_H$. These equations can then be solved to yield

$$\sigma_h = \sigma_H = \nu/(1 - \nu)\sigma_v \ .$$

In terms of the total stresses, this becomes

$$S_h = S_H = \nu/(1 - \nu)(S_v - \alpha P) + \alpha P.$$

This equation is used indiscriminately by most modelers, even when there is no justification for this severe assumption.

The effect of temperature is isotropic if the material is isotropic, and is given by

$$\Delta S_h = \Delta S_H = \alpha_T E \Delta T/(1 - \nu),$$

where α_T is the coefficient of linear thermal expansion, E is Young's modulus, and ΔT is the temperature change causing the thermal stresses. For typical values of α_T (6×10^{-6} in/in/°F) and E (5×10^6 psi), a 10°F change in temperature will induce a 300 psi change in stress, a significant amount for any engineering calculations. (See also Appendix F.)

Many authors have suggested that stress anisotropies measured in undeformed/platform-area strata are due to continental-scale plate tectonics, i.e., to drag at the base of the lithosphere, several tens of kilometers deep, by convection currents in the ductile aesthenosphere (e.g., Zoback et al., 1989,), or to distant ridge-push forces at the edges of global plates (e.g., Bott, 1991). Hydrocarbon reservoirs and most of the subsurface stress measurements that have been made occur in the shallowest parts of the lithosphere. Stresses derived from base-of-crust drag or ridge-push are likely to be secondary effects at best within the shallow strata of interest to petroleum geologists.

Rather, the stresses of interest for this report are those that have been imposed laterally on strata in a basin from nearby tectonism, from local structure and topography, and from volume constraints during basin subsidence and uplift. Stress from two or more sources may be superimposed, and there are a number of local phenomena such as high topographic relief that can alter local stresses. The following section outlines common sources of horizontal stress anisotropy in sedimentary basins where hydrocarbon reservoirs occur and notes causes for the superposition of stresses that complicate exploration for, and production from, fractured reservoirs.

4.1 Horizontal Compression as a Source of Stress

4.1.1 Thrusting

Numerous linear thrust belts around the world have been produced by horizontal compression at plate margins. Some of this compression is often transmitted through the thrust belt into the stable platform area beyond, where it combines with horizontal compression due to the impingement of the thrust belt itself into the strata of the adjacent foredeep. Several good examples exist of measured maximum horizontal stresses and regional fractures trending normal to thrust fronts, although the relationship between thrusting and stress in adjacent strata is not universally accepted (e.g., Bell and Adams, 1990). Where significant plan-view curvature of a thrust belt is present, the stress trajectory and/or fracture strikes commonly change regionally to maintain an angular relationship that is essentially normal to the thrust front.

Such thrust-front-normal stresses are apparently effective for a few hundreds of kilometers in front of the source of stress (e.g., Europe in front of the Alps, the Arabian platform in front of the Zagros Mountains; Hancock and Bevan, 1987), although the stress magnitude diminishes with distance (e.g., in front of the Canadian Rockies; Woodland and Bell, 1988). At present, there is no reliable way to predict magnitudes of stresses based on amount of thrusting because of the complexities inherent in geologic systems. However, although the magnitudes must be measured directly, the stress orientations in many cases can be predicted in the absence of structural complexity (discussed below) simply by drawing stress trajectories normal to thrust fronts.

More localized thrusts, such as the thick-skinned Laramide block uplifts of the Rocky Mountain foreland province, produce stresses in adjacent strata in the same manner. However, because they impinge on relatively small areas, the stress trajectories commonly radiate out from the thrust front as if it were a point source once a sufficient distance from the thrust front is reached. For example, a fan-shaped pattern of natural fractures radiates across part of the Piceance basin directly in front of the White River Uplift (Figure 5). This

pattern has been duplicated by a stress trajectory array modeled from an indenter stress superimposed on a regional stress (Lorenz et al., 1991).

The depths at which these thrust-derived stresses are present depends on an number of factors, including the depths at which the thrust fronts indent the adjacent strata (Hafner, 1951). Horizons of weaker strata may also dissipate stresses similar to thrust decollements, such that stresses below the weaker strata may not reflect nearby indentation of the thrust whereas stresses in overlying strata will. This is discussed further below.

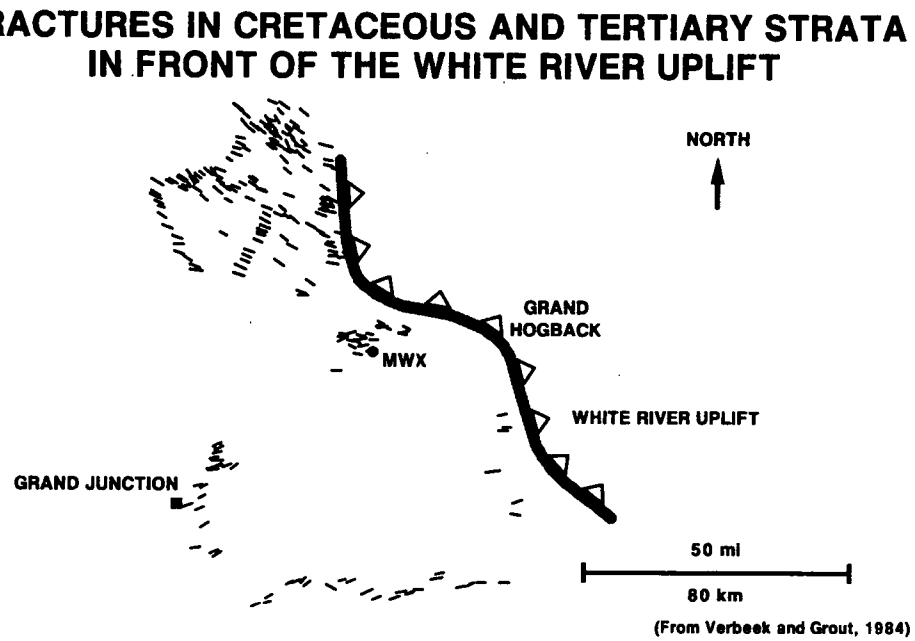

Figure 5. Natural fracture pattern that radiates out from the White River Uplift, created by stress trajectories radiating away from the thrust front during thrusting.

4.1.2 Basin Subsidence

Few if any basins subside at equal rates in all parts of the basin, as this would require vertical, parallel basin margins and a nonspherical earth. Rather, subsidence is commonly greatest in certain parts of the basin (a faulted margin, the center of a basin, etc). The strata must accommodate strain as volume constraints are met during subsidence within the basin boundaries into a sphere of diminishing radius. Because most basins are wider than they are deep by orders of magnitude, and because the radius of the earth is so large relative to the common depths of basin subsidence, this mechanism rarely adds significant strains to the strata in a basin.

However, significant strain can result during subsidence in especially narrow, deep basins. For instance, Upper Cretaceous strata in the foredeep adjacent to the Idaho/ Wyoming thrust belt are about 6000 m thick, whereas they are less than 2000 m thick over the Moxa Arch 55 km to the east (Weimer, 1961). In order to lengthen the 55 km line along the original depositional surface to its position as the hypotenuse of a triangle after deposition and burial, about 0.2% strain must be accommodated (Figure 6). Moreover, because the hypotenuse is not a straight line but is convex upward due to lithospheric elasticity, an additional strain of 0.06% is imposed for a total strain of nearly 0.3%, which is sufficient to fracture in situ strata over geologic time. Thus the strain (which produces stress) across the short axis of a narrow, deep basin exceeds the strain/stress along its long axis, and

anisotropic stresses result. If the stresses are of sufficient magnitude, they may produce fractures aligned parallel to the long basin axis.

Strain from Lengthening Line to Hypotenuse

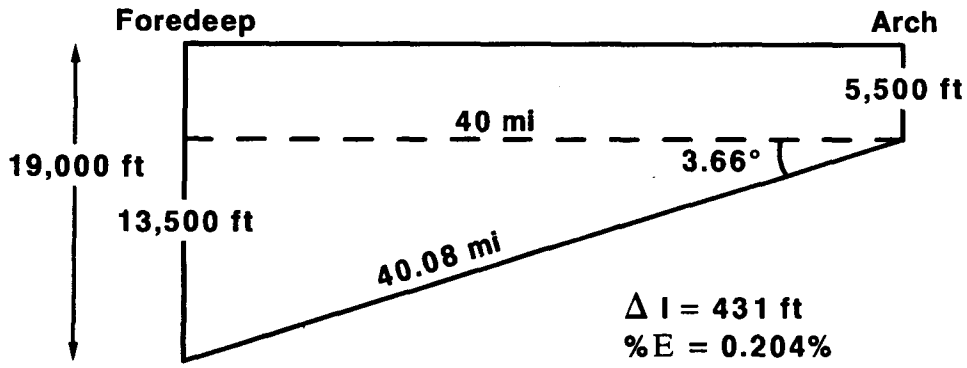

Figure 6. Strain due to lengthening of a depositional surface to a hypotenuse during asymmetric subsidence in a narrow, deep basin such as the Late Cretaceous foredeep in southwestern Wyoming.

Price (1974) recognized a variant of this phenomenon that involves consideration of the curvature of the earth's surface. Ideally, as the strata in a basin subside, they are subjected initially to lateral compression as their length, measured along the curved surface of the earth, is shortened to the length of the line measured across the chord of the earth between the edges of the basin. This assumes that there is no subsidence at the basin margins.

The magnitudes of the stresses and strains set up by the compression will be a function of the width of the basin, i.e., how far the strata must subside, and therefore how much shortening there will be before the originally curved surface line is concordant with the straight chord line. Less subsidence will be required in a narrow basin than in a wide basin to achieve this condition, and if a basin has a long and a short axis, the stress set up across its short axis will be less than that across its wide axis, leading to asymmetric horizontal stresses. Chord-line depth is actually relatively shallow. For instance, for the Piceance basin, the two main axes are 100 and 250 km across, and depths to chord lines at the middle of the basin are less than 100 m and 600 m for each axis respectively.

Stress anisotropy remains as subsidence continues beyond a chord line, but for the opposite reason: extensional strain results as the reference line, theoretically pinned at the basin edges, is lengthened in an arc during continued subsidence. Extension across the narrow axis of the basin will always be greater because the radius of the theoretical circle is smaller, and short-axis-parallel extension would be initiated at shallower depths than that across the greater dimension of the basin. This again would cause asymmetric horizontal stresses that could lead to fracturing. (Note that the extensional strain referred to does not lead to true tension, but rather merely decreases the subsurface compressional stress in that direction.)

4.1.3 Basin Uplift

As strata in a basin are uplifted, an opposite effect to that just described may occur *if* the basin edges are pinned. However, this is rarely the case. It is more likely, since uplift takes the strata out of the realm of lateral constraints, that the basin margins will have little effect

on the strata. As the strata are uplifted, however, they will be subtending an arc of a sphere of slightly larger radius and will be subject to a release of some percentage of the previous horizontal stresses, equally in all horizontal directions if uplift is uniform (Figure 7).

If the previous horizontal stresses were asymmetric, as is most likely, then an equilateral stress release will still leave a remnant stress anisotropy, which will govern the orientation of any stress-release fracturing. Thus, stress-release fractures will form parallel to the previous minimum horizontal stress, as the locked-in elastic stresses rebound against the direction of the previous maximum horizontal stress (see experimental results of Gallagher et al., 1974; Rathore et al., 1989).

4.2 Calculating Stress Trajectories Due to Thrusts

There are simple analytical solutions that can be adapted for estimating the stress trajectories induced by a thrust fault, such as the White River thrust which is found on the east side of the Piceance basin. Given the geometry of a distributed load (Figure 8), the stresses can be calculated (Jaeger and Cook, 1976) as

$$\sigma_x = X/\pi\{\theta_1 - \theta_2 - \sin(\theta_1 - \theta_2)\cos(\theta_1 + \theta_2)\},$$
$$\sigma_y = X/\pi\{\theta_1 - \theta_2 - \sin(\theta_1 - \theta_2)\cos(\theta_1 + \theta_2)\}, \text{ and}$$
$$\tau_{xy} = X/\pi\{\sin(\theta_1 - \theta_2)\sin(\theta_1 + \theta_2)\},$$

where $\theta_1 = \tan^{-1}(x/(y-a))$ and $\theta_2 = \tan^{-1}(x/(y+a))$, and X is the load per unit length.

Such simple solutions can be superposed to yield more complicated thrust geometries. For example, a calculation of the effect of the White River thrust in the Piceance basin (Figure 9) is obtained by superposing two separate thrust plates located in offset positions. The stress trajectories fan out from the source of the load, giving a radial pattern. It should be noted that these calculations assume plane strain behavior, so they may not be appropriate right at the surface. At depth, they should provide good estimates of the stress trajectories.

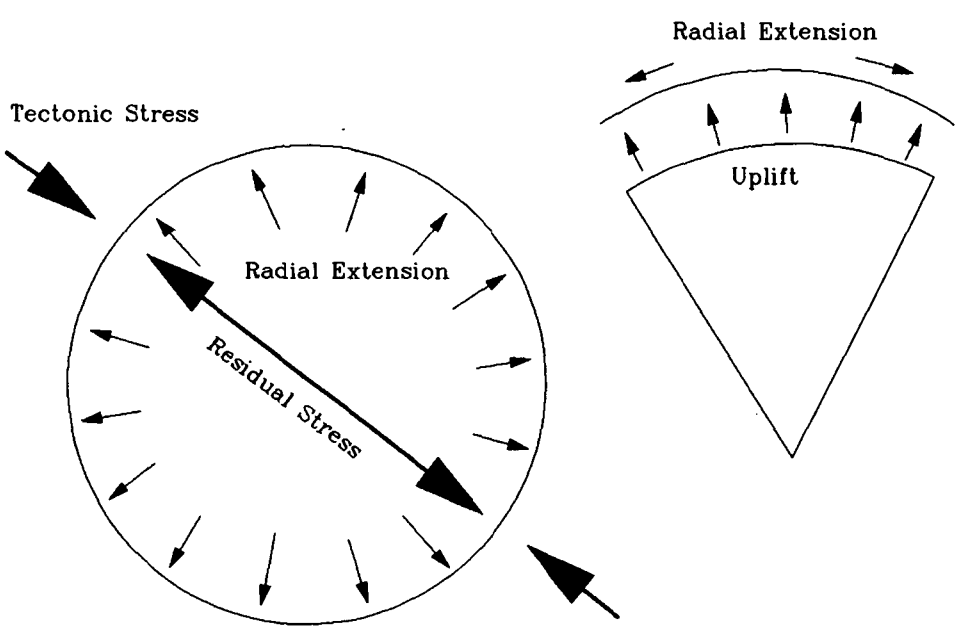

Figure 7. Stresses in strata created by uniform uplift and radial release of confining stresses.

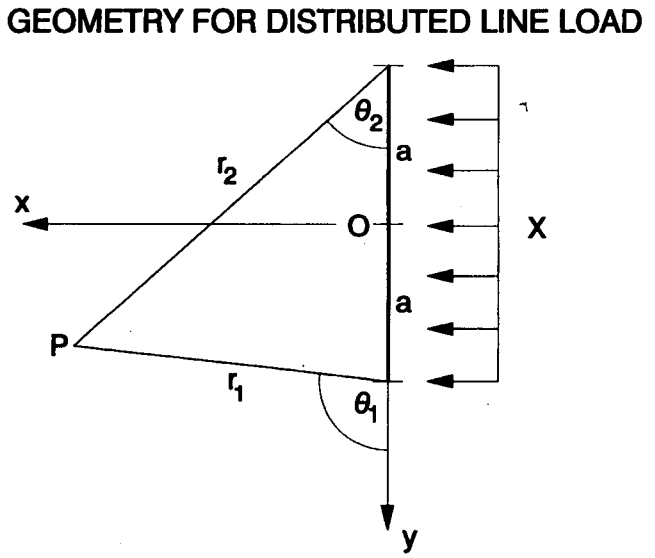

Figure 8. Schematic of the geometry for a constant distributed load applied to a semi-infinite region.

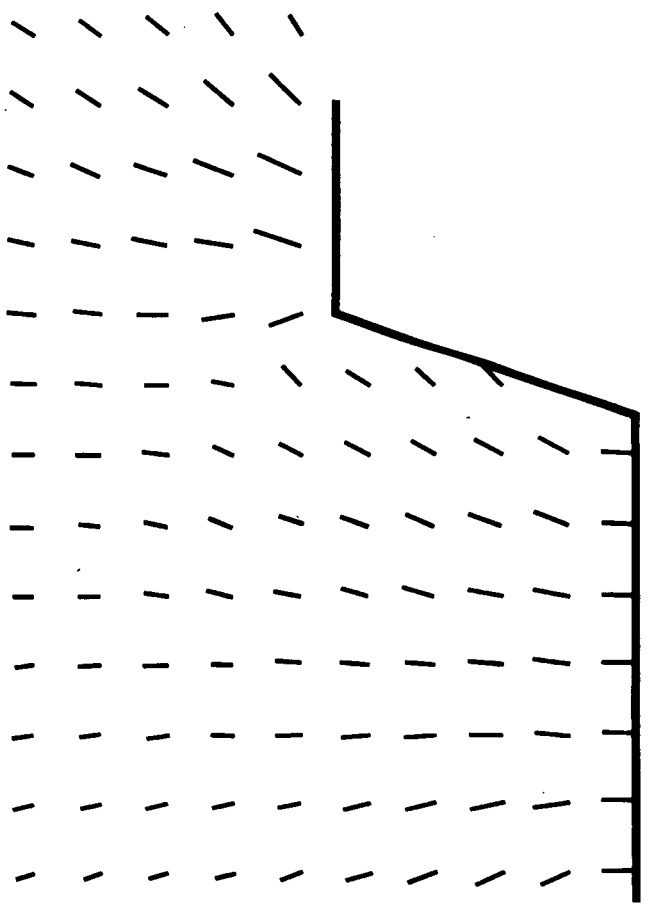

Figure 9. Stress trajectories calculated from simple distributed loads as representations of the White Rover thrusts. Line orientations indicate the orientations of the maximum stress; length of the line indicates the relative stress magnitudes. (Compare to Figure 5.)

4.3 Calculating the Horizontal Stress Due to Basin-Wide Strain

The component of the horizontal stresses due to the horizontal strains imposed on a basin can be calculated in a straightforward manner. Assuming that there are tectonic strains, ϵ_h and $_H$ (also, since ϵ_H is defined as the maximum stress direction, $\epsilon_H > \epsilon_h$), then the stress components due to tectonics, S_{ht} and S_{Ht}, are

$$S_{ht} = E\epsilon_h/(1 - \nu^2) + \nu E\epsilon_H/(1 - \nu^2) \text{ and}$$

$$S_{Ht} = E\epsilon_h/(1 - \nu^2) + \nu E\epsilon_h/(1 - \nu^2)$$

Thus the stress in each of the horizontal directions depends on the strain in its direction *and* the strain in the orthogonal horizontal direction.

5. Local Modifications of Regional Stresses in a Basin

In the absence of heterogeneity, stresses will be uniform or will at least change uniformly over large areas. This ideal condition is rare. Among other effects, formation properties change laterally and vertically, stresses change with time or may be superimposed, geologic structures may provide significant "free" surfaces within a formation that may alter the local stress array, and strata may be warped by flexure to create local, structurally produced stresses. These effects and others are examined below.

5.1 Variations in Pore Pressure

Pore pressure is an important factor in determining whether strata are susceptible to being fractured. Formations containing high pore pressure are more likely to fracture under otherwise similar conditions of anisotropic stress and rock properties than formations with normal pore pressure. Therefore, if conditions of concurrent high pressure and anisotropic stress are reconstructed for some time within the geologic history of a formation, natural fracturing can be expected. Moreover, if parts of a formation were more highly pressured than others, the high-pressure areas are more promising targets for fractured-reservoir exploration.

Pore pressure varies through both time and space as a function of mechanisms such as relative rates of sedimentation, burial, dewatering, compaction (e.g., Fertl, 1976; Dickey, 1979), and the onset of hydrocarbon maturation and the resultant generation of gas. Overpressured conditions may be reversed over time due to pressure leak-off. Underpressured conditions may be present where rapid uplift and erosion has occurred. Reconstructing the geologic history of a formation in order to decide whether overpressured conditions once existed is not overly difficult, although the magnitude of such conditions can rarely be quantified or dated precisely.

Spatial variation in pore pressure within a formation is just as important. Some parts of formations are often buried more deeply and/or more rapidly so that they may be more highly pressured than shallower areas of the same formation. Similarly, if hydrocarbons capable of generating gas are only present locally in a formation, that area may become more highly pressured than other areas despite otherwise similar conditions.

The Mesaverde Formation provides an example of present-day lateral variation in pore pressure (ranging from normal pressures in reservoirs at the western margins of the basin to significant overpressuring in the deeply buried reservoirs near the MWX site). The formation also contains evidence to suggest that paleo-pore pressure varied. The latter condition is

suggested by a set of fractures that is apparently limited to the deeply buried, central parts of the basin. These are dominantly west-northwest trending fractures that formed between about 36–40 m.y. ago under conditions of high pore pressure and regional anisotropic horizontal stress. The less deeply buried, less pressurized parts of the formation along the western edges of the basin were subjected to the same stresses, yet did not fracture at this time. Fracturing of these zones of the formation did not occur until several million years later under conditions of stress anisotropy that were slightly different in origin and orientation (Lorenz and Finley, 1991). Thus the fracture domains in the strata of the Mesaverde Group are vertically and laterally separated, depending on variations in the magnitude of the formation pore pressure. Fracture domains are not zoned parallel to formation boundaries.

Pore pressure variations also affect the total stress in strata, as αP is one component of the total horizontal stress. Data from the Vicksburg formation (Salz, 1977) provide the classic example of how pore pressures influence horizontal stress (Figure 10). Data from MWX (Figure 11), while more limited, show the same trend of increasing horizontal stress with increasing pore pressure.

5.2 Stress Decollements

Vertical zonation of stresses and fractures may also be caused by layers of weaker strata that allowed physical, lateral motion of rock, as in a thrust decollement. An example of this is given by Becker et al. (1987) for the Jura Mountains area in front of the Alpine thrust belt of Europe. In this locality, a zone of relatively ductile anhydrites and halites separates a lower domain of regional northwest-trending stress from an upper domain of stresses which radiate from north-northeast to west (Figure 12 a and b). The upper, radiating pattern is due to the indentation of the Jura Mountain block into the European craton, which was in turn a result of the regional northwest compressive stress.

Thus the ductile strata allowed thin-skinned thrusting, and the thrusting imposed a secondary stress on the strata in front of the thrusting, but only at the shallower levels above the ductile zone. Whether the shallow strata also contain a secondary fracture pattern is not reported, but would be a function of their fracture susceptibility and the magnitude of the secondary stress. Regardless, if fractures had been formed by the northwest regional stress in these strata prior to thrusting, the present oblique stress orientation would act to close most of the fractures.

This type of vertical stress zonation may occur within as well as in front of thrust sheets, resulting from several structural configurations. If a thrust impinges on a basement high or other structural "buttress," a secondary thrust plane may form. Strata below this plane will remain highly stressed (unless strain is accommodated by folding or other deformation), whereas stress within the strata above the plane may be partially released during the relatively unopposed motion of the strata above the buttress (Figure 13).

Conversely, in an unbuttressed situation, the stresses within the strata below a new thrust plane may be the ones relieved by the formation of the new thrust. Thus once a thrust plane forms within a previously uniformly stressed section of strata, the stress below the plane is relieved as strain along the fault plane, whereas the stress above the fault plane is maintained by the force needed to move the thrust sheet. This assumes that the regional stress no longer acts on the lower strata, but rather is directed only against the moving strata of the upper plate, as is probably the case in the Piceance basin. In this instance, the relatively ductile Mancos Shale provides a stress and motion decollement much as does the anhydrite layer in the Alpine foreland, and blind thrusts die out within a tectonically thickened section of Mancos Shale over the Divide Creek anticline (Grout et al., 1991).

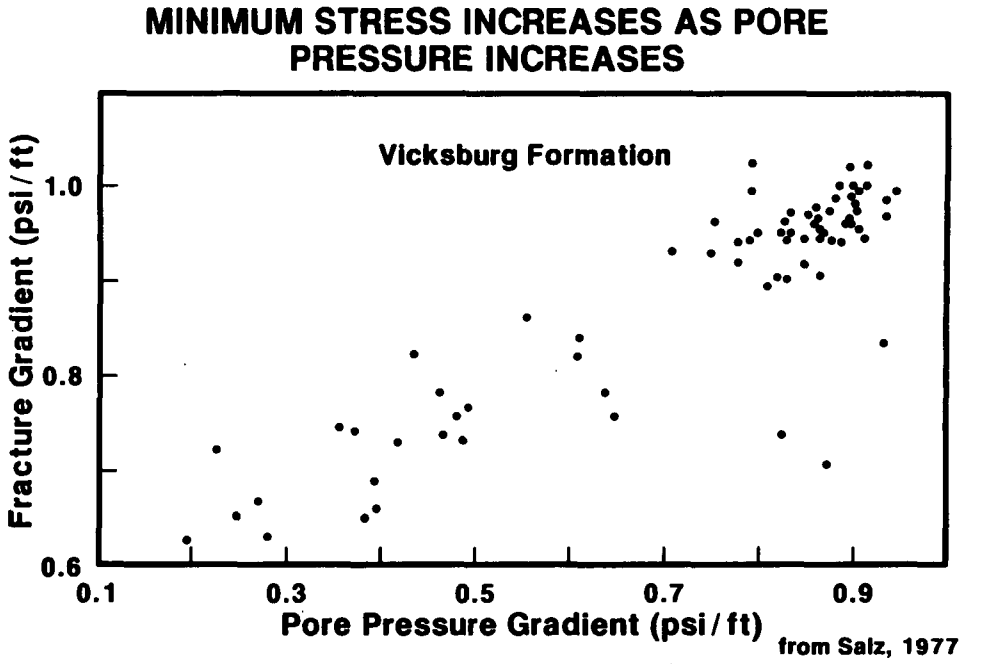

Figure 10. Measured variation in the minimum horizontal stress, as represented by the fracture gradient, as a function of the pore pressure for the Vicksburg Formation.

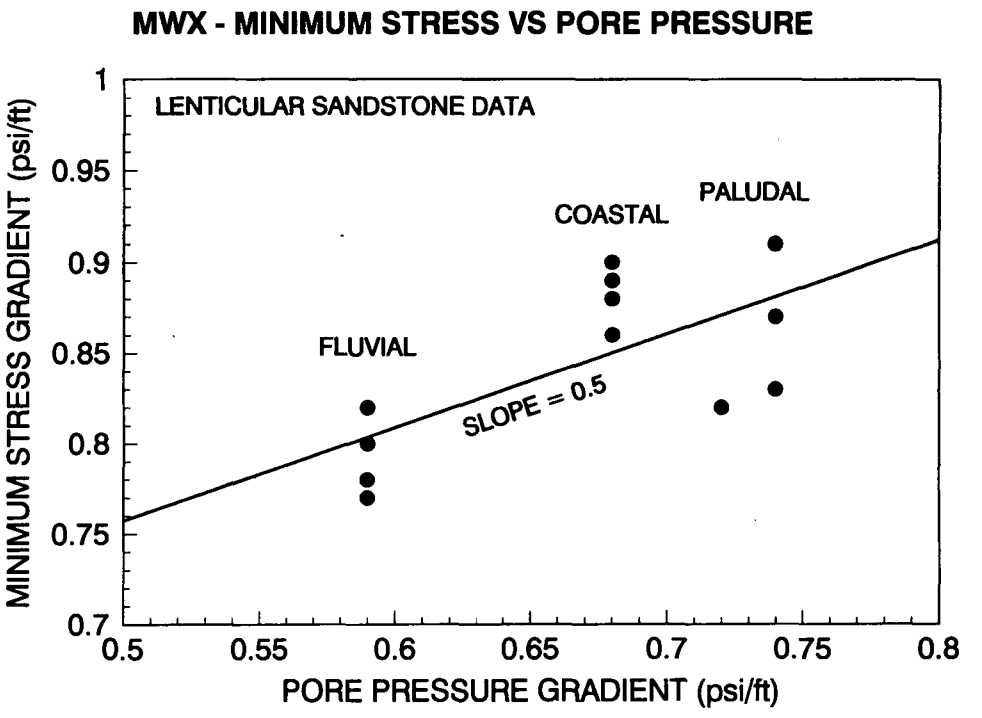

Figure 11. Measured variation in the minimum horizontal stress, as represented by the fracture gradient, as a function of the pore pressure for the MWX site.

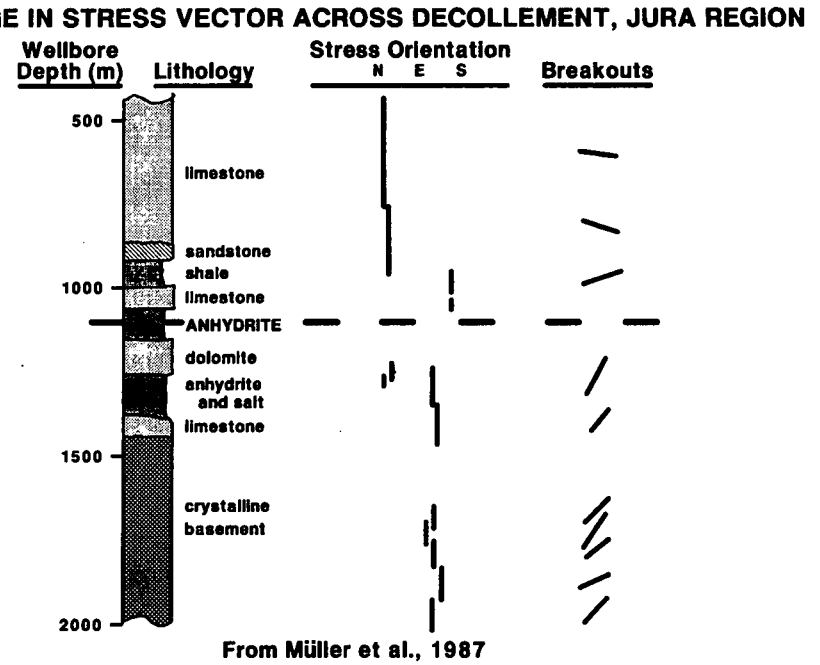

(a) Stress variations across a ductile boundary layer in front of the Alpine thrust belt (from Mueller et al., 1987).

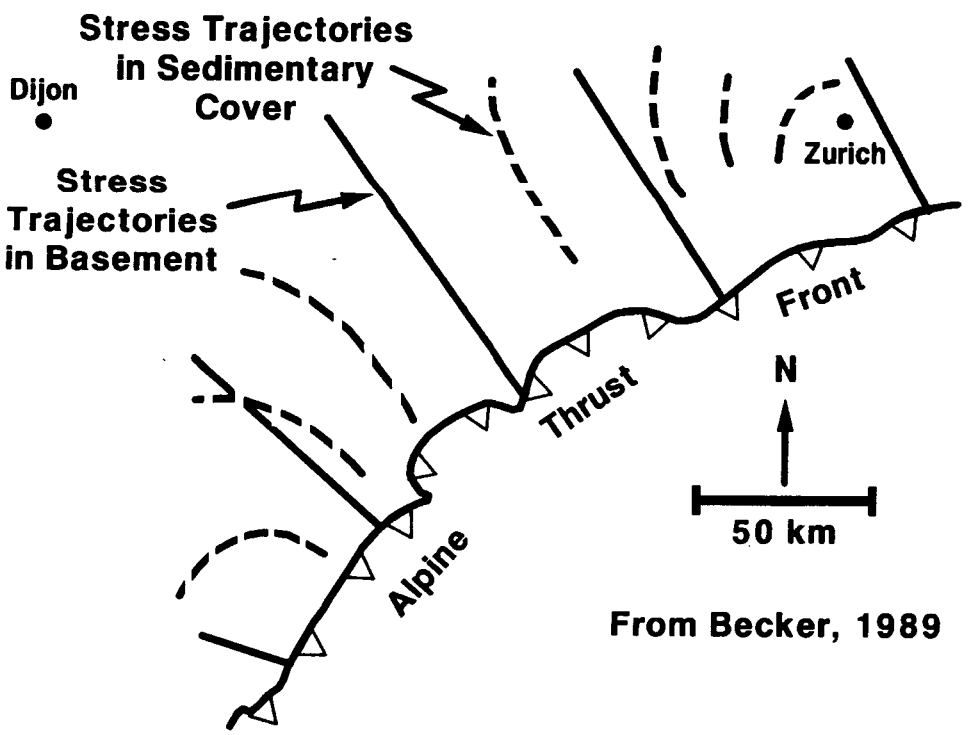

(b) Inferred planview stress trajectories of upper stress array and lower stress array in the same area as (a) (from Becker, 1989).

Figure 12. Stress in the Jura Region

DIFFERENT LAYERS WILL BE SUBJECT TO DIFFERENT STRESSES

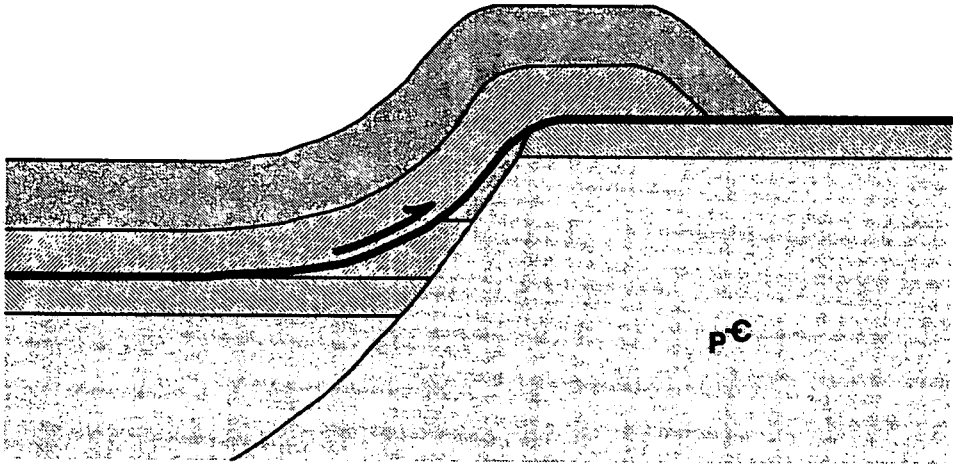

From Kulick and Schmidt, 1988

Figure 13. Example of horizontally layered stress domains caused by buttress-induced thrusting (from Kulick and Schmidt, 1988). Measurements of paleostresses within strata with a similar configuration have suggested that the stresses in the upper, unbuttressed layers had been largely relieved (Genovese and Schmidt, 1989).

5.3 Stress Refraction

Changes in stress orientation due to inhomogeneities in strata have been hypothesized and can be demonstrated at the laboratory scale, but have not yet been proven at the basin scale. However, there is every reason to believe that stress refraction at this scale can be real, and the concept has been used to explain observations of otherwise anomalous stress trajectories. Bell and Lloyd (1989) have suggested that an observed change in stress orientation across the Peace River Arch in western Canada is due to the refraction of regional stresses. Refraction is inferred to be the result of stress propagation through the higher modulus granitic/basement rock brought up by the uplift (Figure 14). It is conceivable that stress orientations within lenticular reservoirs could be oblique to stresses in the encasing strata if the rock properties of the two strata are different. In fact, it is not uncommon for adjacent layers of strata in outcrop to display a 10°–20° divergence in strike between fractures of the same set.

On a somewhat smaller scale, normal faults may provide a sufficiently "free" surface so that the local stress trajectories are reoriented to curve away from the regional trend and abut the fault at a right angle. This requires that the mechanical continuity of the formation be broken at the fault (1) by changes in rock properties such as filling of the fault by gouge, (2) by fluid pressure in the fault or fault asperity offsets so that the fault walls are not in solid contact, or (3) by the juxtaposition of strata with differing rock properties due to large displacement along the fault.

If a free-surface fault juxtaposes two different formations, the trajectories may merely refract across the surface. However, if the original stresses are normal or parallel to the fault, little change in orientation would be expected across it.

Regional stress trajectories oblique to a shear fault will also be affected by the local inhomogeneity. As shown by Anderson (1942), where shear creates local tension along the

fault, trajectories will reorient to trend normal to the fault, as with a normal fault. However, where the shear creates compression along the fault, the regional trajectories will reorient to become parallel to the fault. Such a mechanism probably explains the various patterns of secondary fracturing in the Arches National Monument area described by Dyer (1988); locally the secondary fractures curve to become normal to the primary fractures, but elsewhere they curve to become parallel.

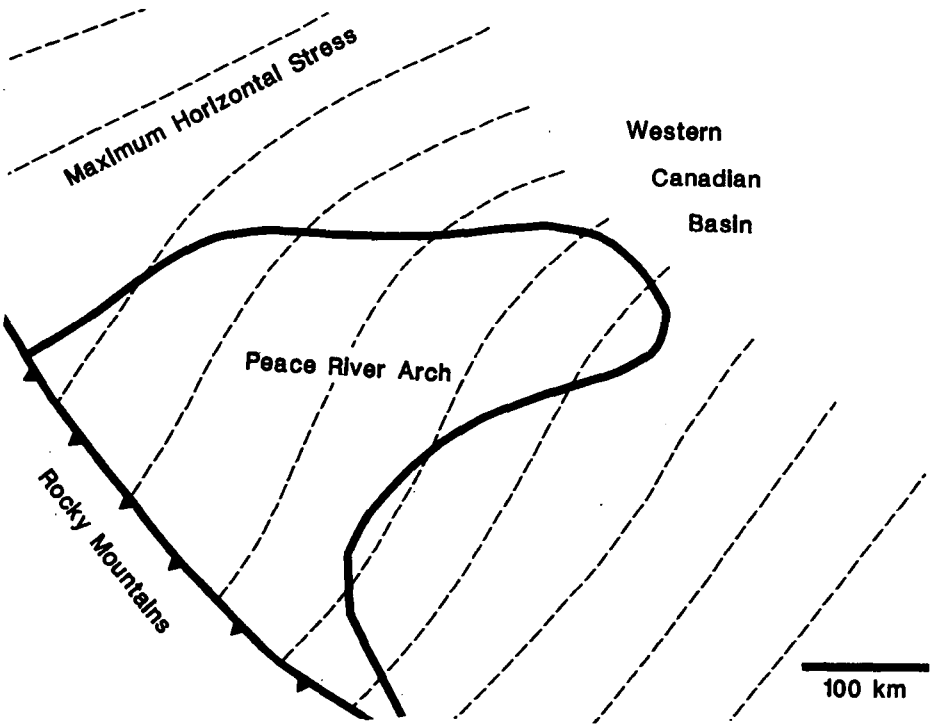

Figure 14. Stress trajectories deflected by inhomogeneities in strata (from Bell and Lloyd, 1989).

5.4 Local Stress Due to Flexure

Fracturing is often one of the earliest structural responses of a formation to anisotropic stresses. Stresses may continue to build despite fracturing, however, and the ultimate response of the strata may be manifest as folds or faults. Flexure imposes a secondary set of localized stresses on the formation, stresses that may locally be quite high and that may result in the development of local fracture sets (Stearns and Friedman, 1972). If the rocks within the fold have not fractured previously, several sets of fractures may develop with a geometrically predictable relationship to the trend of the fold because of the flexural stresses. However, if regional fractures are present in the formation prior to folding, they may act as planes of weakness and accommodate most of the flexural strain by reactivation. The angular relationship between the early fractures (if any), the flexural fractures, and the stresses imposed by flexure will vary from place to place on the fold; thus the permeability of the fracture system and the producibility of a reservoir will vary. The system of stresses, radial fractures, and regional fractures in chalks on the domal structure of the Ekofisk Field is a good example of this interaction (Teufel and Farrell, 1990).

5.5 Effects of Severe Topography

The weight of the mass of rock present in a mountain range will add a component of stress with predictable orientation and magnitude to the regional stress system in adjacent areas if the load is supracrustal and not isostatically compensated. The greater the relief and the more abrupt the relief, the greater the stress it imposes and the deeper it will be significant.

This phenomenon is present at the MWX site, where a topographic stress is imposed on the regional west-northwest stress. The topographic stress derives from the 4000 to 5000 ft of relief between the valley floor and adjacent highlands located only a few miles immediately to the north and south (Clark, 1983). The topographic stress component trends north-south at the MWX site, and its effect is to rotate the total stress trajectory a maximum of about 15° to a more east-west orientation in the shallower parts of the MWX holes (Figure 15). This effect diminishes with depth.

Another probable example of topographic effects occurs in reservoirs in the DOE and Barrett wells that are located immediately to the south of the Anvil Points escarpment, north of the MWX site. The fractures in these reservoirs formed at the same time as those at the MWX site and therefore trend west-northwest, yet these wells responded favorably to hydraulic stimulation fractures, whereas the MWX wells, for the most part, did not. At MWX, the principal horizontal in situ stress trends nearly parallel to the fractures; thus the stimulation fractures did not intersect many natural fractures. Near the escarpment, however, the superimposed topographic stress is strong and is inferred to have rotated the trend of the maximum compressive stress sufficiently to direct the hydraulic stimulation fractures transverse to the natural-fracture permeability trend. Data from one of the Barrett wells suggests that the stresses are rotated 20°–40° from that found at MWX.

A calculation of the stresses due to topography can be simply made (a finite element solution will be more accurate, but also much more difficult) using the same stress solutions as for the thrust-induced stress trajectories given earlier. Given the solutions (Jaeger and Cook, 1976) for a constant distributed load,

$$\sigma_x = X/\pi\{\theta_1 - \theta_2 - \sin(\theta_1 - \theta_2)\cos(\theta_1 + \theta_2)\},$$
$$\sigma_x = X/\pi\{\theta_1 - \theta_2 + \sin(\theta_1 - \theta_2)\cos(\theta_1 + \theta_2)\}, \text{ and}$$
$$\tau_{xy} = X/\pi\{\sin(\theta_1 - \theta_2)\sin(\theta_1 + \theta_2)\},$$

and those for a linearly increasing load (Figure 16),

$$\sigma_x = (X/2\pi)\{[1 + (y/a)](\theta_1 - \theta_2) - \sin 2\theta_1\},$$
$$\sigma_x = (X/2\pi)\{[1 + (y/a)](\theta_1 - \theta_2) + \sin 2\theta_1 - (x/a)\ln[(r_2/r_1)^2]\}, \text{ and}$$
$$\tau_{xy} = (p/2\pi)\{1 - (x/a)(\theta_1 - \theta_2) - \cos 2\theta_1\},$$

the effects of many types of topographies can be modeled.

An example calculation (Figure 17) is shown for Anvil Points in the vicinity of MWX and the Barrett wells (See also Appendix E). Using stress data for strata at 6000 ft depth and adding in the effects of the high Anvil Points mesa, the reorientation of the stress field was calculated as a function of the angle of the mesa escarpment relative to the maximum principal stress, with the distance from the escarpment as a parameter. It can be clearly seen that the topography can significantly reorient the stress field, even at a distance of three miles.

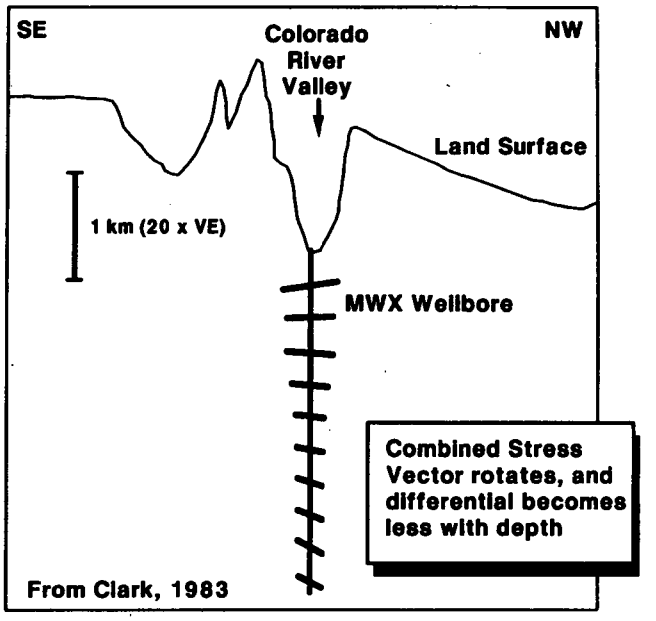

Figure 15. The changes in stress orientation and magnitude with depth, due to topographic loading near the MWX site (from Clark, 1983).

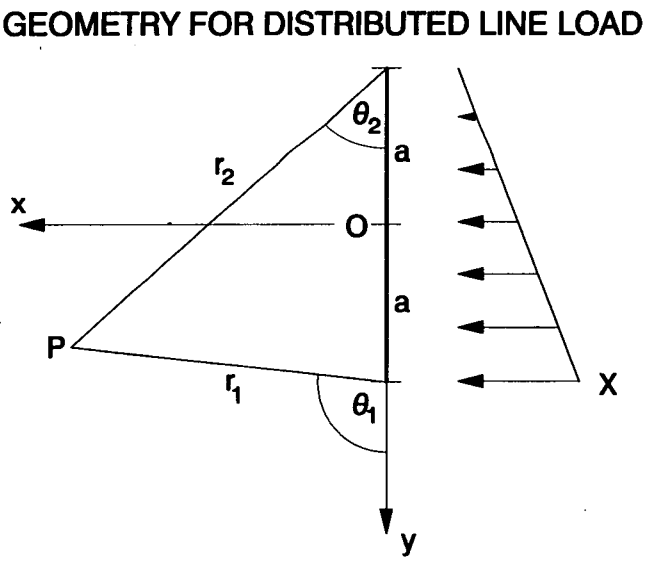

Figure 16. Schematic of the geometry for a linearly increasing distributed load applied to a semi-infinite region.

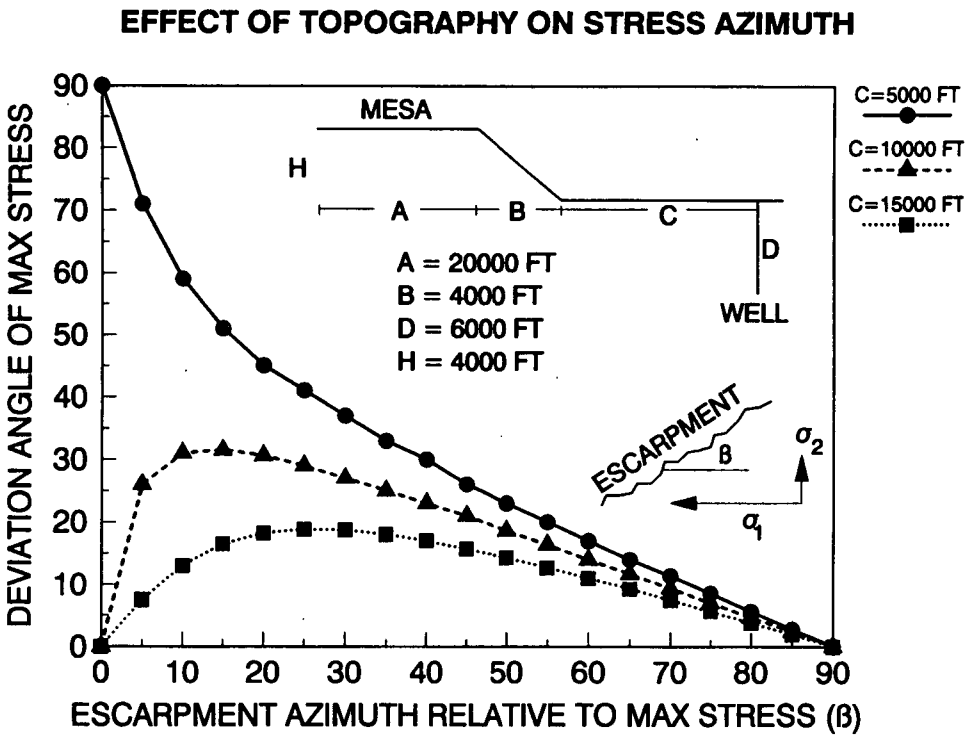

Figure 17. Calculated stress reorientation due to a mesa and escarpment as a function of the angle of the escarpment relative to the far-field maximum stress orientation. A high mesa can significantly reorient the stress field.

5.6 Relaxation of Stresses

When a confining stress is removed from strata, as during uplift, erosion, or regional change of tectonic regime to extension, the response of the strata varies according to the petrophysical properties and history of the rock. Some rocks, such as sandstones, commonly display a remnant, locked-in stress even after all external confining stress is removed. This stress originates when the component grains of the rock are cemented together by diagenesis while they are elastically deformed by external stress. Some of the elastic deformation of each grain may be "locked in" by cementation, such that when the external stress on such a rock is released, the cementation prevents the relaxation of this strain, which sets up secondary, internal stresses in the rock between the grains and the cement (Gallagher et al., 1974; Rathore et al., 1989).

If the grains were originally deformed anisotropically, the remnant/locked-in stress will be anisotropic. This internal stress will, in fact, behave similarly to an active tectonic stress in affecting the behavior of hydraulic fractures or stress-sensitive reservoirs (Figure 7). Thus a reservoir may be located in a currently inactive tectonic area, yet may display anisotropic stress behavior.

Stress-release fracturing is another effect of locked-in stress. If external confining stress is released, the strength of the locked-in elastic stresses may be sufficient to break the rock, producing fractures that trend normal to the maximum confining stress at the time the stress was locked in. If fractures parallel to that stress had also formed prior to stress release, a reticulate fracture pattern may develop. This is a common occurrence in surficial rocks where stresses are released during quarrying activities and where preferred cleavage directions are apparent in rock without visible fabric. It also is probably responsible for the formation of

many of the short, orthogonal, connecting fractures between throughgoing fractures in strata exposed by erosion at the surface.

In the Piceance basin, the F_4 fracture set mapped by Verbeek and Grout (1983) may have such an origin. These fractures maintain an abutting and orthogonal relationship to a radiating, regional (F_2) fracture set. A related phenomenon is documented in core from the MWX site in the numerous Anelastic Strain Recovery (ASR) measurements made. When rock samples were released from the confining stress at depth during coring, some of the locked-in stress was relieved by the development of microcracks oriented normal to the in situ maximum horizontal compressive stress. Microcrack development over the course of several hours was measured as microstrains on strain gauges (Warpinski and Teufel, 1989).

Stress-release fractures would not be expected to be present in the subsurface in most instances, as significant stress release at depth is not common. Therefore such fractures mapped on outcrops should not be extrapolated indiscriminantly into reservoirs at depth.

If stress is not locked in (poor cementation or no cementation at all), the rocks would relax elastically, and no fracturing would be expected on stress release. Alternatively, if the components of the rock are ductile, remnant locked-in stress anisotropy would not be possible, and stress-release fracturing would not occur.

The ductility of some strata, notably of clay-rich shales, commonly allows much of the stress in a rock to dissipate over time and distance when the stress is removed, or even under conditions of constant stress. Ductile strata typically are not fractured. Many "shales" contain fractures, commonly those with high percentages of carbonate and/or silica components, and not all "shales" are ductile. Moreover, high pore pressure may make otherwise ductile strata relatively brittle; shales with a high organic content may, under conditions of organic maturation and high local pore pressure, become more susceptible to fracturing than adjacent strata that would be more brittle under atmospheric conditions.

Some of these phenomena are illustrated at the MWX site by measurements of the different in situ stresses in the shales and sandstones of the Mesaverde Formation. The minimum stress in the shales has relaxed since the last tectonic stress episode and now is (1) horizontally isotropic and (2) has a magnitude which reflects only the weight of the overburden strata (Warpinski et al., 1985, Warpinski and Teufel, 1989). The horizontal stresses in the sandstones, however, are anisotropic. They are less than that which would be generated by the weight of the overburden because of a degree of strength inherent in the sandstone rock structure that helps to support this weight. Since the surrounding shales are horizontally isotropic, they are not presently transmitting a horizontal tectonic stress. However, they must have transmitted enough stress at some point in their history to have caused the sandstones to fracture. Therefore the stress anisotropy in the sandstone reservoirs must be a remnant one, transmitted through the shales before they relaxed.

Another example of locked-in stress is documented by McLellan (1988) in describing the foredeep basin of Alberta. The situation is essentially that found at the MWX site, with horizontally isotropic, relaxed shales at overburden stress and horizontally anisotropic stresses in the sandstones. In Alberta, however, the stresses in the sandstones are *higher* than the overburden stress, arguing for a significant horizontal tectonic stress during cementation (which is entirely likely given the adjacent thrust belt) and/or the erosional removal of a significant thickness of overburden strata (also likely in this area).

Theoretically, limestones would be less likely than siliciclastic sandstones to retain a locked-in stress because their ductility under high confining pressure and elevated temperature commonly exceeds that of shale (e.g., Handin, et al., 1963). Moreover, carbonates are typically soluble under these conditions, especially when nonuniformly stressed, and strain in limestones may therefore also be accommodated through pressure solution and recrystallization. The ductility of dolomite, however, is nearly as low as that of clean, quartzitic sandstone.

There are good examples of anisotropic stresses measured in chalk reservoirs (e.g., Ekofisk field), and many of these rocks behave elastically in the laboratory on a short time

scale. Thus carbonates may exhibit not only the record of an active tectonic stress anisotropy, but they also seem to have the potential for preserving a remnant stress anisotropy. If so, stress-release fractures may develop in limestones under the right conditions.

The difference in behavior between an elastic rock, such as a well-cemented sandstone, or a more ductile one such as clay-rich shale, probably represents the extremes of a spectrum. Shales have a short relaxation time constant (the MWX shales fit a 5 million year time constant; Warpinski, 1989), whereas sandstones seem to have vastly longer relaxation time constants, probably on the order of tens to hundreds of millions of years. Accordingly, sandstones are essentially elastic during the time scales of interest.

Stress may dissipate laterally as it is "diluted" radially from a point source and/or as it is accommodated by strain in the rocks. This is not a stress release, but it may limit the size of an area that is subject to sufficient stress to cause fracturing.

6. Analysis: Reconstructing the Stress/Fracture History of a Basin

In reconstructing the tectonic history and ultimately the stress/fracture history of a potentially fractured reservoir, it is necessary to be able to read the fossilized record of stress in the rocks. It is also useful to be able to measure the present-day in situ stresses. Such stress records may include but are not limited to the kinematic indicators used by structural geologists. Many stress records do not record actual motion of the rocks, only the orientation of the contemporaneous stress.

Some measurement techniques can be used to calculate *present*-day stress magnitudes, but there are few if any reliable ways to measure *paleo*stress magnitudes.

6.1 Paleostress Indicators

Paleostress records range in size from microscopic crystal deformation to the trends of mountain ranges. The reliability of each indicator can vary with local circumstances, and each should be evaluated accordingly. A suite of mutually supporting indicators of different categories and magnitudes offers the most reliable evidence. Such a suite has been documented within the Piceance basin (Figure 18), and this will be used as the primary example in the discussions below.

6.1.1 Microscopic Indicators

Calcite is subject to crystallographic twinning when stressed anisotropically. This produces characteristic deformation lamellae that can (laboriously) be measured in thin section with a petrographic microscope and universal stage in order to determine the stress orientation (e.g., Groshong et al., 1984; Teufel, 1980). Several samples of calcite cement in sandstone core from the MWX wells were analyzed in this manner, yielding maximum horizontal paleostress orientations of northwest to west-northwest.

Quartz also deforms under stress, but instead of twinning, crystallographic shear planes are produced (McLaren et al., 1970). These shear planes can also be measured under the microscope and analyzed for the maximum compressive stress. Dula (1981) analyzed quartz deformation planes in the White River Uplift (the mountainous Laramide uplift just east of the Piceance Basin), concluding that the recorded maximum paleostress was horizontal and that it trended west-northwest.

These measurements of the paleostress in the vicinity of the MWX site are consistent and suggest that the horizontal stress locally exceeded the vertical, overburden stress. This fits well with the concept of the White River Uplift as a thick-skinned, overthrust indenter into the basin. The direction of thrusting indicated by the crystallographic evidence is west-northwest, which fits with evidence from the microscale configuration of the Grand Hogback (the boundary between the basin and the uplift). This will be discussed below.

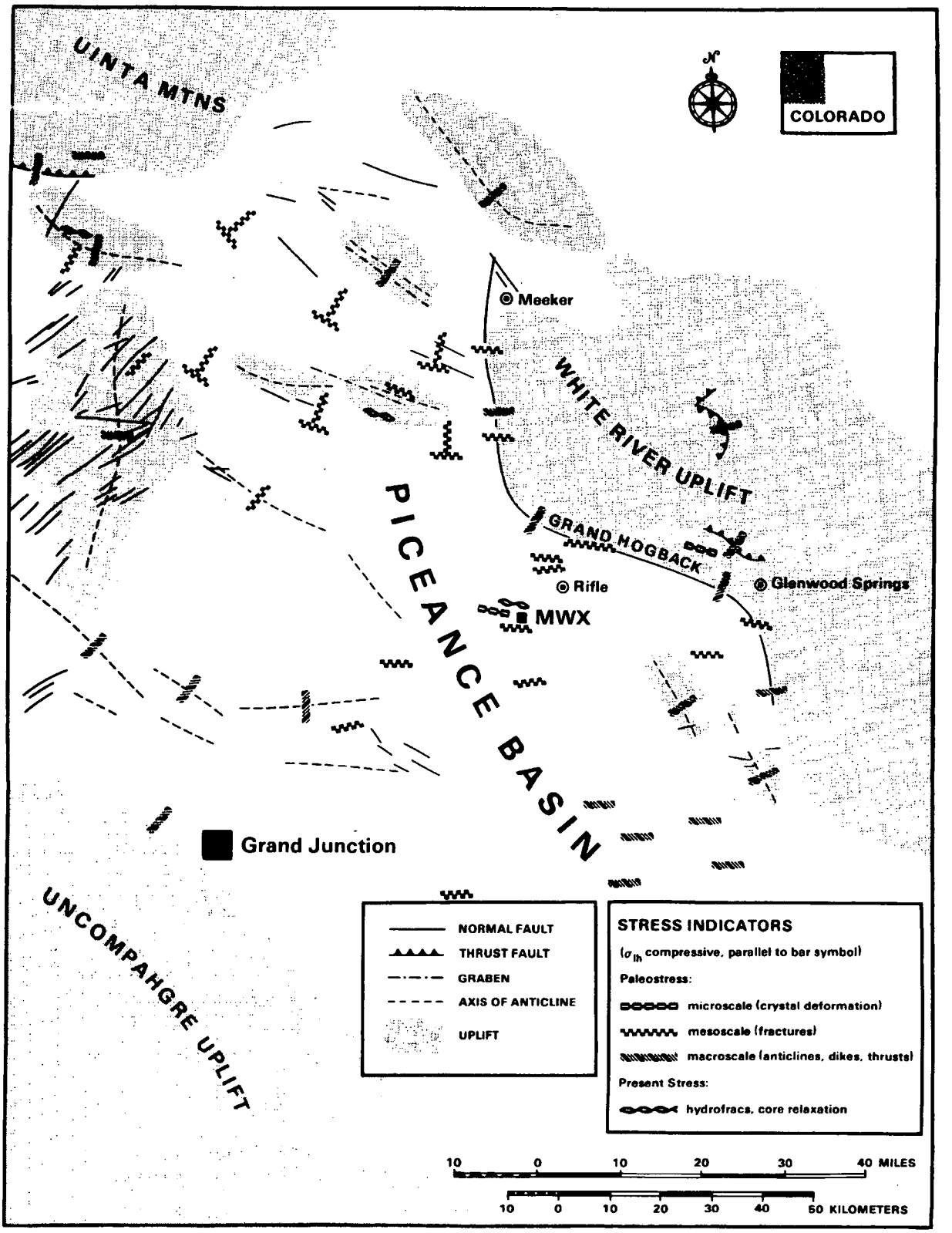

Figure 18. Map of the Piceance basin showing the trends and occurrences of paleostress indicators.

Stress domains may vary rapidly both laterally and vertically, and isolated microscopic stress indicators should not be relied on for the reconstruction of stress trajectories across entire basins. Nevertheless, they do offer important information on stresses at local sites and corroborating evidence for more regional stress history reconstructions. For calcite twin lamellae, estimates of the differential stress at the time of formation can be made, and a threshold of at least 100 bars must be achieved before twins are formed (Jamison and Spang, 1976). However, the actual stress magnitudes cannot be derived.

6.1.2 Mesoscopic Indicators

The intermediate scale of stress records includes most of what are usually measured as "kinematic indicators" (e.g., slickensides, veins/gashes, conjugate shears, etc., e.g., Arthaud and Choukroune, 1973) by structural geologists when reconstructing the relative motion between great masses of rock. However, since relatively few hydrocarbon reservoirs are located under mountain ranges, we will concentrate here on the more subtle indicators that occur in less-deformed, sedimentary strata, i.e., vertical extension fractures. (See also Appendices A, B.)

Vertical extension fractures are present in almost all sedimentary strata, despite the absence of other evidence of deformation. Such fractures form as a result of horizontal stress anisotropy in the strata acting on rocks that fail in a brittle mode despite high confining stresses; pore pressure partially negates the confining stresses, creating brittle strata. Stress anisotropy not only creates fractures, but it also dictates fracture orientation and maintains fracture aperture. Extension fractures will be oriented in the plane of the maximum and intermediate compressive stresses and will be normal to the least confining stress. Since the overburden stress is most commonly the maximum stress, most extension fractures are vertical. Even if one of the horizontal stresses is the maximum stress, extension fractures will be vertical as long as the overburden stress remains at least the intermediate stress.

Thus vertical extension fractures may be used to determine the orientation of the horizontal stress anisotropy. Because horizontal stresses will be isotropic in the absence of tectonic influence, fracture orientations may often be used to infer the presence, type, and location of tectonic activity at the time of fracturing.

At the MWX site and in the Piceance basin, several sets of fractures have been documented by numerous authors. (See summary in Lorenz and Finley, 1991.) West-northwest fracture orientations suggest a west-northwest maximum horizontal compressive stress in strata throughout most of the basin. These are interpreted to reflect the stresses derived from the Sevier overthrust belt to the west and locally from the incipient thrusting of the White River Uplift.

Several exceptions to this west-northwest trend occur, most notably (1) in fractures that form an array spreading westward across the basin in the Tertiary strata and (2) in fractures that are younger than and orthogonal to other fractures. The former are interpreted as having followed an arcuate stress trajectory formed by the point stress source as the White River Uplift was thrust into the basin. (See Figures 5 and 9.) The latter are inferred to be stress-release fractures, as discussed above, formed during uplift and erosion.

Vertical extension fractures may also form where no obvious source of compressional tectonism exists, or may even be normal to an expected trend if extension in another direction exceeds that from an obvious but superficial source of compression. An example of this is the Cretaceous strata of southwestern Wyoming, where asymmetric subsidence in a narrow, deep basin produced significant extension transverse to the narrow axis of the basin. This strain exceeded the extension due to compression from the adjacent thrust belt; thus the fractures were formed parallel to the axis of the basin and parallel to the thrust belt (Laubach and Lorenz) (Figure 19).

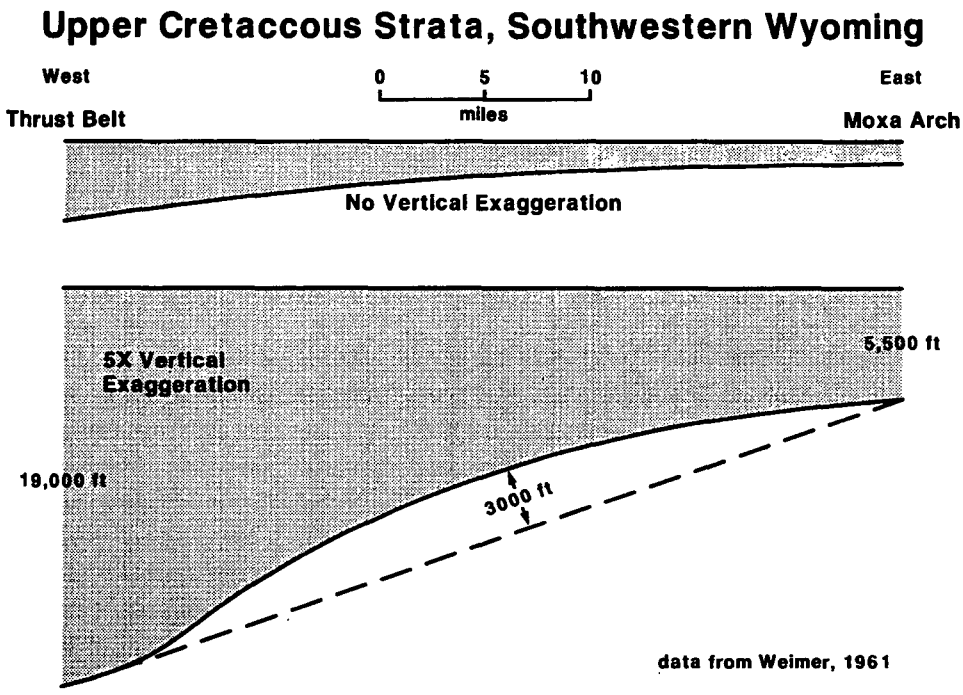

Figure 19. Rapid subsidence in a narrow basin that led to asymmetric stresses and fracturing parallel to the basin axis despite thrust-fault compression normal to the basin axis: Cretaceous foredeep of the Green River basin, southwestern Wyoming.

6.1.3 Macroscopic Indicators

Large-scale stress records are perhaps the easiest to see and measure, yet are also potentially the most deceptive. Examples of mesoscopic stress indicators that occur in the Piceance basin include normal faults and thrust faults, anticlines, graben, and igneous dikes. There have also been remote-sensing studies of various "lineaments" in the basin, but the significance of lineaments is highly questionable when their origin is unknown, and they will not be discussed further here.

The least ambiguous of these indicators are igneous dikes. Several Tertiary dikes have been mapped in the south-central part of the basin, and others exist in the central basin, all of which trend east-west. A dike is a natural hydraulic fracture and will be oriented normal to the least compressive stress; therefore, the maximum horizontal stress in the basin at the time of intrusion was east-west. The dikes are up to 5 miles long and reflect a consistent stress orientation in the strata to a depth of at least this magnitude. Stress rotation with depth would be apparent as an en echelon segmenting of the dikes, which does not occur. Thus the dikes are good paleostress records, and their orientation is consistent with other stress indicators discussed thus far because the strikes of extension fractures in this part of the basin rotate to become east-west or even slightly west-southwest.

Faults must be interpreted more carefully. Ideally, normal faults and graben form in extension normal to the least compressive stress while thrust faults form normal to the maximum compressive stress. However, there may be a component of strike-slip motion in addition to the dip-slip motion in either type of fault. The magnitude of this oblique motion can be considerable and is the result of stresses that are not entirely at right angles to the fault plane. A pre-existing weakness in the rock may also dictate the location and trend of the fault, whereupon the stresses only activate that weakness, do not control the fault orientation, and cannot be directly inferred from fault orientation.

Normal faults and the one graben within the Piceance basin trend primarily northwest, consistent with the dominant northwest maximum compressive stress suggested by other indicators. There is some scatter, which probably reflects basement heterogeneity, but no evidence for strike-slip motion has been reported from these faults.

A major thrust fault is present at the eastern margin of the basin, forming the Grand Hogback and creating the White River Uplift. Smaller thrusts are buried below the Divide Creek and Wolf Creek Anticlines in the southeastern part of the basin (Grout et al., 1991). The edge of the Uncompahgre Uplift at the southwestern margin of the basin may also be located at a thrust fault, but this has not been documented.

The smaller, buried thrusts apparently record east-west thrusting. Although they are complex, they may be interpreted in a relatively straightforward manner once suitable subsurface/seismic data is available. The Grand Hogback thrust, however, displays an ambiguous dogleg in the middle sector that has been interpreted to indicate a thrust event directed toward the south or southwest (Perry et al., 1988). Southwest thrusting would be in addition to (and at a different time from) the eastward-directed thrusting suggested by the north-south trending segments of the hogback. Strata along the dogleg are rotated more nearly vertical than strata on other parts of the hogback, and an overhang has been demonstrated near the center by industry drilling.

Study of this zone is incomplete, but none of the fracture patterns directly south of the dogleg support local north-south compression. Alternatively, the dogleg may an artifact of basement heterogeneity, and the true structure may be a tear-fault discontinuity in the north-south thrust that is obscured by blind, eastward-directed thrusting beneath the Mesozoic cover. In any case, the major thrust fault in the Piceance basin is an ambiguous stress indicator despite its large size and large-scale movement.

Anticlines within the Piceance basin are the least reliable of all of the local stress indicators. An anticline is typically interpreted as the result of horizontal compression normal to its axis, especially where numerous en echelon anticlines are present as in the Appalachian fold belt. However, most of the examples of antiform strata in the Piceance basin are out of phase. Most also trend west-northwest, suggestive of a north-northeast compressive stress that is nearly normal to any other stress record present in the basin. These "anticlines" seem to have been draped passively over faulted basement blocks. Each block was uplifted by stresses that were only loosely related to folding of the overlying strata, and the fold axes were commonly oblique to the stresses that uplifted the fault blocks. In such cases, the trend of the antiform reflects primarily the heterogeneity of the faulted basement, not a dominant stress orientation.

6.2 Present-Day, In Situ Stress Indicators

Several techniques can be used to measure the modern in situ stress orientation, and some also provide a measure of the stress magnitudes. Most of the methods provide only site-specific information.

Core and wellbore analysis were used to measure site-specific stresses at the MWX site. Among the techniques used to measure stress from core samples were Anelastic Strain Recovery (ASR), Differential Strain Curve Analysis (DSCA), Circumferential Velocity Anisotropy (CVA) (see Appendix D), and the measurement of coring-induced petal/petal-centerline, scribe-line, and disc fractures (see Kulander et al., 1990; Lorenz et al., 1990; Strickland and Ren, 1980; Teufel, 1983). The first three techniques measure the orientation of microscopic stress-release fractures that develop in the rock normal to the maximum in situ horizontal stress when the confining stress is released. Coring-induced fractures form with a strike (petal, petal-centerline, and scribe-line fractures) or plume axis (disc fractures) that usually parallels the in situ maximum horizontal stress. All of these methods provide information on the maximum horizontal stress direction *only* if the core is or can be oriented.

Stress magnitudes may also be calculated from the ASR technique in ideal cases (Warpinski and Teufel, 1989). Another procedure that measures the magnitude of the minimum in situ stress is the mini-or micro-frac technique, where small volumes of fluid are

injected into the formation from the wellbore while the injection pressure is monitored (Warpinski, 1985). Pressure continues to be monitored after injection is stopped, giving a measure of the stress the formation exerts on the fluid as the induced fracture is forced closed.

Analysis of the breakouts in a borehole, using caliper, borehole images, or other downhole tools will also indicate the local maximum horizontal stress direction (e.g., Fordjor et al., 1983; Plumb and Cox, 1987). A borehole commonly becomes elliptical as breakouts develop preferentially on the borehole walls that are aligned with the minimum horizontal compressive stress.

Finally, the direction of propagation of a hydraulic fracture may be monitored seismically (Hart et al., 1984) or by the use of instruments such as tiltmeters. The direction of propagation is controlled by and will parallel the maximum horizontal in situ stress. All of these methods (except tiltmeters) have been used successfully at the MWX site, and they consistently indicate a west-northwest maximum horizontal compressive stress.

There have been reports of success in determining the local subsurface stress direction by measuring seismic shear wave anisotropy (e.g., Crampin, 1985). In theory, since horizontal stress anisotropy preferentially holds open those natural microcracks in the rock that are aligned with the maximum compressive stress, shear waves will be impeded in the direction transverse to the open microcracks. A unidirectional set of macrofractures will have the same effect, whether they are aligned with the present maximum stress or not. Although fractures and stresses are commonly so aligned, care must be taken to be sure that stress is being measured with this technique and not an oblique fracture orientation.

Earthquake focal mechanisms have been used to determine the direction of stress orientations in large tectonically active areas (Liang and Wyss, 1991). Although such measurements are valid, they commonly measure the stresses at much greater depths than most reservoirs, and they are not sensitive to the local variations in stress that structures and topography can cause.

In the Piceance basin, the orientation of the stress field has been successfully measured at several sites. The orientation of the stress field at MWX (Figure 20) has been measured using several techniques, all of them showing a stress orientation that is slightly north of west with a possible rotation with depth. Measurements farther north (Bredehoeft et al., 1976) showed a similar stress orientation (Figure 18), as did velocity anisotropy measurements on a Fuelco well about 15 mi to the southwest of MWX. The only data in disagreement are velocity-anisotropy and coring-induced fracture results from the Barrett MV8-4 well in Grand Valley. However, this well is under the severe topography of Anvil Points and probably suffers a rotation due to the additional load.

ASR results at the MWX site suggest that differences in the two horizontal stresses in the Mesaverde vary from about 600–1200 psi, depending upon the depth and the zone.

6.3 Pore Pressure

One of the major uncertainties in reconstructing the fracture history of a basin is the fracture susceptibility of the strata through time. This is largely dependant on formation pore pressure, though other factors such as changing rock properties (a function of cementation, compaction, diagenesis, etc.) are also important. Pore pressure will change as the organic material in a formation matures and produces gas, as burial/compaction ratios evolve, as the strata are compressed laterally by tectonism, and/or as temperature gradients change. Reconstruction of pore pressure histories is difficult. Uncertainties include the gross estimates that must be made of organic volumes contained by formations and the percentages of the gasses produced that may have been lost or adsorbed.

Nevertheless, geologically reasonable estimates can often be made at least of the probable timing of elevated pore pressures, if not of their magnitude, and of how the pressure history interacted with the tectonic/stress history of a formation. Such estimates were made for the Piceance basin at the MWX site, where it can be demonstrated that elevated pressure produced by gas generation in the formation (Spencer, 1987) coincided with enhanced

tectonic compression to create natural fractures (Lorenz and Finley, 1991). An important piece of corroborative data for this interpretation came from fluid-inclusion analyses, which provided an indication of the in situ temperatures and pressures during fracturing.

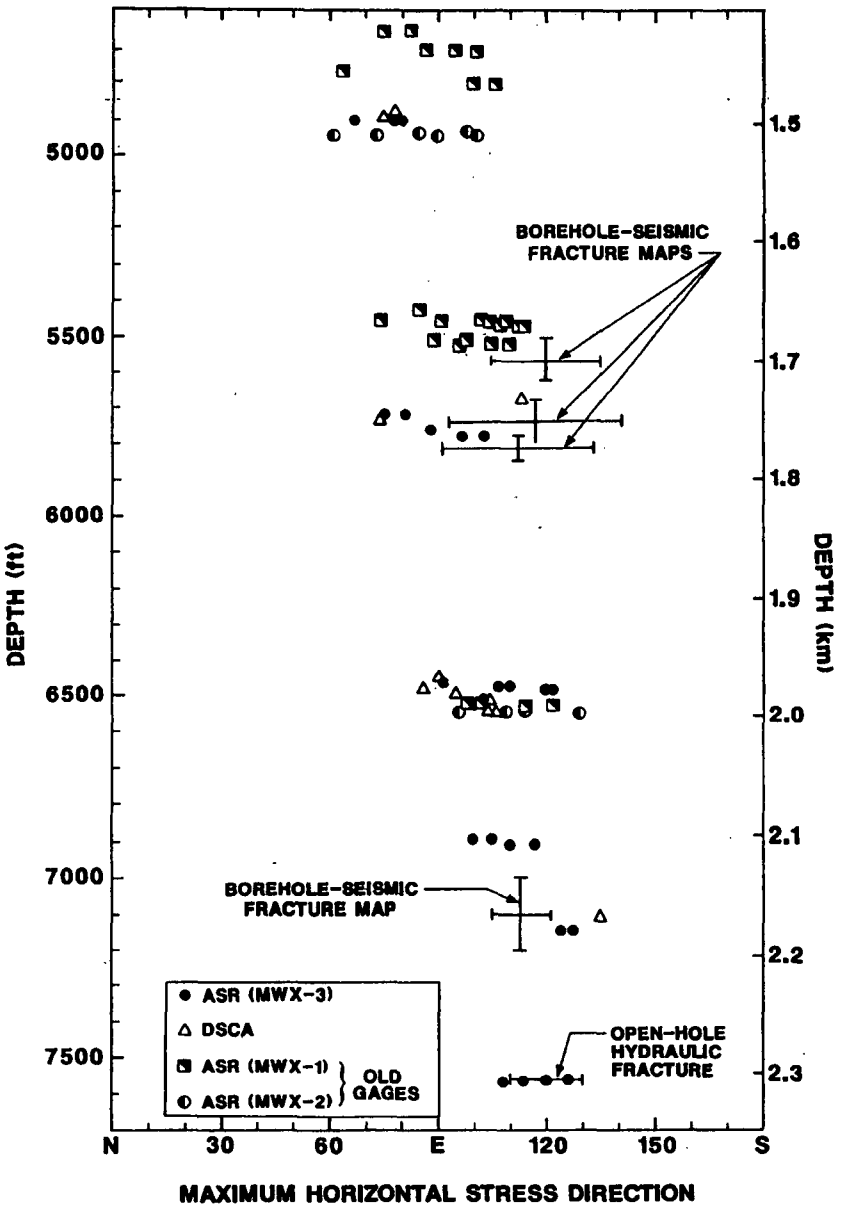

Figure 20. Orientation of the stress field at MWX based on Anelastic Strain Recovery (ASR) data in three wells, Differential Strain Curve Analysis (DSCA) on selected samples, an open-hole hydraulic fracture (impression packer), and four hydraulic fracture experiments where borehole seismic instrumentation was used to map the fracture azimuth.

6.4 Summary

Paleostress indicators should be used in conjunction with tectonic reconstructions to create a conceptual stress-history model of the strata in question. An integrated numerical model is within the capabilities of computer programs (e.g., Warpinski, 1989), but is only as accurate as the geologic data available. Any model must use or correctly predict the measured paleo-stress indicators and the known present-day stresses as known tie points.

A tectonic and stress history model was constructed for the Mesaverde strata at the MWX site (Lorenz, 1985; Warpinski, 1989; Lorenz and Finley, 1991) that incorporates most of the factors discussed above. The principal components of the model include (1) a curve depicting the depth of burial relative to the changing-elevation land surface through time (Figure 21), (2) an analysis of the timing and probable effects of the different tectonic events in and around the basin (regional uplift, volcanism, basin-margin thrusting, etc.), (3) a conceptual model of the pore pressure in the formation through time, (4) basement heterogeneities, (5) empirical evidence of the natural fracture characteristics and distribution throughout the basin, and (6) measurements of the modern in situ stresses.

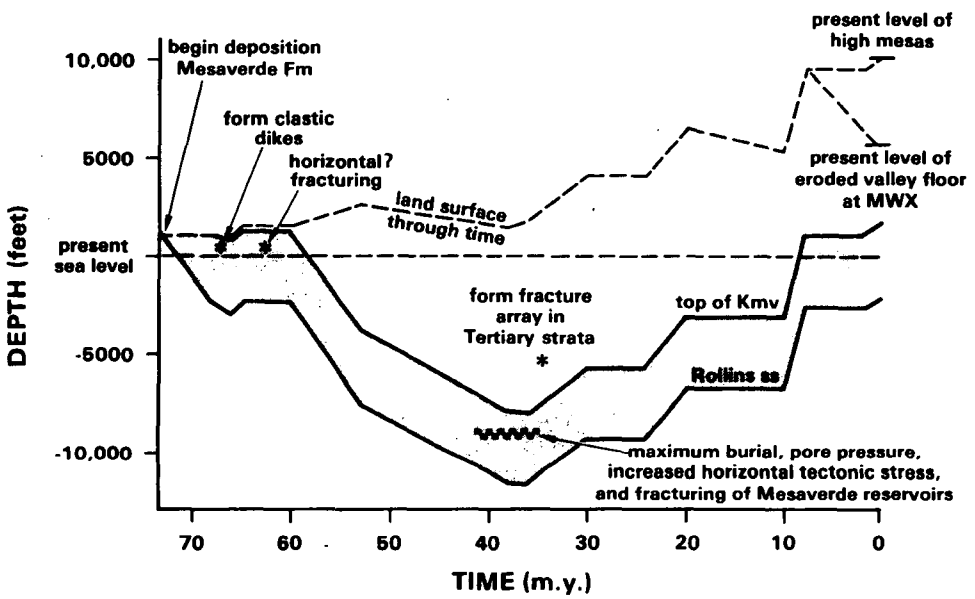

Figure 21. Time/Burial-depth/Surface-elevation diagram for the strata at the MWX site in the Piceance basin.

These data and the synthesis suggest that natural fracturing occurred during a time of elevated pore pressure, at maximum depth of burial, and under conditions of enhanced compressive stress due to basin-margin tectonic compression about 36–40 million years ago. Significantly, the shales that surround the sandstones are in a relaxed state and reflect the overburden stress. Therefore, the present stresses in the reservoir sandstones must be locked-in/remnant stresses because no horizontal tectonic compression is being transmitted to the sandstones through the shales. The maximum horizontal stresses (both paleo and present) caused fracturing and are therefore parallel to the natural fractures. Accordingly, most of the fractures comprise a single, west-northwest trending, regional set. However, the local high-relief topography may rotate the present shallow stress orientations by 10°–15°.

7. Prediction of Fracture and Stress Orientations in a Basin and at a Well Site

The above criteria can be used to infer paleo and present stress patterns in a basin and thus to predict (1) the potential for fracturing in a given set of reservoir strata and (2) the probable relative orientations of fractures and the in situ stresses. With this information, the effects of the stresses on reservoir deliverability may be inferred.

As with any predictions, the larger the data base, the better the prediction. Moreover, once a well is drilled based on predictions, new data become available, allowing for the incremental refinement (or sometimes the drastic modification) of original predictions until the prediction eventually matches reality when all factors are known. The goal, of course, is to make as accurate a prediction as possible as early as possible. Unfortunately, time and money often dictate that the initial prediction will be based on a limited data set. Given the complexity of geologic systems, which usually contain hidden factors that are revealed only at inopportune times, one should be prepared to modify predictions.

A summary list of the data desirable for predicting stresses and fractures in the generic basin is given in Table 1. This is a short table, but, as shown above, each category admits numerous possible sources of data and contains numerous potential ambiguities.

Table 1. Information for Predicting Subsurface Stress and Fracture Patterns at a Well Site

Present regional stress orientations
Present regional stress magnitudes
Surface fracture patterns
Time-depth history of the strata
Regional structural patterns and timing
Formation pressures, past and present
Topographic profiles of the site

There are two parallel studies that must be made and then integrated in order to reconstruct the fracturing events and to predict fracture orientation. One is to estimate the fracture susceptibility of the strata through time, and the other is to reconstruct the stress-anisotropy (tectonic) history of the basin. Time intervals where high susceptibility coincides with high anisotropy are the most likely times of fracturing, and the stress orientations at these times will control fracture trends.

A numerical example of this approach has been constructed for the Piceance basin (Warpinski, 1989). Stresses were calculated through time based on geologic estimates of compressive tectonic stress and depth of burial (Figure 22), and fracture susceptibility was calculated based on varying rock properties (derived from geologic estimates of the pore pressure, temperature, and diagenesis histories). In this study, the likelihood of fracture was based on a comparison of the stress conditions with a laboratory-derived failure envelope for samples of the reservoir sandstones (Figure 23). Calculated end-result stresses correlated best with those measured in the strata when a visco-elastic model of the strata was used.

An alternative, empirical, and complementary approach to modeling the same basin is presented by Lorenz and Finley (1991). In this analysis it was noted that the timing of maximum compression due to basin-margin thrusting coincided with maximum burial and with maximum organic maturation (therefore with maximum formation pore pressure). Therefore, maximum fracture susceptibility was contemporaneous with maximum stress anisotropy, and fracturing was inferred to have occurred at this time. The orientation of the fractures is compatible with the compressive stress trajectories produced by thrusting.

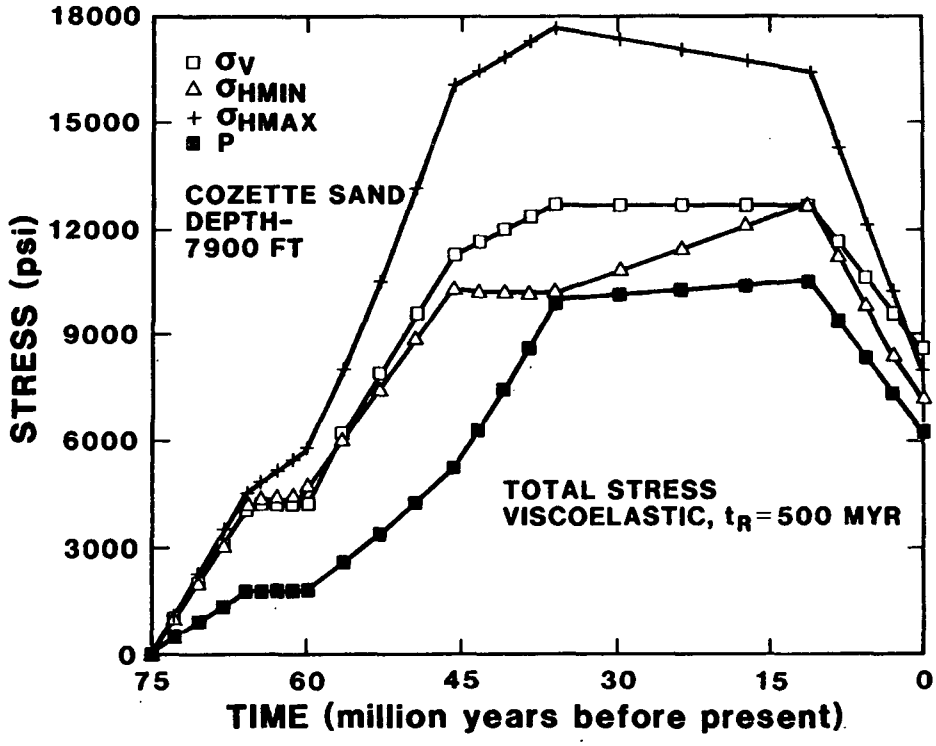

Figure 22. Reconstructed stress history for the strata at the MWX site

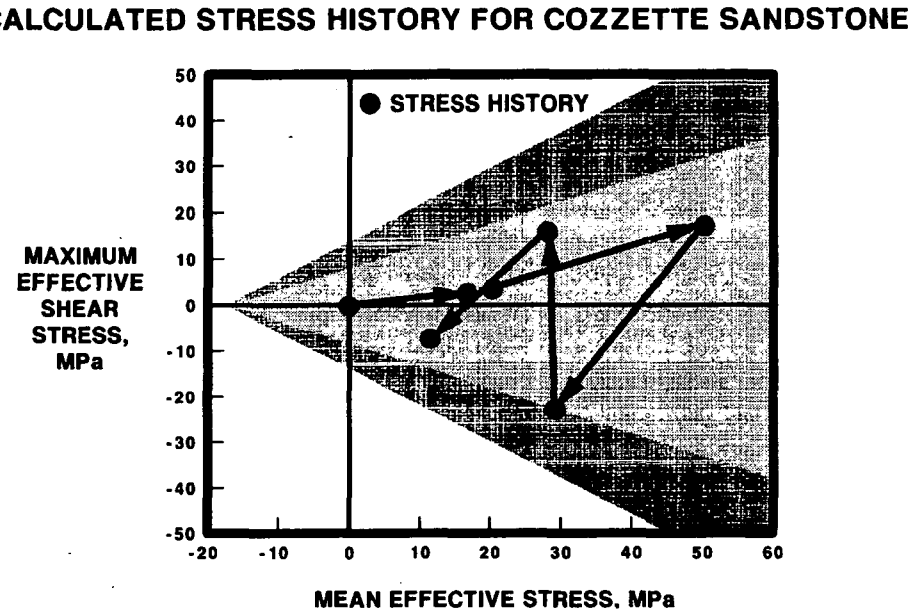

Figure 23. Stresses (from previous figure) plotted within an empirical failure envelope, indicating the most likely times of fracturing. Outer envelope is failure plane from laboratory data. Inner envelope indicates failure plane corrected for geologic criteria.

Similar approaches may be taken to predict fracturing and fracture/stress orientations without foreknowledge of the fracture character or of the present stress state at depth. However, there will be fewer definitive tie points between the model and reality, and the reconstruction will be commensurately less reliable.

7.1 Tectonic Stress History

1. The tectonic history of a basin must first be understood. All potential sources of anisotropic stress in the basin (asymmetric basin subsidence, thrusting, flexure, topography, etc., as discussed earlier) must be identified and mapped, and the probable orientations or trajectories of the stresses produced by each source plotted. Differentiate between regional stresses and local stress-modifying features.
2. The time intervals during which each stress was a factor must be determined as closely as possible. Stratigraphic dating and radiometric dating are essential in this exercise, but, unfortunately, the two time scales do not always coincide, and they rarely offer the desired precision.
3. The magnitudes of stresses should be estimated if possible. This may be approached by measuring indentation distances, radii of curvature, amounts of uplift, or the amounts of strain that resulted from each source. Use geologic principles and inventiveness.
4. A time-depth curve (e.g., Figure 21) should be constructed for the specific site of interest. Again, dating may be less precise than desirable. Most time-depth curves do not account for more than the position of the strata relative to the land surface, but more insight may be gained by (a) plotting the strata relative to sea level, which allows uplift events to be seen in context, and (b) plotting the local land surface relative to sea level in order to retain a plot of total burial depth. Moreover, the thicknesses of strata removed by erosion should be estimated and included in the plot.
5. All paleostress indicators should be identified and plotted along with any constraints on their time of origin in map form or even on a series of time-slice maps. These maps may be the same ones on which the structures/stress sources are located, where correlations between the two often become apparent.
6. Note potential vertical discontinuities in stresses such as depths of indentation or ductile stratigraphic layers.
7. The result should be a 4-dimensional concept of stresses in the basin (vertically, 2-dimensional laterally, and time) that is as quantitative as possible. This will commonly be more quantitative than the geologist is comfortable with, yet less so than an engineer would like.

7.2 Calculated Stress History

Stress-strain relationships for a linear-elastic, homogeneous, and isotropic material are well known and can be written as

$$E d\epsilon_x = d\sigma_x - \nu(d\sigma_y + d\sigma_z) - \alpha E dT$$
$$E d\epsilon_y = d\sigma_y - \nu(d\sigma_x + d\sigma_z) - \alpha E dT$$

for the horizontal directions, where E is Young's modulus, ν is Poisson's ratio, α is the coefficient of thermal expansion, $d\epsilon$ is a differential strain, $d\sigma$ is an effective differential stress, and dT is a differential temperature change. The stresses, strains, and temperature are written as differentials because they will need to be integrated later to account for changes in material properties. In addition, σ will always denote an effective stress. Also, compression

is positive; thus increasing dT results in expansion, and a minus sign precedes the thermal strain term.

These equations can be solved for the stresses as

$$d\sigma_x = \frac{\nu}{1-\nu} d\sigma_z + \frac{E d\epsilon_x}{1-\nu^2} + \frac{\nu E d\epsilon_y}{1-\nu^2} + \frac{\alpha E dT}{1-\nu}$$

$$d\sigma_y = \frac{\nu}{1-\nu} d\sigma_z + \frac{E d\epsilon_y}{1-\nu^2} + \frac{\nu E d\epsilon_x}{1-\nu^2} + \frac{\alpha E dT}{1-\nu} .$$

Each of these components was separately discussed earlier. In this form, σ_z is recognized as the effective differential overburden stress caused by a change in depth, pore pressure or properties. It is given by

$$d\sigma_z = d[(\rho g - \lambda)D] ,$$

where ρ is the rock bulk density, g is the gravitational constant, λ is the pore pressure gradient (psi/ft or kPa/m), and D is the depth. Throughout the analysis, σ_x will be the minimum compressive stress and σ_y the maximum compressive stress. Without more information, it is tacitly assumed that Biot's modulus is unity.

These equations are the basis for both elastic and viscoelastic analyses. The simplest solution is for elastic behavior with constant rock properties and pore pressure gradient. This results in

$$\sigma_x = \frac{\nu}{1-\nu} \sigma_z + \frac{E\epsilon_x}{1-\nu^2} + \frac{\nu E\epsilon_y}{1-\nu^2} + \frac{\alpha E dT}{1-\nu}$$

$$\sigma_y = \frac{\nu}{1-\nu} \sigma_z + \frac{E\epsilon_y}{1-\nu^2} + \frac{\nu E\epsilon_x}{1-\nu^2} + \frac{\alpha E dT}{1-\nu}$$

$$\sigma_z = (\rho g - \lambda)D,$$

with the obvious implication that the stresses at depth can be calculated at any time if the properties, strains, pressure, and temperature are known. There are many limitations to this approach (Voight, 1974; Prats, 1981), and these equations will not provide accurate stress calculations for most applications. The strains are assumed to be tectonic or geometric and are applied at the edge of the basin.

In general, rocks in a sedimentary basin have time-varying properties: strains, temperature, and pore pressure, with "locked-in" or cumulative stresses. The solution now requires an integration as

$$\Delta\sigma_x = \int_{t_1}^{t_2} \frac{\nu}{1-\nu} \frac{d[(\rho g-\lambda)D]}{dt} dt + \int_{t_1}^{t_2} \frac{E}{1-\nu^2} \frac{d\epsilon_x}{dt} dt$$

$$+ \int_{t_1}^{t_2} \frac{\nu E}{1-\nu^2} \frac{d\epsilon_y}{dt} dt + \int_{t_1}^{t_2} \frac{\alpha E}{1-\nu} \frac{dT}{dt} dt$$

$$\Delta\sigma_y = \int_{t_1}^{t_2} \frac{\nu}{1-\nu} \frac{d[(\rho g-\lambda)D]}{dt} dt + \int_{t_1}^{t_2} \frac{E}{1-\nu^2} \frac{d\epsilon_y}{dt} dt$$

$$+ \int_{t_1}^{t_2} \frac{\nu E}{1-\nu^2} \frac{d\epsilon_x}{dt} dt + \int_{t_1}^{t_2} \frac{\alpha E}{1-\nu} \frac{dT}{dt} dt$$

with

$$\sigma_z(t) = [\rho(t)g - \lambda(t)]D \ .$$

The overburden stress is assumed to instantaneously reflect any changing values and can thus always be calculated if the properties, pore pressure, and depth are known at any instant. The horizontal stresses must be integrated through history to arrive at a reasonable estimate of the horizontal stresses at depth. The integrals have been taken with respect to time because it is always possible to make some simple assumptions about the way properties and other parameters will vary through time (assuming the burial, tectonic, and diagenetic history are known). These equations can now be used to include the effect of lithification and changes in load parameters.

A comparable analysis can be performed for viscoelastic behavior of the rocks, and the equations are given in Appendix C. For the viscoelastic case, it is also necessary to estimate a relaxation time for the rocks. It is generally expected that sandstones will behave elastically over reasonable geologic time periods (<100 million years) while shales probably behave viscoelastically over very short time periods (<5 million years).

An example calculation for the stress history of three wells in the Piceance basin (Figure 24) shows that large stress anisotropies are expected at the time of maximum burial, but pore pressure is also high at this time. Thus conditions are conducive to the formation of regional fractures. (See also Appendix C.)

7.3 Fracture-Susceptibility History

1. Estimate the rate of lithification of the strata. This will be a function of diagenesis, burial (compaction), cementation, etc., and will be qualitative since no standard or universal rate exists. However, the more a sediment turns into a rock, the higher the modulus it will have, and the more it will be prone to fracture.
2. Create a pore-pressure history for the strata. This is another difficult and qualitative exercise, but is important because pore pressure acts to negate confining pressure, and a less confined rock is brittle and prone to fracture. Organic maturation, rate of compaction, ease of formation dewatering, and lateral compression of strata are all factors to consider. It may also be important to note the lateral distributions of certain pore pressure domains (i.e., if certain parts of a formation contain coal, organic maturation may generate formation pressures higher than in zones without coal). Since pore pressure will also contribute to the total stress of a system, its effects should also be considered when constructing the stress history above.
3. Determine thermal and overburden-stress histories. Thermal strains can be very high, and a large component of the lateral stresses comes from the overburden stress. Isotropic stresses from these two factors will add to the total stress of a system, and deep burial and/or a high geothermal gradient will increase the fracture susceptibility of strata.

The result should again be a 4-dimensional concept of lateral and vertical pore pressure variation through time, although this will in all probability be more qualitative than the stress-history model.

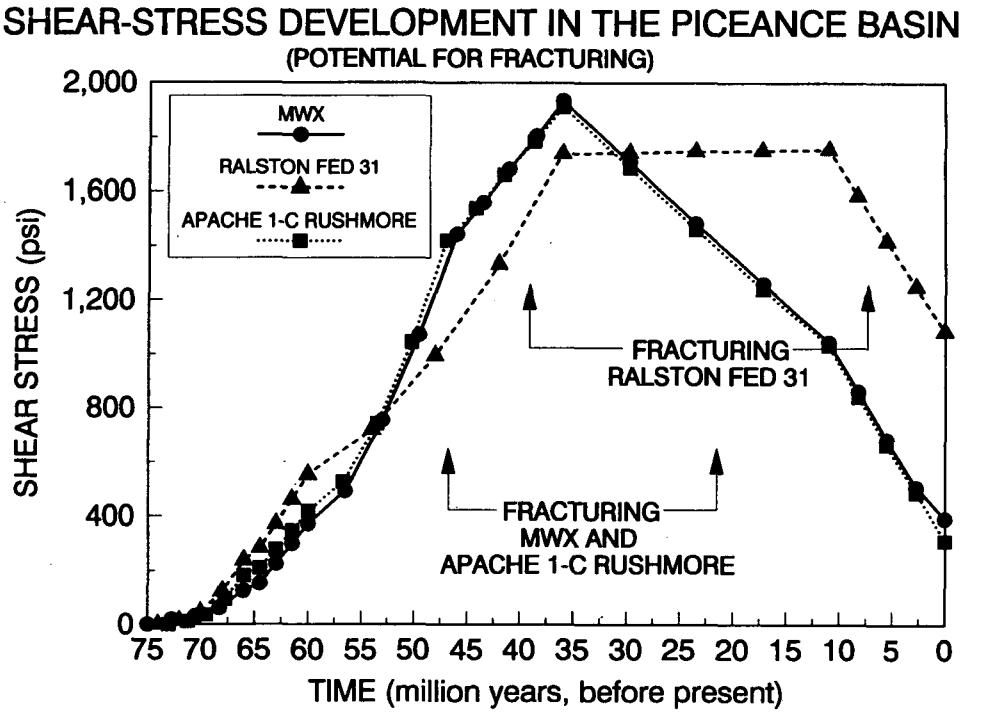

Figure 24. Calculation of the shear stress, through time, that would have developed at three sites in the southern Piceance basin. Increased shear stress indicates increased potential for fracturing.

7.4 Integration

The optimum conditions for fracturing, and therefore the most probable times of fracturing, occur at the intersections of maximum stress anisotropy and maximum fracture susceptibility. This may not always be the case, for if earlier, less ideal conditions allowed fracturing, subsequent ideal conditions may only reactivate existing fractures. Moreover, there may be more than one fracturing event in a basin, and fracture sets may be superimposed. Thus the interpretation of fracturing in a basin must be made carefully and with full knowledge of the geological history of the basin.

Regardless of when the fracturing actually occurs, fracture planes should be aligned with the maximum and intermediate compressive stresses at the time of fracturing. These orientations are derived from the stress trajectories created by the combined stress sources in the basin. Thus the maps of stress sources and of stress indicators provide the basis for predicting fracture orientations in a given set of strata in a given area. These maps can also be used to predict the present-day in situ stress orientations (which commonly, but not always, parallel the paleo-stress orientation).

Once regional fracture and regional stress orientations are known, the probable details of specific well sites can be predicted, and specific exploration prospects may be generated. The latter may consist of searching for anomalies where the regional stress has been altered due to local structure or radical topography, providing a mechanism to direct hydraulic stimulation fractures across the natural fracture trend for enhanced efficiency. They may also consist of areas of the basin where the reconstructed tectonic stresses or fracture susceptibility of the strata were maximized, increasing the likelihood of fractured reservoirs.

Conclusion

The multi-discipline processes described above for assessing the fracture history of a basin, a specific site within it, and the probable effects of the fractures on the reservoir in question can be summarized in a flow diagram (Figure 25). This figure lists, as the "Fracture Analysis Toolbox," the techniques that can be used to measure current stresses and to reconstruct paleostresses, as well as the methodologies used to infer probable fracture types and their effects on a reservoir. Application of as many of these techniques as possible to a given problem, although expensive and time consuming, is desirable in order to constrain the modeling and inferences that follow at the ensuing interpretive-level procedures.

Use of these techniques allows for a scientifically-based evaluation of the potential for fractures to be present in the subsurface, and if present, their probable importance to permeability and thus to the recovery of hydrocarbons from the reservoirs in the system.

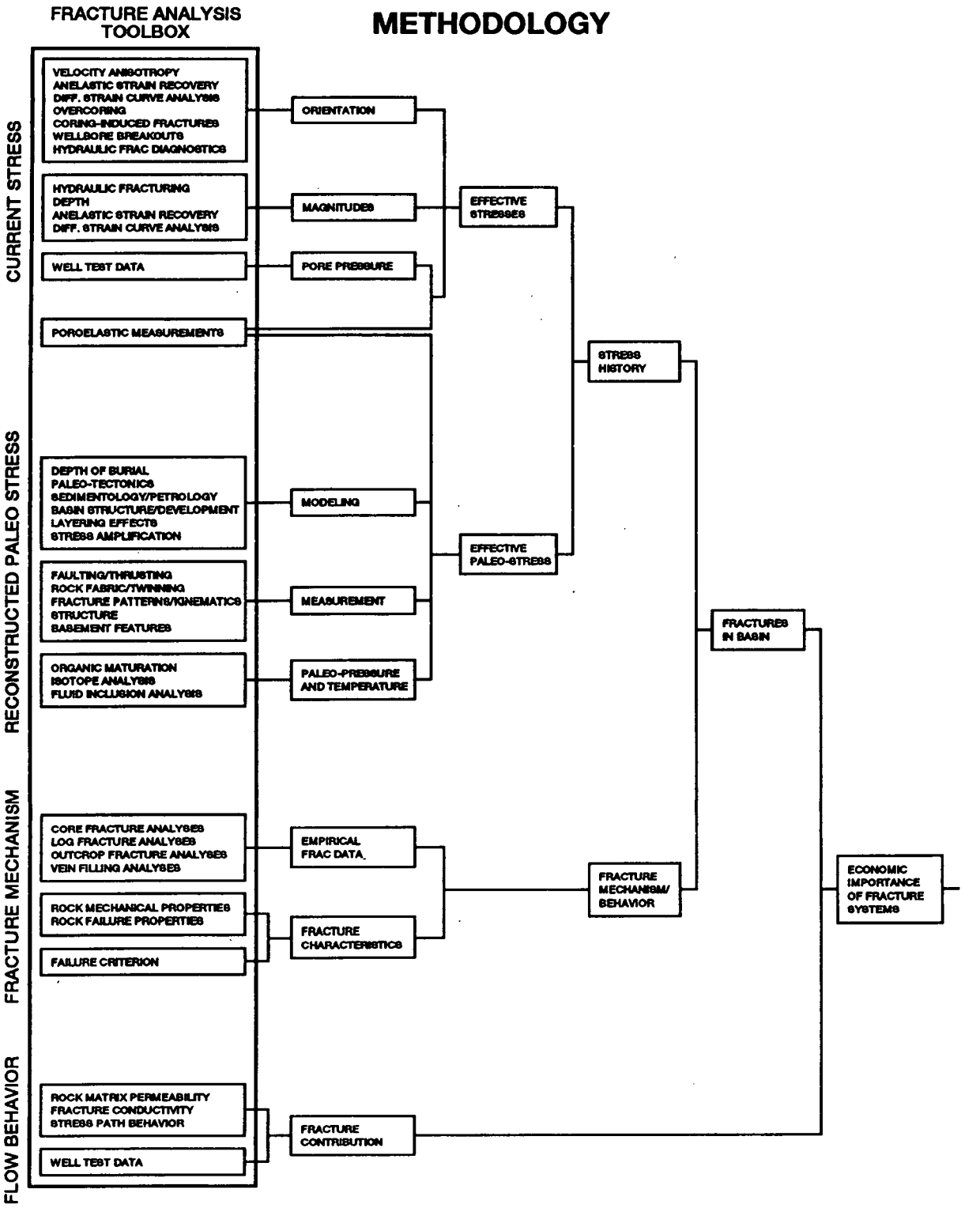

Figure 25. Flow diagram summarizing fracture-assessment techniques and their integration into the procedures described in this paper.

References

Anderson, E.M., 1942, The Dynamics of Faulting: Oliver and Boyd, London. 183 p.

Arthaud, F., and Choukroune, P., 1973, Method d'analyse de la tectonique cassante a l'aide des microstructures dans les zones peu deformees: exemple de la plate-forme Nord-Aquitaine: Revue de l'Institute Francais du Petrole, v. 27, p. 175–732.

Becker, A., 1989, Detached neotectonic stress field in the northern Jura Mountains, Switzerland: Geologische Rundschau, v. 78, p. 459–475.

Becker, A., Blumling, P., and Muller, W.H., 1989, Recent stress field and neotectonics in the eastern Jura Mountains, Switzerland: Tectonophysics, v. 135, p. 277–288.

Bell, J.S., and Lloyd, P.F., 1989, Modelling of stress refraction in sediments around the Peace River Arch, western Canada: Current Research, Part D, Geological Survey of Canada, Paper 89-1D, p. 49–54.

Bell, J.S., and Adams, J., 1990, Do the rocks remember? How contemporary are the regional stresses in Canada?, in Herget, G., Arjang, B., Betournay, M., Gyenge, M., Vongpaisal, S., and Yu, Y.S., eds., Proceedings of Specialty Conference: Stresses in Underground Structures: Mining Research Laboratories, Canada Centre for Mineral and Energy Technology, EMR, p. 13–22.

Bott, M.H.P., 1991, Ridge push and associated plate interior stress in normal and hot spot regions: Tectonophysics, v. 200, p. 17–32.

Branagan, P.T., 1984, Interference testing of the naturally fractured Cozzette sandstone: a case study at the DOE MWX site: Society of Petroleum Engineers paper number 12869, SPE Unconventional Gas Recovery Symposium, Pittsburgh, p. 359–366.

Branagan, P. T., Cipolla, C. L., Lee, S. J. and Wilmer, R. H., 1985, Comprehensive well testing and modeling of pre- and post-fracture well performance of the MWX lenticular tight gas sands: Society of Petroleum Engineers paper number 13867, Proceedings, 1985 SPE Symposium on Low Permeability Reservoirs, Denver, CO, p. 191–202.

Bredehoeft, J.D., Wolff, R.G., Keys, W.S. and Shuter, E., 1976, Hydraulic fracturing to determine the regional in situ stress field: Geologic Society of America Bulletin, Vol. 87, p. 250–258.

Clark, J.A., 1983, The prediction of hydraulic fracture azimuth through geological, core, and analytical studies: Society of Petroleum Engineers paper number 11611, SPE/DOE Joint Symposium on Low Permeability Reservoirs, Denver, CO, p. 107–114.

Crampin, S., 1985, Evaluation of anisotropy by shear-wave splitting: Geophysics, v. 5048, p. 142–152.

Dickey, P.A., 1979, Petroleum development geology: PPC Books, Tulsa, Oklahoma.

Dula, W.F.Jr., 1981, Correlation between deformation lamellae, microfractures, macrofractures, and in situ stress measurements, White River Uplift, Colorado: Geological Society of America Bulletin, v. 92, p. 37–46.

Elkins, L.F., and Skov, A.M., 1960, Determination of fracture orientation from pressure interference: Petroleum Transactions, AIME, v.219, p. 301–304.

Fertl, W.H., 1976, Global occurrence and evaluation of abnormal formation pressures, *in* Abnormal Formation Pressures: Elsevier, New York, p. 325–347.

Fordjor, C.K., Bell, J.S., and Gough, D.I., 1983, Breakouts in Alberta and stress in the North American plate: Canadian Journal of Earth Sciences, v. 20, p. 1445–1455.

Gallagher, J.J., Friedman, M., Handin, J., and Sowers, G.M., 1974, Experimental studies relating to microfracture in sandstone: Tectonophysics, v. 21, p. 203–247.

Genovese, P.W., and Schmidt, C.J., 1989, A calcite twin-strain analysis of thrust sheets, southwestern Montana: evidence for stress field concentration by Rocky Mountain foreland anticlines.

Griggs, D. and Handin, J., 1960, Observations on fracture and a hypothesis of earthquakes: Geological Society of America Memoir 79, p. 347–364.

Groshong, R.H.Jr., Teufel, L.W., and Gasteiger, C., 1984, Precision and accuracy of the calcite strain-gage technique: Geological Society of America Bulletin, v.95, p. 357–363.

Grout, M.A., Abrams, G.A., Tang, R.L., Hainsworth, T.J., and Verbeek, E.R., 1991, Late Laramide thrust-related and evaporite-domed anticlines in the southern Piceance basin, Northeastern Colorado plateau: American Association of Petroleum Geologists Bulletin, v. 75, p. 205–218.

Hafner, W., 1951, Stress distribution and faulting: Geological Society of America Bulletin, v. 62, p. 373–398.

Hancock, P.L., and Bevan, T.G., 1987, Brittle modes of foreland extension, *in* M.P. Coward, J.F. Dewey, and P.L. Hancock, eds., Continental Extensional Tectonics: Geological Society Special Publication no. 28, p. 127–137.

Handin, J., Hager, R.V., Friedman, M., and Feather, J.N., 1963, Experimental deformation of sedimentary rocks under confining pressure: pore pressure tests: American Association of Petroleum Geologists Bulletin, v.47, p.717–755.

Hart, C.M., Engi, D., Fleming, R.P. and Morris, H.E., 1984, Fracture diagnostics results for the Multiwell Experiment's paludal zone stimulation: Society of Petroleum Engineers paper number 12852, Proceedings, SPE/DOE Unconventional Gas Recovery Symposium, Pittsburgh, PA, p. 221–228.

Jaeger, J.C. and Cook, N.G.W, 1976, *Fundamentals of Rock Mechanics*, Halsted Press, New York.

Jamison, W.R., and Spang, J.H., 1976, Use of calcite twin lamellae to infer differential stress: Geological Society of America Bulletin, v. 87, p. 868–872.

Kempthorne, R.H., and Irish. J.P.R., 1981, Norman wells—a new look at one of Canada's largest oil fields: Journal of Petroleum Technology, v. 33, p. 985–991.

Kulander, B.R., Dean, S.L., and Ward, B.J.Jr., 1990, Fractured core analysis: interpretation, logging, and use of natural and induced fractures in core: American Association of Petroleum Geologists, Methods in Exploration Series, No. 8, 88 p.

Kulick, D.M., and Schmidt, C.J., 1988, Region of overlap and styles of interaction of Cordilleran thrust belt and Rocky Mountain foreland: Geological Society of America Memoir 171, p. 75–98.

Laubach, S.E., and Lorenz, J.C., 1992, Preliminary assessment of natural fracture patterns of Frontier Formation sandstones, southwestern Wyoming, *in* Mullen, C.E. (ed.), Rediscover the Rockies; Wyoming Geological Association, 43rd Field Conference Guidebook, p. 87–96.

Liang, B. and Wyss, M., 1991, Estimates of orientation of stress and strain tensors based on fault-plane solutions in the epicentral area of the great Hawaiian earthquake of 1868: Bulletin of the Seismological Society of America, Vol. 81, p. 2320–2334.

Lorenz, J.C., 1989, Reservoir sedimentology of rocks of the Mesaverde Group at the Multiwell Experiment site and east central Piceance basin, *in* B.E. Law and C.W. Spencer, eds., Geology of tight gas reservoirs in the Pinedale anticline area, Wyoming, and at the Multiwell Experiment site, Colorado: U.S. Geological Survey Bulletin 1886, p. K1–K24.

Lorenz, J.C., 1985, Tectonic and stress histories of the Piceance Creek basin and the MWX site, from 75 million years ago to the present: Sandia National Laboratories Report SAND84-2603, 55 p.

Lorenz, J.C., and Finley, S.J., 1991, Regional fractures II: fracturing of Mesaverde reservoirs in the Piceance basin, Colorado: American Association of Petroleum Geologists Bulletin, v. 75, p. 1738–1757.

Lorenz, J.C., Teufel, L.W., and Warpinski, N.R., 1991, Regional fractures I: a mechanism for the formation of regional fractures at depth in flat-lying reservoirs: American Association of Petroleum Geologists Bulletin, v. 75, p. 1714–1737.

Lorenz, J.C., Finley, S.J., and Warpinski, N.R., 1990, Significance of coring-induced fractures in Mesaverde core, northwestern Colorado: American Association of Petroleum Geologists Bulletin, v. 74, p. 1017–1029.

McLaren, A.C., Turner, R.G., Boland, J.N., and Hobbs, B.E., 1970, Dislocation structure of the deformation lamellae in synthetic quartz; a study by electron and optical microscopy: Contributions to Mineralogy and Petrology, v. 29, p. 104–115.

McLellan, P., 1988, In situ stress prediction and measurement by hydraulic fracturing, Wapiti, Alberta: Journal of Canadian Petroleum Technology, v. 27, p. 85–95.

Morrow, N.R., Brower, K.R., Ma, S. and Buckley, J.S., 1990, Fluid flow in healed tectonic fractures: Journal of Petroleum Technology, p. 1310–1318.

Muller, M., Nieberding, F., and Wanninger, M., 1988, Tectonic style and pressure distribution at the northern margin of the Alps between Lake Constance and the River Inn: Geologische Rundschau, v. 77, p. 787–796.

Myal, F.R., and Frohne, K.-H., 1991, Drilling the SHCT well in the Piceance Creek basin, Colorado: Society of Petroleum Engineers paper number 21866, Society of Petroleum Engineers Joint Rocky Mountain Regional Meeting and Low-Permeability Reservoir Symposium, Denver, p. 611–622.

Northrop, D.A., and Frohne, K.-H., 1990, Insights and contributions from the Multiwell Experiment: a field laboratory in tight sandstone reservoirs: Journal of Petroleum Technology, v. 42, p. 772–779.

Perry, W.J. Jr., Grout, M.A., Tang, R.L., and Hainesworth, T.J., 1988, Wedge model for late Laramide basement-involved thrusting, Grand Hobgback Monocline and White River uplift, western Colorado [abstract]: Geological Society of America, Abstracts with Programs, v. 20, p. 384–385.

Plumb. R.A., and Cox, J.W., 1987, Stress directions in eastern North America determined to 4.5 km from borehole elongation measurements: Journal of Geophysical Research, v. 92, p. 4805–4816.

Prats, M., 1981, Effect of burial history on the subsurface horizontal stresses of formations having different material properties: Society of Petroleum Engineers Journal, Vol 21, p. 658–662.

Price, N.J., 1974, The development of stress systems and fracture patterns in undeformed sediments: Proceedings of the 3rd Congress of the International Society of Rock Mechanics, v. 1-A, p. 487–496.

Rathore, J.S., Holt. R.M., and Fjaer, E., 1989, Effects of stress history on petrophysical properties of granular rocks; Proceedings of the 30th U.S. Symposium on Rock Mechanics, p. 765–772.

Salz, B., 1977, Relationships between fracture propagation pressure and pore pressure: Society of Petroleum Engineers paper 6870, Proceedings, 52nd Annual SPE Annual Technical Conference.

Spencer, C.W., 1987, Hydrocarbon generation as a mechanism for overpressuring in the Rocky Mountain region: American Association of Petroleum Geologists Bulletin, v. 71, p. 368–388.

Stearns, D.W., and Friedman, M., 1972, Reservoirs in fractured rock: American Association of Petroleum Geologists Memoir 16, p. 82–105.

Strickland, F.G., and Ren, N.-K., 1980, Prediction the in-situ stress for deep wells using differential strain curve analysis: Society of Petroleum Engineers paper no. 8954, SPE/DOE Symposium on Unconventional Gas Recovery, Pittsburgh, p. 251–258.

Teufel, L.W., 1983, Determination of in-situ stress from anelastic strain recovery measurements of oriented core: Society of Petroleum Engineers paper no. 11649, SPE/DOE Symposium on Low-Permeability Gas Reservoirs, Denver, p. 421–430.

Teufel, L.W., 1980, Strain analysis of experimental superposed deformation using calcite twin lamellae: Tectonophysics, v.65, p. 291–309.

Teufel, L.W., and Farrell, 1990, In situ stress and natural fracture distribution in the Ekofisk Field, North Sea, *in* 3rd North Sea Chalk Symposium, Copenhagen, Denmark, June 11–12: Norwegian Petroleum Directorate and Danish Energy Agency, Joint Chalk Research Program, 33 p.

Teufel, L.W. and Farrell, 1992, Interrelationship between in situ stress, natural fractures, and reservoir permeability anisotropy, a case study of the Ekofisk field, North Sea: Proceedings, Fractured and Jointed Rock Mass Conference, Lake Tahoe, CA, 9 p.

Voight, B., 1974, Stress History and Rock Stress, Proceedings, Third International Congress of Society for Rock Mechanics, Vol.2, pt A, p. 580–582.

Warpinski, N.R., Branagan, P.T. and Wilmer, R., 1985, In situ stress measurements at U.S. DOE's Multiwell Experiment site, Mesaverde, group, Rifle, Colorado: Journal of Petroleum Technology, Vol. 37, p. 527–536.

Warpinski, N.R., 1989, Elastic and viscoelastic calculations of stresses in sedimentary basins: SPE Formation Evaluation, v. 4, p. 522–530.

Warpinski, N.R. and Teufel, L.W., 1989, A viscoelastic constitutive model for determining in situ stress magnitudes from anelastic strain recovery of core: Society of Petroleum Engineers Production Engineering, Vol. 3, p. 272–280.

Warpinski, N.R. and Teufel, L.W., 1989, In situ stresses in low-permeability rocks: Journal of Petroleum Technology, Vol. 41, p. 405–414.

Warpinski, N. R., 1991, Hydraulic fracturing in tight, fissured media: Journal of Petroleum Technology, p. 146–152, 208–209.

Weimer, R.J., 1961, Uppermost Cretaceous rocks in central and southern Wyoming, and northwest Colorado: Wyoming Geological Association, 16th Annual Field Conference Guidebook, p. 17–28.

Woodland, D.C., and Bell, J.S., 1988, In-situ stress magnitudes from mini-frac records in western Canada: Petroleum Society of CIM, paper no. 88-39-67, 39th Annual Technical Meeting, Calgary, p. 67-1 to 67-27.

Zoback, M.L., and Zoback, M.D., 1980, State of stress in the coterminous United States: Journal of Geophysical Research, v. 85, p. 6113–6156.

Zoback, M.L., and 29 co-authors, 1989, Global patterns of tectonic stress: Nature, v. 341, p. 291–298.

APPENDIX A

Wellbore Geometries for Optimum Fracture Characterization and Drainage

(From: Lorenz, J.C., 1992, paper in West Texas Geological Society Bulletin, v. 32, p. 5–8).

Abstract

There are two problems that are rarely considered when drilling a deviated well for the purpose of draining naturally fractured reservoirs: (1) how to intersect enough fractures with the pilot hole to accurately characterize the fracture population; and (2), does reservoir heterogeneity limit vertical permeability, despite fractures, such that a horizontal well provides little benefit in enhanced drainage volume?

The first problem can be addressed with slightly deviated wellbores. A 30-degree deviation from vertical will enhance the probability of intersecting a vertical fracture in a 35-ft thick reservoir by up to 6200%. The optimum 6200% occurs if the wellbore azimuth is oriented normal to fracture strike. However, even if fracture strike is unknown, there is a two-thirds chance of intersecting at least half of this percentage with a randomly oriented wellbore azimuth.

The second problem becomes severe in horizontally laminated reservoirs where fractures are bounded by bedding and where lateral wellbore lengths are limited due to lease lines or small reservoir sizes. In these reservoirs, there is a quantifiable advantage to drilling slant holes with deviations of less than 80 degrees. Increases in reservoir heterogeneity increase the drainage-volume advantage of the short slant hole over that of the horizontal hole. Thus, there is still a need for sedimentary characterization of fractured reservoirs.

Fracture Characterization

The Problem

Vertical to near-vertical fractures do not have a high probability of being intersected by vertical wells. Therefore, the absence of fractures in vertical core does not constrain the possible occurrence of fractures and fracture-dominated production in a reservoir. Conversely, the presence of any fractures in core should be cause to consider the probability that the reservoir contains significant fracture porosity (Figure A1).

An example of this problem is presented by Lorenz and Hill (1991), where 85 ft of vertical core from the Cozzette Sandstone (Upper Cretaceous Mesaverde Group) at the MWX site, Garfield County, Colorado, contains no fractures. However, core from the deviated hole at the same site shows that natural fractures in this reservoir are abundant, with an average spacing of only three ft (Figure A2). The fractures in this reservoir create an increase in permeability of two orders of magnitude, and cause a horizontal permeability anisotropy of between 10:1 and 100:1.

Therefore, if the objective of a pilot well is to characterize natural fractures for the purpose of designing horizontal holes, the probability of intersecting natural fractures in the well must be enhanced.

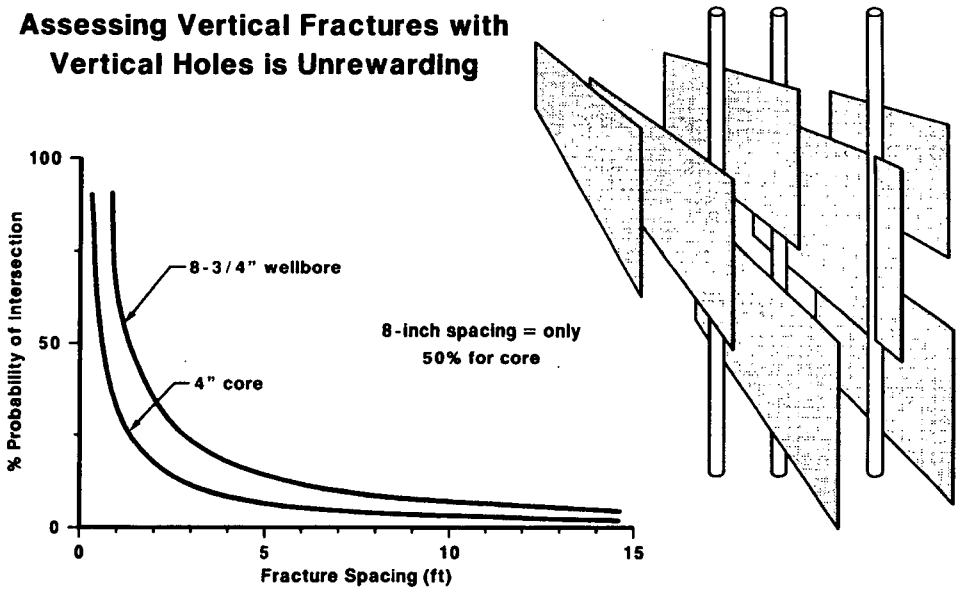

Figure A1. Relationship between fracture spacing and the probability of intersecting a fracture with a vertical hole/core.

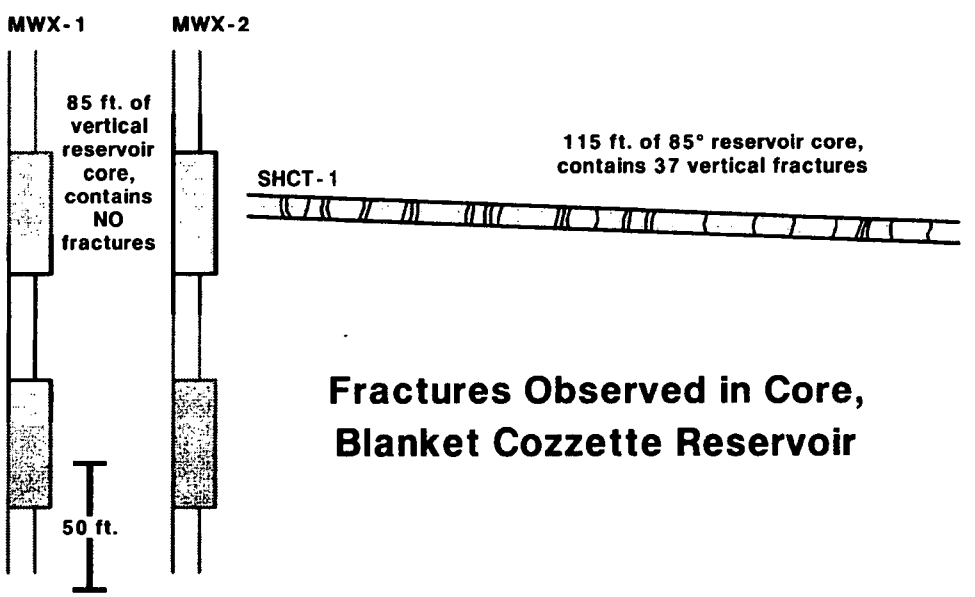

Figure A2. Fractures observed in vertical vs deviated core from the same reservoir at the same site: Cozzette Sandstone Member (Upper Cretaceous Mesaverde Group), Garfield County, Colorado.

One Solution

Relatively small deviations of a wellbore will dramatically increase the chances of fracture intersection. Whereas vertical core typically spans only four inches of reservoir width, the width interrogated by a deviated hole is a function of the tangent of the deviation angle and the reservoir thickness (Figure A3). For example, a hole deviated by 30 degrees in a 35-ft thick reservoir samples more than 20 ft of the reservoir width, for a lateral-interrogation advantage over vertical core of 6200%.

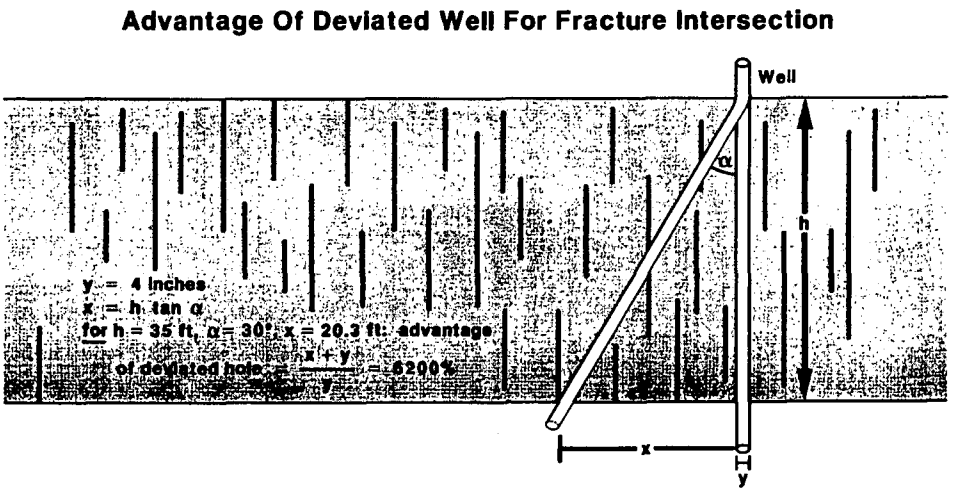

Figure A3. Advantage of a deviated well for fracture intersection.

The advantage of a 30-degree wellbore can also be viewed in terms of how it would compare to the optimum sampling allowed by a 90-degree (horizontal) wellbore. Because the horizontal distance sampled is a function of the sine of the deviation angle, the 90-degree wellbore yields a sampled width of only twice that of the more easily drilled and maintained 30-degree wellbore of the same length (Figure A4).

A bonus in coring a deviated hole is that, in many cases, the expense of a core orientation survey need not be incurred (Lorenz and Hill, 1992). The geometric relationships are such that if the uphole direction and top-hole side of the core can be determined (usually apparent if bedding is present and arguably horizontal), the orientation of fractures can be derived using the standard wellbore survey, which gives wellbore inclination and azimuth (Figure A5). Moreover, there is commonly less ambiguity in distinguishing between natural and coring-induced fractures in deviated core. (Note that Figure 5 shows core from a hole deviated by 60 degrees, but that the same principle works for deviations between about 20 and 85 degrees).

It has been assumed, until this point, that the deviated wellbore azimuth is oriented normal to a known fracture trend (strike). However, if the fracture strike is poorly constrained or even unknown, a deviated wellbore still may offer a considerable advantage over the vertical wellbore. This is because the planview number of fractures hit, expressed as a percentage of the optimum of those that would be hit if the wellbore azimuth was exactly normal to fractures, is a simple sine function of the angle between fracture strike and wellbore azimuth (Figure A6). The distance normal to fracture strike traversed by the wellbore is computed by multiplying the horizontal length of the wellbore by the sine of the angle between its azimuth and the fracture strike. Thus, as the angle decreases from 90 degrees, the rate of fracture intersection efficiency drops off slowly for the first plus or minus 30 degrees. In fact, this efficiency is at least 50% for a sweep of plus or minus 60 degrees, which encompasses two-thirds of the possible directions of drilling. If fracture orientation is known, the azimuth of well deviation should be normal to the fractures. If strike is not known, even a random azimuth is apt to be useful, as shown in Figure A7. Preliminary geologic studies can usually narrow the range of uncertainty.

The percentage of fractures hit by a wellbore will be a function of both the angle between fractures and the wellbore azimuth in the horizontal plane, and the angle of deviation in the vertical plane. It can be quite high even where the angular relationships are not optimum. (If the strata are not horizontal, or the fractures are not vertical, there will be a third geometric factor to consider.) In horizontal strata with vertical fractures, the fracture intersection efficiency is the sine of the angle between wellbore azimuth and fracture strike, times the sine of the angle by which the wellbore is deviated from vertical.

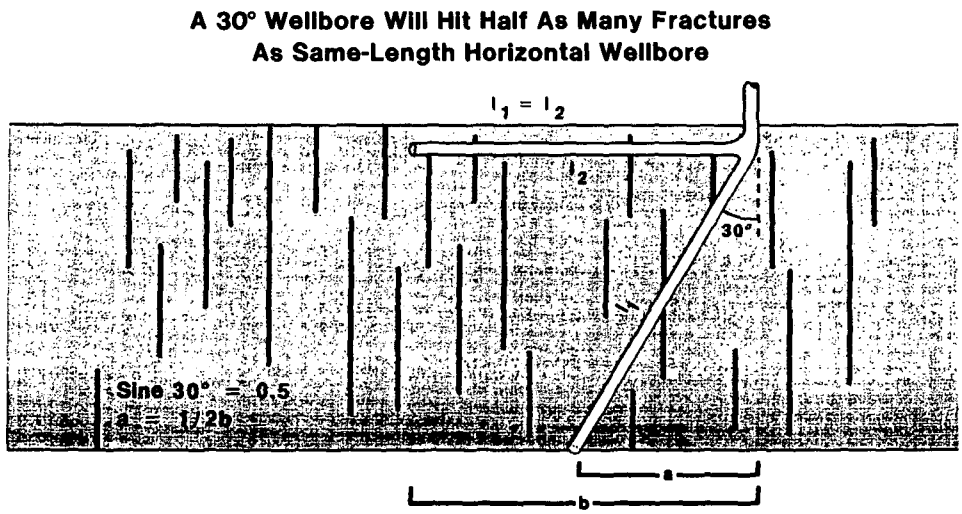

Figure A4. A 30-degree wellbore will hit half as many fractures as a horizontal hole of the same length.

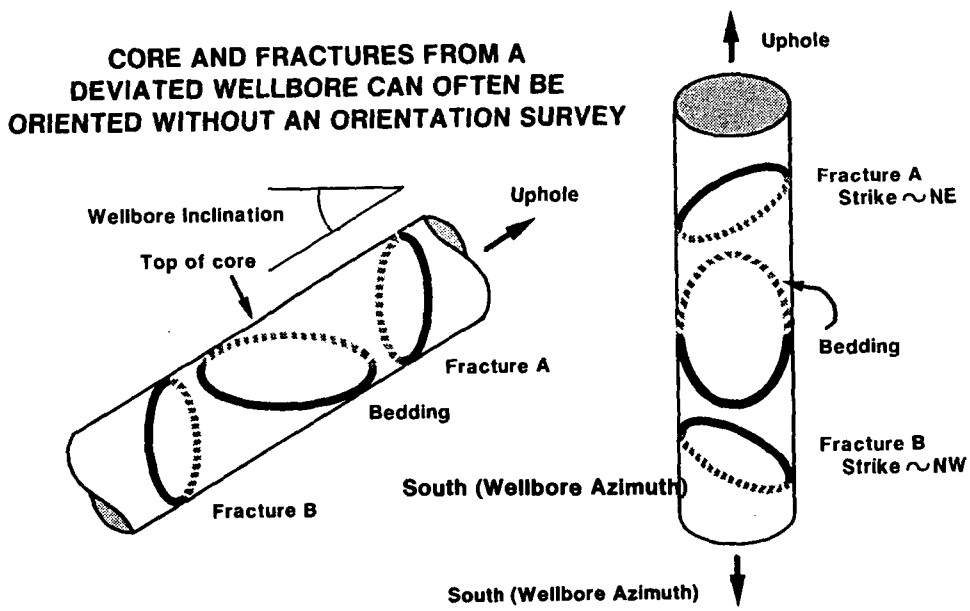

Figure A5. Core and fractures from a deviated wellbore can often be oriented without an orientation survey.

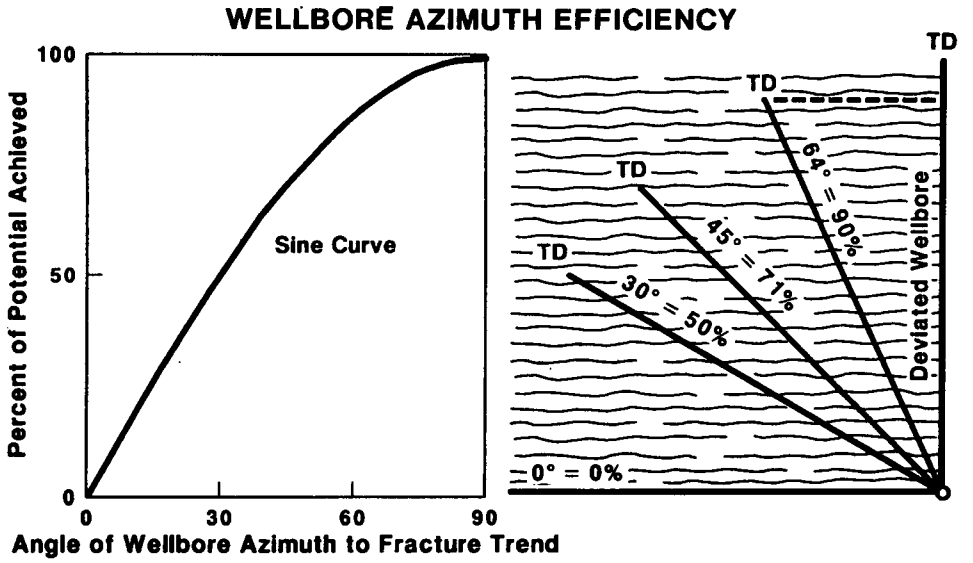

Figure A6. Relationship between a wellbore azimuth and its efficiency in fracture intersection.

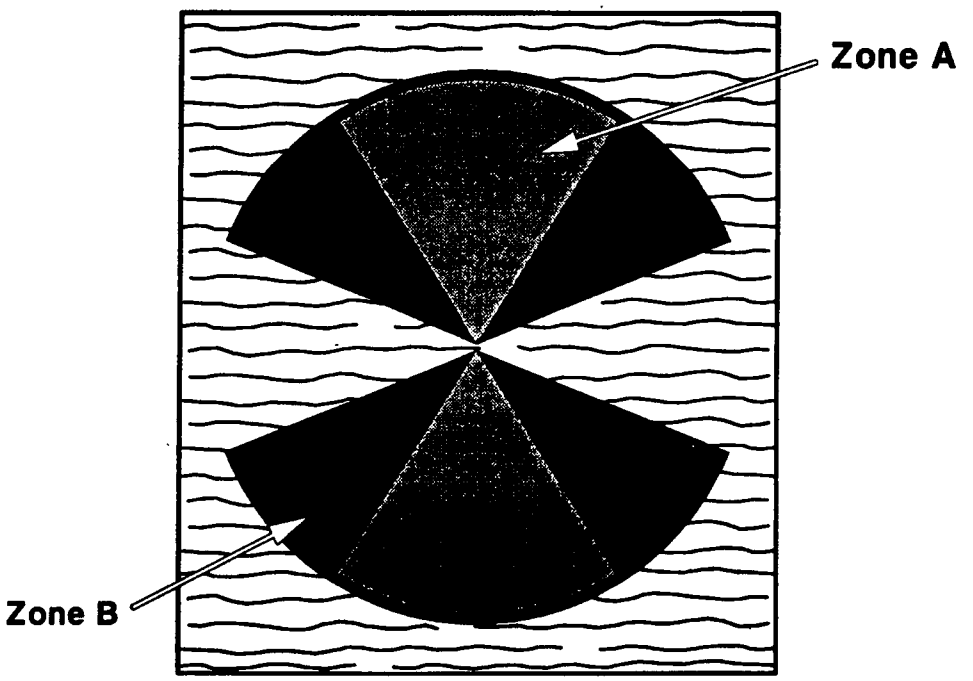

Figure A7. Horizontal wellbore azimuth efficiency (planview). Any wellbore azimuth drilled within zone A (within 30 degrees of normal to the fracture trend) will encounter at least 87% of the fractures that a fracture-normal wellbore would have hit. Similarly, a wellbore drilled anywhere within plus or minus 60 degrees of fracture-normal (zone B) will have at least a 50% fracture-intersection efficiency. A randomly oriented horizontal wellbore azimuth will have a two-thirds chance of having at least a 50% efficiency.

This relationship is advantageous for any deviated wellbore. High percentages of fractures are easy to hit with deviated holes. Where fracture strike is uncertain or unknown, there is an excellent chance of intersecting, and thus characterizing, a large number of fractures with deviated holes. This is a cost-effective approach to obtaining vital information for the design of horizontal wells.

Drainage Efficiency of Deviated Holes in Heterogeneous Reservoirs

Once a reservoir fracture system has been characterized, production considerations may dictate an optimum wellbore geometry. If the fractured reservoir is otherwise homogeneous, with unlimited vertical drainage, increasing deviations from vertical access more and more of the reservoir, with an unlimited-length horizontal wellbore being the most desirable (Joshi, 1988). However, reservoir heterogeneity commonly restricts vertical communication, even in fractured strata, and drainage efficiency suffers accordingly.

For a vertical well in a homogeneous but fractured reservoir, the drainage volume is limited only by the lateral permeability and radius of drainage. For simplicity, this is considered only in two dimensions, and the "area" of drainage ("A") will be used as the standard of comparison: i.e., drainage from hypothetical reservoirs described here will be presented as a percentage of "A" (Figure A8). For example, a deviation of 45 degrees allows drainage from a similar radius on either side of the well, but also accesses the area within the reservoir that is traversed by the well, and the drainage area is 225% of "A." (Addition of the third dimension will change the results by a constant figure that is the length of the drainage radius in that third dimension, along the natural fracture trend).

Once barriers to vertical permeability are inserted into this idealized, hypothetical reservoir, the improvement in drainage area created by a deviated hole is diminished, because there are now areas (compartments) above and below the wellbore that are no longer easily drained (Figure A9). With two beds, a 45-degree hole provides only 163% drainage, and with five beds, drainage is diminished to 125%.

Increasing the wellbore deviation increases drainage efficiency, the addition of bedding discontinuities offsets this advantage at a rapid rate (Figure A10).

Unfortunately, more numerous permeability barriers/lithologic discontinuities also decrease the efficiency of a horizontal hole. A single bed bisecting the reservoir decreases the immediate drainage by half. If there are five beds and only one is accessed by the horizontal hole, drainage as a percent of "A" still increases dramatically with the length of hole in the reservoir, but the area not drained increases four times as fast (Figure A11). If there are 10 beds, the situation is that much worse.

For limited-length wellbores in heterogeneous reservoirs, slant holes offer an advantage in drainage area over horizontal holes (Figure A12). With five beds, 400% of "A" is achieved with a 610-ft, 85-degree slant hole. The same length horizontal hole in this reservoir yields only about 300% of "A." To achieve 400% with a horizontal hole, the hole must be 760 ft long. The more heterogeneous the reservoir, the longer a horizontal wellbore must be to equal the drainage efficiency of a slant hole.

Additional Drainage from Slant Hole in Homogeneous Reservior

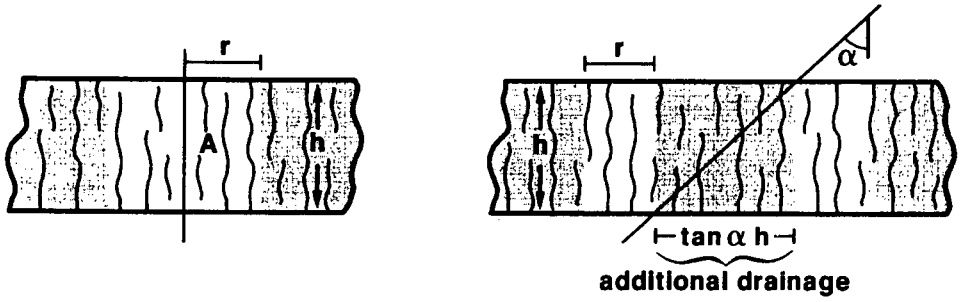

Vertical Well:
Drainage = 2rh = A
= Standard, or 100%

Deviated Well:
Drainage = 2rh + tan α h • h

Figure A8. Additional volume can be drained from a slant hole in a homogeneous reservoir.

Reservoir Heterogeneity Reduces Advantage of Slant Hole

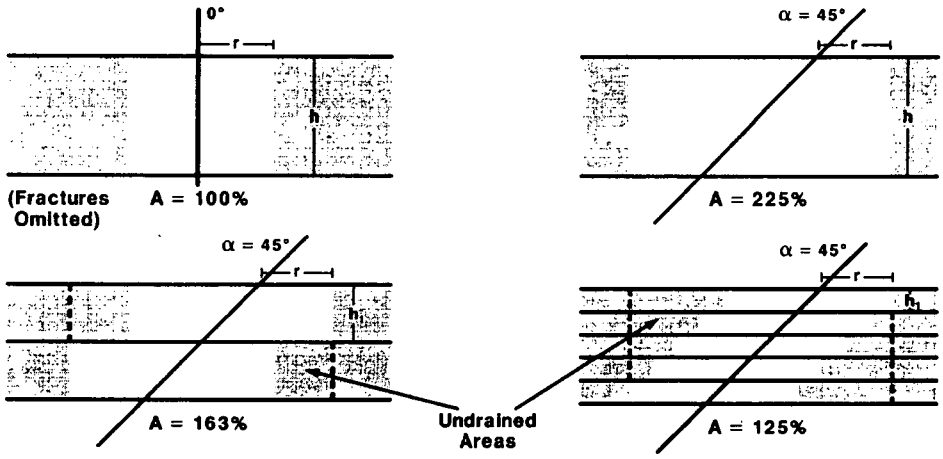

$$\left(\% \text{ of } A = \frac{(2rh) + (\tan \alpha\ h_i \cdot h_i)(\text{No. Beds})}{2rh} \cdot 100\right)$$

Figure A9. Reservoir heterogeneity reduces the advantage of a slant hole.

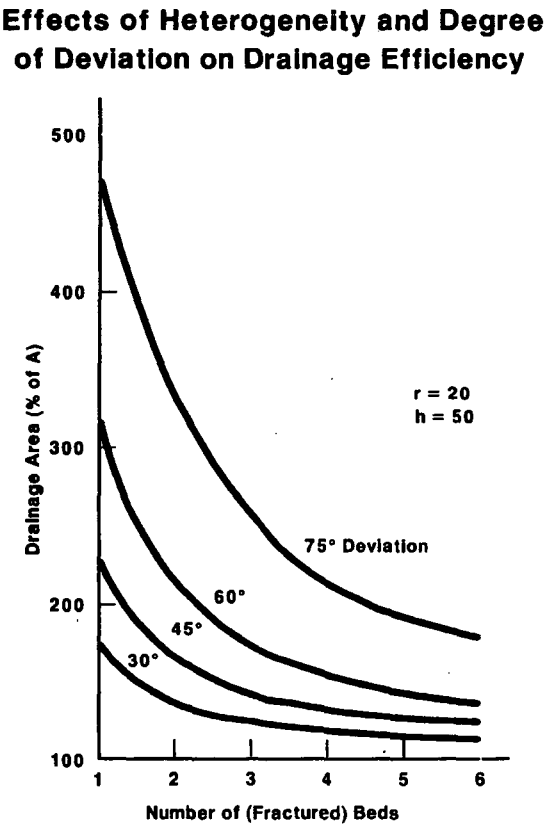

Figure A10. Relationship of reservoir heterogeneity and wellbore deviation to drainage efficiency.

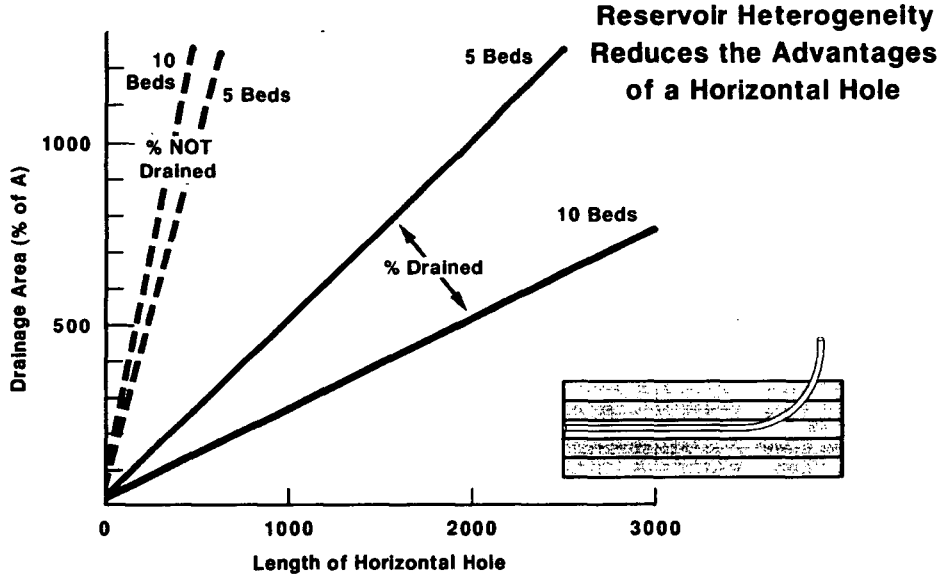

Figure A11. Relationship of reservoir heterogeneity to drainage efficiency for a horizontal hole.

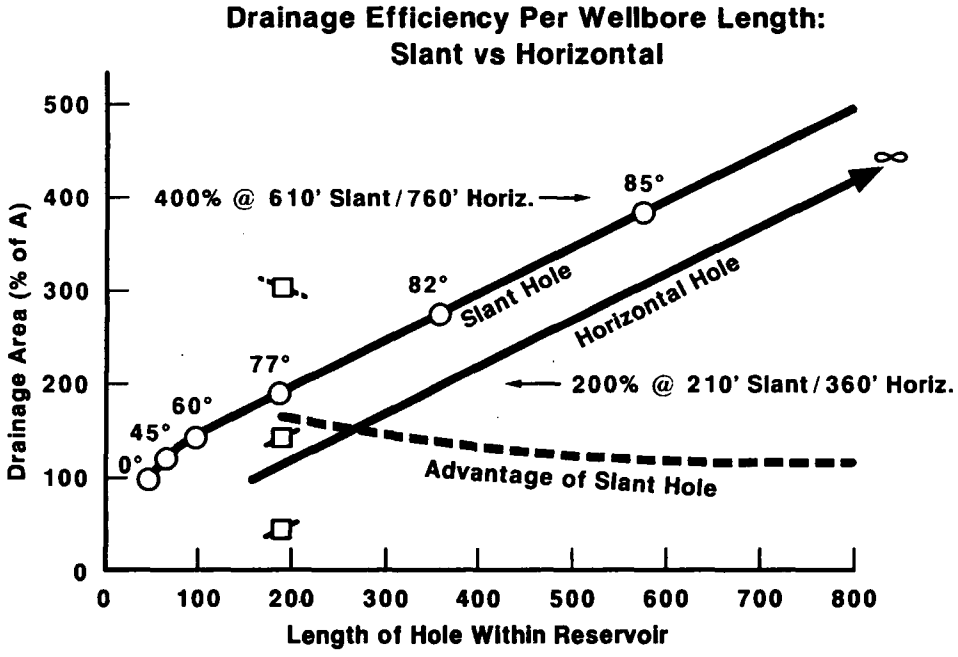

Figure A12. Comparison of the drainage efficiency per wellbore length for slant and horizontal wells in a reservoir with five hypothetical permeability discontinuities. Note that the difference between slant and horizontal hole efficiency is significantly greater for a ten-bed configuration (boxes).

Conclusions

Slightly deviated pilot holes will significantly increase the chances of intersecting and characterizing vertical and near-vertical natural fractures, thereby improving the data base for a horizontal well design. Although initially it may be more costly to deviate a pilot hole, it would be a waste of money to drill a vertical hole that does not intersect fractures if that is the purpose of the hole.

Slant wellbores should be considered when fractured reservoirs are heterogeneous, especially where the length of a horizontal lateral is limited due to lease or reservoir size. A slant well may also offer a greater probability that, given time, the relatively inaccessible compartments of a reservoir will be drained through lateral permeability restrictions, because they are commonly more permeable than vertical restrictions.

References

Joshi, S.D., 1988, Augmentation of well productivity with slant and horizontal wells: Journal of Petroleum Technology, v. 44, p. 729–739.

Lorenz, J.C., and Hill, R.E., 1991, Subsurface fracture spacing: Comparison of inferences from slant/horizontal core and vertical core in Mesaverde reservoirs: Society of Petroleum Engineers, paper number 21877, Proceedings of the Rocky Mountain Regional Meeting and Low-Permeability Reservoirs Symposium, Denver, CO, April 15–17, 1991, p. 705–716.

Lorenz, J.C., and Hill, R.E., 1992, Measurement and analysis of fractures in core; *in* Schmoker, J.W., Coalson, E.B., and Brown, C.A. (eds.), Geological studies relevant to horizontal drilling: Examples from western North America: Rocky Mountain Association of Geologists, p. 47–59 (see appendix B of this report).

APPENDIX B

Measurement and Analysis of Fracture in Core

(From: Lorenz, J.C., and Hill, R.E., 1992, paper in Geological Studies Relevant to Horizontal Drilling: Examples from Western North America, J.W. Schmoker, E.B. Coalson, and C.A. Brown, eds.; Rocky Mountain Association of Geologists, p. 47–59).

Abstract

Optimum analysis of natural fracture characteristics and distributions in reservoirs requires conscientious supervision of coring operations, on-site core processing, careful layout and marking of the core, and detailed measurement of fracture characteristics. Natural fractures provide information on the in situ permeability system, and coring-induced fractures provide data on the in situ stresses. Fracture data derived from vertical core should include fracture height, type and location of fracture terminations with respect to lithologic heterogeneity, fracture planarity and roughness, and distribution with depth. Fractures in oriented core from either a vertical or a deviated well yield information on dip, dip azimuth, strike, mineralization, and the orientation of fractures relative to in situ stresses. Only measurements of fractures in core from a deviated/horizontal well will provide estimates of fracture spacing and fracture porosity. These data can be graphed and cross-plotted to yield semi-quantitative fracture characteristics for reservoir models. Data on the orientations of fractures relative to each other in unoriented core can be nearly as useful as the absolute orientations of fractures.

Introduction

Published detailed characterizations of fractures in core are not common, since non-proprietary data bases that are large enough to allow a reasonable characterization of a 3-D, in-situ fracture network are rare. When data are available, important parameters have often been left unmeasured, and analyses often omit important relationships such as fracture orientations with respect to each other in unoriented core, and fracture distribution with respect to sedimentary heterogeneity. We offer here a set of descriptions and measurements of fractures in cores that illustrate different "nuts and bolts" techniques for relatively complete measurements of fractures from vertical and deviated wells. We further suggest how the data derived from these techniques may be analyzed for the characterization of a fracture system.

Several prominent references precede this paper: Kulander et. al. (1979, 1990), and Norman and Garrett (1988) list criteria for making the critical distinction between natural fractures and fractures that are artificially induced by the coring and handling processes, and offer excellent descriptions of the types of fractures in core. Skopec et. al. (1990; in press), and Nelson et. al. (1987) describe core handling procedures, and the process for correlating oriented core with an orientation survey. In this paper, we recommend several additional steps for processing core for fracture analysis.

Several methods have been offered for converting fracture measurements in vertical core to fracture spacing (Lerche and Narr, 1986; Aguilera, 1988; Narr, 1991). These techniques assume a relatively regular fracture distribution in evenly bedded strata, whereas fractures commonly occur in irregular swarms (e.g., Laubach, 1991), and are irregularly distributed within heterogeneous reservoirs (Lorenz and Hill, 1991). Other references, such as Van Golf-Racht (1982), approach fractured reservoirs from the petroleum engineer's point of view, and build fractured reservoir models around idealized fracture characteristics. More often than not an engineer can and does take the mere fact that fractures are present, modified perhaps by data on fracture orientation, to model reservoir production. It may not be possible to quantify heterogeneous fracture distributions into absolute terms usable by a reservoir engineer, but a useful, working, semi-quantitative characterization of fractures can be constructed if enough core is available.

Much of the fracture-characterization problem derives from the fact that core data are one-dimensional and usually vertical. Moreover, vertical fractures are hard to intersect, and therefore hard to characterize, with vertical core. However, data from one- dimensional core can be analyzed, and, within limits, turned into a concept of the three-dimensional fracture distribution. We present examples of fractures in core from vertical, horizontal, and moderately deviated wells, that show which types of fracture information and measurements can and cannot be derived from each type of core, and compare their value for fracture characterization.

Our most complete example is from the Piceance basin, northwestern Colorado. At this site, 4200 ft (1280 m) of vertical core containing 275 vertical-extension fractures, 236 ft of 60°-from-vertical core containing 28 fractures, and 115 ft of near-horizontal core containing 37 fractures were taken from the Upper Cretaceous Mesaverde Formation from the U.S. Department of Energy's Multiwell Experiment (MWX) and Slant Hole Completion Test (SHCT) wells (Lorenz and Hill, 1991). These projects were designed to assess and develop technologies for recovery of natural gas from low-permeability reservoirs (Northrop and Frohne, 1990; Myal and Frohne, 1991). The sandstone reservoirs in this formation at this site would have sub-microdarcy in situ permeabilities, and would be unproducible, without the pervasive natural fracture system that is present in the sandstones (Lorenz et. al., 1989). The fractures at this site are irregularly spaced, unidirectional, regional fractures, created by basin-wide dilatancy of the strata during horizontal compression rather than by flexure (Lorenz and Finley, 1991). The abundance of core from wells of different deviations at this site has allowed a greater degree of subsurface fracture characterization than would normally be possible, but this example points the way toward analysis of fractures in wells where less core is available.

Coring, Processing, and Preliminary Measurements

Monitoring Coring Operations

Significant information on core condition and fracture character can be obtained by on-site monitoring of coring operations. If this is not possible, such information (though without as much detail), can sometimes be gleaned from the coring engineer's report, the geolograph, and the mud log. High or erratic torque is often used as evidence of fractured formations, but may also indicate points of correlation between rubbleized sections of the core and breaks in the orientation survey record. Abrupt increases in pump pressure or weight-on-bit may induce fractures in the core, and knowing the exact depths of such increases may help determine whether an otherwise ambiguous fracture in the core is natural or induced. At the very least, the depth at which the drill-pipe connections were made during coring should be noted, as these are often associated with spinoffs in the core and abrupt scribe rotations, and are therefore useful in determining whether the orientation of a fracture

in one piece of core can be compared with that in another piece, or whether a discontinuity exists in the core between them.

Core Processing Procedures

Core processing can be divided into four different activities: 1) recovery, 2) layout, reassembly, and marking, 3) description and measurement, and 4) packaging. Aspects of the procedures for layout, and for recovery and packaging have been discussed by Skopec et al. (in press) and description and measurement are described by Kulander et al. (1990). We suggest several additions to these procedures, and emphasize that steps 2 and 3 can and should be performed, at least in a preliminary fashion, at or near the wellsite. The benefits of so doing usually outweigh the logistical difficulties of field processing. The cost of a coring operation begs for maximized data acquisition.

Importance of Field Processing

There is a trend toward the use of liners in core barrels, especially in formations that are prone to jam the barrel during coring. While this may improve core recovery, it also removes the geologist one step from the raw data since the geologist usually does not examine the core until it is shipped to the laboratory and therefore is rarely on site during coring. The locations of incipient jamming, increased bit weight or revolutions per minute, or other events that can affect the condition of the core are rarely recorded by on-site personnel.

A significant loss of data also occurs with each successive manipulation of the core, as pieces of rubble are discarded, pieces of core become inverted, samples (and souvenirs) are removed, and additional breakage of the core, especially across fractures, occurs. Thus, logging of core for fractures is increasingly difficult after each handling procedure, and is especially frustrating if the core has been extensively sampled for other analyses. This is because all of the core is significant for fracture logging: lengths of unfractured intervals are important to measurements of fracture spacing, and even rock chips with fracture-face mineralization in rubble zones yield data on the presence and location of fractures.

When core is slabbed, some of the smaller fractures are often revealed, but the advantage of waiting to log fractures until after slabbing is usually outweighed by the loss of information during slabbing. Information is lost due to (1) additional breakage and removal of core, destroying core continuity and decreasing the potential for comparison of the relative orientation of fractures, and (2) the significantly smaller volume of rock that is left for examination in the slabs. However, the logging of fractures in unslabbed core requires that the entire core surface be carefully inspected.

The location and nature of fracture terminations are also important, but cannot be determined if critical pieces of core have been lost or sampled. Fracture width cannot be measured in horizontal core if a core sample with a fracture face on one end has been removed. Unfortunately, horizontal core often breaks at fractures, and these end pieces are commonly the ones taken for samples. Unless stringent operating procedures are followed, under strict wellsite supervision, core data will be lost. To minimize this, core should be cut in an unlined, standard core barrel if possible (not likely if the strata are highly fractured) or else the core from core-barrel liners should be processed in the field before significant data loss occurs.

Another advantage of field processing is that it allows problems with orientation and coring equipment to be corrected between core runs. Murphy's Law tends to be especially applicable to most wellsite operations, and the value of field processing and monitoring cannot be overemphasized.

Further checks on orientation quality can be made after the fracture orientation data have been collected. For example, a plot of fracture strike with depth can be used to cross check the orientation survey: if fractures have consistent orientations within each core run, but the trend varies from run to run, one or more of the orientation surveys may be suspect.

Core Recovery, Layout, and Marking Procedures

Fracture measurement cannot begin until the core has been removed from the core barrel, laid out, the core pieces reassembled as accurately as possible, and the appropriate markings made for footage, orientation, and uphole direction.

1. Core Recovery: Core damage can be avoided when using a conventional (unlined) barrel by laying the barrel down on the wellsite pipe rack and pumping the core out hydraulically with a high-pressure, low-volume pump. A rubber plug should be inserted in the barrel to prevent water from contacting the core. Except where the core is highly fractured and wedges itself in the barrel, it can be slowly pumped out into numbered trays. This procedure avoids the damage to the core that is commonly associated with the sledge-hammer/gravity-feed removal method on the rig floor, and preserves the smaller pieces of core, along with their orientation, allowing long intervals of continuously-fit core to be reassembled.
2. Core Layout: Layout and reassembly of the core pieces as much as possible are critical steps in orienting any core, since the strength of a data set is proportional to the length of the intervals of continuous fit. Even if core is not oriented, it should be processed as though it were, because cores can often be oriented after they have been cut and because the relative orientations of fractures to each other are useful.
3. Marking for Orientation: The basic procedures for orienting core have been published (e.g., Bleakly et. al., 1985; Nelson et. al., 1987; Skopec et. al., 1990). We elaborate here on the technique for deriving fracture orientations from oriented core. Oriented core has three grooves scribed into the core surface as it is cut, with two lines close together and an isolated line on the opposite side of the core. The isolated scribe is called the Principal Scribe Line (PSL); its orientation relative to true north is recorded by the core orientation survey.

Because of the rotation of the bit, the scribe lines commonly drift clockwise downhole, despite the bearing assembly designed to decouple the inner core barrel from the rotation of the outer core barrel. For this reason, a straight, artificial Master Orientation Line (the MOL) is useful (1) for comparing the relative orientations of features in the core, and (2) as an oriented reference point (with respect to the oriented PSL, and thus to true north) for calculations of true fracture orientations. The MOL is marked on the core, after the core is laid out and fit together, as follows: at the uphole end of each continuous-fit section of core pieces, the core is rotated so that the PSL is at the "top" of the core. A pipe-welder's level helps to position this line at the exact top. A chalk line is snapped along the top of the core, and is then scribed by hand and marked in blue. Red and black lines are marked on either side of the MOL, with the red on the right side of the MOL looking uphole, to prevent pieces of core from becoming inverted.

Thus the core is marked with both a rotating PSL (usually green) and a straight, blue MOL. The MOL is most useful for comparing relative orientations of fractures within each continuous-fit interval and for absolute fracture orientation. The MOL is re-set to coincide with the PSL at each rubble zone, spinoff, or other core discontinuity. Knowledge of where the connections and bit rotation-speed changes were made during coring, and the continuity of the orientation survey, can aid in determining whether the PSL and MOL were continuous through these discontinuities, and whether a feature to be oriented correlates to an orientation-survey data point located above or below the discontinuity.

Once the core is marked, the first measurement to make is the angular deviation of the PSL from the MOL with depth. The deviation of the PSL from the MOL should correlate with the changes in magnetic toolface orientation reported by the orientation survey (Bleakly et. al., 1985, Skopec et. al., 1990). If a significant discrepancy exists between the two, or if the PSL rotates more than 10–15°/ft (so that the common plus-or-minus one-foot depth correlation uncertainties between core and the survey cause significant orientation uncertainties), then absolute-orientation calculations for fractures may be worthless.

Measurement of Fracture Dip and Strike

Fracture dip and strike in core can be most accurately measured with an electromagnetic goniometer, but adequate preliminary results may be obtained with a dime-store protractor, or, preferably, with a 0–360° annular protractor with an inside diameter equal to the core diameter. To measure the relative orientation of fractures, the MOL is used as a 0° reference point, with the true azimuth of the MOL added to the measured orientations later to obtain true fracture orientation.

Dip angle may be approximated with a protractor aligned with the core axis. If the fracture extends diagonally through the core, dip angle may be also obtained from the arc tangent of the height of the fracture along the core axis divided by the core diameter. Apparent dip angle must be corrected for hole deviation in non-vertical wells, which requires oriented core. Where fractures are not vertical, measuring dip azimuth resolves a possible 180° ambiguity in dip direction that is present if only fracture strike is measured, and which would mask the difference between a set of parallel inclined fractures, and two sets of opposite-dipping inclined fractures with the same strike.

The strike of fractures in core can be calculated several ways:

1. In vertical core, obtain the angle from the MOL to each intersection of the fracture with the core surface ($\alpha 1$ and $\alpha 2$, Figure B1), measured counter-clockwise looking down-core. If the fracture dips, these angles must be measured at two different depths along the core axis, and the distance between the measurement points recorded (Figure B2). With these 5 measurements, the relative strike and dip of the fracture can be calculated using the equations shown on Figure B2. True strike is obtained by correcting for deviation of the MOL from the PSL and for the true orientation of the PSL.

2. For vertical core, the relative fracture strike may also be taken as 90° to the line estimated normal to the fracture plane and bisecting it midcore, with the position of that line measured clockwise from the MOL with a protractor. Degrees on the protractor must increase clockwise looking down-core. (If the fracture dips with respect to the core axis, strike is 90° to the uppermost or lowermost intersection of the fracture with the core surface). True fracture orientation is then derived by adding the MOL and PSL deviation components. Alternately, the PSL can be aligned directly against its true orientation value on the circular protractor, and the true orientation of the line 90° to the fracture can be read directly (Figure B3), provided that the core depth can be accurately correlated to the orientation survey depth.

3. The orientation of a fracture relative to the core axis in deviated core is measured in the same manner, but the orientation must then be reoriented by means of a stereonet (e.g., Ragan, 1973), or a computer program. In core from a deviated hole, the orientation survey gives the position of the PSL in degrees clockwise (looking downhole) from the "high side" or roof of the hole, not its position relative to true north. This position must be geometrically combined with the true azimuth and dip of the core axis provided by the wellbore survey to provide a 3-D framework for reorienting the fractures.

Geometric relationships useful for this process include: (1) An originally horizontal reference plane (pre-coring/in situ orientation) may be demarcated on the core by bedding if the strata are horizontally laminated (Figure B4) but otherwise must be reconstructed from the PSL orientation survey and the wellbore deviation survey. This plane will cut the deviated core with an apparent angle of dip, measured relative to the core axis, equal to the deviation of the well from vertical. (2) The apparent dip azimuth of this plane (relative to the core axis) will be parallel to the wellbore azimuth, and the downhole end of the plane terminates on the high side of the core. (3) The strike of this plane relative to the core axis is the horizontal axis for rotating the core back to its in situ position.

4. For a rough, field estimation, fracture orientations in deviated core can be estimated with a protractor if the core is held in the appropriate in situ position with sand bags. The core position is based on the wellbore orientation survey, and bedding or the PSL orientation. The geometry of this method may be visualized in Figure B4: bedding and/or the core orientation survey define the top of the core and its uphole direction, while the wellbore survey provides core-axis dip angle and azimuth.

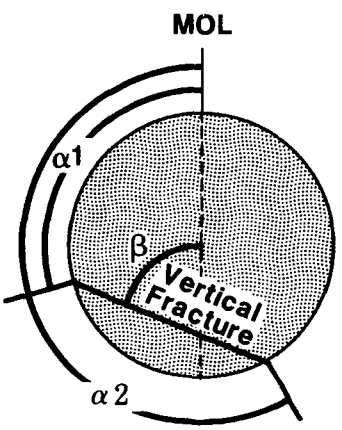

View is looking down on core

The strike (β) can be calculated:

$$\beta = \tan^{-1}\left(\frac{\sin\alpha_2 - \sin\alpha_1}{\cos\alpha_1 - \cos\alpha_2}\right)$$

Figure B1. Schematic of core cross-section, showing the angles to be measured, and the formula for converting the angles into strike relative to the MOL, for fractures in vertical core. MOL is the Master Orientation Line, β is the strike angle relative to the MOL, $\alpha 1$ and $\alpha 2$ are the angles between the MOL and the two edges of the fracture on the core surface.

Case 1

Dip = 90 - Φ where

$$\Phi = \tan^{-1}\left[\frac{\frac{d}{2}\left\{1 - \cos\left(\frac{\alpha 1}{2}\right)\right\}}{L}\right]$$

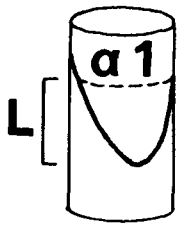

d = core diameter and must be in the same units as L

Case 2

Dip = 90 - Φ where

$$\Phi = \tan^{-1}\left[\frac{\frac{d}{2}\left\{\cos\left(\frac{\alpha 2}{2}\right) - \cos\left(\frac{\alpha 1}{2}\right)\right\}}{L}\right]$$

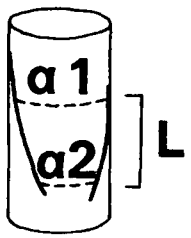

Figure B2. Diagrams of fractures in core, showing the angles to be measured between the intersections of a fracture on a core surface ($\alpha 1$ and $\alpha 2$), and the formula for converting the angles into fracture dip angle with respect to the core axis for two cases: Case 1: The dip can be calculated with one strike measurement and the distance from the angle to the apex of the fracture trace (L) if the fracture exits the core; Case 2: Dip can be calculated by measuring two angles and the vertical distance between them (L).

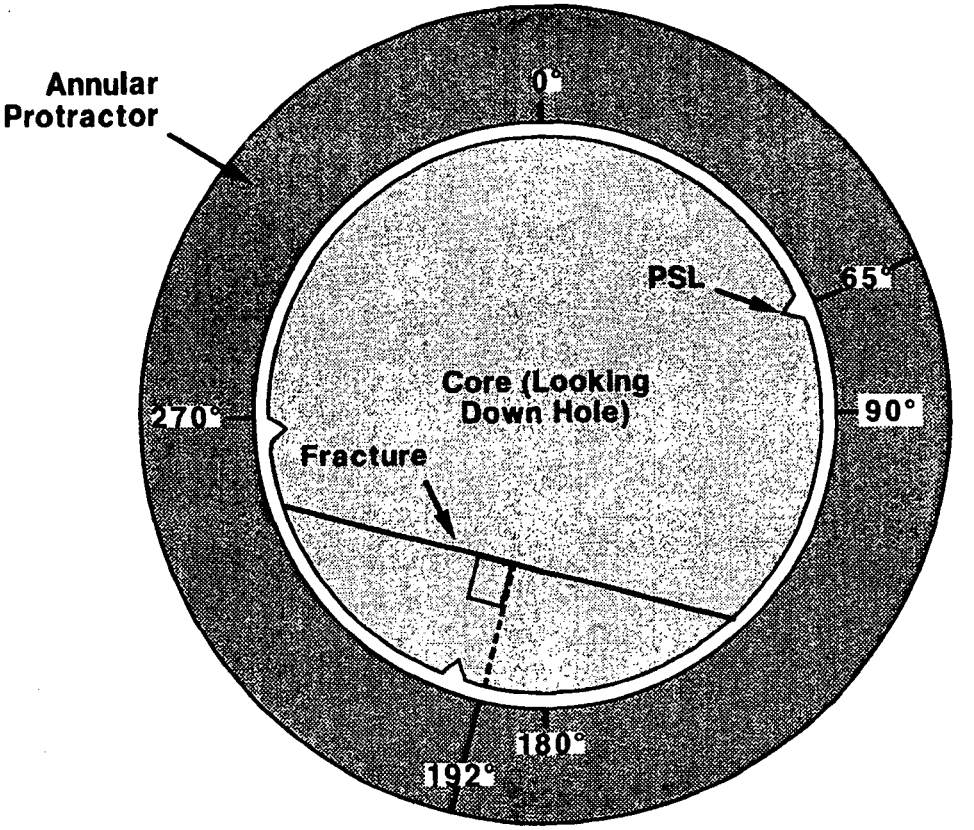

Figure B3. Schematic of core cross section and annular protractor: Fracture strike in the core can be read directly, *if* the orientation survey is good and *if* the scribe rotation is minimal, as follows: (1) the principal scribe-line groove (PSL) is aligned on the protractor with its true orientation at that depth, provided by the orientation survey, of 65°, (2) an imaginary line normal to the midpoint of the fracture at that horizon is measured at 192°, and (3) true fracture strike is calculated as 90° from the imaginary line, at 102°. Fracture strike can be read from its direct intersection with the protractor **only** if it exactly bisects the core.

However, if scribe rotation is a significant factor, more precise measurements are obtained as follows: zero on the protractor is aligned with the PSL, and relative fracture strike read from the imaginary 90° line to the fracture; thus 127° minus 90° equals 37°. The true PSL orientation is then added to the relative strike to give true strike: 37° plus 65° equals 102°. This becomes slightly cumbersome whenever sums exceed 360°, and this method requires that the depths of the orientation survey be correlated exactly with equivalent depths of the core, for which a PSL-deviation-from-MOL diagram must be made (see Skopec et al., 1990), and compared to the orientation-survey deviation.

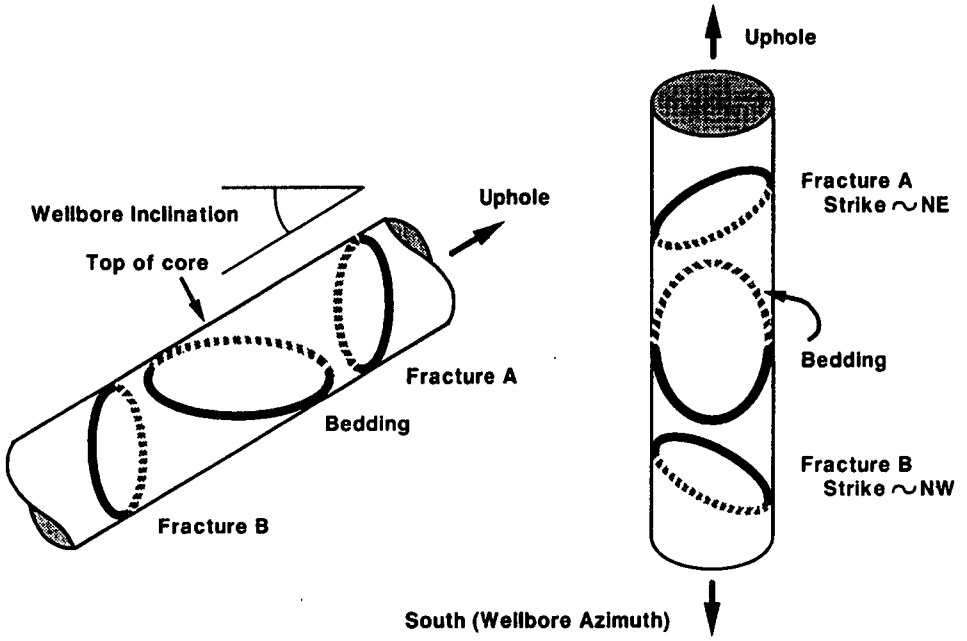

Figure B4. Diagram showing two views of fractures in the same piece of core, and portraying (1) how a rough, field measurement of fracture orientation may be obtained, and (2) how core from a deviated well may sometimes be oriented without an orientation survey. The latter technique requires that bedding is sufficiently planar and horizontal to indicate the top of the core, that the uphole direction of the core is known (an asymmetric scribe shoe is valuable here), and that the wellbore azimuth and deviation for the cored interval are available from a wellbore survey.

Orienting Unoriented Core

Unoriented core can be oriented after the fact in some cases, by comparing features indicative of the in situ stress orientation that may be present in both the unoriented core and in oriented downhole logs. If an oriented four-arm caliper log has been run in the hole, and if it shows definitive breakouts indicating anisotropic horizontal stresses, the borehole elongation will commonly trend normal to the strike of stress-controlled, coring-induced scribe-line, petal, and petal-centerline fractures. If no petal fractures are present, other stress-identification techniques may apply. Anelastic Strain Recovery (ASR) or Differential Strain Curve Analysis (DSCA) measurements must be made on the core immediately after it is removed from the core barrel, but laboratory measurements of acoustic velocity anisotropy may be made on core years after it was cut (e.g., Strickland and Ren, 1980; Teufel, 1983). All of these tests are designed to indicate the orientation of the principal horizontal stress, and thus the core can be oriented relative to the stress directions indicated by breakouts. Similarly, features recognized in both core and oriented wellbore-image logs may correlated and used to orient core, as discussed later.

Paleomagnetic core orientation may be used to orient small segments of core where fractures occur, long after the core has been collected (Van Alstine et. al., 1991). A disadvantage is that numerous plugs must often be taken from a short interval of core.

Descriptions of Fractures in Core from Vertical Wells

Vertical core provides the most commonly available data base for characterizing fractures. In fact, it is common to attempt to assess the fractures in a formation by drilling and coring a vertical pilot hole prior to drilling a horizontal well (Skopec, 1991). When fractures are intersected in this way, significant data are obtained. A list of fracture parameters that can and should be measured in core in order to characterize fracture permeability systems is given in Table B1.

Table B1. Fracture Parameters that Should Be Measured in Core

- Host Lithology:
  - type and thickness
  - number and type of sedimentary heterogeneities
- Depth of Fracture and Position within Bed:
- Vertical Fracture Terminations:
  - location and character
  - relationship to sedimentary heterogeneity
  - relationship to core surface
- Fracture Height in Core:
  - note if minimum due to fracture exiting core
  - note if minimum due to missing core
- General Fracture Character:
  - single, en echelon, anastamosed, etc.
- Type of Fracture:
  - direction of separation/offset
- Strike and Dip (Dip Azimuth):
  - absolute (if possible)
  - relative to other fractures and stress indicators (if not)
- Spacing between Fractures:
- Mineralization:
  - type
  - character (crystal size, amorphous, slickencrysts, etc.)
  - percent of fracture filled
- Total and Remnant Fracture Width:
  - character of remnant porosity
- Surface Ornamentation Beneath Mineralization:
  - slickensides, plumose structure, etc.
  - planarity
  - orientation of linear features
  - orientation relative to fracture plane
- Number of Fracture Sets:
  - relationship to nearby fractures (abutting, crossing, etc.)

Unfortunately, the probability of intersecting vertical fractures with vertical core is not high. In the simplest case, where one set of evenly spaced fractures is present, the probability of encountering a fracture is the ratio of the core diameter (or borehole diameter when using logs) to fracture spacing. Thus, even if fractures are only eight inches apart, the probability of coring a fracture with a four-inch diameter core is only 50%. This probability decreases rapidly as fracture spacing increases (Figure B5).

Drilling-induced fractures are common in vertical core, and the strike of induced petal and petal-centerline fractures supplies an important measure of the in situ stress orientation (Kulander et. al., 1990; Lorenz et. al., 1990). This type of fracture must be distinguished from natural fractures, and the petal fracture strike should always be measured, if only relative to the strike of adjacent natural fractures. This relationship is important because hydraulic stimulation fractures will parallel the principal horizontal stress, and therefore the angular relationship between stimulation fractures and natural fractures, as well as the probability of a natural fracture set being open or closed at depth, may be predicted.

Characteristics Measurable Only in Vertical Core

Fracture planes that parallel the axis of the core (vertical fractures and vertical wells) provide some types of information that are important, but that are not available from horizontal wells. Specifically, vertical core allows for the measurement of fracture heights (Figure B6a, b, and c), and for the locations and types of fracture terminations (Figure B7). For regional fractures, such as those in the heterogeneous Mesaverde reservoirs in the Piceance Basin, fracture heights are commonly less than gross bed thickness because they are limited by the numerous internal sedimentary heterogeneities. Fractures are also commonly limited by ductile reservoir-bounding strata.

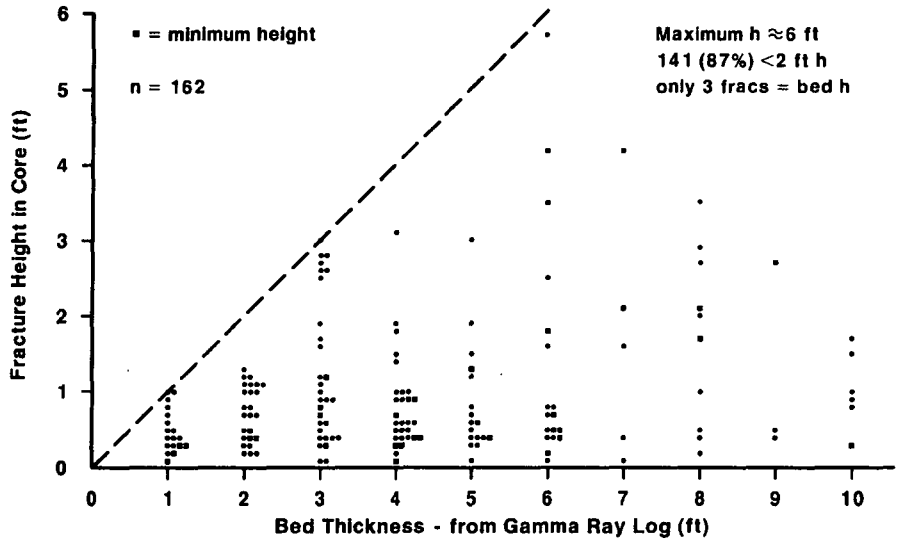

a. Individual fracture height in core as a function of bed thickness for sandstone beds no more than 10 ft thick. "Minimum height" indicates that the total fracture height is unknown due to missing core or other factor. Dashed line indicates the 1:1 bed thickness to fracture height ratio that is rarely attained.

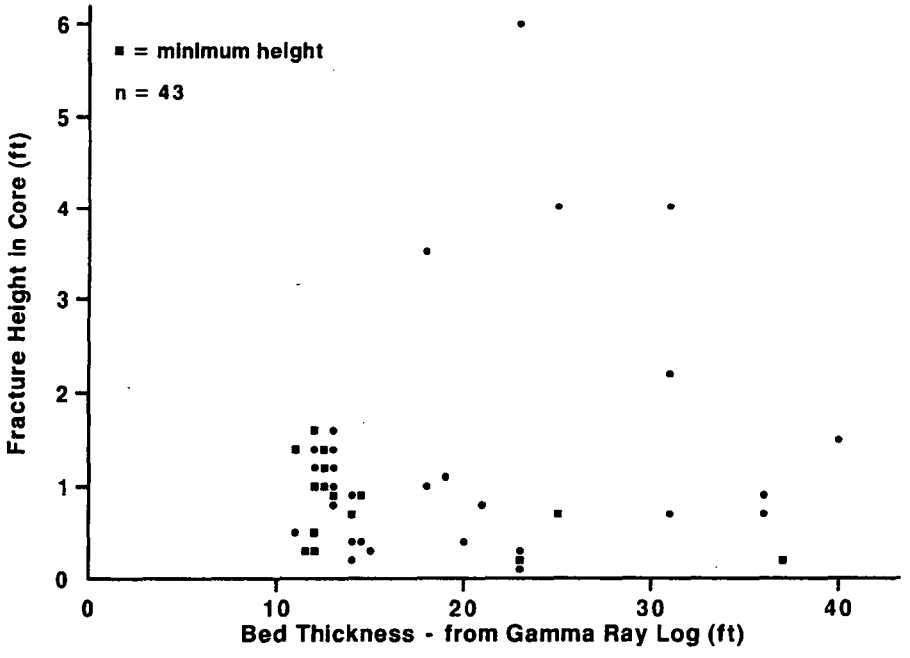

b. Individual fracture height as a function of gross bed thickness for sandstone beds greater than 10 ft thick. A horizontally compressed version of Figure 6A would fit into the space at the left of this graph, showing that most of the fractures cored are in the thinner sandstone and siltstone beds.

Figure B6. (Continued on next page)

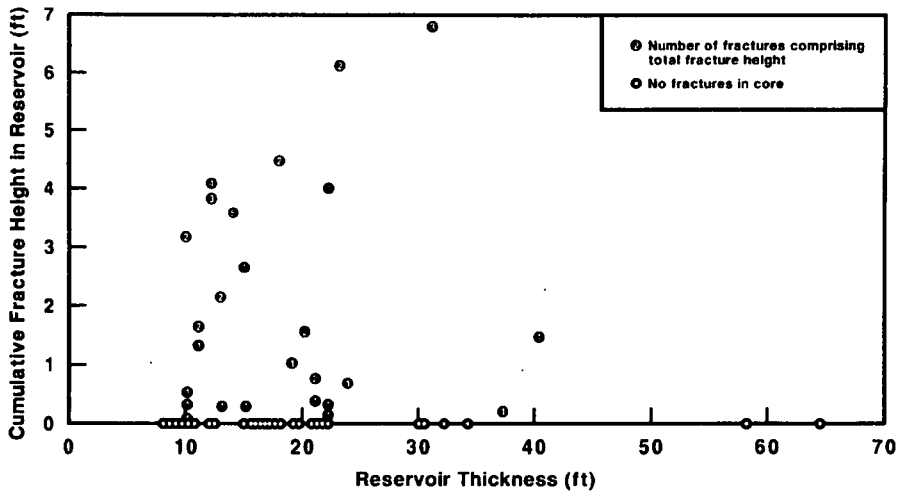

c. Cumulative fracture height in core in sandstones that are at least ten feet thick. Note that core from over half (52%) of the reservoirs, including the thickest ones, displayed *no* fractures, yet deviated core shows that these same sandstones are in fact highly fractured.

Figure B6. Plots of fracture-height data from vertical core, that highlight the irregular fracture distribution within heterogeneous fluvial sandstone reservoirs of the Mesaverde Formation in the Piceance Basin, Colorado. (Data are from the MWX wells.)

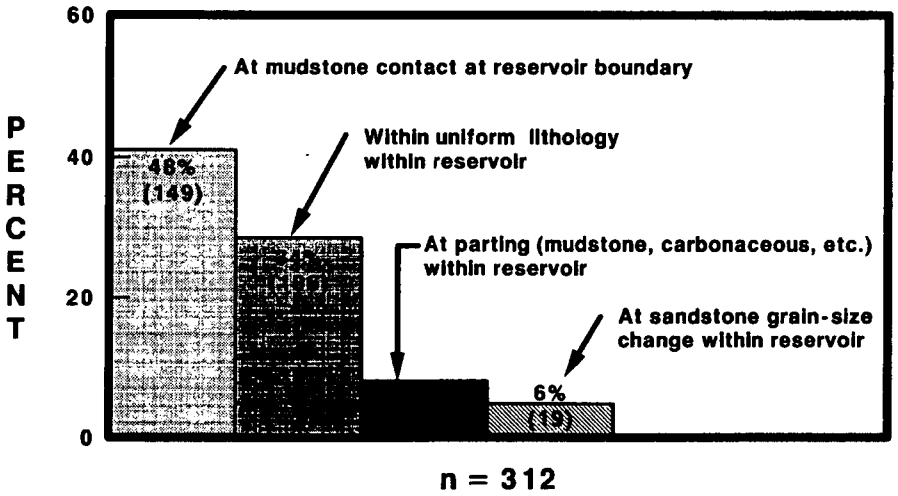

Figure B7. Histogram showing the locations of fracture terminations in vertical core from heterogeneous, fluvial sandstone reservoirs in the Mesaverde Formation in the Piceance Basin, Colorado. (Data are from the MWX wells.) The percentage of fracture terminations at bounding mudstone lithologies is high in this plot because many of the fractures occur in relatively thin beds. These data suggest that fractures that extend the full thickness of any reservoir are rare to absent.

Core lithology and fractures should be described together, because the distribution of fractures relative to lithology is important. Thus if measurements show (1) that the fractures are limited to the reservoir strata, and (2) that fracture heights are significantly less than bed thickness, then vertical fracture permeability between and within reservoirs will be severely limited, and both horizontal drilling and cubic-block reservoir-engineering models may be inappropriate. Fracture planarity and surface roughness (due to mineralization and/or fracture-surface ornamentation) are also more readily measured in vertical core simply because larger samples of the fracture planes are obtained, if fractures are intersected, than in horizontal core. Estimates of these parameters can be used by the reservoir engineer to determine flow rates and turbulence, and by the geologist as clues to the origin of the fractures.

Finally, vertical core can provide a measurement of fracture distribution with depth (Figure B8), and of the variation in fracture characteristics as different formations are penetrated by a well. As noted in Figure B8, however, such vertical distributions should be used with caution, as changes may be facies controlled and more apparent than real.

Vertical core in heterogeneous reservoirs will not provide definitive data on the presence or absence of vertical fractures, much less on fracture spacing and fracture porosity, but it will allow the measurement of dip, strike, and permeability. These will be discussed below, together with dimensions tha0t can be measured from either vertical or deviated core.

Descriptions of Fractures in Core from Deviated Wells

The chances of intersecting vertical to near-vertical fractures increase dramatically when wells are deviated. The ratio of the horizontal distances within the reservoir sampled by (1) a deviated well, and (2) vertical four-inch diameter core, varies as the thickness of the reservoir times the tangent of the deviation angle (Figure B9). Thus a well with a 30° deviation in a 35-ft bed will sample 20.3 ft of horizontal distance, or 6200% more than vertical four-inch core. If the deviated wellbore azimuth is normal to the fracture strike, chances of intersecting vertical fractures are increased by 6200%. Therefore deviated pilot holes should be considered when planning horizontal wells.

Even though fractures are not difficult to intersect with a deviated well, an irregular fracture distribution and the resulting limited vertical fracture permeability will significantly decrease the production advantage of such a well. Therefore it is important to characterize the nature of the fractures and fracture-permeability system in the reservoir in order to properly design wells, and fracture analysis beyond notations of fracture dip, strike, and depth is needed.

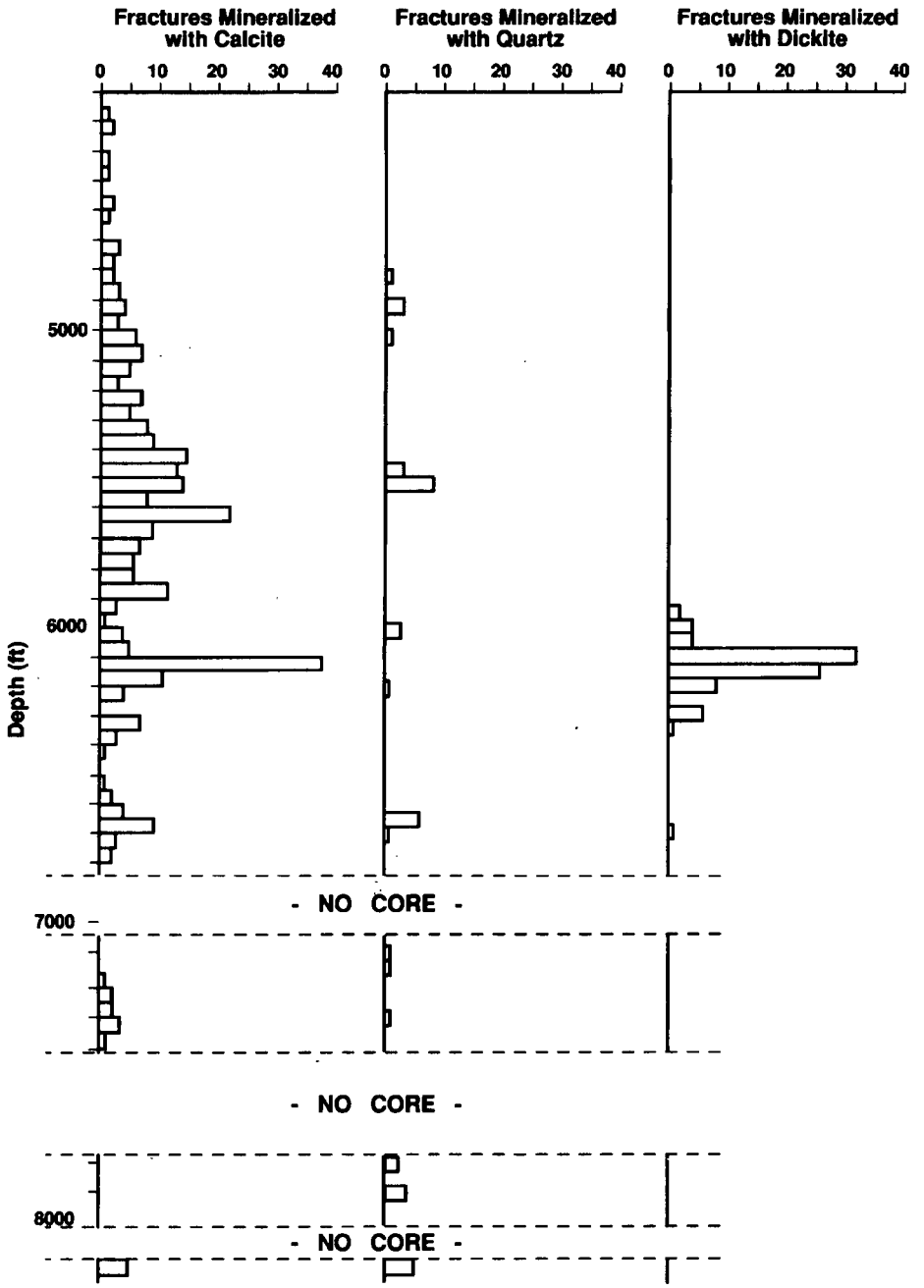

Figure B8. Histogram showing fracture frequency in vertical wells as a function of depth in the Mesaverde Formation in the MWX wells in the Piceance Basin of Colorado. These wells are relatively straight, but apparent high frequencies could be caused in other wells by deviated segments of a wellbore. New data from the deviated SHCT-1 well (Lorenz and Hill, 1991) show the measured paucity of fractures in the lower intervals to be misleading, as deviated core contains numerous closely spaced fractures in these same zones. The apparent decrease in fracture frequency is a function of a decrease in the number of highly fractured, interbedded thin sandstones in the lower zones, caused by changing depositional facies. Fracture spacing within the actual reservoirs of these lower strata is not significantly less than spacing in the higher reservoirs.

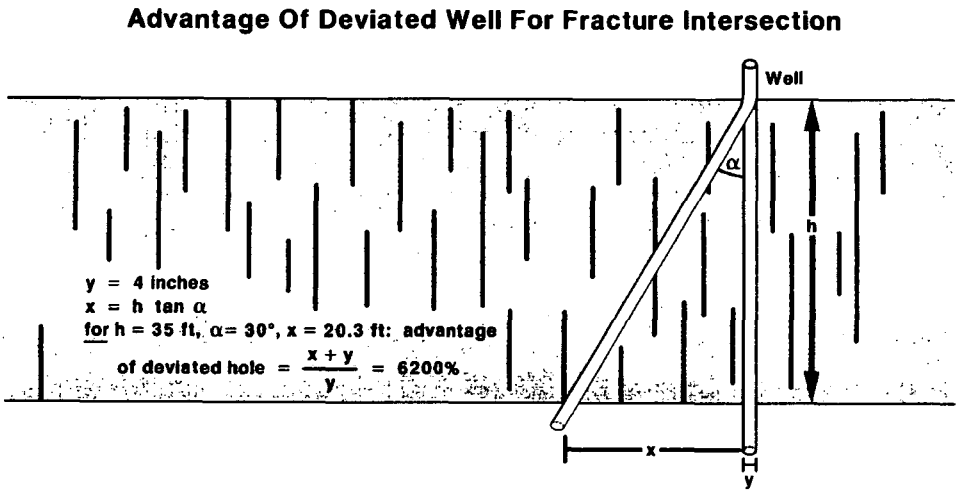

Figure B9. Schematic drawing showing the increased chance of encountering vertical fractures in a deviated well, as a ratio between the lateral distance crossed by the deviated hole, and the four inches "traversed" laterally by four-inch core. For the purpose of fracture characterization, a slant hole offers a significant advantage over vertical holes. h is bed thickness, α is the angle the hole is deviated from vertical, y is the core diameter, and the heavy vertical lines are fractures.

Characteristics Measurable Only in Deviated Core

The principal characteristic of fractures measurable only in core from deviated holes is fracture spacing. However, although an absolute spacing can be measured in the core, the data are still one-dimensional, measured along the core axis. Measured spacing along the core axis must be converted into true horizontal spacing by accounting for the geometric relationships between hole deviation, hole azimuth, and fracture strike. Once this is done, the distribution of spacings can be analyzed.

The extrapolation of measured fracture spacing in core to the rest of the reservoir, based on the principle that extensional strain should be constant throughout the reservoir, may or may not be valid depending on reservoir heterogeneity. However, the precise number derived from core for the average or the range of fracture spacings is rarely applicable to reservoir engineering models. For the horizontal SHCT-1 core in the relatively homogeneous, marine Cozzette sandstone, fracture spacing varies between a minimum of less than one inch to a maximum of 17 ft with an average of 3 ft (Lorenz and Hill, 1991). The "average fracture spacing" value in this case is of little use as a direct input parameter to reservoir engineering models because it ignores the wide range of spacings. It may, in fact, be misleading, because it includes the spacings of isolated fractures as well as the spacings within fracture swarms, even though swarms are effectively single fractures in an engineering sense (P.T. Branagan, personal communication, 1991), while single, isolated fractures may contribute little to the system.

For comparison, 17 distinct gas shows in the mud log from a side-track of the SHCT-1 well have spacings of 2 to 35 ft. Such spacing compares more favorably to the 2.5–17.6 ft range of swarm and isolated fracture spacings than to individual fracture spacings seen in the correlative core (Figure B10). Swarms of closely spaced fractures appear on the mud log as single gas shows. If some of the isolated fractures are deleted from the core spacing computation on the assumption that they may not show on the mud log, the upper limit of the fracture spacing range for core approaches the observed upper spacing limit of the mud log gas shows.

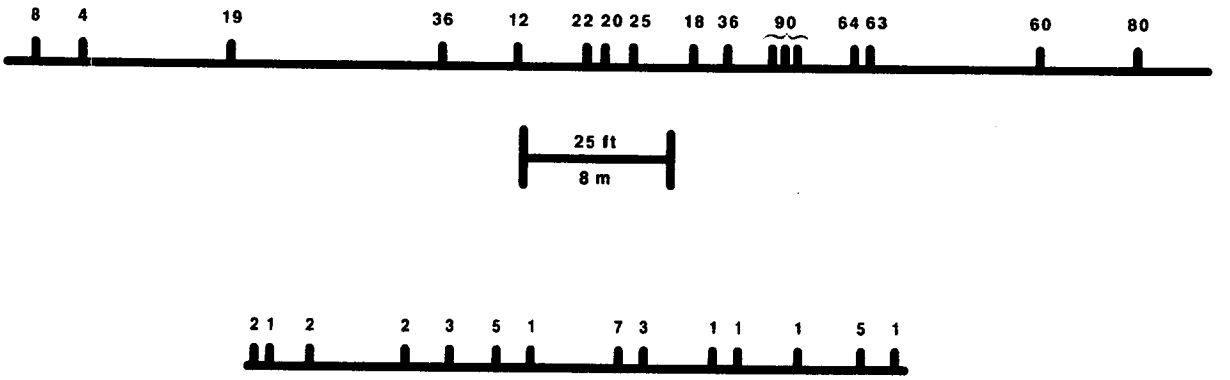

Figure B10. A comparison between the location and volume of gas shows in the horizontal portion of the SHCT-1 sidetrack (top line; volume of gas in gas units X 10 indicated above line), and the spacings of isolated fractures and fracture swarms in horizontal SHCT-1 core (bottom line; numbers of fractures per location indicated above line) in the same reservoir at the same depth. The two traces are from parallel holes, so there is no direct correlation, but swarm spacing is comparable to gas show spacing, whereas the average spacing of all fractures is considerably less than the spacings of gas shows. Data from the Mesaverde Formation, Piceance Basin, Colorado.

If the average spacing of fracture swarms is more useful to the engineer, then the spacing populations must be characterized so that this figure can be determined. Fractal analysis is one approach to fracture characterization (e.g., LaPoint, 1988; Nelson, 1991), but for the limited data set commonly available in core, a somewhat simpler statistical approach based on cumulative probability distribution plots of fracture spacings may be equally useful. An example of such plots of fracture spacings in the SHCT-1 core (Figure B11a) highlights the difference between two sub-populations of spacings. The closely spaced swarm population can be removed to leave the spacings of probable engineering significance, and compares favorably to the spacings of gas shows (Figure B11b).

Fracture spacing is significantly less than gross reservoir thickness in the heterogeneous Mesaverde reservoirs at the MWX/SHCT site. This holds true for both the narrow, lenticular, 25 to 35-ft thick channel sandstones and the 60-ft thick, blanket, marine sandstones (bed-thickness to fracture-spacing ratios of 10–15 and 20 respectively).

Once the spacing of fractures has been measured, an estimate of fracture porosity can be made using average fracture open width and average fracture spacing, and can be compared to the rock matrix porosity. A quantitative estimate of fracture porosity can be made with core from a deviated hole, whereas only a qualitative estimate can be derived from vertical core.

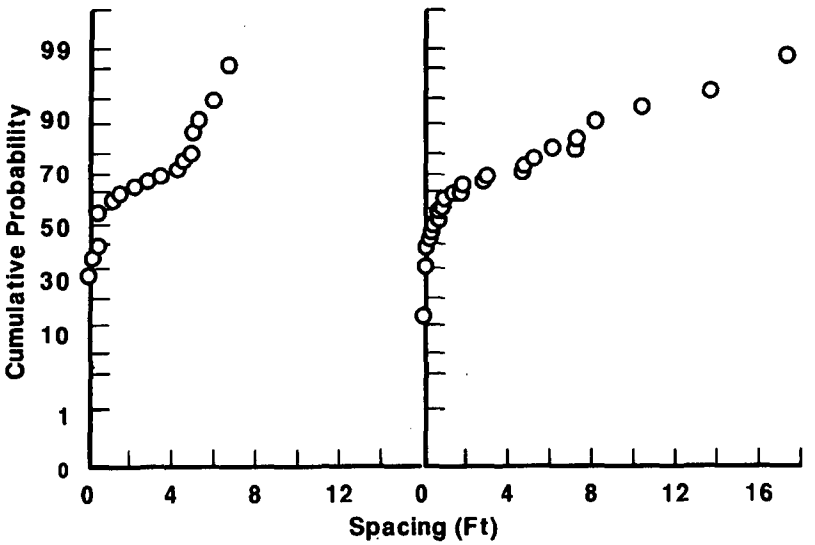

a. Cumulative probability plots of fracture spacings in the SHCT-1 core. These data show (1) populations that are not normally distributed, and (2) sub-populations of spacings, as defined by different slopes. The steep slopes of closely spaced fractures represent fracture swarms (left: plot for lenticular channel sandstones 25–35 ft thick; right: plot for blanket-shaped marine sandstone 60 ft thick).

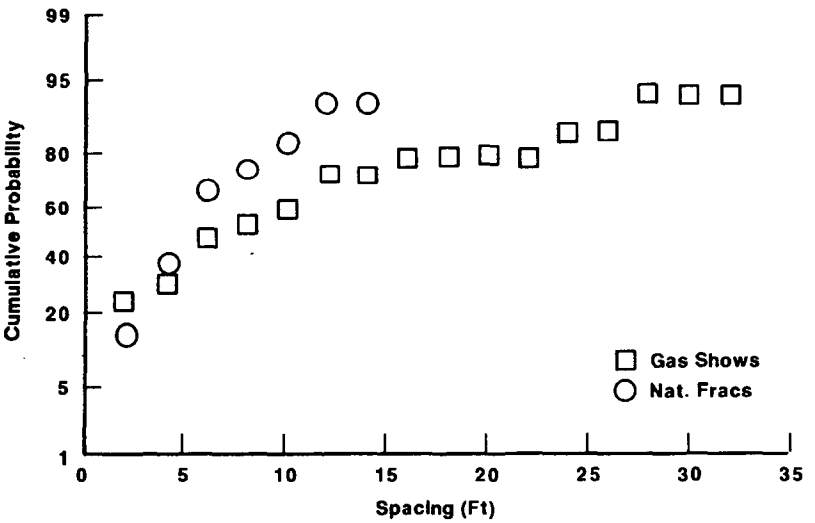

b. Cumulative probability plots of the spacings of gas shows (data from Figure B10), and the Cozzette core fracture spacings greater than 2 ft. This figure suggests that the widely spaced fractures are those that influence production. (Data are from the SHCT-1 well, Mesaverde Formation, Piceance Basin, Colorado. Cumulative probability plots are described by D'Agostino and Stephens, 1986.)

Figure B11. Characterization of fracture spacing in horizontal wells.

Fracture Characteristics Measurable in Both Vertical and Deviated Core

Fracture dip and strike can be obtained from either deviated or vertical core if the core is oriented. Even if core is not oriented, the fracture orientations relative to each other and relative to any stress indicators such as petal fractures should be made, and referenced to an arbitrary orientation line (the MOL described above) if sufficient lengths of continuous-fit core are available for study. Fractures that are consistently parallel to each other argue for a single set of sub-parallel fractures, and thus for significant permeability anisotropy in the subsurface (Figure B12). Parallel or oblique strike relationships between fracture sets and the principal horizontal stress can also be determined from consistent angular relationships between petal fractures and natural fractures. This relationship is important to (1) prediction and understanding the effects of hydraulic stimulation fractures, (2) determining which of multiple fracture sets is most important to permeability, and (3) determining the sensitivity of fracture permeability to changes in stress during production-induced pore pressure changes.

Many natural fractures are mineralized, which reduces the permeability along the fracture (Figure B13). Smaller fractures may appear to be completely mineralized and to have little or no permeability, although many apparently mineralized fractures provide significant permeability under in situ conditions. Moreover, such fractures may parallel more open fractures that have not been cored, and thus should be measured as an indication of fracture trend.

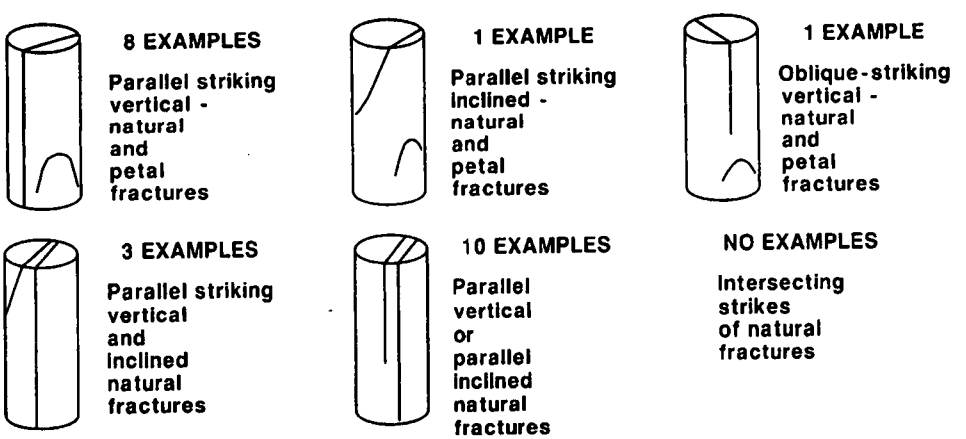

Figure B12. An example of fractures in a core that can be demonstrated to be parallel to each other, and to the maximum horizontal stress, by measuring fractures relative to an arbitrary orientation line (MOL—see text) over several short, continuous-core intervals. This was possible despite the breakdown of the core orientation survey and badly rubbleized core. (Data are from the Austin-Mississippian limestone at 13,000-ft depth, in the Heyco Duncan Unit 3 well in the Tatum basin, NM, courtesy of Larry Brooks and the Harvey E. Yates Co.) The fracture trend is still unknown, but the data suggest that the fractures will create anisotropic horizontal permeability, and that a hydraulic stimulation would be relatively ineffective.

Direct measurement of fracture permeability is a tricky operation. Cutting a plug that contains the fracture is difficult, as only fractures that are well cemented will hold together during the plugging process (e.g., Morrow et. al., 1990). Unfortunately, the tightly cemented fractures may not contribute as much to the system permeability as less easily plugged, open fractures. Whole-core measurements of permeability can give more realistic, and commonly much higher, values for system permeability (e.g., Lamb and Ferguson, 1988). Poorly cemented fractures may sometimes be artificially cemented, plugged, the artificial glue dissolved, and the plug then tested.

Table B2 compares the types of fracture data that can be obtained from core from vertical and deviated wells. Both types of data are desirable for optimum characterization of subsurface fracture systems. Only a limited number of fracture measurements are exclusive to horizontal core, but these parameters, spacing and porosity, are important.

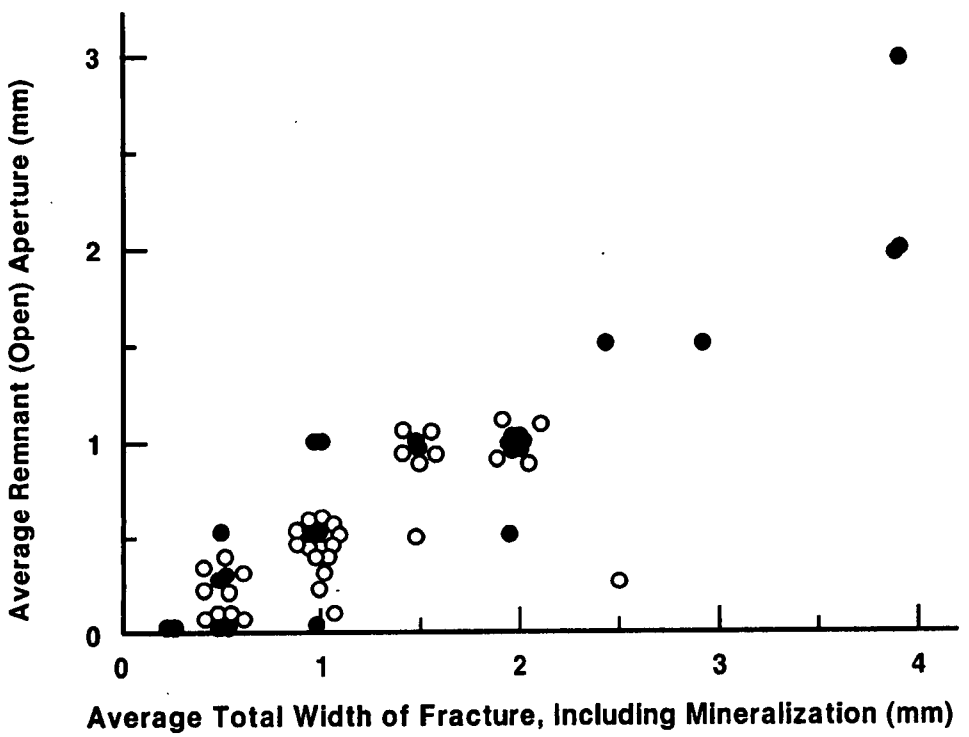

Figure B13. Total fracture width plotted against remnant (unmineralized) fracture aperture of the same fracture. The smaller fractures tend to be more completely mineralized. Solid circles from lenticular channel sandstones; open circles from marine sandstones. (Data are from core from the SHCT-1 well, Mesaverde Formation, Piceance Basin, Colorado.)

Table B2. Comparison of Types of Data Measurable in Core from Vertical and Deviated Wells

Measurable Characteristic	Vertical Core	Deviated Core
Spacing	–	x
Total Width	x	x
Remnant Aperture/Mineralization	x	x
Formation Fracture Porosity	–[1]	x
Fracture Permeability	x	x
Strike and Dip	x	x[2]
Number of Fracture Sets	x	x
Vertical Termination Locations	x[3]	–
Height	x[3]	–
Preferred Host Rock	x[3]	–
Surface Morphology	x	–
Fracture Type	x	x[3]

Comments: 1. Qualitative estimate may be possible
2. May not require oriented core
3. Requires sufficient core

Note that *if* fractures are intersected, vertical core will provide more attributes than deviated core, but *not* the important factors of spacing and porosity.

Fracture-Identification Logs

Fractures in fracture-identification logs can be analyzed in much the same fashion as fractures in core (e.g., Emmendorfer, 1989). Unfortunately, no fracture-identification logs were run in the SHCT-1 well or its side track, and other wells will be used to illustrate this section.

Comparison With Core Data

Fracture-identification logs can provide a check on the fracture orientations obtained from oriented cores. Figure B14a and b shows an example of agreement between fracture orientations derived from image-log analysis and from correlative core. Although agreement in fracture orientation is common, in most cases it is difficult to correlate specific individual fractures between core and image logs. It is always desirable to have core to calibrate the images seen on logs, as apparent fractures on logs, especially in horizontal holes, can be the products of tool malfunction.

In some cases, natural fractures can be distinguished from induced fractures on image logs. In such cases, the different orientations of the two types of fractures, seen in the log and corroborated by core observations, may allow the initial distinction to be made. Once this criterion is established, other characteristic image differences such as width and brightness of the fracture image may become apparent. Image logs can identify open fractures which are commonly filled with drilling mud near the wellbore and therefore offer a resistivity and density contrast. Mineral-filled fractures can only be seen if there is a significant resistivity or density contrast between the mineralization and the rock matrix.

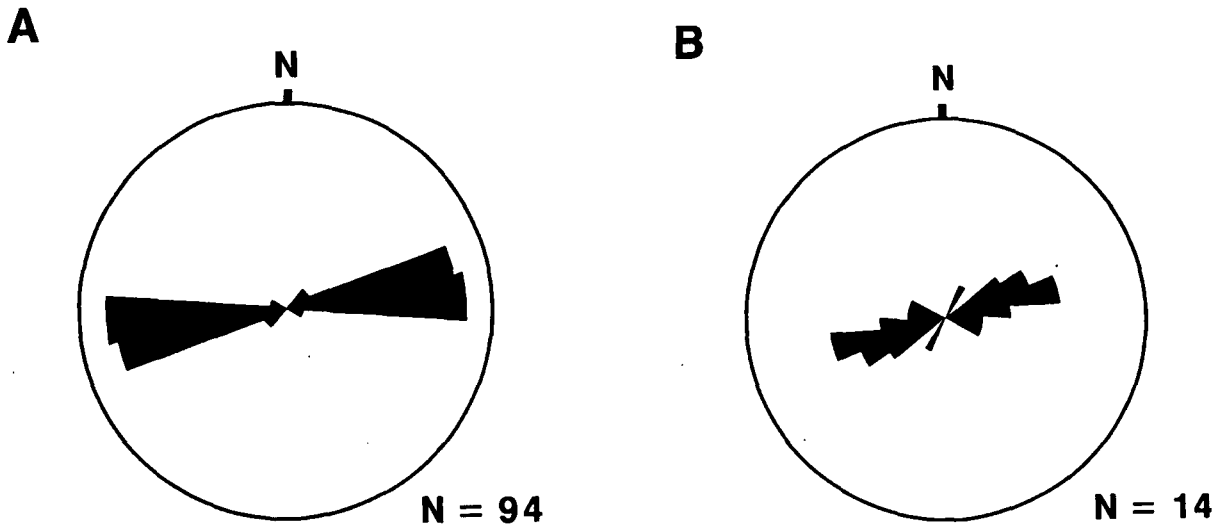

a. Pass through 1740 ft of the Mesaverde Formation, Piceance Basin, Colorado, by Schlumberger's FMS log

b. Strikes from 109 ft of oriented core within the same section. (Data are from the Barrett MV 8-4 well in the central Piceance basin, CO, courtesy of Kurt Reinecke and Barrett Resources Corp.)

Figure B14. Rose diagrams showing the strikes of coring-and drilling-induced fractures in a vertical well.

Orienting Core Using Fracture Identification Logs

Image logs can be used to orient vertical and deviated cores. The unoriented core is processed as though it was oriented, as described above, and measurements of fracture orientations are made relative to an MOL. Orientation is achieved by correlation of an orientable feature such as inclined bedding on the log to the same structure in the core. The log orientation of the feature is then used to determine the true orientation of the MOL for that section of core. Crossbeds and large fractures are commonly good features for correlation purposes. By orienting the MOL in this manner, it is possible to orient other fractures visible in the core but not in the log. Caution should be used as some types of coring-induced fractures do not extend from the core into the wellbore wall, and vertical natural fractures seen in a vertical wellbore image log need not intersect the smaller-diameter core.

Interpretation Without Core Data

When core data are not available, fractures on image logs must be interpreted carefully, especially as to their origin (induced vs natural) and therefore their significance. Experience with the common orientations and unique log signatures of different types of fractures in an area may allow classification of fractures (e.g., Standen, 1991).

Most classifications of fractures using logs alone are somewhat subjective, and conclusions from such classifications should be made with caution. It is possible to analyze the orientations of fractures from image logs on stereoplots or rose diagrams, and to attempt to isolate different populations. For instance, drilling-induced fractures commonly have high dips, and a population of fractures with average dips of less than 70° is likely to be one of natural fractures. However, if a formation has not previously been well characterized, core is essential for reliable interpretation of borehole image logs.

Discussion and Summary

The more core that is available from wellbores of different orientations, and the more fracture identification logs that are run, the more complete will be the resulting characterization of the subsurface fracture system. For the Mesaverde reservoirs at the MWX/SHCT site, core measurements of fractures demonstrated the existence of a dominant fracture trend. This trend creates a pronounced horizontal permeability anisotropy (up to 100:1 as indicated by well tests), and results in highly elliptical drainage patterns in the reservoirs (Lorenz et. al., 1989). However, analysis of the fractures and lithologies together suggested that the fractures are irregularly distributed within the heterogeneous fluvial reservoirs, and commonly terminate within the reservoirs at minor lithologic discontinuities. Few, if any, fractures extend the full thickness of the reservoirs. Thus the vertical fracture permeability in the reservoirs is limited. Except in the more homogeneous marine sandstones, even horizontal wells may not drain the gas with optimum efficiency.

Moreover, the relative inefficiency of the hydraulic stimulation-fracture experiments at this site could have been predicted from the parallelism between natural and induced fractures in the core. Hydraulic fractures parallel the principal horizontal stress (as do the strikes of the induced fractures), and therefore propagate parallel to, rather than across, the high-permeability trend created by the natural fractures.

Fractures that are normal to the maximum horizontal in situ stress, even if numerous, may not be as important to the system permeability as a set of less numerous fractures that are parallel to this stress (Teufel, and Farrell, 1992). Most of the stress-normal fractures would be closed, whereas the less numerous, stress-parallel fractures would be open and relatively permeable if they are not completely mineralized. The induced fractures that commonly record stress orientation should be measured as well as the natural fractures.

Measurements of parameters such as spacing, width, and vertical distribution of fractures cannot be put directly into a numerical reservoir model. Even when abundant data are available as from the MWX/SHCT projects, once the measurements described above have been made, the task of further refining the fracture model devolves into the realm of assumptions, extrapolations, and alchemy. Moreover, the significance of the precision of the measurements is questionable when core samples such a limited area of the reservoir. The measurements may be most useful as relative indications of degree of fracturing of the reservoir and degree of heterogeneity of fracture distribution. Other important dimensions, such as horizontal fracture length, interconnectedness of fractures, and variations in remnant aperture along individual fractures cannot be measured in core, and remain to be inferred intuitively or from filtered outcrop data.

Nevertheless, attention to detail during the logging of a core for fractures will yield significantly more insight into the characteristics of a fracture system. In order to optimize the amount of information that can be derived from fractures in core, procedures such as on-site core processing, measuring fractures before slabbing, monitoring coring operations, and deviating pilot wells should be seriously considered. Thought should also be given to using the relative orientations of fractures even in core that is not oriented and to the possibility of orienting cores after they have been cut.

References

Aguilera, R., 1988, Determination of subsurface distance between vertical parallel natural fractures based on core data: American Association of Petroleum Geologists Bulletin, v. 72, p. 845–851.

Bleakly, D.C., Van Alstine, D.R., and Packer, D.R., 1985, How to evaluate orientation data; quality control: Oil and Gas Journal, v. 85, p. 46–54.

D'Agostino, R.B., and Stephens, M.A., 1986, Goodness-of-fit techniques: Marcel Dekker, Inc., New York, 560 p.

Emmendorfer, A., 1989, Fracture orientation: use of the dipmeter type fracture log: The Mountain Geologist, v. 26, p. 63–67.

Kulander, B.R., Barton C.C., and Dean, S.L., 1979, The application of fractography to core and outcrop fracture investigations: U.S. Department of Energy, Morgantown Energy Technology Center, MECT/SP-79/3, 174 p.

Kulander, B.R., Dean, S.L., and Ward, B.J. Jr., 1990, Fractured core analysis: Interpretation, logging, and use of natural and induced fractures in core: American Association of Petroleum Geologists, Methods in Exploration Series, No.8, 88 p.

Lamb, C.F., and Ferguson, D.G., 1988, The role of core analysis in fractured reservoir evaluation: Canadian Institute of Mining and Metallurgy, paper number 88-39-86, 39th Annual Technical Meeting, Calgary, June 12–16, p. 86-1 to 86-10.

LaPoint, P.R., 1988, A method to characterize fracture density and connectivity through fractal geometry: International Journal of Rock Mechanics and Geomechanics Abstracts, v. 25, p. 421–429.

Laubach, S.E., 1991, Fracture patterns in low-permeability sandstone gas reservoir rocks in the Rocky Mountain region: Society of Petroleum Engineers paper number 21853, *in* Society of Petroleum Engineers Joint Rocky Mountain Section Meeting and Low Permeability Reservoir Symposium, April 15–17, 1991, Denver, CO, p. 501–510.

Lerche, I., and Narr, W., 1986, Estimating subsurface fracture density in core: Effects resulting from variable fracture spacing: SPE Formation Evaluation, v. 2, p. 249–258.

Lorenz, J.C., and Hill, R.E., 1991, Subsurface fracture spacing: Comparison of inferences from slant/horizontal core and vertical core in Mesaverde reservoirs: Society of Petroleum Engineers paper number 21877, *in* Society of Petroleum Engineers Rocky Mountain Regional Meeting and Low-Permeability Reservoirs Symposium, April 15–17, 1991, Denver, CO, p. 705–716.

Lorenz, J.C., and Finley, S.J., 1991, Regional fractures II: Fracturing of Mesaverde reservoirs in the Piceance Basin, Colorado: American Association of Petroleum Geologists Bulletin, v. 75, p. 1738–1757.

Lorenz, J.C., Warpinski, N.R., Branagan, P.T., and Sattler, A.R., 1989, Fracture characteristics and reservoir behavior of stress-sensitive fracture systems in flat-lying lenticular formations: Journal of Petroleum Technology, v. 41, p. 615–622.

Lorenz, J.C., Teufel, L.W., and Warpinski, N.R., 1991, Regional fractures I: A mechanism for the formation of regional fractures at depth in flat-lying reservoirs: American Association of Petroleum Geologists Bulletin, v. 75, p. 1714–1737.

Lorenz, J.C., Finley, S.J., and Warpinski, N.R., 1990, Significance of coring-induced fractures in Mesaverde core, northwestern Colorado: American Association of Petroleum Geologists Bulletin, v. 74, p. 1017–1029.

Morrow, N.R., Brower, K.R., Shouxiang, M., and Buckley, J.S., 1990, Fluid flow in healed tectonic fractures: Journal of Petroleum Technology, v. 42, p. 1310–1318.

Myal, F.R., and Frohne, K.-H., 1991, Slant-Hole Completion Test in the Piceance Basin, Colorado: Society of Petroleum Engineers paper number 21866, *in* Society of Petroleum Engineers Rocky Mountain Regional Meeting and Low-Permeability Reservoirs Symposium, April 15–17, 1991 Denver, CO, p. 611–622.

Narr, W., 1991, Fracture density in the deep subsurface: Techniques with application to Point Arguello oil field: American Association of Petroleum Geologists Bulletin, v. 75, p. 1300–1323.

Nelson, R.A., 1991, Multi-scale natural fracture development and its effect on reservoir modeling (abstract): American Association of Petroleum Geologists Bulletin, v. 75, p. 645.

Nelson, R.A., Lenox, L.C., and Ward, B.J. Jr., 1987, Oriented core: Its use, error, and uncertainty: American Association of Petroleum Geologists Bulletin, v. 71, p. 357–367.

Norman, D.K., and Garrett, C.H., 1988, Advances in fractured reservoir characterization: Petroleum Society of the Canadian Institute of Mining and Metallurgy, paper number 88-39-111, 39th Annual Technical Meeting, Calgary, June 12–16, 1988, p. 111-1 to 111-21.

Northrop, D.A., and Frohne, K.-H., 1990, The Multiwell Experiment: A field laboratory in tight gas sandstone reservoirs: Journal of Petroleum Technology, v. 42, p. 772–779.

Ragan, D.M., 1973, Structural geology: An introduction to geometrical techniques: John Wiley and Sons, New York, 207 p.

Skopec, R.A., 1991, Rock characterization in reservoirs targeted for horizontal drilling: Society of Petroleum Engineers, paper number 22709, 66th Annual Technical Conference and Exhibition, Dallas, TX, October 6–9 (in press).

Skopec, R.A., Mann, M.M., Jeffers, D., and Grier, S.P., 1990, Horizontal core acquisition and orientation for formation evaluation: Society of Petroleum Engineers paper number 20418, *in* Society of Petroleum Engineers 65th Annual Technical Conference and Exhibition, September 23–26, New Orleans, LA, p. 153–166.

Skopec, R.A., (chairman), (in press), Wellsite core handling procedures: Work group report prepared for the American Petroleum Institute, Subcommittee on Core Analysis.

Standen, E., 1991, Tips for analyzing fractures on electrical wellbore images: World Oil, v. 212, p. 99–118.

Strickland, F.G., and Ren, N.-K., 1980, Predicting the in-situ stress for deep wells using differential strain curve analysis: Society of Petroleum Engineers paper number 8954, Society of Petroleum Engineers/Department of Energy Symposium on Unconventional Gas Recovery, Pittsburgh, PA, May 18–21, 1980, p. 251–258.

Teufel, L.W., 1983, Determination of in-situ stress from anelastic strain recovery measurements of oriented core: Society of Petroleum Engineers paper number 11649, Society of Petroleum Engineers/Department of Energy Symposium on Low-Permeability Gas Reservoirs, Denver, CO, March 14–16, 1983, p. 421–430.

Teufel, L.W., and Farrell, H.E., 1992, Interrelationship between in situ stress, natural fractures, and reservoir permeability, a case study of the Ekofisk Field: Symposium on Fractured and Jointed Rock Mass, International Society or Rock Mechanics, Lake Tahoe, CA, June 3–5, 1992, (in press).

Van Alstine, D.R., Butterworth, J.E., Willemse, E.J.M., and Evert Van de Graaff, W.J., 1991, Paleomagnetic core-orientation for characterizing reservoir anisotropy: Case histories from fractured reservoirs in Abu Dhabi and Venezuela (abstract): American Association of Petroleum Geologists Bulletin, v. 75, p. 687.

Van Golf-Racht, T.D., 1982, Fundamentals of fractured reservoir engineering: Developments in Petroleum Science, No. 12, Elsevier, Amsterdam, 253 p.

APPENDIX C

Viscoelastic Stress History Equations for Basin Stress Modeling

The viscoelastic solution to the problem is obtained using the Viscoelastic Correspondence Principle. This principle states that if a solution to an elastic problem is known, then the LaPlace transform of the solution to the corresponding viscoelastic problem may be found by replacing the elastic constants (μ and E) by appropriate quotients of operator polynomials, and the actual loads by their LaPlace transforms. Using the Viscoelastic Correspondence Principle, the viscoelastic solutions can be determined directly from the elastic solutions.

The major problem is development of an appropriate viscoelastic model to describe the behavior of rocks over geologic time. Since little is known about such behavior, we have chosen three requirements.

1. Initial elastic response as if the rock is linear-elastic.
2. As time $\rightarrow \infty$, the material approaches a uniform state, that is, all shear stresses will eventually relax out.
3. Keep it as simple as possible. No good data are available to justify a complex model.

The simplest case which yields acceptable initial and long-term behavior is one in which the rock is:

1. Elastic in dilation
2. Maxwell material in distortion

After performing the necessary transformations and inversions, the viscoelastic solution is given as

$$d\sigma_x = A_1(t)\frac{\nu}{1-\nu}d[(\rho g-\lambda)D] + A_2(t)\frac{E}{1-\nu}2\,d\epsilon_x$$

$$+ A_3(t)\frac{\nu E}{1-\nu^2}d\epsilon_y + A_4(t)\frac{\alpha E}{1-\nu}dT$$

for the x term. (The corresponding y term is formed by a transposition of x and y subscripts.) The A_i are the relaxation functions and are given by

$$A_1(t) = \frac{(1-\nu)}{\nu} - \frac{(1-2\nu)}{\nu}e^{-t/t_R},$$

$$A_2(t) = \frac{(1+\nu)}{2}e^{-t/t_R} + \frac{(1-\nu)}{2}e^{-\beta t/t_R},$$

$$A_3(t) = \frac{(1+\nu)}{2\nu}e^{-t/t_R} - \frac{(1-\nu)}{2\nu}e^{-\beta t/t_R}, \text{ and}$$

$$A_4(t) = e^{-t/t_R}$$

where t_R is the relaxation time of the rock, and β is given by

$$\beta = \frac{3(1-\nu)}{(1+\nu)}$$

These equations are identical to the elastic solution if the A_i are all unity.

These results can be summed over an arbitrarily large number of time intervals, t_1 to t_2, to obtain

$$\Delta\sigma_x = \int_{t_1}^{t_2} A_1\,(t-t')\,\frac{\nu}{1-\nu}\,\frac{d[(\rho g-\lambda)D]}{dt'}\,dt'$$

$$+ \int_{t_1}^{t_2} A_2\,(t-t')\,\frac{E}{1-\nu^2}\,\frac{d\epsilon_x}{dt'}\,dt'$$

$$+ \int_{t_1}^{t_2} A_3\,(t-t')\,\frac{\nu E}{1-\nu^2}\,\frac{d\epsilon_y}{dt'}\,dt'$$

$$+ \int_{t_1}^{t_2} A_4\,(t-t')\,\frac{\alpha E}{1-\nu}\,\frac{dT}{dt'}\,dt'$$

and a similar result for the y direction. While these equations are similar to the elastic solution, the presence of time, t, in the A_i considerably complicates the calculations and bookkeeping chores. As time advances, each of these integrals must be reevaluated with the new value of t in the relaxation functions. This is required because the viscoelastic material has a memory of previous disturbances and will continue to relax from previous disturbances even as it is responding to new ones. Because of this feature of viscoelastic materials, the stresses are "naturally" locked in (or cumulative).

APPENDIX D

Techniques for In Situ Stress Measurement: Anelastic Strain Recovery (ASR), and Circumferential Velocity Anisotropy (CVA)

The orientation of the principal horizontal stresses can often be determined from various types of core analyses. Types of measurements include anelastic strain recovery (ASR; Teufel, 1983; Blanton, 1983, Warpinski and Teufel, 1989), differential strain curve analysis (DSCA; Strickland and Ren, 1980), and circumferential velocity analysis (CVA; Sayers, 1988). DSCA is offered by service companies to the industry and will not be discussed here.

Anelastic Strain Recovery (ASR)

ASR has considerable appeal because it is a direct measurement of the strain relief process as it is occurring. This strain relaxation occurs because the original in situ stresses at depth have been relieved through drilling. Since this process is likely to be irreversible, ASR provides the only true measurement of this behavior. The appeal of ASR, however, is somewhat negated by the difficulty of the measurement.

ASR is conducted by selecting samples at the drill site, instrumenting them with clip-on displacement gages as quickly as possible, and monitoring the subsequent relaxation of the core for 1–2 days. Three gages, spaced 45° apart, are placed around the horizontal plane, while one axial gage is optionally placed on the core. The axial gage serves no purpose for fracture azimuth, but it is necessary for estimating stress magnitudes.

The orientation of the maximum stress is the direction of the maximum strain recovery; recovery occurs due to microcracking in response to the unloading of the in situ stresses. More unloading, and therefore more strain recovery, occurs in the direction of the maximum horizontal stress than it does in the direction of the minimum stress. This behavior is shown in Figure D1. The direction of the maximum strain recovery can be quickly computed by using the strain-rosette equations, yielding

$$\theta = \frac{1}{2}\tan^{-1}\left(\frac{\epsilon_{45} - (\epsilon_0 + \epsilon_{90})}{\epsilon_0 - \epsilon_{90}}\right)$$

The angle, θ, has to be determined by inspection, as it is always less than or equal to 45°, and it is the angle with respect to the largest of the ϵ_0 or the $\epsilon_{90}0$ strains.

There are many complications that can occur with ASR, so it should never be used alone. If the rock is extremely tight, pore pressure may be trapped within the sample and cause contractions in the core as it slowly escapes. Pore pressure contractions are usually larger than the strain recovery, and are due to a volumetric shrinkage of the core as the pore pressure is reduced. Pore pressure effects can be accounted for, but they add another uncertainty to the analysis (Warpinski and Teufel, 1989).

Rock fabric, as due to tectonic cracks, bedding, burrows, and other aligned features, is probably the most serious difficulty in performing these measurements. ASR will often produce a large response to many types of fabric. In using this techniques, it is always important to inspect the core carefully, both before and after monitoring, to ensure that fabric is not affecting the results. Thin sections can also be useful. Employing more than one of these procedures is often a good double check.

Figure D2 shows the type of strain relaxation that typically occurs on sandstone rocks. This test is on a MWX coastal sandstone at a depth of 6517 ft, and yields a maximum recovery of 364 $\mu\epsilon$ on the axial gage and 100–200 $\mu\epsilon$ on the horizontal gages. Note that data is first obtained about 7 hours after the core was cut. The solid lines are theoretical fits of the data, using an analysis procedure described in Warpinski and Teufel (1989).

Analysis of these results yield:

maximum principal horizontal strain	237 $\mu\epsilon$
minimum principal horizontal strain	101 $\mu\epsilon$
overburden strain	364 $\mu\epsilon$
angle with respect to 0° gage	−30°
maximum stress angle	N87°E

These results can also be used to estimate the stress magnitudes, as given by Blanton (1983), and Warpinski and Teufel (1989).

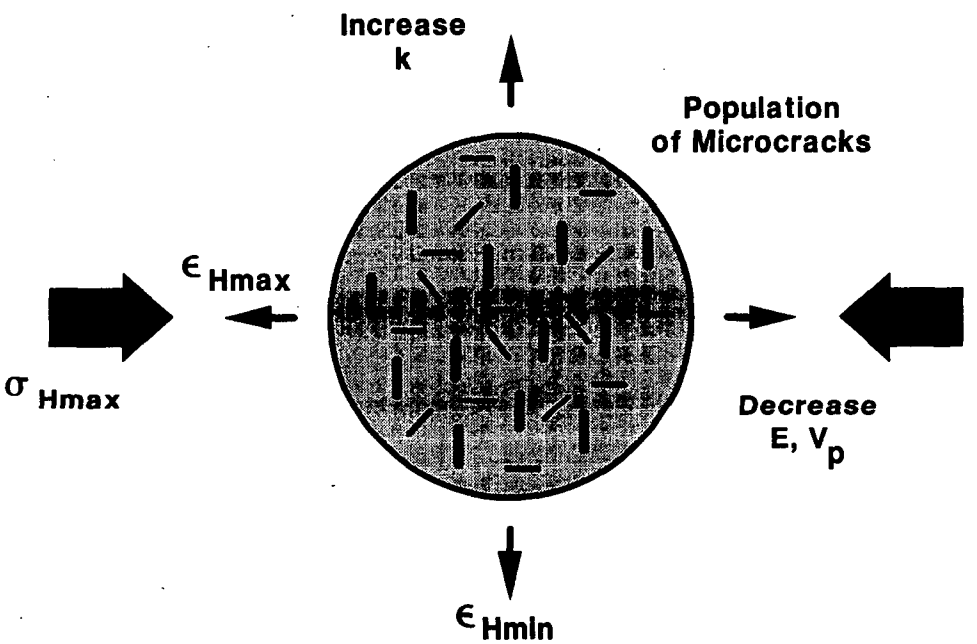

Figure D1. Preferential development of microcracks aligned normal to the maximum in situ stress, during anelastic strain recovery after rock has been cored.

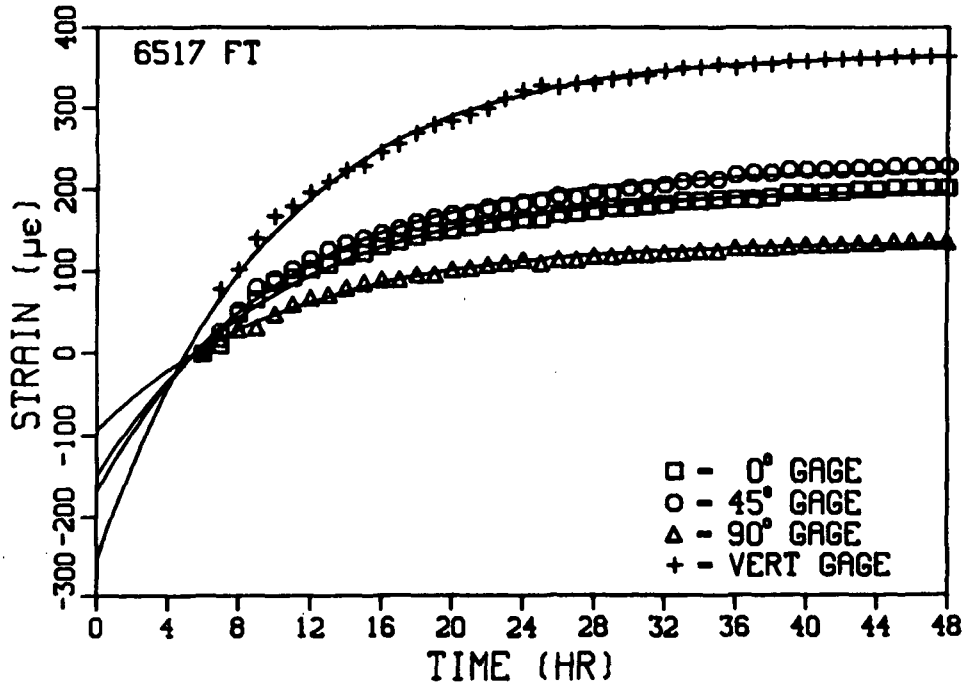

Figure D2. Time-dependent strain profiles for strain gauges with different orientations around a core during anelastic strain recovery.

Circumferential Velocity Anisotropy (CVA)

The relaxation of a piece of core from its in situ stress state at depth produces microcracks that perturb the acoustic velocity through the core sample. Measurement of the circumferential velocity anisotropy (CVA) of the core then provides information about what orientation has the most open microcracks (slowest velocity), which can be related to the in situ stress orientation, or occasionally to the rock fabric if one exists. The theoretical velocity distribution for a preferentially oriented population of microcracks has been worked out by Sayers (1988), yielding a velocity distribution given by

$$V(\theta) = V_{avg} + A\cos(2\theta+\phi) + B\cos(4\theta+\phi)$$

In this equation, the velocity at any orientation, $V(\theta)$, is a function of the average velocity through the sample plus a 2θ and a 4θ component. The phase angle, ϕ, is simply the offset angle that makes $V(\theta)$ a maximum at $2\theta+\phi=0°$ (assuming B is much smaller than A).

Because acoustic waves will be slowed primarily in the direction in which they cross the most cracks, the orientation of the minimum velocity, $2\theta+\phi=180°$, is the direction in which the most cracks are crossed. Since more microcracks will open up against the largest principal stress, the minimum velocity orientation should be aligned with the maximum stress direction. A schematic of this behavior is shown in Figure 1, which shows that many petrophysical properties are affected by the cracks.

While application of this technique is straightforward, there are a number of factors that can cause problems. Some rocks exhibit little or no relaxation so that few microcracks are formed and the velocity anisotropy is small. High porosity rock, where additional microcracks have a minimal effect on velocity through the highly voided rock, can also yield questionable results. Whenever the velocity variations are 2–3% or less, the inferred stress orientation should be considered unreliable.

Another major problem for the CVA technique is the prior existence of a rock fabric due to cracks, layering, oriented grains or crystals, or many other factors. Such a fabric can often produce a velocity anisotropy that overwhelms the microcracks velocity anisotropy, thus yielding a fabric orientation rather than a stress orientation. However, fabrics tend to have a different velocity character than microcracks, and this becomes very apparent in fitting the theoretical curve to the data. When the velocity distribution is controlled by relaxation microcracks, the theoretical fit is generally good, and the sinusoidal character of the anisotropy is evident. When the anisotropy is due to fabric, there is generally a poor fit of the theoretical curve, and the velocity data has a blocky structure. This difference provides a qualitative diagnostic for fabric problems.

An occasional problem is the presence of a damaged zone around the core surface, which can often cause significant velocity slowing. It is easiest to run velocity surveys on as-received core, but if the data are not satisfactory, the surface of the core should be ground down about ⅛ in. and the velocity survey rerun. This procedure often improves the quality of the data.

Figure D3 shows and example of the velocity anisotropy obtained from a MWX core sample taken from the coastal zone at 6520 ft. This sandstone rock had a 14% anisotropy with a well-defined minimum at N96°E, the orientation of the stress field at this depth. Note also that the data are well-fit by the theoretical curve using a least-square regression (the solid line); this good fit assures that the anisotropy is not controlled by fabric.

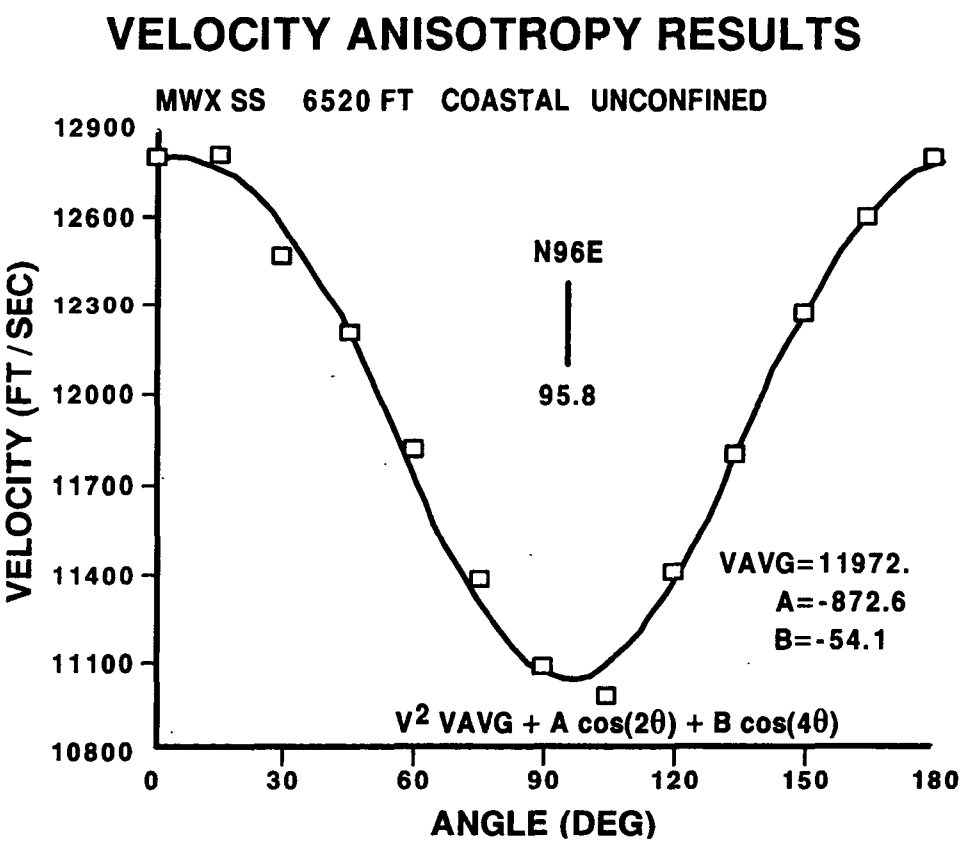

Figure D3. Velocities at different locations around a core, showing differences due to preferentially aligned microcracks.

References

Blanton T.L, 1983, The relation between recovery deformation and in situ stress magnitudes: SPE Symposium on Low Permeability, Denver, CO, p. 213–218.

Sayers, C. M., 1988, Stress-induced ultrasonic S-wave velocity anisotropy in fractured rock: Ultrasonics, v. 26, p. 311–317.

Strickland, F.G. and Ren, N.K., 1980, Predicting the in situ stress state for deep wells using differential strain curve analysis: SPE 8954, SPE Unconventional Gas Recovery Symposium, Pittsburgh, PA, p. 251–258.

Teufel, L. W., 1983, Determination of the principal horizontal stress directions from anelastic strain recovery measurements of oriented core: application to the Cotton Valley Formation, East Texas: Proc., ASME Symposium on Geomechanics, Houston, TX, June 20–22, 1983.

Warpinski, N.R., and Teufel, L.W, 1989, A viscoelastic constitutive model for determining in situ stress magnitudes from anelastic strain recovery of core: SPE Production Engineering, v. 4, p. 272–280.

APPENDIX E

Computer Codes for Calculating the Effects of Topography on Stress

Two simple computer codes are given as examples of how topographic effects can be easily estimated. The first code is used for estimating the change in stress orientation due to a mesa and escarpment. The second code is a general 3-D code for calculating the additional stress imparted by any type of topographic high, although the example given is for a ridge of finite width and length.

Mesa Topographic Calculations

The effect of a mesa can be evaluated using the equations described in the text. In this code, the geometric input parameters are the height of the mesa, its width, the width of the escarpment, the distance from the edge of the escarpment to the well, and the depth of interest in the well. From these data, the induced stresses at the point of interest (assuming a rock weight gradient of 1.0 psi/ft) are calculated. Next, the far-field in situ stress magnitudes and their orientation relative to the escarpment are input. The two sets of stresses are summed appropriately, and a new principal stress orientation is determined. The following pages contain a listing of the FORTRAN source code for the program.

COMPUTER PRINT OUTS FOLLOW THIS SECTION!

```
      PROGRAM TOPO
C ***  PROGRAM TO CALCULATE THE EFFECT OF A MESA ON THE STRESS
C ***  ORIENTATION AT DEPTH
      CHARACTER*1 IUN,IST
      PRINT*,'                    TOPOGRAPHY PROGRAM'
      PRINT*,' PRESS ENTER TO START: '
      READ(*,100) IST
      PRINT*,' '
      PRINT*,'*****************                                '
      PRINT*,'   |              *                               '
      PRINT*,'   |                *                             '
      PRINT*,'   H                  *'
      PRINT*,'   |                    *'
      PRINT*,'   +                     ***************************'
      PRINT*,'                 |         |                     | * '
      PRINT*,'+------ A ------+--- B ---+------------ C --------* '
      PRINT*,'                 |         |                     | * '
      PRINT*,'                                                 D * '
      PRINT*,'                                                 | * '
      PRINT*,'                                                 + * '
      PRINT*,' INPUT DISTANCES A,B,C,D,H IN SAME UNITS: '
      READ(*,*) A,B,C,D,H
      PRINT*,' ARE UNITS FEET (F) OR METERS (M): '
      READ(*,100) IUN
  100 FORMAT(A1)
      IF(IUN .EQ. 'F' .OR. IUN .EQ. 'f') GRAV=0.433
      IF(IUN .EQ. 'M' .OR. IUN .EQ. 'm') GRAV=9.8
      PRINT*,' INPUT DENSITY IN GM/CC: '
      READ(*,*) RHO
      P=RHO*GRAV*H
      PRINT*,' INPUT POISSONS RATIO: '
      READ(*,*) POISS
      PI=3.141592654
C  ****   BEGIN CALCULATION OF FLAT PART OF MESA + FLAT OVER ESCARP
      THET1=ATAN(D/C)
      IF(C .LT. 0.0) THET1=THET1+PI
      ARG=D/(A+B+C)
      THET2=ATAN(ARG)
      ARG1=THET1-THET2
      ARG2=THET1+THET2
      TA=SIN(ARG1)
      TB=COS(ARG2)
      TC=SIN(ARG2)
      SIGX=P/PI*(THET1-THET2-TA*TB)
      SIGY=P/PI*(THET1-THET2+TA*TB)
      TAUXY=P/PI*(TA*TC)
      WRITE(*,200) SIGX,SIGY,TAUXY
  200 FORMAT(' FOR THE FLAT PART: SIGX=',F12.3,' SIGY=',F12.3,
     1       'TAUXY=',F12.3)
C   ********   SUBTRACT OUT EXCESS ESCARPMENT PART
      ARG=D/(B+C)
      THET2=ATAN(ARG)
      R1=SQRT(C**2+D**2)
      R2=SQRT((B+C)**2+D**2)
      Y=B/2.0+C
```

```
      TA=THET1-THET2
      TB=1+Y/B*2.0
      ARG=2.0*THET1
      SIGX=SIGX-0.5*P/PI*(TB*TA-SIN(ARG))
      SIGY=SIGY-0.5*P/PI*(TB*TA+SIN(ARG)-D/B*2.0*ALOG((R2/R1)**2))
      TAUXY=TAUXY-0.5*P/PI*(1.0-D/B*2.0*TA-COS(ARG))
      SIGZ=POISS*(SIGX+SIGY)
      WRITE(*,201) SIGX,SIGY,TAUXY,SIGZ
  201 FORMAT(' ALL PARTS: SIGX=',F12.3,' SIGY=',F12.3/
     1       ' TAUXY=',F12.3,' SIGZ=',F12.3)
C   ********   GET INFO ON THE GLOBAL STRESS FIELD
      PRINT*,' INPUT THE MAGNITUDES OF THE TWO HORIZONTAL STRESSES '
      PRINT*,' SMAX (S1) THEN SMIN (S2): '
      READ(*,*) S1,S2
      PRINT*,'                        P  *              ^     '
      PRINT*,'                     R  *                 |     '
      PRINT*,'                  A  *                    |     '
      PRINT*,'               C  *                       2     '
      PRINT*,'            S  *  *                       |     '
      PRINT*,'         E  * BETA *                      |     '
      PRINT*,'         * ---------     <------- 1 ------|     '
      PRINT*,' INPUT ANGLE BETA BETWEEN SMAX & ESCARPMENT AZIMUTH:'
      PRINT*,' INPUT -100 FOR RANGE OF BETA (0-90 BY 5 DEG): '
      READ(*,*) BETA
      IF(BETA .GT. -99) THEN
         BETA=BETA/180.0*PI
         N=1
      DBETA=0.0
      ELSE
         BETA=0.0
         DBETA=5.0/180.0*PI
         N=19
      ENDIF
C   ********   CALCULATE PERTURBATION ON GLOBAL STRESSES
      DO 50 I=1,N
         BETAD=BETA*180.0/PI
         WRITE(*,205) BETAD
  205    FORMAT(' BETA=',F8.2)
         S1P=S1+SIGZ*COS(BETA)**2+SIGY*SIN(BETA)**2
         S2P=S2+SIGZ*SIN(BETA)**2+SIGY*COS(BETA)**2
         ARG=2.0*BETA
         TAU12P=0.5*(SIGY-SIGZ)*SIN(ARG)
C   ********   CALCULATE NEW PRINCIPAL STRESS ORIENTATION
         ARG=2.0*TAU12P/(S1P-S2P)
         ALPHA=0.5*ATAN(ARG)
         ALPHA=ALPHA*180.0/PI
         IF(S2P .GT. S1P) ALPHA=ALPHA+90.0
         WRITE(*,202) S1P,S2P,TAU12P,ALPHA
   50    BETA=BETA+DBETA
  202 FORMAT(' NEW STRESSES: S1=',F12.3,' S2=',F12.3,' TAU=',F12.3/
     1       'ANGLE FROM OLD STRESS DIRECTION=',F8.2)
      PRINT*,' PRESS ENTER TO END: '
      READ(*,100) IST
      STOP
      END
```

General 3-D Code for Stress Magnitude Calculations

A general code for any 3-D topographic high can be easily assembled if the topographic feature can be simply represented by a surface or several pieces of surfaces. In this case, equations given by Jaeger and Cook (1976) can be directly applied. Given the geometry shown in Figure E1, where a load is applied at point P and the stress is calculated at point Q, the equations for the stresses are given by:

$$\sigma_x = \frac{1}{2\pi}\iint\left[\frac{3(x-\xi)^2 z}{\rho^5} + \frac{G[(y-\eta)^2+z^2]}{(\lambda+G)\,\rho^3\,(z+\rho)} - \frac{Gz}{(\lambda+G)\,\rho^3} - \frac{G(x-\xi)^2}{(\lambda+G)\,\rho^2\,(z+\rho)^2}\right] p(\xi,\eta)\,d\xi\,d\eta$$

$$\sigma_y = \frac{1}{2\pi}\iint\left[\frac{3(y-\eta)^2 z}{\rho^5} + \frac{G[(x-\xi)^2+z^2]}{(\lambda+G)\,\rho^3\,(z+\rho)} - \frac{Gz}{(\lambda+G)\,\rho^3} - \frac{G(y-\eta)^2}{(\lambda+G)\,\rho^2\,(z+\rho)^2}\right] p(\xi,\eta)\,d\xi\,d\eta$$

$$\sigma_z = \frac{3z^3}{2\pi}\iint \rho^{-5}\,p(\xi,\eta)\,d\xi\,d\eta$$

$$\tau_{yz} = \frac{3z^2}{2\pi}\iint (y-\eta)\,\rho^{-5}\,p(\xi,\eta)\,d\xi\,d\eta$$

$$\tau_{zx} = \frac{3z^2}{2\pi}\iint (x-\xi)\,\rho^{-5}\,p(\xi,\eta)\,d\xi\,d\eta$$

$$\tau_{xy} = \frac{1}{2\pi}\iint\left[\frac{3z(x-\xi)\,(y-\eta)}{\rho^5} - \frac{G(x-\xi)\,(y-\eta)\,(z+2\rho)}{(\lambda+G)\,\rho^3\,(z+\rho)^2}\right] p(\xi,\eta)\,d\xi\,d\eta$$

with $\rho = [(x-\xi)^2 + (y-\eta)^2 + z^2]^{1/2}$

The double integration is not difficult if $p(\xi,\eta)$ can be defined. In this example code, a subroutine is called to provide $p(\xi,\eta)$ at any point in a normalized form (i.e., the height of the topographic feature is divided by the maximum height). Because a subroutine provides the load data, the only input parameters needed for the main program are Poisson's ratio, the maximum height, the density of the rocks, and the depth of the calculation. This program calculates the all six stresses along any line of constant x or constant y values. The following pages are a listing of the FORTRAN source code for this example.

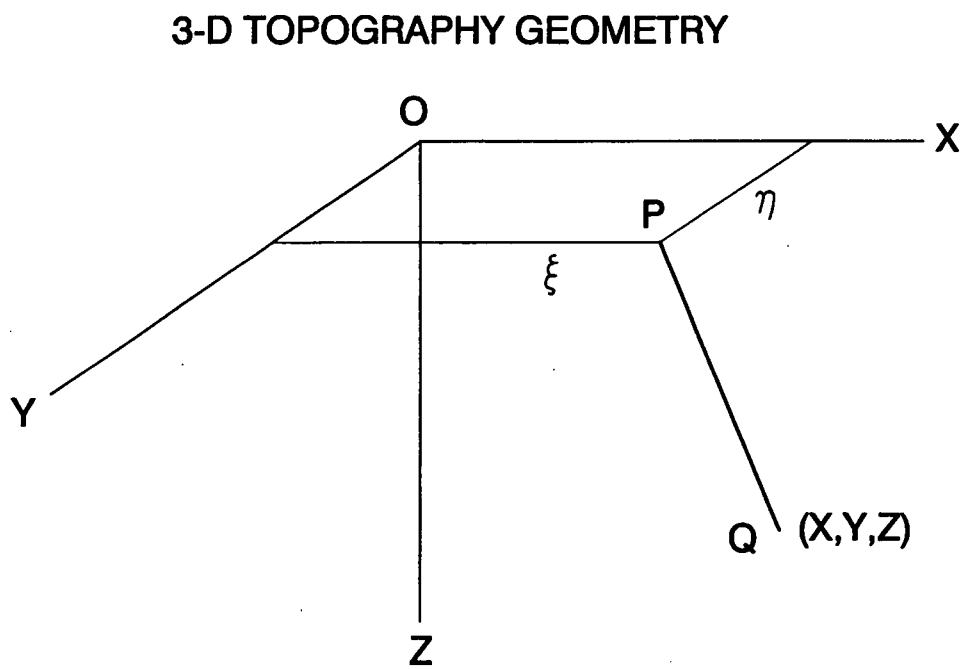

Figure E1. Three-dimensional topography geometry.

```
      PROGRAM TOPO3D
C     PROGRAM TO CALCULATE THE EFFECT OF TOPOGRAPHY ON THE STRESS
C     FIELD AT DEPTH
C        INPUT DATA FOR MAIN PROGRAM INCLUDE:
C                  POISSON'S RATIO
C                  MAXIMUM HEIGHT OF TOPOGRAPHY
C                  DENSITY OF ROCKS IN THE TOPOGRAPHIC HIGH
C                  DEPTH WHERE STRESSES ARE TO BE CALCULATED
C
C        INPUT DATA ON THE RIDGE GEOMETRY ARE HANDLED IN SUBROUTINE
C        PLOAD.  THE CURRENT PLOAD IS AN EXAMPLE FOR A RIDGE
C
C        RESULTS ARE WRITTEN TO AN OUTPUT FILE OF OPERATORS CHOICE
C
C        CALCULATIONS ARE PERFORMED AT THE SPECIFIED DEPTH,Z, ALONG
C        A LINE FOR WHICH EITHER X OR Y ARE CONSTANT
C
      CHARACTER*1 IXY
      CHARACTER*20 FILEOUT
      DIMENSION FA(6,3),FB(6,3),SUMU(6),SUMV(6)
      PRINT*,' INPUT POISSONS RATIO: '
      READ(*,*) POISS
      POI=1.0-2.0*POISS
      PRINT*,' INPUT MAXIMUM HEIGHT (ABOVE SURFACE) OF TOPO: '
      READ(*,*) H
      PRINT*,' INPUT DENSITY OF ROCKS (GM/CC): '
      READ(*,*) DENS
      PFAC=0.433*DENS*H
      PRINT*,' INPUT DEPTH FOR CALCULATION: '
      READ(*,*) Z
      PI=3.141592654
      PRINT*,' INPUT A PATH AND NAME FOR THE OUTPUT FILE: '
      READ(*,101) FILEOUT
  101 FORMAT(A20)
      OPEN(8,FILE=FILEOUT)
C  ***  U=ZETA=X
C  ***  V=ETA=Y
C  ***  CALL PLOAD TO GET MAX AND MIN VALUES FOR INTEGRATION
      CALL PLOAD(0.0,0.0,UMAX,UMIN,VMAX,VMIN,0.0,0)
      WRITE(*,200) UMIN,UMAX,VMIN,VMAX
      WRITE(8,200) UMIN,UMAX,VMIN,VMAX
  200 FORMAT(' ZETA RANGE: ',2F12.2,'   ETA RANGE: ',2F12.2)
      PRINT*,' YOU CAN CALCULATE STRESS ALONG X OR Y LINE'
      PRINT*,' WHICH ONE IS CONSTANT (X OR Y): '
      READ(*,100) IXY
  100 FORMAT(A1)
C  ***  SET UP MIN AND MAX VALUES FOR CALCULATION & NUMBER OF STEPS
      IF(IXY .EQ. 'X' .OR. IXY .EQ. 'x') THEN
C  ***  FOR LINES OF CONSTANT X
         PRINT*,' INPUT X VALUE: '
         READ(*,*) X
         PRINT*,' INPUT MIN & MAX Y VALUES AND NUMBER OF STEPS'
         PRINT*,' FOR ONE POINT, NUMBER OF STEPS = 0: '
         READ(*,*) YMIN,YMAX,N
```

```
         IF(N .NE. 0) THEN
            DY=(YMAX-YMIN)/FLOAT(N)
         ELSE
            DY=0
         ENDIF
         N=N+1
         Y=YMIN
      ELSE
C  ***  FOR LINES OF CONSTANT Y
         PRINT*,' INPUT Y VALUE: '
         READ(*,*) Y
         PRINT*,' INPUT MIN & MAX X VALUES AND NUMBER OF STEPS'
         PRINT*,' FOR ONE POINT, NUMBER OF STEPS = 0: '
         READ(*,*) XMIN,XMAX,N
         IF(N .NE. 0) THEN
            DX=(XMAX-XMIN)/FLOAT(N)
         ELSE
            DX=0
         ENDIF
         N=N+1
         X=XMIN
      ENDIF
      DU=(UMAX-UMIN)/100.0
      DV=(VMAX-VMIN)/100.0
      U=UMIN
      V=VMIN
C **  START CALCULATIONS -- FIRST LOOP FOR DIFFERENT X AND Y VALUES
      DO 50 NI=1,N
C **  PERFORM DOUBLE INTEGRATION, OVER ZETA AND ETA
C **  START ZETA INTEGRAL
         IF(IXY .EQ. 'X' .OR. IXY .EQ. 'x') THEN
            WRITE(*,202) Y
            WRITE(8,202) Y
  202       FORMAT(' Y=',F12.2)
         ELSE
C           WRITE(*,203) X
C           WRITE(8,203) X
C 203       FORMAT(' X=',F12.2)
         ENDIF
         U=UMIN
         DO 8 J=1,6
    8       SUMU(J)=0.0
         KSTART=1
   10    DO 30 K=KSTART,3
            V=VMIN
            DO 12 J=1,6
   12          SUMV(J)=0.0
C **  START ETA INTEGRAL FOR CURRENT ZETA
            ISTART=1
   15       DO 20 I=ISTART,3
               RHO=SQRT((X-U)**2+(Y-V)**2+Z**2)
               AA=3.0*(X-U)**2*Z/RHO**5
               AB=3.0*(Y-V)**2*Z/RHO**5
               AC=POI*((X-V)**2+Z**2)/(RHO**3*(Z+RHO))
```

```
                AD=POI*Z/RHO**3
                AE=POI*(X-U)**2/(RHO**2*(Z+RHO)**2)
                AF=1.0/RHO**5
                AG=AF*(Y-V)
                AH=AF*(X-U)
                AI=3.0*Z*(X-U)*(Y-V)*AF
                AJ=POI*(X-U)*(Y-V)*(Z+2.0*RHO)/(RHO**3*(Z+RHO)**2)
C **  CALL SUBROUTINE PLOAD FOR LOAD INFORMATION
                CALL PLOAD(U,V,UMAX,UMIN,VMAX,VMIN,P,1)
C               IF(I .EQ. 1) WRITE(*,210) U,V,P
C 210           FORMAT(' U=',F12.2,'  V=',F12.2,'  P=',F12.6)
C **  GET FACTORS FOR EACH STRESS COMPONENT
                FB(1,I)=(AA+AC+AD+AE)*P
                FB(2,I)=(AB+AC+AD+AE)*P
                FB(3,I)=AF*P
                FB(4,I)=AG*P
                FB(5,I)=AH*P
                FB(6,I)=(AI+AJ)*P
                VOLD=V
   20           V=V+DV
             ISTART=2
C **  GET SUMS FOR EACH STRESS COMPONENT
             DO 25 J=1,6
                SUMV(J)=SUMV(J)+DV*(FB(J,1)+4.0*FB(J,2)+FB(J,3))/3.0
   25           FB(J,1)=FB(J,3)
C            WRITE(*,207) VOLD,(SUMV(J),J=1,6)
C            WRITE(8,207) VOLD,(SUMV(J),J=1,6)
C 207        FORMAT(' V=',F12.2,'  V SUMS: ',2F12.6/4E12.4)
             IF((VOLD-VMAX) .LT. -1.E-03) GO TO 15
C  **  END OF FIRST INTEGRAL LOOP
C  ** FACTORS FOR OUTSIDE INTEGRAL TAKEN DIRECTLY FROM INSIDE ONE
             DO 28 L=1,6
   28           FA(L,K)=SUMV(L)
             UOLD=U
   30        U=U+DU
          KSTART=2
C **  GET SUMS FOR EACH STRESS COMPONENT
          DO 35 J=1,6
             SUMU(J)=SUMU(J)+DU*(FA(J,1)+4.0*FA(J,2)+FA(J,3))/3.0
   35        FA(J,1)=FA(J,3)
C            WRITE(*,208) UOLD,(SUMU(J),J=1,6)
C            WRITE(8,208) UOLD,(SUMU(J),J=1,6)
C 208        FORMAT(' U=',F12.2,'  U SUMS: ',2F12.6/4E12.4)
          IF((UOLD-UMAX) .LT. -1.E-03) GO TO 10
C **  END OF SECOND INTEGRAL LOOP
C **  CALCULATE STRESSES
          SIGX=SUMU(1)*0.5/PI*PFAC
          SIGY=SUMU(2)*0.5/PI*PFAC
          SIGZ=1.5*Z**3/PI*SUMU(3)*PFAC
          TAUYZ=1.5*Z**2/PI*SUMU(4)*PFAC
          TAUXZ=1.5*Z**2/PI*SUMU(5)*PFAC
          TAUXY=0.5/PI*SUMU(6)*PFAC
          WRITE(*,205) X,Y,Z,SIGX,SIGY,SIGZ,TAUYZ,TAUXZ,TAUXY
          WRITE(8,205) X,Y,Z,SIGX,SIGY,SIGZ,TAUYZ,TAUXZ,TAUXY
```

```
205    FORMAT('     X= ',F12.2,'     Y= ',F12.2,'     Z= ',F12.2/
   '          '  SIGX= ',F12.2,'  SIGY= ',F12.2,'  SIGZ= ',F12.2/
   2          ' TAUYZ= ',F12.2,' TAUXZ= ',F12.2,' TAUXY= ',F12.2)
       IF(IXY .EQ. 'X' .OR. IXY .EQ. 'x') THEN
          Y=Y+DY
       ELSE
          X=X+DX
       ENDIF
 50    CONTINUE
    CLOSE(8)
    STOP
    END


    SUBROUTINE PLOAD(ZETA,ETA,ZETAMAX,ZETAMIN,ETAMAX,ETAMIN,SUM,
   1           IQ)
C  **  SUBROUTINE FOR A SHORT RIDGE
C
C                       FRONT                              SIDE
C
C                ********************                         *
C              * |        |        | *                      *|*
C            *   |        |        |   *                  * | *
C          *     |        H        |     *                *  |  *
C        *       |        |        |       *            *   |   *
C      *         |        |        |         *         *    |    *
C    *           |        |        |           *      *     |     *
C -ZETA1      -ZETAO      o      ZETAO       ZETA1  -ETAO   o  ETAO
C
C
C  ETA CONTRIBUTION
C  ETA< ABS(ETAO)                        [ETAO-ABS(ETA)]/ETAO
C  ETA> ABS(ETAO)                                  0
C  ZETA CONTRIBUTION
C  ZETA < ABS(ZETAO)                               1
C  ABS(ZETAO) < ZETA < ABS(ZETA1)  [ZETA1-ABS(ZETA)]/[ZETA1-ZETAO]
C  **   ZETA > ABS(ZETA1)                              0
C
C
C  **  SIZE OF MOUNTAIN RIDGE
      ETAO=5000
      ZETAO=5000
      ZETA1=10000
      ETAMIN=-ETAO
      ETAMAX=ETAO
      ZETAMIN=-ZETA1
      ZETAMAX=ZETA1
      IF(IQ .EQ. 0) RETURN
C  **  GET CONTRIBUTIONS
      SUM=1.0
      IF(ABS(ETA) .LT. ETAO) THEN
         SUM=SUM*(ETAO-ABS(ETA))/ETAO
```

```
ELSE
   SUM=0.0
   RETURN
ENDIF
IF(ABS(ZETA) .GT. ZETA1) THEN
   SUM=0.0
   RETURN
ELSE IF(ABS(ZETA) .LT. ZETAO) THEN
   SUM=SUM*1.0
ELSE
   SUM=SUM*(ZETA1-ABS(ZETA))/(ZETA1-ZETAO)
ENDIF
RETURN
END
```

References

Jaeger, J.C. and Cook, N.G.W, 1976, *Fundamentals of Rock Mechanics,* Halsted Press, New York.

APPENDIX F

Computer Code for Stress-History Calculations

A computer code, which was originally developed to calculate the stress history of the Multiwell site, has been modified for general use in calculating the stress history at any site. This model assumes that the rock is viscoelastic, although large relaxation times result in an elastic calculation, and that the stresses are controlled by the weight of the overburden, the pore pressure, the temperature, the tectonic strains in both horizontal directions, and the properties of the rocks, which are functions of time. The difficulty in running this model lies primarily in determining the input parameters with sufficient accuracy.

The equations governing the response of the rock are first developed in the text in elastic form and are given in Appendix C in viscoelastic form. The primary input parameters are the material and formation characteristics at each time step. These include:

TIME	time point (million years before present time)
DEPTH	depth at this time (ft)
POISSPC	Poisson's ratio in percent of (final-initial) Poisson's ratio
EPC	Young's modulus in percent of (final-initial) Young's modulus
EPSX	tectonic strain in minimum direction, accumulated at this time step ($\mu\xi$)
EPSY	tectonic strain in maximum direction, accumulated at this time step ($\mu\xi$)
RHO	density of the rocks (gm/cc)
PGRAD	pore pressure gradient (psi/ft)
TGRAD	temperature gradient (deg F/1000 ft)
ALPHA	coefficient of thermal expansion (in/in/deg F)

Other input parameters include:

Number of time steps
The present Poisson's ratio and Young's modulus (psi)
The initial Poisson's ratio and Young's modulus (psi)
The rock relaxation time (million years)
The number of integration steps (usually 4 is sufficient)

The time dependent inputs for Poisson's ratio and Young's modulus were set up as percentages of the (final-initial) values because the initial value is not well-constrained. This way, initial values and the subsequent lithification rates could be easily changed for parametric studies without changing the entire input file at each time step. The strain input is set up so that the strains are cumulative. If the calculation is elastic (large relaxation time) with constant properties, then the total tectonic strain at any time is the sum of all the previous strains. If a large compressive strain (positive strain) has occurred for some period, then relaxation of this compressive strain is accomplished with an extensional strain (negative strain) at the next time steps. Example input data sets for the three cases run in this study are given in Tables F1, F2, and F3.

Table F1. MWX Cozzette Input Data

```
COZZETTE SANDSTONE   PICEANCE BASIN
            7
75.0      0.0 0.000 0.000  0.00000  0.00000 2.100 0.4330  0.00 0.60E-05
66.0   4100.0 0.380 0.380  0.00000  0.00050 2.300 0.4330 19.96 0.60E-05
60.0   4100.0 0.400 0.400  0.00000  0.00050 2.400 0.4330 19.96 0.60E-05
46.0  10400.0 0.890 0.890 -0.00100  0.00100 2.500 0.5000 20.23 0.60E-05
36.0  11700.0 1.000 1.000 -0.00100 -0.00040 2.500 0.8500 20.25 0.60E-05
11.0  11700.0 1.000 1.000  0.00050 -0.00040 2.500 0.9000 20.25 0.60E-05
 0.0   7900.0 1.000 1.000  0.00036 -0.00040 2.500 0.8000 20.17 0.60E-05
   0.220     0.45000E+07   0.400     0.30000E+06
    1000.00000000
            4
```

Table F2. Ralston Federal 31 Cozzette Input Data

```
RALSTON FEDERAL 31
            6
74.0      0.0 0.000 0.000  0.00000  0.00000 2.100 0.4330  0.00 0.60E-05
66.0   4000.0 0.500 0.500  0.00000  0.00050 2.300 0.4330 24.00 0.60E-05
60.0   4000.0 0.550 0.550  0.00000  0.00050 2.400 0.4330 24.00 0.60E-05
36.0   8500.0 1.000 1.000 -0.00100  0.00100 2.500 0.6000 24.00 0.60E-05
11.0   8500.0 1.000 1.000 -0.00050 -0.00040 2.500 0.7000 24.00 0.60E-05
 0.0   6370.0 1.000 1.000  0.00030 -0.00040 2.500 0.6500 24.00 0.60E-05
   0.220     0.45000E+07   0.400     0.30000E+06
    1000.00000000
            4
```

Table F3. Apache 1-C Rushmore Cozzette Input Data

```
APACHE 1-C US RUSHMORE
            7
73.0      0.0 0.000 0.000  0.00000  0.00000 2.100 0.4330  0.00 0.60E-05
66.0   3700.0 0.350 0.350  0.00000  0.00050 2.200 0.4330 25.70 0.60E-05
60.0   3700.0 0.380 0.380  0.00000  0.00050 2.300 0.4330 25.70 0.60E-05
47.0   9900.0 0.900 0.900 -0.00100  0.00100 2.400 0.5000 23.70 0.60E-05
36.0  11000.0 1.000 1.000 -0.00100 -0.00040 2.500 0.8000 24.50 0.60E-05
11.0  11000.0 1.000 1.000  0.00050 -0.00040 2.500 0.8500 24.50 0.60E-05
 0.0   8550.0 1.000 1.000  0.00036 -0.00040 2.500 0.8000 24.50 0.60E-05
   0.220     0.45000E+07   0.400     0.30000E+06
    1000.00000000
            4
```

This program was written, compiled, and linked using Ryan-McFarland FORTRAN and the PLOT88 software library for graphics. The main program contains the evaluation of the integrals through all time steps. Subroutine INPUT is used to enter the data, either by hand or by file. Subroutine TABLE writes the data in a tabular form. Subroutine SPLOT is a plotting routine that can produce the following output as a function of time:

Total stresses (SHMAX, SHMIN, SV, P)
Effective stresses (EFFSHMAX, EFFSHMIN, EFFSV)
Stress components (S1 (gravity), S2 (thermal), S3X (x tectonic), S3Y (y tectonic))
Strains (EPSX, EPSY)
Temperature (T)
Depth (D)

Subroutine FAIL calculates the failure behavior of the rocks and compares this behavior to actual failure data input by the user. Mohr-Coulomb failure data are used for this routine, and an example of input failure data for the Cozzette case is given below.

```
5
    -2320.00        0.00
    11237.50        11165.00
    17980.00        16457.50
    22910.00        20010.00
    29145.00        24795.00
```

The first input is the number of data points, followed by any points on the Mohr-Coulomb envelope, with the first point being mean effective stress and the second point being maximum shear stress. There is also an option for a reduced strength envelope. Most failure data are obtained on dry samples at strain rates of 1×10^{-5}. Under in situ geologic conditions, where water is present and strain rates are several orders of magnitude lower, the failure envelope can be expected to be 20–50% lower, and this can be accounted for using a reduction factor of 0.8–0.5. Failure results are also plotted in subroutine FAIL. A listing of the FORTRAN source code and example output for the Cozzette case are given in the following pages.

A sample output for the Cozzette sandstone is presented. These results were obtained using the input from Tables F1, F2, and F3. The accompanying plots (Figures F1–F7), were produced during the running of the output example. They show all the data that can be plotted using this program.

Program

```
      PROGRAM SHIST
      PARAMETER (IT=20,ID=20)
      CHARACTER*1 IINTST,IRELAX,ITIME,IUNITS,IPLOT,ITABLE,IFAIL,ICONT
      CHARACTER*40 DEFZONE
      DIMENSION SV(IT,ID),SHMIN(IT,ID),SHMAX(IT,ID),PO(IT,ID),EPSY(IT),
     1T(IT),D(IT),TIN(IT),DIN(IT),S1(IT,ID),S2(IT,ID),S3X(IT,ID),
     2S3Y(IT,ID),ESV(IT,ID),ESHMIN(IT,ID),ESHMAX(IT,ID),EPSX(IT),
     3PGRAD(IT),RHO(IT),ALPHA(IT),TGRAD(IT),TDEPTH(3),TEMP(IT,ID)
      DIMENSION POISPC(IT),EPC(IT),SUM(9),ADD(9),
     1EO(IT),EM(IT),POISSO(IT),POISSM(IT),PGRADO(IT),PGRADM(IT),
     2ALPHAO(IT),ALPHAM(IT),FEPSXM(IT),FEPSYM(IT),
     3FDTDT(IT),FGRAV(IT),TREL(IT,ID),TINC(IT),DREL(IT,ID)
C  INITIALIZE DATA
      IINTST='N'
      IRELAX='N'
    1 DO 2 I=1,IT
        T(I)=0.0
      DO 2 J=1,ID
        SV(I,J)=0.0
        PO(I,J)=0.0
        S1(I,J)=0.0
        S2(I,J)=0.0
        S3X(I,J)=0.0
        S3Y(I,J)=0.0
        SHMIN(I,J)=0.0
        SHMAX(I,J)=0.0
        ESHMIN(I,J)=0.0
        ESHMAX(I,J)=0.0
    2   ESV(I,J)=0.0
      TSURF=50.
      T(1)=TSURF
C  INPUT DATA IF NEEDED
      IF(IINTST .EQ. 'Y' .OR. IRELAX .EQ. 'Y') GO TO 3
      CALL INPUT(TIN,DIN,POISPC,EPC,EPSX,EPSY,DEPTH,POISS,E,RHO,TGRAD,
     1           ALPHA,DDEPTH,N,POISSI,EI,PGRAD,NSTEPS,TR,DEFZONE)
      TEMP(1,NSTEPS)=TSURF
      TREL(1,NSTEPS)=TIN(1)
      DREL(1,NSTEPS)=0.0
      DPOISS=POISS-POISSI
      DE=E-EI
      POISSO(1)=POISSI
      EO(1)=EI
C  CALCULATE TIMES FOR EACH INCREMENT
    3 DO 5 LL=2,N
         TINC(LL)=TIN(LL-1)-TIN(LL)
         DTINC=TINC(LL)/REAL(NSTEPS)
         DO 4 JJ=1,NSTEPS
    4       TREL(LL,JJ)=TIN(LL-1)-DTINC*REAL(JJ)
    5 CONTINUE
      D(1)=0.0
```

```
C  START THE CALCULATIONS; DO LOOP ON LARGE TIME INTERVALS
      DO 50 L=2,N
      PRINT 100,TIN(L),EPSX(L),EPSY(L),POISPC(L),EPC(L)
      WRITE(10,100)TIN(L),EPSX(L),EPSY(L),POISPC(L),EPC(L)
      PRINT 202,RHO(L),TGRAD(L),ALPHA(L),PGRAD(L)
      WRITE(10,202) RHO(L),TGRAD(L),ALPHA(L),PGRAD(L)
      DDELTA=DIN(L)-DIN(L-1)
      D(L)=D(L-1)+DDELTA
C  DETERMINE SLOPE AND INTERCEPTS FOR THE PROPERTIES
      POISSO(L)=POISPC(L-1)*DPOISS+POISSI
      EO(L)=EPC(L-1)*DE+EI
      POISSM(L)=(POISPC(L)-POISPC(L-1))*DPOISS/TINC(L)
      EM(L)=(EPC(L)-EPC(L-1))*DE/TINC(L)
      PGRADO(L)=PGRAD(L-1)
      PGRADM(L)=(PGRAD(L)-PGRAD(L-1))/TINC(L)
      ALPHAO(L)=ALPHA(L-1)
      ALPHAM(L)=(ALPHA(L)-ALPHA(L-1))/TINC(L)
C  DETERMINE THE FORCING LOADS AND STRAINS FOR THIS TIME STEP
      FEPSXM(L)=EPSX(L)/TINC(L)
      FEPSYM(L)=EPSY(L)/TINC(L)
      T(L)=TSURF+D(L)*TGRAD(L)/1000.
      FDTDT(L)=(T(L)-T(L-1))/TINC(L)
      FGRAV(L)=(((0.433*RHO(L)-PGRAD(L))*D(L))-((0.433*
     1RHO(L-1)-PGRAD(L-1))*D(L-1)))/TINC(L)
C  START THE INTEGRATION
C  REMEMBER, EACH INTEGRAL MUST BE CARRIED THROUGH ALL TIME
C  THE FIRST LOOP IS FOR EACH OF THE INCREMENTAL TIMES THAT THE
C     RELAXATION FUNCTION IS TO BE EVALUATED
      DZ1=DDELTA/REAL(NSTEPS)
      DO 35 MTIME=1,NSTEPS
      TIME=TREL(L,MTIME)
C     PRINT 504,L,MTIME,TIME
C     WRITE(10,504)L,MTIME,TIME
C 504 FORMAT(' L=',I2,'  MTIME=',I2,'  TIME=',F12.4)
C  THE 2ND LOOP IS FOR EACH STEP IN HISTORY WHERE A FORCING FUNC. OCCURS
      DO 30 MFF=2,L
C     PRINT 503,MFF,FGRAV(MFF),FDTDT(MFF),FEPSXM(MFF),FEPSYM(MFF)
C     WRITE(10,503)MFF,FGRAV(MFF),FDTDT(MFF),FEPSXM(MFF),FEPSYM(MFF)
C 503 FORMAT(' MFF=',I2,'  FG=',E12.4,' FDT=',E12.4,' FEPSX=',E12.4,
C    1' FEPSY=',E12.4)
C  NEED THE INCREMENTAL TIME STEP FOR EACH LARGE TIME PERIOD
C  REMEMBER, EACH LARGE TIME PERIOD IS DIIFERENT SIZE, SO THE
C  INCREMENTAL TIME STEPS ARE IRREGULAR ALSO
      DZ=TINC(MFF)/(REAL(NSTEPS)*2.0)
      Z=0.0
C     PRINT 502,MFF,TINC(MFF),DZ
C     WRITE(10,502)MFF,TINC(MFF),DZ
C 502 FORMAT(' MFF=',I2,'  TINC=',F12.4,'  DZ=',F12.6)
```

```
C  START THE SUMMATION FOR EACH INCREMENTAL TIME STEP
C  THE 3RD LOOP CALCULATES INCREMENTAL STRESS FOR EACH INCREMENTAL TIME
      DO 20 I=1,NSTEPS
      IF(MFF .EQ. L .AND. I .GT. MTIME) GO TO 20
C     PRINT 501,I,Z
C     WRITE(10,501)I,Z
C 501 FORMAT(' I=',I2,'  Z=',F12.4)
      DO 8 JJ=1,6
    8 SUM(JJ)=0.0
C  EVALUATE PROPERTIES AT THREE POINTS(ENDS AND MIDDLE)
      DO 15 J=1,3
      POISSF=POISSO(MFF)+POISSM(MFF)*Z
      EF=EO(MFF)+EM(MFF)*Z
      ALPHAF=ALPHAO(MFF)+ALPHAM(MFF)*Z
C  CALCULATE THE DELTA TIME OVER WHICH RELAXATION OCCURS
C  REMEMBER, TIME INCREASES AS WE GO BACK IN HISTORY
      TINTEG=TIN(MFF-1)-Z
      RELAXT=TINTEG-TIME
C  EVALUATE THE RELAXATION FUNCTION AT THIS TIME
      C1=1.0-POISSF
      C2=1.0+POISSF
      C3=1.0-2.0*POISSF
      C4=3.0*C1/C2
      C5=EXP(-RELAXT/TR)
      C6=EXP(-C4*RELAXT/TR)
      A1=C1/POISSF-C3/POISSF*C5
      A2=C2/2.0*C5+C1/2.0*C6
      A3=0.5*C2/POISSF*C5-0.5*C1/POISSF*C6
      A4=C5
C     PRINT 500,J,TIME,TINTEG,RELAXT,A1,A2,A3,A4,A5,A6
C     WRITE(10,500)J,TIME,TINTEG,RELAXT,A1,A2,A3,A4,A5,A6
C 500 FORMAT(' J=',I2,'  TIME=',F12.4,'  TINTG=',F12.4,' RELXT=',F12.4
C    1,' THE A''S ARE',/6E12.4)
C  CALCULATE TOTAL CONTRIBUTION TO INTEGRAL (RELAX. + PROP + FOR FUN)
      ADD(1)=POISSF/(1.0-POISSF)*FGRAV(MFF)*A1
      ADD(2)=ALPHAF*EF/(1.0-POISSF)*FDTDT(MFF)*A4
      ADD(3)=EF/(1.0-POISSF**2)*FEPSXM(MFF)*A2
      ADD(4)=EF/(1.0-POISSF**2)*FEPSYM(MFF)*A2
      ADD(5)=POISSF*ADD(3)*A3/A2
      ADD(6)=POISSF*ADD(4)*A3/A2
C     PRINT 505,(ADD(IJK),IJK=1,6)
C     WRITE(10,505)(ADD(IJK),IJK=1,6)
C 505 FORMAT('ADD(I)=',6E12.4)
      FAC=1.0
      IF(J .EQ. 2) FAC=4.0
C  ADD THIS CONTRIBUTION TO THE RUNNING SUM (3 POINTS FOR EACH SUM)
      DO 12 K=1,6
   12 SUM(K)=SUM(K)+ADD(K)*FAC
   15 IF(J .LT. 3) Z=Z+DZ
```

```
C  NOW CALCULATE THE STRESS COMPONENTS FOR THIS INCREMENT
      S1(L,MTIME)=S1(L,MTIME)+DZ/3.0*SUM(1)
      S2(L,MTIME)=S2(L,MTIME)+DZ/3.0*SUM(2)
      S3X(L,MTIME)=S3X(L,MTIME)+DZ/3.0*(SUM(3)+SUM(6))
      S3Y(L,MTIME)=S3Y(L,MTIME)+DZ/3.0*(SUM(4)+SUM(5))
C     PRINT 506,S1(L,MTIME),S2(L,MTIME),S3X(L,MTIME),S3Y(L,MTIME)
C     WRITE(10,506)S1(L,MTIME),S2(L,MTIME),S3X(L,MTIME),S3Y(L,MTIME)
C 506 FORMAT(' S1=',E12.4,'  S2=',E12.4,'  S3X=',E12.4,'  S3Y=',E12.4)
   20 CONTINUE
C  END OF THE THIRD LOOP
C  END OF THE SECOND LOOP
   30 CONTINUE
C  CALCULATE OVERBURDEN STRESS, PORE PRESSURE AND TEMPERATURE
      DREL(L,MTIME)=D(L-1)+DZ1*REAL(MTIME)
      SV(L,MTIME)=RHO(L)*0.433*DREL(L,MTIME)
      PO(L,MTIME)=(PGRADO(L)+PGRADM(L)*(TIN(L-1)-TREL(L,MTIME)))*
     1DREL(L,MTIME)
      TEMP(L,MTIME)=T(L-1)+FDTDT(L)*TINC(L)*REAL(MTIME)/REAL(NSTEPS)
C  CALCULATE THE HORIZONTAL STRESSES
      SHMIN(L,MTIME)=S1(L,MTIME)+S2(L,MTIME)+S3X(L,MTIME)+PO(L,MTIME)
      SHMAX(L,MTIME)=S1(L,MTIME)+S2(L,MTIME)+S3Y(L,MTIME)+PO(L,MTIME)
C  CALCULATE THE EFFECTIVE STRESSES
      ESV(L,MTIME)=SV(L,MTIME)-PO(L,MTIME)
      ESHMIN(L,MTIME)=SHMIN(L,MTIME)-PO(L,MTIME)
      ESHMAX(L,MTIME)=SHMAX(L,MTIME)-PO(L,MTIME)
      PRINT 201,DREL(L,MTIME),SV(L,MTIME),S1(L,MTIME),S2(L,MTIME),S3X(L
     1,MTIME),S3Y(L,MTIME),SHMIN(L,MTIME),SHMAX(L,MTIME),PO(L,MTIME),
     2TEMP(L,MTIME),ESV(L,MTIME),ESHMIN(L,MTIME),ESHMAX(L,MTIME)
      WRITE(10,201) DREL(L,MTIME),SV(L,MTIME),S1(L,MTIME),S2(L,MTIME),
     1              S3X(L,MTIME),S3Y(L,MTIME),SHMIN(L,MTIME),
     2              SHMAX(L,MTIME),PO(L,MTIME),TEMP(L,MTIME),
     3              ESV(L,MTIME),ESHMIN(L,MTIME),ESHMAX(L,MTIME)
C END OF FIRST LOOP
   35 CONTINUE
   50 CONTINUE
C  PREPARE FOR OUTPUT
      IPU=1
      PRINT*,' DO YOU WANT OUTPUT IN SI(S) OR CONV(C) UNITS: '
      READ 111,IUNITS
      IF(IUNITS .EQ. 'S') THEN
         A=0.0068948
         IPU=2
         DO 55 J=1,N
         DO 55 K=1,NSTEPS
         SV(J,K)=SV(J,K)*A
         PO(J,K)=PO(J,K)*A
         S1(J,K)=S1(J,K)*A
         S2(J,K)=S2(J,K)*A
         S3X(J,K)=S3X(J,K)*A
         S3Y(J,K)=S3Y(J,K)*A
         SHMIN(J,K)=SHMIN(J,K)*A
         SHMAX(J,K)=SHMAX(J,K)*A
```

```
         ESV(J,K)=ESV(J,K)*A
         ESHMIN(J,K)=ESHMIN(J,K)*A
   55    ESHMAX(J,K)=ESHMAX(J,K)*A
      ENDIF
C  PREPARE FOR PLOTS
      PRINT*,' DO YOU WANT PLOTS: '
      READ 111,IPLOT
  111 FORMAT(A1)
      IF(IPLOT .EQ. 'N') GO TO 60
      D(1)=0.0
      CALL SPLOT(D,TIN,SV,SHMIN,SHMAX,PO,S1,S2,S3X,S3Y,T,ESV,ESHMIN,
     1           ESHMAX,EPSX,EPSY,N,DEPTH,IPU,NSTEPS,TREL,DEFZONE)
C  PREPARE FOR A TABLE OF THE DATA
   60 PRINT*,' DO YOU WANT A TABLE OF THE DATA: '
      READ 111,ITABLE
      IF(ITABLE .NE. 'Y') GO TO 70
      CALL TABLE(N,TREL,SV,SHMIN,SHMAX,ESV,ESHMIN,ESHMAX,
     1S1,S2,S3X,S3Y,PO,TEMP,EPSX,EPSY,PGRAD,RHO,POISSO,EO,ALPHA,
     2IPU,NSTEPS,DREL)
C  FAILURE ANALYSIS
   70 PRINT*,' DO YOU WANT A FAILURE ANALYSIS: '
      READ 111,IFAIL
      IF(IFAIL .EQ. 'N') GO TO 80
      CALL FAILURE(N,ESV,ESHMIN,ESHMAX,PO,TIN,DIN,IPU,NSTEPS,TREL,
     1             DREL,DEFZONE)
C  CONTINUATION SEQUENCE
   80 PRINT*,' DO YOU WANT TO CONTINUE: '
      READ 111,ICONT
      IF(ICONT .EQ. 'N') STOP
      PRINT*,' DO YOU WANT SAME DATA WITH A NEW RELAXATION TIME: '
      READ 111,IRELAX
      IF(IRELAX .EQ. 'Y') THEN
         PRINT*,' INPUT THE NEW RELAXATION TIME IN MY: '
         READ(11,*) TR
         GO TO 85
      ENDIF
      PRINT*,' DO YOU WANT SAME DATA WITH NEW INTEGRATION STEP: '
      READ 111,IINTST
      IF(IINTST .EQ. 'N') GO TO 1
   85 PRINT*,' INPUT THE NUMBER OF INTEGRATION STEPS: '
      READ (11,*) NSTEPS
      GO TO 1
  100 FORMAT(/' TIME IN MILLIONS OF YEARS BEFORE PRESENT =',F5.2/
     1' EPSX=',E12.4,'    EPSY=',E12.4/'  POISPC=',F10.8,'    EPC=',
     2F10.8/)
  201 FORMAT(' D=',F10.2,' SV=',F10.2,' S1=',F10.2,' S2=',F10.2/
     1' S3X=',F10.2,' S3Y=',F10.2,' SHMIN=',F10.2,' SHMAX=',F10.2/
     2' PO=',F10.2,' TEMP=',F7.1,/
     3' EFF SV=',F10.2,' EFF SHMIN=',F10.2,' EFF SHMAX=',F10.2)
  202 FORMAT(3X,'INPUT PARAMETERS'/'  RHO=',F8.4,' GM/CM**3'/
     1'  TGRAD=',F8.4,' DEG F/100 FT'/'  ALPHA=',E14.4,'  1/DEG F'/
     2'  PGRAD=',F8.5,' PSI/FT'/)
      END
```

```
C
C
      SUBROUTINE INPUT(TIN,DIN,POISSPC,EPC,EPSX,EPSY,DEPTH,POISS,E,
     1                 RHO,TGRAD,ALPHA,DDEPTH,N,POISSI,EI,PGRAD,
     2                 NSTEPS,TR,DEFZONE)
      CHARACTER*1 IFH,IWR
      CHARACTER*20 FILEIN,FILEOUT
      CHARACTER*40 DEFZONE
      PARAMETER (IT=20)
      DIMENSION TIN(IT),DIN(IT),POISSPC(IT),EPC(IT),EPSX(IT),EPSY
     1(IT),PGRAD(IT),TGRAD(IT),ALPHA(IT),RHO(IT)
C  INPUT DATA
C
C         POISSPC ------- POISSONS RATIO--% INCREASE FROM INITIAL TO
C                                           PRESENT DAY VALUE
C         EPC ----------- YOUNGS MODULUS--% INCREASE FROM INITIAL TO
C                                           PRESENT DAY VALUE
C         EPSX ---------- TECTONIC STRAIN IN MIN DIRECTION--MICROSTRAIN
C         EPSY ---------- TECTONIC STRAIN IN MAX DIRECTION--MICROSTRAIN
C         RHO ----------- DENSITY--GM/CC
C         PGRAD --------- PORE PRESSURE GRADIENT--PSI/FT
C         TGRAD --------- TEMPERATURE GRADIENT--DEG F/1000 FT
C         ALPHA --------- COEFFICIENT OF LINEAR THERMAL EXPANSION
C
C
C                 INPUT FILE
C
C     1: DESCRIPTION OF ZONE (40 CHARACTERS)
C     2: NUMBER OF TIME STEPS (N)
C     3: I=1,N  TIME, DEPTH,POISSPC,EPC,EPSX,EPSY,RHO,PGRAD,TGRAD,ALPHA
C     4: POISSON'S RATIO, YOUNG'S MODULUS, INITIAL POISS, INITIAL YOUNG
C     5: RELAXATION TIME IN MYRS
C     6: NUMBER OF INTEGRATION STEPS
C
C
C
      PRINT*,' DO YOU WANT TO INPUT BY FILE (F) OR HAND (H): '
      READ(*,100) IFH
  100 FORMAT(A1)
      IF(IFH .EQ. 'F' .OR. IFH .EQ. 'f') THEN
         PRINT*,' WHAT IS THE NAME OF THE INPUT FILE: '
         READ(*,101) FILEIN
         OPEN (8,FILE=FILEIN)
         REWIND 8
         READ(8,102) DEFZONE
  101    FORMAT(A20)
  102    FORMAT(A40)
         READ(8,*) N
         DO 2 I=1,N
    2       READ(8,*) TIN(I),DIN(I),POISSPC(I),EPC(I),EPSX(I),EPSY(I),
     1                RHO(I),PGRAD(I),TGRAD(I),ALPHA(I)
         READ(8,*) POISS,E,POISSI,EI
```

```
         READ(8,*) TR
         READ(8,*) NSTEPS
         CLOSE (8)
         PRINT*,' DATA FILE READ '
      ELSE
         PRINT*,' INPUT A DESCRIPTION OF THE ZONE/BASIN (40 CHARS): '
         PRINT*,' '
         READ(*,102) DEFZONE
    5    PRINT*,' HOW MANY TIMES AT WHICH YOU HAVE DATA: '
         READ (*,*) N
         IPP=7
         ITEMPD=1
         WRITE(*,300)
  300    FORMAT(' INPUT THE DATA FOR EACH TIME INTERVAL; START AT',
     1       ' EARLIEST PERIOD')
         WRITE(*,301)
  301    FORMAT(' TIME(MYBP),DEPTH OF ZONE(FT),POISSPC,EPC,EPSX,EPSY,',
     1          'RHO,PGRAD,TGRAD,ALPHA')
         DO 10 I=1,N
            WRITE(*,333) I
  333       FORMAT(' TIME STEP #',I3,': ')
   10       READ (*,*) TIN(I),DIN(I),POISSPC(I),EPC(I),EPSX(I),EPSY(I)
     1           ,RHO(I),PGRAD(I),TGRAD(I),ALPHA(I)
C  INPUT DATA FOR CURRENT TIME
   11    PRINT*,' INPUT: PRESENT POISS AND E: '
         READ (*,*) POISS,E
         PRINT*,' INPUT: INITIAL POISS AND E: '
         READ (*,*) POISSI,EI
         DDEPTH=DIN(N)
C  VISCOELASTIC DATA
         PRINT*,' INPUT THE RELAXATION TIME IN MILLIONS OF YEARS: '
         READ(*,*) TR
         PRINT*,' INPUT THE NUMBER OF INTEGRATION STEPS: '
         READ (*,*) NSTEPS
         PRINT*,' DO YOU WANT THESE DATA WRITTEN TO A FILE: '
         READ(*,100) IWR
         IF(IWR .EQ. 'Y' .OR. IWR .EQ. 'y') THEN
            PRINT*,' DATA WILL BE SAVED; WHAT FILE NAME: '
            READ(*,101) FILEOUT
            OPEN(9,FILE=FILEOUT)
            REWIND 9
            WRITE(9,102) DEFZONE
            WRITE(9,*) N
            DO 20 I=1,N
   20          WRITE(9,400) TIN(I),DIN(I),POISSPC(I),EPC(I),EPSX(I),
     1                    EPSY(I),RHO(I),PGRAD(I),TGRAD(I),ALPHA(I)
  400       FORMAT(1X,F7.1,1X,F7.1,1X,F5.3,1X,F5.3,1X,F8.5,1X,F8.5,1X,
     1             F6.3,1X,F6.4,1X,F6.2,1X,E11.4)
            WRITE(9,401) POISS,E,POISSI,EI
  401       FORMAT(1X,F7.3,1X,E14.5,1X,F7.3,1X,E14.5)
            WRITE(9,*) TR
            WRITE(9,*) NSTEPS
            CLOSE (9)
            PRINT*,' DATA FILE WRITTEN '
```

```
         ENDIF
      ENDIF
      PRINT*,' WHAT OUTPUT FILE NAME: '
      READ(*,101) FILEOUT
      OPEN(10,FILE=FILEOUT)
      REWIND 10
      WRITE(*,200) DEFZONE
  200 FORMAT(1X,A40)
      WRITE(10,200) DEFZONE
      WRITE(*,201) N
  201 FORMAT(5X,I2,' TIME STEPS')
      WRITE(10,201) N
      WRITE(*,202)
  202 FORMAT(2X,'I',3X,'TIME',3X,'DEPTH',3X,'NU%',3X,'E%',6X,'EPSX',
     14X,'EPSY',4X,'RHO',2X,'PGRAD',3X,'TGRAD',3X,'ALPHA')
      WRITE(10,202)
      DO 40 I=1,N
         WRITE(*,203) I,TIN(I),DIN(I),POISSPC(I),EPC(I),EPSX(I),EPSY(I)
     1                ,RHO(I),PGRAD(I),TGRAD(I),ALPHA(I)
  203    FORMAT(1X,I2,1X,F7.2,1X,F7.0,1X,F5.3,1X,F5.3,1X,F8.5,1X,F8.6,
     1          1X,F5.3,1X,F5.3,1X,F7.3,1X,E9.2)
   40    WRITE(10,203) I,TIN(I),DIN(I),POISSPC(I),EPC(I),EPSX(I),
     1                EPSY(I),RHO(I),PGRAD(I),TGRAD(I),ALPHA(I)
      WRITE(*,204) POISS,E,POISSI,EI
  204 FORMAT(/20X,'POISSONS RATIO     YOUNGS MODULUS'/
     1       3X,'PRESENT VALUE',8X,F7.3,10X,E10.3/
     2       3X,'INITIAL VALUE',8X,F7.3,10X,E10.3)
      WRITE(10,204) POISS,E,POISSI,EI
      WRITE(*,205) TR,NSTEPS
  205 FORMAT(/' RELAXATION TIME=',F14.4,' MYRS'/
     1     ' EACH TIME STEP SUBDIVIDED INTO ',I2,' INTEGRATION STEPS'/)
      WRITE(10,205) TR,NSTEPS
      RETURN
      END
C
C
C
      SUBROUTINE TABLE(N,TREL,SV,SHMIN,SHMAX,ESV,ESHMIN,
     1ESHMAX,S1,S2,S3X,S3Y,PO,TEMP,EPSX,EPSY,PGRAD,RHO,POISSO,EO,
     2ALPHA,IPU,NSTEPS,DREL)
      PARAMETER (IT=20,ID=20)
      DIMENSION TREL(IT,ID),SV(IT,ID),SHMIN(IT,ID),SHMAX(IT,ID),
     1ESV(IT,ID),ESHMIN(IT,ID),ESHMAX(IT,ID),DREL(IT,ID),
     2S1(IT,ID),S2(IT,ID),S3X(IT,ID),S3Y(IT,ID),PO(IT,ID),
     3TEMP(IT,ID),EPSX(IT),EPSY(IT),PGRAD(IT),RHO(IT),POISSO(IT),
     4EO(IT),ALPHA(IT)
C  WRITE OUTPUT IN A TABLE
      IF(IPU .EQ. 1) PRINT*,'       STRESS UNITS ARE IN PSI'
      IF(IPU .EQ. 2) PRINT*,'       STRESS UNITS ARE IN MPA'
      DO 50 I=1,N
      IF(I .EQ. 1) JSTART=NSTEPS
      IF(I .NE. 1) JSTART=1
      PRINT 210,(TREL(I,J),J=JSTART,NSTEPS)
```

```
      PRINT 211,(DREL(I,J),J=JSTART,NSTEPS)
      PRINT 212,(SV(I,J),J=JSTART,NSTEPS)
      PRINT 213,(SHMIN(I,J),J=JSTART,NSTEPS)
      PRINT 214,(SHMAX(I,J),J=JSTART,NSTEPS)
      PRINT 215,(ESV(I,J),J=JSTART,NSTEPS)
      PRINT 216,(ESHMIN(I,J),J=JSTART,NSTEPS)
      PRINT 217,(ESHMAX(I,J),J=JSTART,NSTEPS)
      PRINT 218,(S1(I,J),J=JSTART,NSTEPS)
      PRINT 219,(S2(I,J),J=JSTART,NSTEPS)
      PRINT 220,(S3X(I,J),J=JSTART,NSTEPS)
      PRINT 221,(S3Y(I,J),J=JSTART,NSTEPS)
      PRINT 222,(PO(I,J),J=JSTART,NSTEPS)
      PRINT 223,(TEMP(I,J),J=JSTART,NSTEPS)
      PRINT 224,EPSX(I)
      PRINT 225,EPSY(I)
      PRINT 226,PGRAD(I)
      PRINT 227,RHO(I)
      PRINT 228,POISSO(I)
      PRINT 229,EO(I)
      PRINT 230,ALPHA(I)
      WRITE(10,210) (TREL(I,J),J=JSTART,NSTEPS)
      WRITE(10,211) (DREL(I,J),J=JSTART,NSTEPS)
      WRITE(10,212) (SV(I,J),J=JSTART,NSTEPS)
      WRITE(10,213) (SHMIN(I,J),J=JSTART,NSTEPS)
      WRITE(10,214) (SHMAX(I,J),J=JSTART,NSTEPS)
      WRITE(10,215) (ESV(I,J),J=JSTART,NSTEPS)
      WRITE(10,216) (ESHMIN(I,J),J=JSTART,NSTEPS)
      WRITE(10,217) (ESHMAX(I,J),J=JSTART,NSTEPS)
      WRITE(10,218) (S1(I,J),J=JSTART,NSTEPS)
      WRITE(10,219) (S2(I,J),J=JSTART,NSTEPS)
      WRITE(10,220) (S3X(I,J),J=JSTART,NSTEPS)
      WRITE(10,221) (S3Y(I,J),J=JSTART,NSTEPS)
      WRITE(10,222) (PO(I,J),J=JSTART,NSTEPS)
      WRITE(10,223) (TEMP(I,J),J=JSTART,NSTEPS)
      WRITE(10,224) EPSX(I)
      WRITE(10,225) EPSY(I)
      WRITE(10,226) PGRAD(I)
      WRITE(10,227) RHO(I)
      WRITE(10,228) POISSO(I)
      WRITE(10,229) EO(I)
      WRITE(10,230) ALPHA(I)
   49 PRINT 231
   50 CONTINUE
  210 FORMAT(/' TIME (MY)=',6X,7(1X,F5.1,2X)/)
  211 FORMAT(' DEPTH (FT)=',5X,7F8.1)
  212 FORMAT(' SV=',13X,7F8.1)
  213 FORMAT(' SHMIN=',10X,7F8.1)
  214 FORMAT(' SHMAX=',10X,7F8.1)
  215 FORMAT(' EFF SV=',9X,7F8.1)
  216 FORMAT(' EFF SHMIN=',6X,7F8.1)
  217 FORMAT(' EFF SHMAX=',6X,7F8.1)
  218 FORMAT(' S1-GRAV=',8X,7F8.1)
  219 FORMAT(' S2-TEMP=',8X,7F8.1)
```

```
  220 FORMAT(' S3X-STRAIN=',6X,7F8.1)
  221 FORMAT(' S3Y-STRAIN=',6X,7F8.1)
  222 FORMAT(' PO=',13X,7F8.1)
  223 FORMAT(' TEMP (DEG F)=',3X,7F8.2)
  224 FORMAT(' EPSX (IN/IN)=',3X,F8.5)
  225 FORMAT(' EPSY (IN/IN)=',3X,F8.5)
  226 FORMAT(' PGRAD (PSI/FT)=',1X,F8.3)
  227 FORMAT(' RHO (GM/CC)=',4X,F8.3)
  228 FORMAT(' POISSONS RATIO=',1X,F8.4)
  229 FORMAT(' YOUNG MOD (PSI)=',E8.3)
  230 FORMAT(' ALPHA (1/DEG F)=',E8.3)
  231 FORMAT(//)
      RETURN
      END
C
      SUBROUTINE SPLOT(D,TIN,SV,SHMIN,SHMAX,PO,S1,S2,S3X,S3Y,T,ESV,
     1                 ESHMIN,ESHMAX,EPSX,EPSY,N,DEPTH,IPU,NSTEPS,TREL,
     2                 DEFZONE)
C
C  PLOTTING ROUTINE
C
      PARAMETER (IT=20,ID=20)
      CHARACTER*1 IRP,ICH,IPL,IPLTYP
      CHARACTER*40 DEFZONE
      DIMENSION D(IT),TIN(IT),SV(IT,ID),SHMIN(IT,ID),SHMAX(IT,ID),
     1PO(IT,ID),S1(IT,ID),S2(IT,ID),S3X(IT,ID),S3Y(IT,ID),ESV(IT,ID),
     2ESHMIN(IT,ID),ESHMAX(IT,ID),YO(2,6),YSTEP(2,6),YEND(2,6),
     3TEST(11),T(IT),EPSX(IT),EPSY(IT),PEPSX(IT),PEPSY(IT),TT(400),
     4TREL(IT,ID)
      IOC=97
      IOPR=0
      MC=97
      MP=60
    1 PRINT*,' PLOTS ARE SETUP FOR IBM EGA AND LASERJET PRINTER'
      PRINT*,' DO YOU WANT TO CHANGE THESE? '
      READ(*,100) ICH
  100 FORMAT(A1)
      IF(ICH .EQ. 'Y' .OR. ICH .EQ. 'y') CALL SETUP(IOC,MC,IOPR,MP)
C  GET MIN OR MAX VALUES FOR PLOT
      DO 3 I=1,11
    3 TEST(I)=0.0
      DO 7 I=1,N
         DO 5 J=1,NSTEPS
C  PLOT 1
            IF(SHMAX(I,J) .GT. TEST(1)) TEST(1)=SHMAX(I,J)
            IF(SV(I,J) .GT. TEST(1)) TEST(1)=SV(I,J)
            IF(SHMIN(I,J) .GT. TEST(1)) TEST(1)=SHMIN(I,J)
            IF(SHMIN(I,J) .LT. TEST(2)) TEST(2)=SHMIN(I,J)
            IF(SHMAX(I,J) .LT. TEST(2)) TEST(2)=SHMAX(I,J)
            IF(SV(I,J) .LT. TEST(2)) TEST(2)=SV(I,J)
```

```
            IF(PO(I,J) .LT. TEST(2)) TEST(2)=PO(I,J)
C  PLOT 2
            IF(ESHMAX(I,J) .GT. TEST(3)) TEST(3)=ESHMAX(I,J)
            IF(ESHMIN(I,J) .GT. TEST(3)) TEST(3)=ESHMIN(I,J)
            IF(ESV(I,J) .GT. TEST(3)) TEST(3)=ESV(I,J)
            IF(ESV(I,J) .LT. TEST(4)) TEST(4)=ESV(I,J)
            IF(ESHMIN(I,J) .LT. TEST(4)) TEST(4)=ESHMIN(I,J)
            IF(ESHMAX(I,J) .LT. TEST(4)) TEST(4)=ESHMAX(I,J)
C  PLOT 3
            IF(S3Y(I,J) .GT. TEST(5)) TEST(5)=S3Y(I,J)
            IF(S2(I,J) .GT. TEST(5)) TEST(5)=S2(I,J)
            IF(S1(I,J) .GT. TEST(5)) TEST(5)=S1(I,J)
            IF(S3X(I,J) .GT. TEST(5)) TEST(5)=S3X(I,J)
            IF(S3X(I,J) .LT. TEST(6)) TEST(6)=S3X(I,J)
            IF(S3Y(I,J) .LT. TEST(6)) TEST(6)=S3Y(I,J)
            IF(S2(I,J) .LT. TEST(6)) TEST(6)=S2(I,J)
            IF(S1(I,J) .LT. TEST(6)) TEST(6)=S1(I,J)
C  PLOT 6
            PEPSX(I)=EPSX(I)*1.E+06
            PEPSY(I)=EPSY(I)*1.E+06
            IF(PEPSY(I) .GT. TEST(7)) TEST(7)=PEPSY(I)
    5       IF(PEPSX(I) .LT. TEST(8)) TEST(8)=PEPSX(I)
C  PLOT 4
         IF(T(I) .GT. TEST(9)) TEST(9)=T(I)
C  PLOT 5
         IF(D(I) .GT. TEST(10)) TEST(10)=D(I)
C  X AXIS (TIME)
    7    IF(TIN(I) .GT. TEST(11)) TEST(11)=TIN(I)
      KDEPTH=INT(DEPTH)
      WRITE(*,201) TEST(11)
  201 FORMAT(' START TIME IS ',F12.3,' YRS BEFORE PRESENT'/
     1       ' INPUT: START TIME, TSTEP AND TEND (E.G. 75,5,0): ')
      READ(*,*) TO,TSTEP,TMAX
      TSTEP=-TSTEP
C  IPLTYP DESCRIBES TYPE OF PLOT
      DO 80 J=1,6
         IDEV=IOC
         JDEV=MC
         IPL='N'
         IF(J.EQ.1) PRINT*,' DO YOU WANT TO PLOT TOTAL STRESS: '
         IF(J.EQ.2) PRINT*,' DO YOU WANT TO PLOT EFF. STRESS: '
         IF(J.EQ.3) PRINT*,' DO YOU WANT TO PLOT STRESS COMP.: '
         IF(J.EQ.4) PRINT*,' DO YOU WANT TO PLOT TEMPERATURE: '
         IF(J.EQ.5) PRINT*,' DO YOU WANT TO PLOT DEPTH: '
         IF(J.EQ.6) PRINT*,' DO YOU WANT TO PLOT STRAINS: '
         READ 100,IPLTYP
         IF(IPLTYP .EQ. 'N') GO TO 80
C  SETUP FOR THE CORRECT PLOT
         IF(J .EQ. 1) THEN
            IAXEP=1
            IAXEN=2
            TEST(IAXEN)=0.0
         ELSE IF(J .EQ. 2) THEN
             IAXEP=3
             IAXEN=4
```

```
      ELSE IF(J .EQ. 3) THEN
          IAXEP=5
          IAXEN=6
      ELSE IF(J .EQ. 6) THEN
          IAXEP=7
          IAXEN=8
      ENDIF
      IF(J .NE. 4 .AND. J .NE. 5) THEN
         PRINT 200,TEST(IAXEP),TEST(IAXEN)
200      FORMAT('THE MAX VALUE IS',F12.2,' THE MIN VALUE IS',F12.2)
         PRINT*,' INPUT YORIG,YSTEP,YMAX: '
         READ(*,*) YO(IPU,J),YSTEP(IPU,J),YEND(IPU,J)
      ELSE
         IF(J .EQ. 4) THEN
            WRITE(*,202) TEST(9)
202         FORMAT(' MAX TEMP =',F10.3,
   1                ' INPUT STEP & MAX FOR PLOT: ')
         ELSE IF(J .EQ. 5) THEN
            WRITE(*,203) TEST(10)
203         FORMAT(' MAX DEPTH =',F12.3,
   1                ' INPUT STEP & MAX FOR PLOT: ')
         ENDIF
         READ(*,*) YSTEP(IPU,J),YEND(IPU,J)
         YO(IPU,J)=0.0
      ENDIF
 10   CALL PLOTS(0,IDEV,JDEV)
      XMAX=10.0
      YMAX=8.0
      CALL WINDOW(0.,0.,12.,10.)
      IF(IPL .EQ. 'Y' .OR. IPL .EQ. 'y') CALL FACTOR(0.68)
      OX=1.7
      OY=1.5
      IF(IPL .EQ. 'Y' .OR. IPL .EQ. 'y') THEN
         OX=2.0
         OY=2.0
         IF(JDEV .EQ. 62) CALL NEWPEN(3)
         IF(JDEV .EQ. 64) CALL NEWPEN(6)
      ENDIF
      CALL COLOR(11,IERR)
      CALL XAXIS(OX,OY,'TIME (MILLION YEARS BEFORE PRESENT)',35,XMAX,
   1             TO,TSTEP,TMAX,0)
      IF(IPU .EQ. 1) THEN
        IF(J .LE. 3)CALL YAXIS(OX,OY,'STRESS (PSI)',12,YMAX,YO(IPU,J)
   1                           ,YSTEP(IPU,J),YEND(IPU,J),0)
      ELSE
        IF(J .LE. 3)CALL YAXIS(OX,OY,'STRESS (MPa)',12,YMAX,YO(IPU,J)
   1                           ,YSTEP(IPU,J),YEND(IPU,J),0)
      ENDIF
      IF(J .EQ. 4) CALL YAXIS(OX,OY,'TEMPERATURE (DEG F)',19,YMAX,
   1                          YO(IPU,J),YSTEP(IPU,J),YEND(IPU,J),0)
      IF(J .EQ. 5) CALL YAXIS(OX,OY,'DEPTH (FT)',10,YMAX,YO(IPU,J),
   1                          YSTEP(IPU,J),YEND(IPU,J),0)
      IF(J .EQ. 6) CALL YAXIS(OX,OY,'STRAIN (MICROSTRAINS)',21,YMAX,
   1                          YO(IPU,J),YSTEP(IPU,J),YEND(IPU,J),0)
```

```
      X1=OX+0.3
      X2=X1+0.8
      Y1=OY+YMAX-0.4
C
C   FIRST PLOT HAS TOTAL STRESSES AND PORE PRESSURES
C
         IF(J .EQ. 1) THEN
            DO 20 MN=1,4
               IF(MN .LT. 4) CALL COLOR(2*MN+8,IERR)
               IF(MN .EQ. 4) CALL COLOR(6,IERR)
               CALL PLOT(OX,OY,3)
               DO 15 I=1,N
                  DO 15 L=1,NSTEPS
                     IF(I .EQ. 1 .AND. L .LT. NSTEPS) GO TO 15
                     IF(MN .EQ. 1) Y=SV(I,L)
                     IF(MN .EQ. 2) Y=SHMIN(I,L)
                     IF(MN .EQ. 3) Y=SHMAX(I,L)
                     IF(MN .EQ. 4) Y=PO(I,L)
                     X=(TREL(I,L)-TO)/(TMAX-TO)*XMAX+OX
                     YP=(Y-YO(IPU,1))/(YEND(IPU,1)-YO(IPU,1))*YMAX+OY
                     CALL SYMBOL(X,YP,0.14,CHAR(MN-1),0.0,-2)
   15                CONTINUE
                  DY=0.4*FLOAT(MN-1)
                  CALL SYMBOL(X1,Y1-DY,0.14,CHAR(MN-1),0.0,-1)
                  CALL SYMBOL(X2,Y1-DY,0.14,CHAR(MN-1),0.0,-2)
                  IF(MN .EQ. 1) CALL SYMBOL(X2+0.3,Y1-DY-0.04,0.22,
     1                                      'SV',0.0,2)
                  IF(MN .EQ. 2) CALL SYMBOL(X2+0.3,Y1-DY-0.04,0.22,
     1                                      'SHMIN',0.0,5)
                  IF(MN .EQ. 3) CALL SYMBOL(X2+0.3,Y1-DY-0.04,0.22,
     1                                      'SHMAX',0.0,5)
                  IF(MN .EQ. 4) CALL SYMBOL(X2+0.3,Y1-DY-0.04,0.22,
     1                                      'PO',0.0,2)
   20          CONTINUE
         ELSE IF(J .EQ. 2) THEN
C
C   SECOND PLOT HAS EFFECTIVE STRESSES
C
            DO 30 MN=1,3
               CALL COLOR(2*MN+8,IERR)
               CALL PLOT(OX,OY,3)
               DO 25 I=1,N
                  DO 25 L=1,NSTEPS
                     IF(I .EQ. 1 .AND. L .LT. NSTEPS) GO TO 25
                     IF(MN .EQ. 1) Y=ESV(I,L)
                     IF(MN .EQ. 2) Y=ESHMIN(I,L)
                     IF(MN .EQ. 3) Y=ESHMAX(I,L)
                     X=(TREL(I,L)-TO)/(TMAX-TO)*XMAX+OX
                     YP=(Y-YO(IPU,2))/(YEND(IPU,2)-YO(IPU,2))*YMAX+OY
                     CALL SYMBOL(X,YP,0.14,CHAR(MN),0.0,-2)
   25                CONTINUE
```

```
                DY=0.4*FLOAT(MN-1)
                CALL SYMBOL(X1,Y1-DY,0.14,CHAR(MN),0.0,-1)
                CALL SYMBOL(X2,Y1-DY,0.14,CHAR(MN),0.0,-2)
                IF(MN .EQ. 1) CALL SYMBOL(X2+0.3,Y1-DY-0.04,0.22,
     1                                    'ESV',0.0,3)
                IF(MN .EQ. 2) CALL SYMBOL(X2+0.3,Y1-DY-0.04,0.22,
     1                                    'ESHMIN',0.0,6)
                IF(MN .EQ. 3) CALL SYMBOL(X2+0.3,Y1-DY-0.04,0.22,
     1                                    'ESHMAX',0.0,6)
   30         CONTINUE
        ELSE IF(J .EQ. 3) THEN
C
C   THIRD PLOT HAS STRESS COMPONENTS
C
           DO 40 MN=1,4
              IF(MN .LT. 4) CALL COLOR(2*MN+8,IERR)
              IF(MN .EQ. 4) CALL COLOR(6,IERR)
              CALL PLOT(OX,OY,3)
              DO 35 I=1,N
                 DO 35 L=1,NSTEPS
                    IF(I .EQ. 1 .AND. L .LT. NSTEPS) GO TO 35
                    IF(MN .EQ. 1) Y=S1(I,L)
                    IF(MN .EQ. 2) Y=S2(I,L)
                    IF(MN .EQ. 3) Y=S3X(I,L)
                    IF(MN .EQ. 4) Y=S3Y(I,L)
                    X=(TREL(I,L)-TO)/(TMAX-TO)*XMAX+OX
                    YP=(Y-YO(IPU,3))/(YEND(IPU,3)-YO(IPU,3))*YMAX+OY
                    CALL SYMBOL(X,YP,0.14,CHAR(MN-1),0.0,-2)
   35               CONTINUE
                DY=0.4*FLOAT(MN-1)
                CALL SYMBOL(X1,Y1-DY,0.14,CHAR(MN-1),0.0,-1)
                CALL SYMBOL(X2,Y1-DY,0.14,CHAR(MN-1),0.0,-2)
                IF(MN .EQ. 1) CALL SYMBOL(X2+0.3,Y1-DY-0.04,0.22,
     1                                    'S1',0.0,2)
                IF(MN .EQ. 2) CALL SYMBOL(X2+0.3,Y1-DY-0.04,0.22,
     1                                    'S2',0.0,2)
                IF(MN .EQ. 3) CALL SYMBOL(X2+0.3,Y1-DY-0.04,0.22,
     1                                    'S3X',0.0,3)
                IF(MN .EQ. 4) CALL SYMBOL(X2+0.3,Y1-DY-0.04,0.22,
     1                                    'S3Y',0.0,3)
   40         CONTINUE
        ELSE IF(J .EQ. 4) THEN
C
C   FOURTH PLOT HAS TEMPERATURE
C
           CALL COLOR(14,IERR)
           CALL PLOT(OX,OY,3)
           DO 45 I=1,N
              X=(TIN(I)-TO)/(TMAX-TO)*XMAX+OX
              YP=(T(I)-YO(IPU,4))/(YEND(IPU,4)-YO(IPU,4))*YMAX+OY
   45         CALL SYMBOL(X,YP,0.14,CHAR(0),0.0,-2)
        ELSE IF(J .EQ. 5) THEN
C
```

```
C   FIFTH PLOT HAS DEPTH
C
            CALL COLOR(14,IERR)
            CALL PLOT(OX,OY,3)
            DO 50 I=1,N
               X=(TIN(I)-TO)/(TMAX-TO)*XMAX+OX
               YP=(D(I)-YO(IPU,5))/(YEND(IPU,5)-YO(IPU,5))*YMAX+OY
   50          CALL SYMBOL(X,YP,0.14,CHAR(0),0.0,-2)
         ELSE IF(J .EQ. 6) THEN
C
C   SIXTH PLOT HAS STRAINS
C
            DO 65 MN=1,2
               CALL COLOR(2*MN+8,IERR)
               CALL PLOT(OX,OY,3)
               DO 60 I=1,N
                  IF(MN .EQ. 1) Y=PEPSX(I)
                  IF(MN .EQ. 2) Y=PEPSY(I)
                  X=(TIN(I)-TO)/(TMAX-TO)*XMAX+OX
                  YP=(Y-YO(IPU,6))/(YEND(IPU,6)-YO(IPU,6))*YMAX+OY
   60             CALL SYMBOL(X,YP,0.14,CHAR(MN),0.0,-2)
               DY=0.4*FLOAT(MN-1)
               CALL SYMBOL(X1,Y1-DY,0.14,CHAR(MN),0.0,-1)
               CALL SYMBOL(X2,Y1-DY,0.14,CHAR(MN),0.0,-2)
               IF(MN .EQ. 1) CALL SYMBOL(X2+0.3,Y1-DY-0.04,0.22,
     1                                   'EPSX',0.0,4)
               IF(MN .EQ. 2) CALL SYMBOL(X2+0.3,Y1-DY-0.04,0.22,
     1                                   'EPSY',0.0,4)
   65          CONTINUE
         ENDIF
      CALL COLOR(12,IERR)
      CALL SYMBOL(OX+0.2,YMAX+0.2+OY,0.2222,DEFZONE,0.0,40)
      CALL PLOT(0.0,0.0,999)
      IF(IPL .EQ. 'Y' .OR. IPL .EQ. 'y') GO TO 80
      PRINT*,' DO YOU WANT A HARDCOPY OF THIS PLOT: '
      READ(*,100) IPL
      IF(IPL .EQ. 'Y' .OR. IPL .EQ. 'y') THEN
         PRINT*,' PLOTTING IN PROGRESS '
         IDEV=IOP
         JDEV=MP
         GO TO 10
      ENDIF
   80 CONTINUE
      PRINT*,' DO YOU WANT TO REPLOT THE DATA? '
      READ(*,100) IRP
      IF(IRP .EQ. 'Y' .OR. IRP .EQ. 'y') GO TO 1
   95 CONTINUE
      RETURN
      END
      SUBROUTINE FAILURE(N,ESV,ESHMIN,ESHMAX,PO,TIN,DIN,IPU,
     1NSTEPS,TREL,DREL,DEFZONE)
C
```

```
C  ESTIMATE FAILURE BEHAVIOR AT EACH STRESS HISTORY TIME STEP
C
      PARAMETER (IT=20,ID=20,IF=50)
      CHARACTER*1 IPLOT,ITABLE,IFD,IWR,IUNITS,ICH,IPL,IRP,IRS
      CHARACTER*20 FILEIN,FILEOUT
      CHARACTER*40 DEFZONE
      DIMENSION ESV(IT,ID),ESHMIN(IT,ID),ESHMAX(IT,ID),PO(IT,ID),
     1          TIN(IT),DIN(IT),PMAX(IF),PMIN(IF),IFLAG(IF),SMEAN(IF),
     2          TAUMAX(IF),ISTATE(IF),TMF(2,10),SMF(2,10),TREL(IT,ID),
     3          TEST(4),DREL(IT,ID),TTA(IF),DTA(IF),TAUF(IF),TAUFR(IF),
     4          XVERT(25),YVERT(25),XNVERT(10),YNVERT(10),XC(7),YC(7),
     5          XRVERT(25),YRVERT(25),XRNVER(25),YRNVER(25)
C  INPUT FAILURE DATA -- MOHR COULOMB CRITERION
      PRINT*,' INPUT FAILURE DATA; BY HAND (H) OR FILE (F): '
      READ(*,100) IFD
  100 FORMAT(A1)
C  INPUT DATA BY FILE
      IF(IFD .EQ. 'F' .OR. IFD .EQ. 'f') THEN
         PRINT*,' WHAT IS THE NAME OF THE INPUT FILE: '
         READ(*,101) FILEIN
         OPEN (8,FILE=FILEIN)
         REWIND 8
  101    FORMAT(A20)
         READ(8,*) NF
         DO 2 I=1,NF
    2       READ(8,*) SMF(1,I),TMF(1,I)
         CLOSE (8)
         PRINT*,' DATA FILE READ '
      ELSE
C  INPUT DATA BY HAND
    5    PRINT*,' HOW MANY DATA POINTS: '
         READ (*,*) NF
         PRINT*,' ARE THE DATA IN CONVENTIONAL (C) OR SI (S) UNITS: '
         READ(*,100) IUNITS
         IPUN=1
         IF(IUNITS .EQ. 'S' .OR. IUNITS .EQ. 's') IPUN=2
         DO 7 I=1,NF
            WRITE(*,333) I
  333       FORMAT(' POINT NUMBER #',I3,': ')
            READ (*,*) SMF(IPUN,I),TMF(IPUN,I)
            IF(IPUN .EQ. 2) THEN
               SMF(1,I)=SMF(2,I)*145.0
               TMF(1,I)=TMF(2,I)*145.0
            ENDIF
    7       CONTINUE
C  SAVE DATA IN A FILE
         PRINT*,' DO YOU WANT THESE DATA WRITTEN TO A FILE: '
         READ(*,100) IWR
         IF(IWR .EQ. 'Y' .OR. IWR .EQ. 'y') THEN
            PRINT*,' DATA WILL BE SAVED; WHAT FILE NAME: '
            READ(*,101) FILEOUT
            OPEN(9,FILE=FILEOUT)
            REWIND 9
```

```
            WRITE(9,420) NF
  420       FORMAT(1X,I2)
            DO 8 I=1,NF
    8          WRITE(9,400) SMF(1,I),TMF(1,I)
  400       FORMAT(1X,F14.2,1X,F14.2)
            CLOSE (9)
            PRINT*,' DATA FILE WRITTEN '
         ENDIF
      ENDIF
C  WRITE OUT FAILURE DATA TO SCREEN AND FILE
      WRITE(*,500) (SMF(IPU,J),TMF(IPU,J),J=1,NF)
      WRITE(10,500) (SMF(IPU,J),TMF(IPU,J),J=1,NF)
  500 FORMAT('  MEAN STRESS      SHEAR STRESS'/
     1       10(1X,F12.2,2X,F12.2/))
      PRINT*,' DO YOU WANT A REDUCED STRENGTH ENVELOPE: '
      READ(*,100) IRS
      IF(IRS .EQ. 'Y' .OR. IRS .EQ. 'y') THEN
         PRINT*,' INPUT REDUCTION FACTOR (E.G., 0.8): '
         READ(*,*) REDF
      ENDIF
C  FIND MIN AND MAX EFFECTIVE STRESSES
   10 IFLAG(1)=0
      DO 15 J=1,4
   15    TEST(J)=0.0
      K=0
      DO 18 I=1,N
         DO 18 J=1,NSTEPS
         IF(I .EQ. 1 .AND. J .NE. NSTEPS) GO TO 18
         K=K+1
         TTA(K)=TREL(I,J)
         DTA(K)=DREL(I,J)
         IFLAG(K)=0
         PMAX(K)=ESHMAX(I,J)
         IF(ESV(I,J) .GT. PMAX(K)) THEN
            IFLAG(K)=1
            PMAX(K)=ESV(I,J)
         ENDIF
         PMIN(K)=ESHMIN(I,J)
         IF(ESV(I,J) .LT. PMIN(K)) THEN
            IFLAG(K)=2
            PMIN(K)=ESV(I,J)
         ENDIF
C  CALCULATE MEAN STRESS AND MAX SHEAR STRESS
         SMEAN(K)=(PMAX(K)+PMIN(K))/2.0
         TAUMAX(K)=(PMAX(K)-PMIN(K))/2.0
         WRITE(*,501) K,SMEAN(K),TAUMAX(K)
  501    FORMAT('  K=',I3,'  SMEAN=',F12.2,'  TAUMAX=',F12.2)
   18    CONTINUE
      KEND=K
C  DETERMINE WHETHER EXTENSION OR COMPRESSION
      STAN=PMIN(2)/SMEAN(2)
      ISTATE(1)=0
      ISTATE(2)=0
```

```
      DO 20 K=3,KEND
         ISTATE(K)=0
         STANNEW=PMIN(K)/SMEAN(K)
         IF(STANNEW .LT. STAN .AND. PMIN(K) .LT. PMIN(K-1)) ISTATE(K)=1
         IF(ISTATE(K) .EQ. 1) TAUMAX(K)=-TAUMAX(K)
   20    STAN=STANNEW
C  SET UP FOR PLOTS
      PRINT*,' DO YOU WANT PLOTS: '
      READ(*,100) IPLOT
      IF(IPLOT .EQ. 'N') GO TO 60
C  GET MIN AND MAX DATA FOR PLOTS
      DO 31 J=1,4
   31   TEST(J)=0.0
      DO 32 J=1,NF
         IF(SMF(IPU,J) .GT. TEST(1)) TEST(1)=SMF(IPU,J)
         IF(TMF(IPU,J) .GT. TEST(2)) TEST(2)=TMF(IPU,J)
         IF(SMF(IPU,J) .LT. TEST(3)) TEST(3)=SMF(IPU,J)
   32    IF(TMF(IPU,J) .LT. TEST(4)) TEST(4)=TMF(IPU,J)
      WRITE(*,310) TEST(3),TEST(1),TEST(4),TEST(2)
  310 FORMAT(' FOR FAILURE DATA:'/' MIN AND MAX MEAN STRESS=',F12.2,
     1       ' AND ',F12.2/' MIN AND MAX SHEAR STRESS=',F12.2,
     2       ' AND ',F12.2)
      DO 34 J=1,4
   34   TEST(J)=0.0
      DO 36 J=1,KEND
         IF(SMEAN(J) .GT. TEST(1)) TEST(1)=SMEAN(J)
         IF(TAUMAX(J) .GT. TEST(2)) TEST(2)=TAUMAX(J)
         IF(SMEAN(J) .LT. TEST(3)) TEST(3)=SMEAN(J)
   36    IF(TAUMAX(J) .LT. TEST(4)) TEST(4)=TAUMAX(J)
      WRITE(*,300) TEST(3),TEST(1)
  300 FORMAT(' MIN AND MAX VALUES OF MEAN STRESS:',F12.2,2X,F12.2/
     1       ' INPUT MIN, STEP AND MAX VALUES FOR PLOT: ')
      READ(*,*) XSTART,XSTEP,XEND
      WRITE(*,301) TEST(4),TEST(2)
  301 FORMAT(' MIN AND MAX VALUES OF SHEAR STRESS:',F12.2,2X,F12.2/
     1       ' INPUT MIN, STEP AND MAX VALUES FOR PLOT: ')
      READ(*,*) YSTART,YSTEP,YEND
C         START PLOTTING
      IOC=97
      IOPR=0
      MC=97
      MP=60
      PRINT*,' PLOTS ARE SETUP FOR IBM EGA AND LASERJET PRINTER'
      PRINT*,' DO YOU WANT TO CHANGE THESE? '
      READ(*,100) ICH
      IF(ICH .EQ. 'Y' .OR. ICH .EQ. 'y') CALL SETUP(IOC,MC,IOPR,MP)
   50 IDEV=IOC
      JDEV=MC
      IPL='N'
   60 CALL PLOTS(0,IDEV,JDEV)
      XMAX=10.0
      YMAX=8.0
      CALL WINDOW(0.,0.,12.,10.)
```

```
      IF(IPL .EQ. 'Y' .OR. IPL .EQ. 'y') CALL FACTOR(0.68)
      OX=1.7
      OY=1.5
      IF(IPL .EQ. 'Y' .OR. IPL .EQ. 'y') THEN
         OX=2.0
         OY=2.0
         IF(JDEV .EQ. 62) CALL NEWPEN(2)
         IF(JDEV .EQ. 64) CALL NEWPEN(4)
      ENDIF
      CALL COLOR(11,IERR)
      IF(IPU .EQ. 1) THEN
         CALL XAXIS(OX,OY,'MEAN EFFECTIVE STRESS (PSI)',27,XMAX,XSTART,
     1              XSTEP,XEND,0)
         CALL YAXIS(OX,OY,'MAXIMUM SHEAR STRESS (PSI)',26,YMAX,YSTART,
     1             YSTEP,YEND,0)
      ELSE
         CALL XAXIS(OX,OY,'MEAN EFFECTIVE STRESS (MPa)',27,XMAX,XSTART,
     1              XSTEP,XEND,0)
         CALL YAXIS(OX,OY,'MAXIMUM SHEAR STRESS (MPa)',26,YMAX,YSTART,
     1              YSTEP,YEND,0)
      ENDIF
      X1=OX+0.3
      X2=X1+0.8
      Y1=OY+YMAX-0.4
C  PLOT THE CALCULATED MEAN STRESS VS SHEAR STRESS DATA
      CALL COLOR(10,IERR)
      IST=-1
      DO 65 K=1,KEND
         IF(I .EQ. 1 .AND. L .LT. NSTEPS) GO TO 65
         X=(SMEAN(K)-XSTART)/(XEND-XSTART)*XMAX+OX
         YP=(TAUMAX(K)-YSTART)/(YEND-YSTART)*YMAX+OY
         IF(K .GT. 2 .AND. ISTATE(K) .NE. ISTATE(K-1)) THEN
C  CHANGE FROM COMPRESSION TO EXTENSION -- DRAW CURVED LINE
            XC(1)=XOLD
            YC(1)=YPOLD
            DIS=SQRT((X-XOLD)**2+(YP-YPOLD)**2)
            RADIUS=DIS/1.5
            IF(ISTATE(K) .EQ. 1 .AND. ISTATE(K-1) .EQ. 0) THEN
               CSIGN=1.0
            ELSE IF(ISTATE(K) .EQ. 0 .AND. ISTATE(K-1) .EQ. 1) THEN
               CSIGN=-1.0
            ENDIF
            AM=-(X-XOLD)/(YP-YPOLD)
            B=(YP+YPOLD)/2.0+0.5*(X**2-XOLD**2)/(YP-YPOLD)
            AA=YP-B
            AB=1.0+AM**2
            XM=(X+AM*AA-CSIGN*SQRT((X+AA*AM)**2
     1         -AB*(X**2+AA**2-RADIUS**2)))/AB
            YM=AM*XM+B
            THET=ASIN(0.5*DIS/RADIUS)
            IF(YP .LT. TPOLD) THET=-THET
            DTHET=THET/3.0
            ALPHA=ATAN(AM)-THET
```

```
            THET=2.0*THET+ALPHA
            DO 777 L=1,5
               THET=THET-DTHET
               XC(L+1)=XM+CSIGN*RADIUS*COS(THET)
 777           YC(L+1)=YM+CSIGN*RADIUS*SIN(THET)
            XC(7)=X
            YC(7)=YP
            CALL CURVE(XC,YC,-7,-0.06)
         ENDIF
         XOLD=X
         YPOLD=YP
         IF(X .GT. (OX+XMAX) .OR. YP .GT. (OY+YMAX)) GO TO 65
         CALL SYMBOL(X,YP,0.14,CHAR(2),0.0,IST)
         IST=-2
  65     CONTINUE
C  PLOT THE FAILURE DATA
      CALL COLOR(12,IERR)
      IYP=0
      NVERT=0
      NRVERT=0
      IST=-1
      XSAV=OX+(0.0-XSTART)/(XEND-XSTART)*XMAX
      YSAV=OY+(0.0-YSTART)/(YEND-YSTART)*YMAX
      DO 67 J=1,NF
         X=(SMF(IPU,J)-XSTART)/(XEND-XSTART)*XMAX+OX
         YP=(TMF(IPU,J)-YSTART)/(YEND-YSTART)*YMAX+OY
         IF(X .GT. (OX+XMAX) .OR. YP .GT. (OY+YMAX)) THEN
            IF(XSAV .LE. (OX+XMAX) .AND. YSAV .LE. (OY+YMAX)) THEN
               SL=(YP-YSAV)/(X-XSAV)
               YYP=YSAV+SL*(OX+XMAX-XSAV)
               IF(YYP .LE. (OY+YMAX)) THEN
                  XX=OX+XMAX
               ELSE
                  YYP=OY+YMAX
                  XX=(YYP-YSAV)/SL+XSAV
                  IYP=1
               ENDIF
               CALL PLOT(XX,YYP,2)
               NVERT=NVERT+1
               XVERT(NVERT)=XX
               YVERT(NVERT)=YYP
               NRVERT=NRVERT+1
               XRVERT(NRVERT)=XX
               YRVERT(NRVERT)=YYP
               GO TO 666
            ENDIF
         ENDIF
         CALL SYMBOL(X,YP,0.14,CHAR(1),0.0,IST)
         NVERT=NVERT+1
         XVERT(NVERT)=X
         YVERT(NVERT)=YP
         NRVERT=NRVERT+1
         XRVERT(NRVERT)=X
```

```
         YRVERT(NRVERT)=YP
         IST=-2
   66    XSAV=X
         YSAV=YP
   67    CONTINUE
C  GET THE REST OF THE VERTICES OF THE UNSTABLE AREA FOR FILL
  666 IF(IYP .EQ. 0) THEN
C IF THE UPPER RIGHT CORNER IS NEEDED FOR THE OUTER SHADING
         NVERT=NVERT+1
         XVERT(NVERT)=OX+XMAX
         YVERT(NVERT)=OY+YMAX
      ELSE
C  IF THERE IS A REDUCED STRENGTH AREA, GET UPPER RIGHT CORNER
         NRVERT=NRVERT+1
         XRVERT(NRVERT)=OX+XMAX
         YRVERT(NRVERT)=OY+YMAX
      ENDIF
      NVERT=NVERT+1
      XVERT(NVERT)=OX
      YVERT(NVERT)=OY+YMAX
      NVERT=NVERT+1
      XVERT(NVERT)=OX
      YVERT(NVERT)=OY
C  PLOT THE NEGATIVE SIDE OF THE FAILURE ENVELOPE
      IYN=0
      IST=-1
      JVERT=0
      XSAV=OX+(0.0-XSTART)/(XEND-XSTART)*XMAX
      YSAV=OY+(0.0-YSTART)/(YEND-YSTART)*YMAX
      DO 69 J=1,NF
         X=(SMF(IPU,J)-XSTART)/(XEND-XSTART)*XMAX+OX
         YP=(-TMF(IPU,J)-YSTART)/(YEND-YSTART)*YMAX+OY
         IF(X .GT. (OX+XMAX) .OR. YP .LT. OY) THEN
            IF(XSAV .LE. (OX+XMAX) .AND. YSAV .GE. OY) THEN
               SL=(YP-YSAV)/(X-XSAV)
               YYP=YSAV+SL*(OX+XMAX-XSAV)
               IF(YYP .GE. OY) THEN
                  XX=OX+XMAX
               ELSE
                  YYP=OY
                  XX=(YYP-YSAV)/SL+XSAV
                  IYN=1
               ENDIF
               CALL PLOT(XX,YYP,2)
               JVERT=JVERT+1
               XNVERT(JVERT)=XX
               YNVERT(JVERT)=YYP
               GO TO 668
            ENDIF
         ENDIF
         CALL SYMBOL(X,YP,0.14,CHAR(1),0.0,IST)
         JVERT=JVERT+1
         XNVERT(JVERT)=X
```

```
         YNVERT(JVERT)=YP
         IST=-2
   68    XSAV=X
         YSAV=YP
   69    CONTINUE
C  FINISH THE VERTICES BY REARRANGING IN REVERSE ORDER
  668 IF(IYN .EQ. 0) THEN
C  IF THE LOWER RIGHT CORNER IS NEEDED
         NVERT=NVERT+1
         XVERT(NVERT)=OX+XMAX
         YVERT(NVERT)=OY
      ENDIF
      DO 70 J=1,JVERT
         NVERT=NVERT+1
         JN=JVERT-J+1
         XVERT(NVERT)=XNVERT(JN)
   70    YVERT(NVERT)=YNVERT(JN)
C  PLOT THE REDUCED STRENGTH ENVELOPE, IF WANTED
      IF(IRS .EQ. 'Y' .OR. IRS .EQ. 'y') THEN
         JRVERT=0
C  POSITIVE SIDE FIRST
         IST=3
         XSAV=OX+(0.0-XSTART)/(XEND-XSTART)*XMAX
         YSAV=OY+(0.0-YSTART)/(YEND-YSTART)*YMAX
         DO 73 J=1,NF
            X=(SMF(IPU,J)-XSTART)/(XEND-XSTART)*XMAX+OX
            YP=(REDF*TMF(IPU,J)-YSTART)/(YEND-YSTART)*YMAX+OY
            IF(X .GT. (OX+XMAX) .OR. YP .GT. (OY+YMAX)) THEN
               IF(XSAV .LT. (OX+XMAX) .AND. YSAV .LE. (OY+YMAX)) THEN
                  SL=(YP-YSAV)/(X-XSAV)
                  YYP=YSAV+SL*(OX+XMAX-XSAV)
                  IF(YYP .LE. (OY+YMAX)) THEN
                     XX=OX+XMAX
                  ELSE
                     YYP=OY+YMAX
                     XX=(YYP-YSAV)/SL+XSAV
                  ENDIF
                  CALL PLOT(XX,YYP,IST)
                  JRVERT=JRVERT+1
                  XRNVER(JRVERT)=XX
                  YRNVER(JRVERT)=YYP
                  GO TO 672
               ENDIF
            ENDIF
            CALL PLOT(X,YP,IST)
            JRVERT=JRVERT+1
            XRNVER(JRVERT)=X
            YRNVER(JRVERT)=YP
            IST=2
   72       XSAV=X
            YSAV=YP
   73       CONTINUE
  672    IST=3
```

```
C  FILL THE POSITIVE SIDE OF THE REDUCED STRENGTH FAILURE ZONE
         DO 74 J=1,JRVERT
            NRVERT=NRVERT+1
            JN=JRVERT-J+1
            XRVERT(NRVERT)=XRNVER(JN)
   74       YRVERT(NRVERT)=YRNVER(JN)
         CALL NEWPEN(1)
         CALL STFILL(6)
         CALL FILL(XRVERT,YRVERT,NRVERT)
         IF(JDEV .EQ. 62) CALL NEWPEN(2)
         IF(JDEV .EQ. 64) CALL NEWPEN(4)
C  PLOT THE NEGATIVE SIDE OF THE REDUCED STRENGTH FAILURE ENVELOPE
         NRVERT=0
         XSAV=OX+(0.0-XSTART)/(XEND-XSTART)*XMAX
         YSAV=OY+(0.0-YSTART)/(YEND-YSTART)*YMAX
         DO 78 J=1,NF
            X=(SMF(IPU,J)-XSTART)/(XEND-XSTART)*XMAX+OX
            YP=(-REDF*TMF(IPU,J)-YSTART)/(YEND-YSTART)*YMAX+OY
            IF(X .GT. (OX+XMAX) .OR. YP .LT. OY) THEN
               IF(XSAV .LT. (OX+XMAX) .AND. YSAV .GE. OY) THEN
                  SL=(YP-YSAV)/(X-XSAV)
                  YYP=YSAV+SL*(OX+XMAX-XSAV)
                  IF(YYP .LE. (OY+YMAX)) THEN
                     XX=OX+XMAX
                  ELSE
                     YYP=OY+YMAX
                     XX=(YYP-YSAV)/SL+XSAV
                  ENDIF
                  CALL PLOT(XX,YYP,IST)
                  NRVERT=NRVERT+1
                  XRVERT(NRVERT)=XX
                  YRVERT(NRVERT)=YYP
                  GO TO 677
               ENDIF
            ENDIF
            CALL PLOT(X,YP,IST)
            NRVERT=NRVERT+1
            XRVERT(NRVERT)=X
            YRVERT(NRVERT)=YP
            IST=2
   77       XSAV=X
            YSAV=YP
   78       CONTINUE
  677    CONTINUE
      ENDIF
C  FILL UNSTABLE AREA
      CALL COLOR(14,IERR)
      CALL NEWPEN(1)
      CALL STFILL(3)
      CALL FILL(XVERT,YVERT,NVERT)
      IF(JDEV .EQ. 62) CALL NEWPEN(2)
      IF(JDEV .EQ. 64) CALL NEWPEN(4)
```

```
C  FILL THE NEGATIVE SIDE OF THE REDUCED STRENGTH FAILURE ZONE
      IF(IRS .EQ. 'Y' .OR. IRS .EQ. 'y') THEN
         IF(IYN .EQ. 1) THEN
            NRVERT=NRVERT+1
            XRVERT(NRVERT)=OX+XMAX
            YRVERT(NRVERT)=OY
         ENDIF
         DO 79 J=1,JVERT
            NRVERT=NRVERT+1
            JN=JVERT-J+1
            XRVERT(NRVERT)=XNVERT(JN)
   79       YRVERT(NRVERT)=YNVERT(JN)
         CALL COLOR(12,IERR)
         CALL NEWPEN(1)
         CALL STFILL(6)
         CALL FILL(XRVERT,YRVERT,NRVERT)
         IF(JDEV .EQ. 62) CALL NEWPEN(2)
         IF(JDEV .EQ. 64) CALL NEWPEN(4)
      ENDIF
C  WRITE LABEL ON PLOT
      CALL COLOR(14,IERR)
      CALL SYMBOL(OX+0.2,YMAX+0.2+OY,0.2222,DEFZONE,0.0,40)
      CALL PLOT(0.0,0.0,999)
      IF(IPL .EQ. 'Y' .OR. IPL .EQ. 'y') GO TO 80
      PRINT*,' DO YOU WANT A HARDCOPY OF THIS PLOT: '
      READ(*,100) IPL
      IF(IPL .EQ. 'Y' .OR. IPL .EQ. 'y') THEN
         PRINT*,' PLOTTING IN PROGRESS '
         IDEV=IOP
         JDEV=MP
         GO TO 60
      ENDIF
   80 IPL='N'
      PRINT*,' DO YOU WANT TO REPLOT THE DATA? '
      READ(*,100) IRP
      IF(IRP .EQ. 'Y' .OR. IRP .EQ. 'y') GO TO 50
   85 PRINT*,'DO YOU WANT A FAILURE TABLE: '
      READ 100,ITABLE
      IF(ITABLE .EQ. 'N') GO TO 90
      IF(IPU .EQ. 1) PRINT*,' UNITS ARE PSI'
      IF(IPU .EQ. 2) PRINT*,' UNITS ARE MPA'
      DO 87 J=1,KEND
         DO 86 K=2,NF
            IF(SMF(IPU,K) .GT. SMEAN(J)) THEN
               SLOPE=(TMF(IPU,K)-TMF(IPU,K-1))/(SMF(IPU,K)
     1               -SMF(IPU,K-1))
               TAUF(J)=TMF(IPU,K-1)+SLOPE*(SMEAN(J)-SMF(IPU,K-1))
               TAUFR(J)=TAUF(J)*REDF
            ENDIF
   86       CONTINUE
   87    CONTINUE
      PRINT 200
      WRITE(10,200)
```

```
      DO 88 J=1,KEND
         WRITE(10,201)TTA(J),DTA(J),SMEAN(J),TAUMAX(J),TAUF(J),TAUFR(J)
 88      PRINT 201,TTA(J),DTA(J),SMEAN(J),TAUMAX(J),TAUF(J),TAUFR(J)
 90   CONTINUE
200   FORMAT(' ********** FAILURE TABLE **********'/1X,'TIME',5X,
     1'DEPTH',3X,'MEAN STRESS',3X,'MAX SHEAR',3X,'FAIL STRESS',3X,
     2'RED. FAIL STRESS')
201   FORMAT(1X,F5.1,2X,F8.1,4X,F8.1,4X,F8.1,6X,F8.1,9X,F8.1)
      RETURN
      END
```

```
 COZZETTE SANDSTONE   PICEANCE BASIN
      7 TIME STEPS
I  TIME DEPTH   NU%  E%     EPSX    EPSY  RHO  PGRAD  TGRAD   ALPHA
1  75.0     0. 0.00 0.00  0.00000 0.00000 2.10 0.433  0.000  0.60E-05
2  66.0  4100. 0.38 0.38  0.00000 0.00050 2.30 0.433 19.960  0.60E-05
3  60.0  4100. 0.40 0.40  0.00000 0.00050 2.40 0.433 19.960  0.60E-05
4  46.0 10400. 0.89 0.89 -0.00100 0.00100 2.50 0.500 20.230  0.60E-05
5  36.0 11700. 1.00 1.00 -0.00100 -.00040 2.50 0.850 20.250  0.60E-05
6  11.0 11700. 1.00 1.00  0.00050 -.00040 2.50 0.900 20.250  0.60E-05
7   0.0  7900. 1.00 1.00  0.00036 -.00040 2.50 0.800 20.170  0.60E-05

                    POISSONS RATIO     YOUNGS MODULUS
   PRESENT VALUE          0.220           0.450E+07
   INITIAL VALUE          0.400           0.300E+06

 RELAXATION TIME=     1000.0000 MYRS
 EACH TIME STEP SUBDIVIDED INTO  4 INTEGRATION STEPS


 TIME IN MILLIONS OF YEARS BEFORE PRESENT =66.00
 EPSX=  0.0000E+00    EPSY=  0.5000E-03
  POISPC=0.38000000    EPC=0.38000000

   INPUT PARAMETERS
  RHO=  2.3000 GM/CM**3
  TGRAD= 19.9600 DEG F/100 FT
  ALPHA=    0.6000E-05  1/DEG F
  PGRAD= 0.43300 PSI/FT

 D=   1025.00 SV=   1020.80 S1=    371.43 S2=    100.48
 S3X=     28.73 S3Y=     73.58 SHMIN=    944.46 SHMAX=    989.31
 PO=    443.83 TEMP=   70.5
 EFF SV=    576.97 EFF SHMIN=    500.63 EFF SHMAX=    545.49
 D=   2050.00 SV=   2041.59 S1=    717.43 S2=    276.19
 S3X=     77.44 S3Y=    203.80 SHMIN=   1958.70 SHMAX=   2085.06
 PO=    887.65 TEMP=   90.9
 EFF SV=   1153.94 EFF SHMIN=   1071.05 EFF SHMAX=   1197.41
 D=   3075.00 SV=   3062.39 S1=   1039.43 S2=    522.95
 S3X=    143.59 S3Y=    388.93 SHMIN=   3037.44 SHMAX=   3282.78
 PO=   1331.47 TEMP=  111.4
 EFF SV=   1730.92 EFF SHMIN=   1705.97 EFF SHMAX=   1951.31
 D=   4100.00 SV=   4083.19 S1=   1338.77 S2=    836.89
 S3X=    224.80 S3Y=    627.40 SHMIN=   4175.76 SHMAX=   4578.37
 PO=   1775.30 TEMP=  131.8
 EFF SV=   2307.89 EFF SHMIN=   2400.46 EFF SHMAX=   2803.07

 TIME IN MILLIONS OF YEARS BEFORE PRESENT =60.00
 EPSX=  0.0000E+00    EPSY=  0.5000E-03
  POISPC=0.40000001    EPC=0.40000001
```

```
 INPUT PARAMETERS
RHO=  2.4000 GM/CM**3
TGRAD= 19.9600 DEG F/100 FT
ALPHA=    0.6000E-05  1/DEG F
PGRAD= 0.43300 PSI/FT

D=   4100.00 SV=   4260.72 S1=   1362.22 S2=    835.64
S3X=    313.19 S3Y=    893.77 SHMIN=   4286.35 SHMAX=   4866.92
PO=   1775.30 TEMP=  131.8
EFF SV=   2485.42 EFF SHMIN=   2511.05 EFF SHMAX=   3091.62
D=   4100.00 SV=   4260.72 S1=   1385.60 S2=    834.38
S3X=    402.20 S3Y=   1162.43 SHMIN=   4397.48 SHMAX=   5157.71
PO=   1775.30 TEMP=  131.8
EFF SV=   2485.42 EFF SHMIN=   2622.18 EFF SHMAX=   3382.41
D=   4100.00 SV=   4260.72 S1=   1408.93 S2=    833.13
S3X=    491.80 S3Y=   1433.38 SHMIN=   4509.17 SHMAX=   5450.74
PO=   1775.30 TEMP=  131.8
EFF SV=   2485.42 EFF SHMIN=   2733.87 EFF SHMAX=   3675.44
D=   4100.00 SV=   4260.72 S1=   1432.20 S2=    831.89
S3X=    582.00 S3Y=   1706.61 SHMIN=   4621.39 SHMAX=   5746.00
PO=   1775.30 TEMP=  131.8
EFF SV=   2485.42 EFF SHMIN=   2846.09 EFF SHMAX=   3970.70

TIME IN MILLIONS OF YEARS BEFORE PRESENT =46.00
EPSX= -0.1000E-02    EPSY=  0.1000E-02
 POISPC=0.88999999    EPC=0.88999999

 INPUT PARAMETERS
RHO=  2.5000 GM/CM**3
TGRAD= 20.2300 DEG F/100 FT
ALPHA=    0.6000E-05  1/DEG F
PGRAD= 0.50000 PSI/FT

D=   5675.00 SV=   6143.19 S1=   1851.31 S2=   1459.20
S3X=    157.17 S3Y=   2123.45 SHMIN=   6020.01 SHMAX=   7986.29
PO=   2552.33 TEMP=  164.0
EFF SV=   3590.86 EFF SHMIN=   3467.68 EFF SHMAX=   5433.96
D=   7250.00 SV=   7848.12 S1=   2231.23 S2=   2205.11
S3X=   -371.58 S3Y=   2644.23 SHMIN=   7446.89 SHMAX=  10462.70
PO=   3382.12 TEMP=  196.1
EFF SV=   4466.00 EFF SHMIN=   4064.76 EFF SHMAX=   7080.57
D=   8825.00 SV=   9553.06 S1=   2574.60 S2=   3061.85
S3X=  -1007.18 S3Y=   3271.89 SHMIN=   8893.96 SHMAX=  13173.03
PO=   4264.68 TEMP=  228.3
EFF SV=   5288.38 EFF SHMIN=   4629.28 EFF SHMAX=   8908.35
D=  10400.00 SV=  11258.00 S1=   2883.79 S2=   4022.38
S3X=  -1752.69 S3Y=   4009.49 SHMIN=  10353.48 SHMAX=  16115.66
PO=   5200.00 TEMP=  260.4
EFF SV=   6058.00 EFF SHMIN=   5153.48 EFF SHMAX=  10915.66
```

```
TIME IN MILLIONS OF YEARS BEFORE PRESENT =36.00
EPSX= -0.1000E-02    EPSY= -0.4000E-03
 POISPC=1.00000000    EPC=1.00000000

  INPUT PARAMETERS
 RHO=  2.5000 GM/CM**3
 TGRAD= 20.2500 DEG F/100 FT
 ALPHA=    0.6000E-05  1/DEG F
 PGRAD= 0.85000 PSI/FT

D=  10725.00 SV=  11609.81 S1=   2631.34 S2=   4225.80
S3X=  -2929.92 S3Y=   3303.86 SHMIN=  10228.16 SHMAX=  16461.94
PO=   6300.94 TEMP=  267.0
EFF SV=   5308.87 EFF SHMIN=   3927.22 EFF SHMAX=  10161.00
D=  11050.00 SV=  11961.62 S1=   2384.48 S2=   4433.32
S3X=  -4131.96 S3Y=   2587.25 SHMIN=  10144.59 SHMAX=  16863.80
PO=   7458.75 TEMP=  273.7
EFF SV=   4502.87 EFF SHMIN=   2685.84 EFF SHMAX=   9405.05
D=  11375.00 SV=  12313.44 S1=   2143.12 S2=   4644.86
S3X=  -5358.52 S3Y=   1859.98 SHMIN=  10102.90 SHMAX=  17321.39
PO=   8673.44 TEMP=  280.3
EFF SV=   3640.00 EFF SHMIN=   1429.46 EFF SHMAX=   8647.96
D=  11700.00 SV=  12665.25 S1=   1907.14 S2=   4860.37
S3X=  -6609.31 S3Y=   1122.36 SHMIN=  10103.19 SHMAX=  17834.86
PO=   9945.00 TEMP=  286.9
EFF SV=   2720.25 EFF SHMIN=    158.19 EFF SHMAX=   7889.86

TIME IN MILLIONS OF YEARS BEFORE PRESENT =11.00
EPSX=  0.5000E-03    EPSY= -0.4000E-03
 POISPC=1.00000000    EPC=1.00000000

  INPUT PARAMETERS
 RHO=  2.5000 GM/CM**3
 TGRAD= 20.2500 DEG F/100 FT
 ALPHA=    0.6000E-05  1/DEG F
 PGRAD= 0.90000 PSI/FT

D=  11700.00 SV=  12665.25 S1=   1870.62 S2=   4830.08
S3X=  -6066.65 S3Y=    757.66 SHMIN=  10725.31 SHMAX=  17549.62
PO=  10091.25 TEMP=  286.9
EFF SV=   2574.00 EFF SHMIN=    634.06 EFF SHMAX=   7458.37
D=  11700.00 SV=  12665.25 S1=   1833.43 S2=   4799.99
S3X=  -5529.89 S3Y=    397.76 SHMIN=  11341.02 SHMAX=  17268.68
PO=  10237.50 TEMP=  286.9
EFF SV=   2427.75 EFF SHMIN=   1103.52 EFF SHMAX=   7031.18
D=  11700.00 SV=  12665.25 S1=   1795.55 S2=   4770.08
S3X=  -4998.98 S3Y=     42.61 SHMIN=  11950.40 SHMAX=  16992.00
PO=  10383.75 TEMP=  286.9
EFF SV=   2281.50 EFF SHMIN=   1566.65 EFF SHMAX=   6608.25
D=  11700.00 SV=  12665.25 S1=   1757.00 S2=   4740.36
S3X=  -4473.85 S3Y=   -307.86 SHMIN=  12553.51 SHMAX=  16719.51
PO=  10530.00 TEMP=  286.9
EFF SV=   2135.25 EFF SHMIN=   2023.51 EFF SHMAX=   6189.51
```

```
TIME IN MILLIONS OF YEARS BEFORE PRESENT = 0.00
EPSX=  0.3600E-03    EPSY= -0.4000E-03
 POISPC=1.00000000    EPC=1.00000000

  INPUT PARAMETERS
 RHO=  2.5000 GM/CM**3
 TGRAD= 20.1700 DEG F/100 FT
 ALPHA=    0.6000E-05  1/DEG F
 PGRAD= 0.80000 PSI/FT

D=  10750.00 SV=  11636.87 S1=   1764.87 S2=   4056.88
S3X=  -4137.72 S3Y=   -688.47 SHMIN=  11090.29 SHMAX=  14539.53
PO=   9406.25 TEMP=  267.5
EFF SV=   2230.62 EFF SHMIN=   1684.04 EFF SHMAX=   5133.28
D=   9800.00 SV=  10608.50 S1=   1772.78 S2=   3375.28
S3X=  -3803.40 S3Y=  -1067.15 SHMIN=   9674.67 SHMAX=  12410.91
PO=   8330.00 TEMP=  248.1
EFF SV=   2278.50 EFF SHMIN=   1344.67 EFF SHMAX=   4080.91
D=   8850.00 SV=   9580.12 S1=   1780.74 S2=   2695.55
S3X=  -3470.88 S3Y=  -1443.91 SHMIN=   8306.66 SHMAX=  10333.64
PO=   7301.25 TEMP=  228.7
EFF SV=   2278.87 EFF SHMIN=   1005.41 EFF SHMAX=   3032.39
D=   7900.00 SV=   8551.75 S1=   1788.74 S2=   2017.69
S3X=  -3140.16 S3Y=  -1818.74 SHMIN=   6986.27 SHMAX=   8307.69
PO=   6320.00 TEMP=  209.3
EFF SV=   2231.75 EFF SHMIN=    666.27 EFF SHMAX=   1987.69

TIME (MY)=        75.0
DEPTH (FT)=          0.0
SV=                  0.0
SHMIN=               0.0
SHMAX=               0.0
EFF SV=              0.0
EFF SHMIN=           0.0
EFF SHMAX=           0.0
S1-GRAV=             0.0
S2-TEMP=             0.0
S3X-STRAIN=           0.0
S3Y-STRAIN=           0.0
PO=                  0.0
TEMP (DEG F)=      50.00
EPSX (IN/IN)=    0.00000
EPSY (IN/IN)=    0.00000
PGRAD (PSI/FT)=    0.433
RHO (GM/CC)=       2.100
POISSONS RATIO=   0.4000
YOUNG MOD (PSI)=.300E+06
ALPHA (1/DEG F)=.600E-05
```

TIME (MY)=	72.7	70.5	68.2	66.0
DEPTH (FT)=	1025.0	2050.0	3075.0	4100.0
SV=	1020.8	2041.6	3062.4	4083.2
SHMIN=	944.5	1958.7	3037.4	4175.8
SHMAX=	989.3	2085.1	3282.8	4578.4
EFF SV=	577.0	1153.9	1730.9	2307.9
EFF SHMIN=	500.6	1071.1	1706.0	2400.5
EFF SHMAX=	545.5	1197.4	1951.3	2803.1
S1-GRAV=	371.4	717.4	1039.4	1338.8
S2-TEMP=	100.5	276.2	522.9	836.9
S3X-STRAIN=	28.7	77.4	143.6	224.8
S3Y-STRAIN=	73.6	203.8	388.9	627.4
PO=	443.8	887.7	1331.5	1775.3
TEMP (DEG F)=	70.46	90.92	111.38	131.84
EPSX (IN/IN)=	0.00000			
EPSY (IN/IN)=	0.00050			
PGRAD (PSI/FT)=	0.433			
RHO (GM/CC)=	2.300			
POISSONS RATIO=	0.4000			
YOUNG MOD (PSI)=	.300E+06			
ALPHA (1/DEG F)=	.600E-05			

TIME (MY)=	64.5	63.0	61.5	60.0
DEPTH (FT)=	4100.0	4100.0	4100.0	4100.0
SV=	4260.7	4260.7	4260.7	4260.7
SHMIN=	4286.3	4397.5	4509.2	4621.4
SHMAX=	4866.9	5157.7	5450.7	5746.0
EFF SV=	2485.4	2485.4	2485.4	2485.4
EFF SHMIN=	2511.0	2622.2	2733.9	2846.1
EFF SHMAX=	3091.6	3382.4	3675.4	3970.7
S1-GRAV=	1362.2	1385.6	1408.9	1432.2
S2-TEMP=	835.6	834.4	833.1	831.9
S3X-STRAIN=	313.2	402.2	491.8	582.0
S3Y-STRAIN=	893.8	1162.4	1433.4	1706.6
PO=	1775.3	1775.3	1775.3	1775.3
TEMP (DEG F)=	131.84	131.84	131.84	131.84
EPSX (IN/IN)=	0.00000			
EPSY (IN/IN)=	0.00050			
PGRAD (PSI/FT)=	0.433			
RHO (GM/CC)=	2.400			
POISSONS RATIO=	0.3316			
YOUNG MOD (PSI)=	.190E+07			
ALPHA (1/DEG F)=	.600E-05			

TIME (MY)=	56.5	53.0	49.5	46.0
DEPTH (FT)=	5675.0	7250.0	8825.0	10400.0
SV=	6143.2	7848.1	9553.1	11258.0
SHMIN=	6020.0	7446.9	8894.0	10353.5
SHMAX=	7986.3	10462.7	13173.0	16115.7
EFF SV=	3590.9	4466.0	5288.4	6058.0
EFF SHMIN=	3467.7	4064.8	4629.3	5153.5
EFF SHMAX=	5434.0	7080.6	8908.3	10915.7

S1-GRAV=	1851.3	2231.2	2574.6	2883.8
S2-TEMP=	1459.2	2205.1	3061.9	4022.4
S3X-STRAIN=	157.2	-371.6	-1007.2	-1752.7
S3Y-STRAIN=	2123.5	2644.2	3271.9	4009.5
PO=	2552.3	3382.1	4264.7	5200.0
TEMP (DEG F)=	163.98	196.11	228.25	260.39
EPSX (IN/IN)=	-0.00100			
EPSY (IN/IN)=	0.00100			
PGRAD (PSI/FT)=	0.500			
RHO (GM/CC)=	2.500			
POISSONS RATIO=	0.3280			
YOUNG MOD (PSI)=	.198E+07			
ALPHA (1/DEG F)=	.600E-05			

TIME (MY)=	43.5	41.0	38.5	36.0
DEPTH (FT)=	10725.0	11050.0	11375.0	11700.0
SV=	11609.8	11961.6	12313.4	12665.2
SHMIN=	10228.2	10144.6	10102.9	10103.2
SHMAX=	16461.9	16863.8	17321.4	17834.9
EFF SV=	5308.9	4502.9	3640.0	2720.2
EFF SHMIN=	3927.2	2685.8	1429.5	158.2
EFF SHMAX=	10161.0	9405.1	8648.0	7889.9
S1-GRAV=	2631.3	2384.5	2143.1	1907.1
S2-TEMP=	4225.8	4433.3	4644.9	4860.4
S3X-STRAIN=	-2929.9	-4132.0	-5358.5	-6609.3
S3Y-STRAIN=	3303.9	2587.3	1860.0	1122.4
PO=	6300.9	7458.7	8673.4	9945.0
TEMP (DEG F)=	267.03	273.66	280.29	286.92
EPSX (IN/IN)=	-0.00100			
EPSY (IN/IN)=	-0.00040			
PGRAD (PSI/FT)=	0.850			
RHO (GM/CC)=	2.500			
POISSONS RATIO=	0.2398			
YOUNG MOD (PSI)=	.404E+07			
ALPHA (1/DEG F)=	.600E-05			

TIME (MY)=	29.7	23.5	17.2	11.0
DEPTH (FT)=	11700.0	11700.0	11700.0	11700.0
SV=	12665.2	12665.2	12665.2	12665.2
SHMIN=	10725.3	11341.0	11950.4	12553.5
SHMAX=	17549.6	17268.7	16992.0	16719.5
EFF SV=	2574.0	2427.7	2281.5	2135.2
EFF SHMIN=	634.1	1103.5	1566.7	2023.5
EFF SHMAX=	7458.4	7031.2	6608.2	6189.5
S1-GRAV=	1870.6	1833.4	1795.6	1757.0
S2-TEMP=	4830.1	4800.0	4770.1	4740.4
S3X-STRAIN=	-6066.6	-5529.9	-4999.0	-4473.9
S3Y-STRAIN=	757.7	397.8	42.6	-307.9
PO=	10091.2	10237.5	10383.7	10530.0
TEMP (DEG F)=	286.92	286.92	286.92	286.92
EPSX (IN/IN)=	0.00050			
EPSY (IN/IN)=	-0.00040			
PGRAD (PSI/FT)=	0.900			

```
RHO (GM/CC)=        2.500
POISSONS RATIO=   0.2200
YOUNG MOD (PSI)=.450E+07
ALPHA (1/DEG F)=.600E-05

TIME (MY)=          8.2     5.5     2.7     0.0
DEPTH (FT)=       10750.0  9800.0  8850.0  7900.0
SV=               11636.9 10608.5  9580.1  8551.7
SHMIN=            11090.3  9674.7  8306.7  6986.3
SHMAX=            14539.5 12410.9 10333.6  8307.7
EFF SV=            2230.6  2278.5  2278.9  2231.7
EFF SHMIN=         1684.0  1344.7  1005.4   666.3
EFF SHMAX=         5133.3  4080.9  3032.4  1987.7
S1-GRAV=           1764.9  1772.8  1780.7  1788.7
S2-TEMP=           4056.9  3375.3  2695.6  2017.7
S3X-STRAIN=       -4137.7 -3803.4 -3470.9 -3140.2
S3Y-STRAIN=        -688.5 -1067.2 -1443.9 -1818.7
PO=                9406.2  8330.0  7301.2  6320.0
TEMP (DEG F)=      267.53  248.13  228.74  209.34
EPSX (IN/IN)=     0.00036
EPSY (IN/IN)=    -0.00040
PGRAD (PSI/FT)=     0.800
RHO (GM/CC)=        2.500
POISSONS RATIO=   0.2200
YOUNG MOD (PSI)=.450E+07
ALPHA (1/DEG F)=.600E-05
 MEAN STRESS       SHEAR STRESS
    -2320.00           0.00
    11237.50       11165.00
    17980.00       16457.50
    22910.00       20010.00
    29145.00       24795.00

********** FAILURE TABLE **********
 TIME     DEPTH   MEAN STRESS   MAX SHEAR   FAIL STRESS   RED. FAIL
STRESS
  75.0       0.0         0.0         0.0        2427.9          1456.7
  72.7    1025.0       538.8        38.2        2841.4          1704.8
  70.5    2050.0      1134.2        63.2        3298.4          1979.0
  68.2    3075.0      1828.6       122.7        3831.3          2298.8
  66.0    4100.0      2555.5       247.6        4389.1          2633.5
  64.5    4100.0      2788.5       303.1        4567.9          2740.8
  63.0    4100.0      2933.9       448.5        4679.5          2807.7
  61.5    4100.0      3080.4       595.0        4792.0          2875.2
  60.0    4100.0      3228.1       742.6        4905.3          2943.2
  56.5    5675.0      4450.8       983.1        5843.7          3506.2
  53.0    7250.0      5572.7      1507.9        6704.6          4022.8
  49.5    8825.0      6768.8      2139.5        7622.6          4573.5
  46.0   10400.0      8034.6      2881.1        8594.0          5156.4
  43.5   10725.0      7044.1     -3116.9        7833.9          4700.3
  41.0   11050.0      6045.4     -3359.6        7067.4          4240.5
  38.5   11375.0      5038.7     -3609.2        6294.8          3776.9
```

36.0	11700.0	4024.0	-3865.8	5516.1	3309.7
29.7	11700.0	4046.2	3412.2	5533.1	3319.9
23.5	11700.0	4067.4	2963.8	5549.4	3329.6
17.2	11700.0	4087.5	2520.8	5564.8	3338.9
11.0	11700.0	4106.5	2083.0	5579.4	3347.6
8.2	10750.0	3408.7	1724.6	5043.9	3026.3
5.5	9800.0	2712.8	1368.1	4509.8	2705.9
2.7	8850.0	2018.9	1013.5	3977.3	2386.4
0.0	7900.0	1449.0	-782.7	3539.9	2124.0

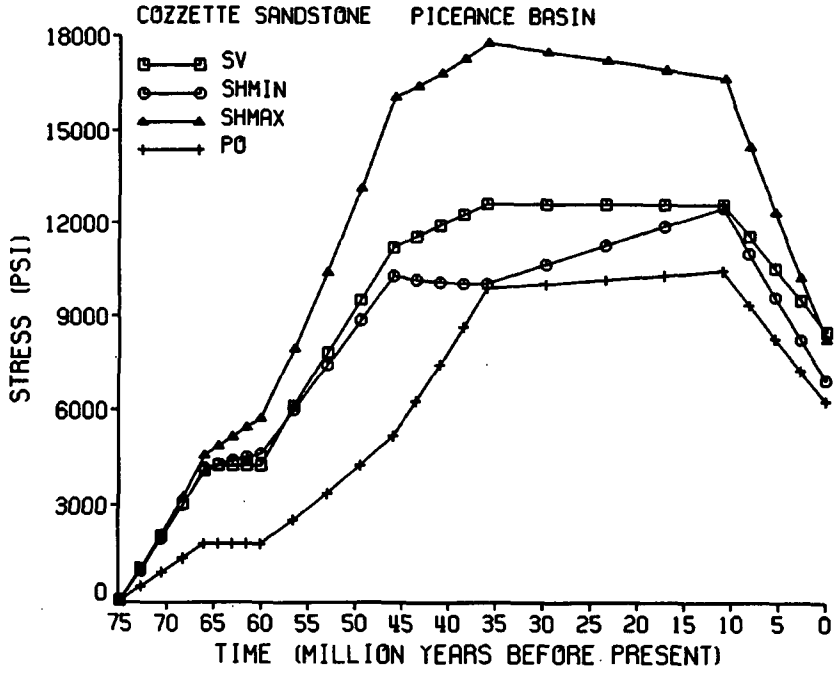

Figure F1. Calculated magnitudes, through time, for the vertical stress (SV), minimum and maximum horizontal stresses (SHMIN and SHMAX), and the pore pressure (PO) for the Cozzette Sandstone at the MWX site.

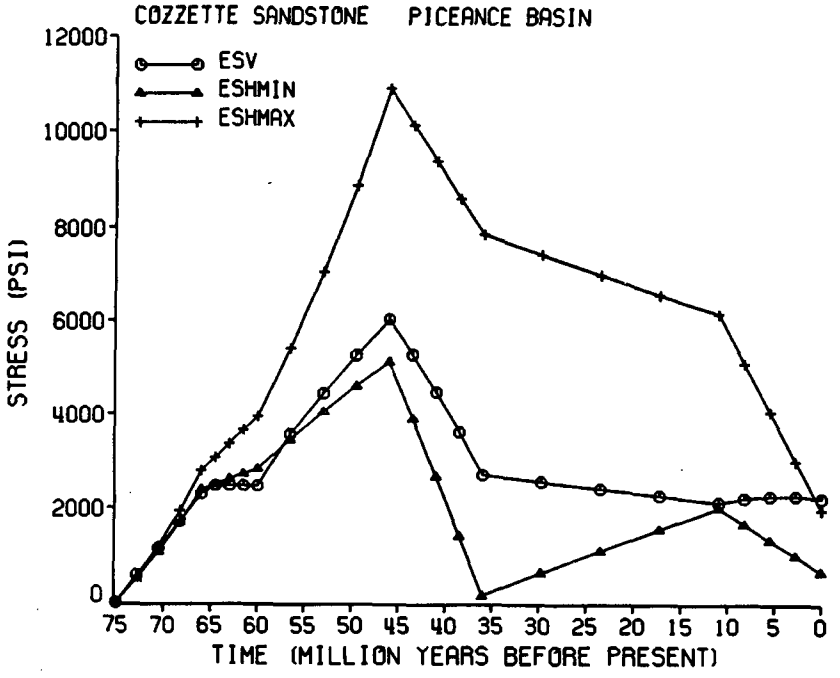

Figure F2. Calculated magnitudes, through time, for the vertical effective stress (ESV), and minimum and maximum effective horizontal stresses (ESHMIN nad ESHMAX).

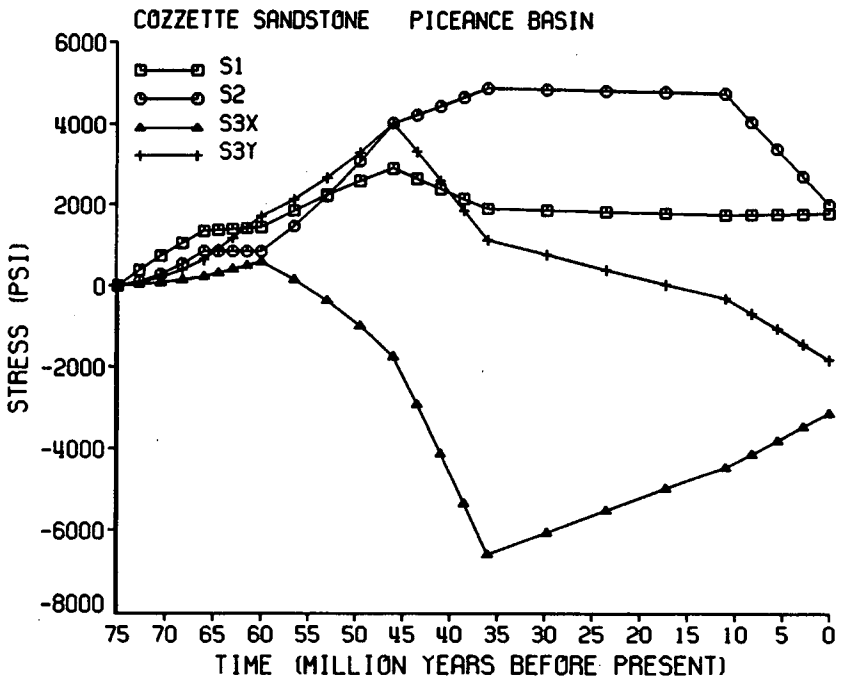

Figure F3. Magnitudes of the different components of the total stress through time: gravity (S1), thermal stress (S2), and the two horizontal tectonic stresses (S3X and S3Y).

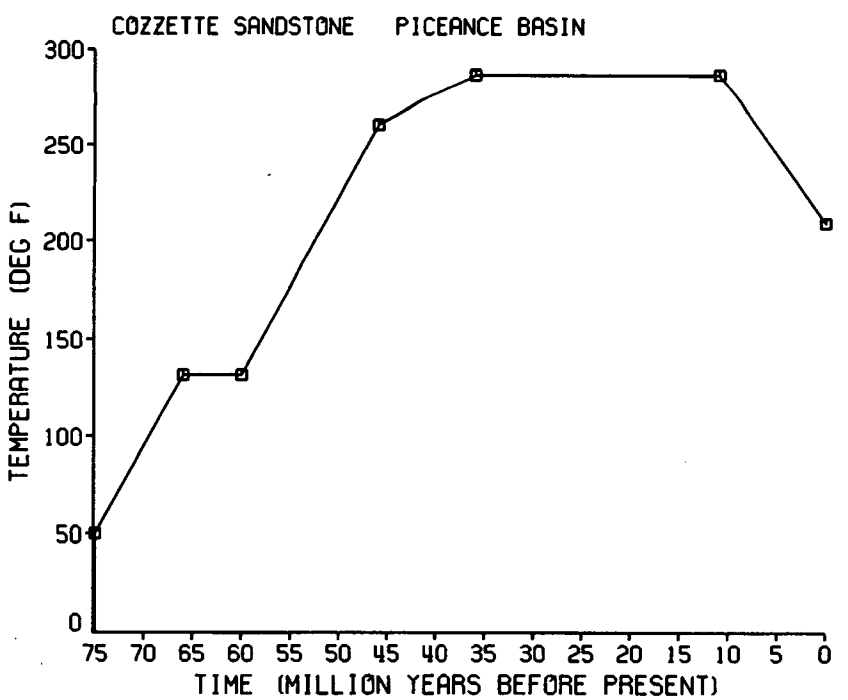

Figure F4. Input values for the temperature through time.

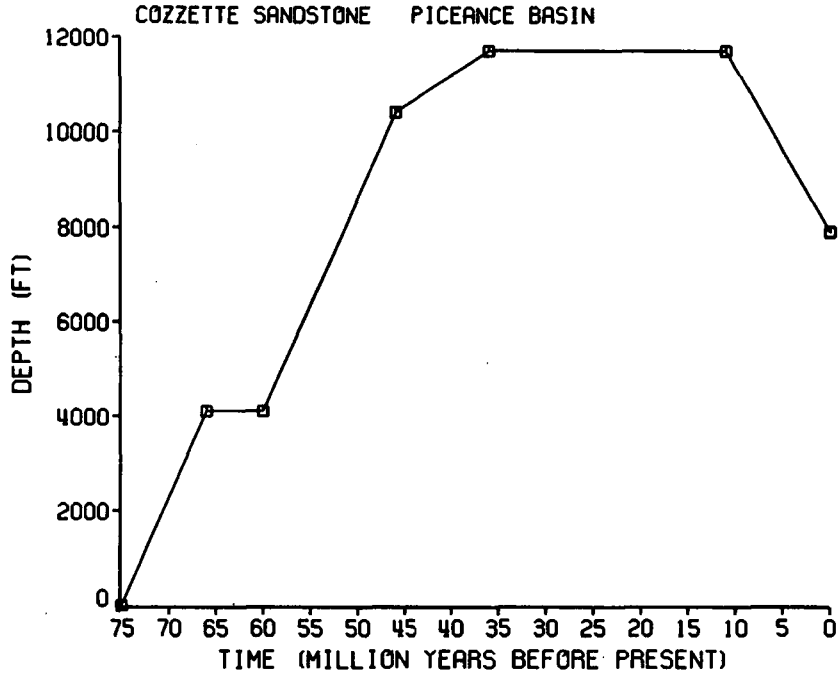

Figure F5. Input values for the depth of burial through time.

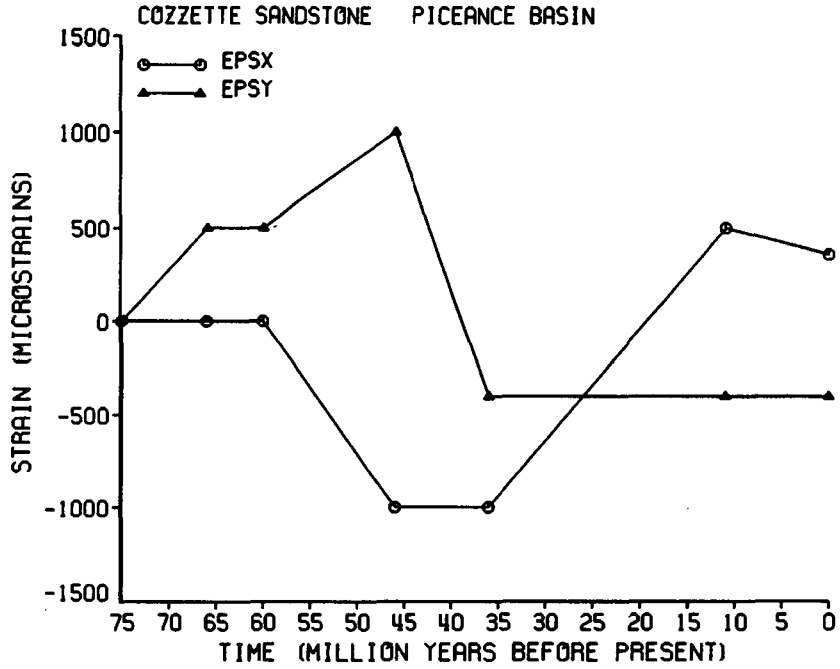

Figure F6. Input parameters for the maximum and minimum tectonic strains (EPSY and EPSX) through time.

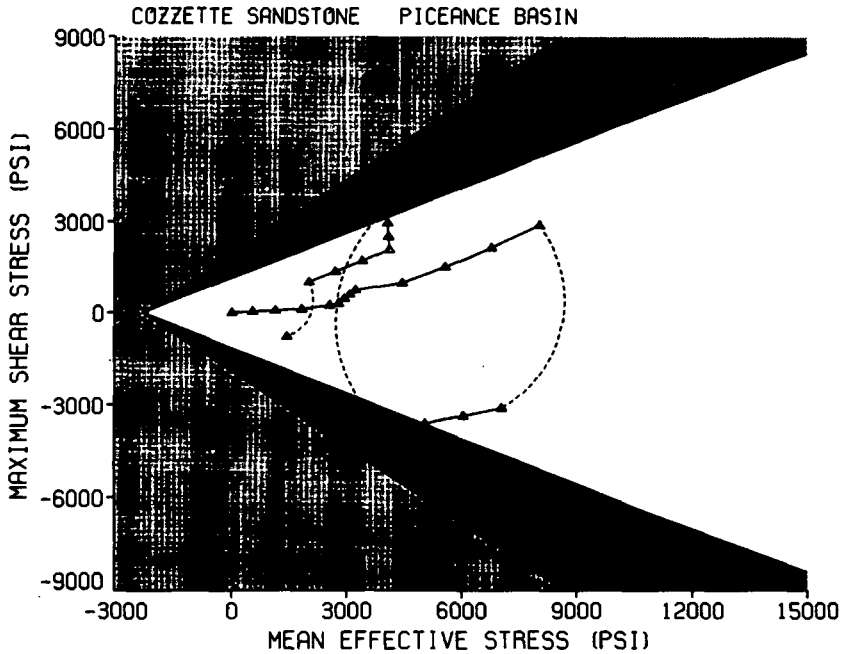

Figure F7. Calculated stress conditions in the Cozzette Sandstone at the MWX site through time, with respect to the limits of laboratory-determined failure (light shading) and the probable failure under true geologic conditions (dark shading) for the rock. The stress condition at the time of deposition 75 million years ago is depicted by the triangle nearest the point of origin of the failure envelope, and the present day stress condition is the triangle at the other end of the circuitous path, just to the lower right of the original triangle. The most likely times of fracturing are the two events depicted by the stress-condition triangles that lie beyond the limits of yielding. (See Warpinski, 1989, for complete details.)

Reference

Warpinski, N.R., 1989, Elastic and viscoelastic calculations of stresses in sedimentary basins: SPE Formation Evaluation, v. 4, p. 522–530.

DISTRIBUTION:

7 U.S. Department of Energy
Office of Oil and Gas Exploration
and Production
Attn: Donald A. Juckett
H. William Hochheiser
Guido Dehoratiis
George Stosur
Arthur Hartstein
Jim R. White
E.B. Nuckolls
FE-30/Forrestal Building
Washington, D.C. 20585

28 U.S. Department of Energy
Morgantown Energy Technology Center
Attn: Leonard Graham
Royal J. Watts (25)
Karl-Heinze Frohne
Charles A. Komar
PO Box 880
Collins Ferry Road
Morgantown, WV 26505

5 U.S. Department of Energy
Bartlesville Project Office
Attn: Thomas C. Wesson
Alex B. Crawley
Robert E. Lemmon
Rhonda Lindsey
Edith Allison
Bartlesville, OK 74005

1 Neil Hurley
Marathon Oil Co.,
PO Box 269
Littleton, CO 80160

3 Oryx Energy Co.
Attn: Harold Illich
Howard White
Robert Skopec
PO Box 2880
Dallas, TX

1 Robert B. Hunter
BP Exploration (Alaska)
PO Box 196612
Anchorage, AK 99519-6612

2 Gas Research Institute
Attn: David Hill
Stephen Wolhart
8600 West Bryn Mawr Ave
Chicago, IL 60631

1 Bruce Cain
Shell Westerns E&P Inc.
PO Box 567
Houston, TX 77001

1 Wm. W. Peabody
Peabody Ventures
125 Lincoln Ave. #400
Santa Fe, NM 87501

1 Stephen H. Leeds
Precision Core Analysis, Inc.
1338 S. Valentia St., Suite 140
Denver, CO 80231

1 Lee Krystinik
Union Pacific Resources Co.
PO Box 7
Fort Worth, TX 76101-0007

1 Jay C. Close
Resources Enterprises
360 Wakara Way
Salt Lake City, UT 84108

1 Byron Kulander
Wright State University
Department of Geology
Dayton, OH 45435

1 Jerry Walker
Sierra Energy Co.
PO Box 20200
Reno, NV 89520

1 Richard Dayvault
Chem-Nuclear Geotech, Inc.
PO Box 14000
Grand Junction, CO 81502

DISTRIBUTION (Continued):

1 Carl Evans
Pennzoil Exploration and Production
PO Box 2967
Houston, TX 77252-2967

1 Robbie Gries
1660 Lincoln, Ste 1640
Denver, CO 80203

1 C. Dennis Irwin
220 Cimmaron Way
Boulder, CO 80303

4 US Geological Survey
Denver Federal Center
Attn: Ben Law, MS 939
Charles SPencer MS 939
Marilyn Grout MS 913
Earl Verbeek MS 913
Denver, CO 80225

1 William Hanson
Amoco Production Co.
PO Box 3092
Houston, TX 77253-5071

1 Stephen Laubach
Bureau of Economic Geology
University Station, Box X
Austin, TX 78713-7508

1 W. Travis Brown
Travis Energy Group
8423 E. Otero Circle
Englewood, CO 80112

1 Ted Campen
Campen Consultants Inc.
7314 Charolais Street
Billings, MT 59106

1 Donald Dayhuff
Chandler & Associates, Inc.
770 Lincoln Tower Bldg
1860 Lincoln
Denver, CO 80203

1 W. Jim Eubanks
ARCo international Oil and Gas Co.
PO Box 260888
Plano, TX 75026-0888

1 Robin Hill
CER Corporation
950 Grier Dr
Las Vegas, NV 89119

4 Harvey E. Yates Co.
One Sunwest Centre
Attn: Larry Brooks
Frank Messa
George Yates
A. J. Deans
PO Box 1933
Roswell, NM 88202

1 Jim Peterson
Dept. of Geology
Univ. of Montana
Missoula, MT 59812

1 Billy Ward, Jr.
1104 E. Dover Pl
Broken Arrow, OK 74012

1 Noel Waechter
Waechter and Associates
Lombardi Bldg, Suite 318
1645 Court Place
Denver, CO 80202

1 Jim Minelli
Meridian Oil
5613 D.T.C. Parkway
Englewood, CO 80111

2 Barrett Resources Corp
Attn: Kurt Reinecke
Terry Barrett
1125 17th St, Suite 2100
Denver, Co 80202

1 Lee Woodward
Dept of Geology
University of New Mexico
Albuquerque, NM 87131

DISTRIBUTION (Continued):

1 Neil Whitehead
NM Bureau Mines & Mineral Resources
Socorro, NM 87081

1 Randall Billingsley
Amoco Production Co
PO Box 800
Denver, Co 80201

1 Norman C. Wardlaw
Department of Geology
University of Calgary
2500 University Drive NW
Calgary, Alberta
T2N 1N4
CANADA

1 Daniel Clark-Lowes
Scott Pickford plc
256 High Street
Croydon, Surrey
CRO 1NF
ENGLAND

1 Chris Garrett
Core Laboratories
Wesgeco House
PO Box 18, 455 London Road
Isleworth, Middlesex
TW7 5AB
ENGLAND

1	6100	R. W. Lynch
10	6112	D. A. Northrop
1	6114	M. W. Scott
5	6114	N. R. Warpinski
1	6117	W. R. Wawersik
5	6117	L. W. Teufel
5	6117	J. C. Lorenz
1	8523-2	Central Technical Files
5	7141	Technical Library
1	7151	Technical Publications
10	7613-2	Document Processing for DOE/OSTI